Development of carbonaceous and polymeric material grafted composites for remediation of pollutants from wastewater

Thesis submitted by

Lopamudra Das

Doctor of Philosophy

(Engineering)

School of Advanced Studies in Industrial pollution Control Engineering

Faculty Council of Interdisciplinary studies, Law & Management

Jadavpur University, Kolkata – 700032, West Bengal, India

Year-2023

Development of carbonaceous and polymeric material grafted composites for remediation of pollutants from wastewater

Thesis submitted for

Doctor of Philosophy (Engineering)

Of

Jadavpur University

by

Lopamudra Das

Under the guidance of

Dr. Avijit Bhowal
Professor
Chemical Engineering Department
Jadavpur University
Kolkata – 700032
India

&

Dr. Papita Das
Professor
Chemical Engineering Department
Jadavpur University
Kolkata – 700032
India

JADAVPUR UNIVERSITY

KOLKATA – 700032, INDIA

INDEX NO.: D-7/ISLM/93/19

1. **Title of thesis**: Development of carbonaceous and polymeric material grafted composites for remediation of pollutants from wastewater

2. **Name, Designation and Institution of Supervisors:**

Dr. Avijit Bhowal
Professor,
Chemical Engineering Department,
Jadavpur University,
Kolkata – 700032, India.
&
Dr. Papita Das
Professor,
Chemical Engineering Department,
Jadavpur University,
Kolkata – 700032, India.

3. **List of Publications in Referred journals:**

1. Das, L., Das, P., Bhowal, A., Bhattachariee, C., 2020. Synthesis of hybrid hydrogel nano-polymer composite using Graphene oxide, Chitosan and PVA and its application in waste water treatment. Environ. Technol. Innov. 18, 100664. https://doi.org/10.1016/j.eti.2020.100664

2. Das, L., Das, P., Bhowal, A., Bhattachariee, C., 2020. Treatment of malachite green dye containing solution using bio-degradable Sodium alginate/NaOH treated activated sugarcane baggsse charcoal beads: Batch, optimization using response surface methodology and continuous fixed bed column study. J. Environ. Manage. 276. https://doi.org/10.1016/j.jenvman.2020.111272

3. Das, L., Das, P., Bhowal, A., Bhattacharjee, C., 2021. Enhanced biosorption of fluoride by extracted nanocellulose/polyvinyl alcohol composite in batch and fixed-bed system: ANN analysis and numerical modeling. Environ. Sci. Pollut. Res. https://doi.org/10.1007/s11356-021-14026-x

4. Das, L., Sengupta, S., Das, P., Bhowal, A., Bhattacharjee, C., 2021. Experimental and Numerical modeling on dye adsorption using pyrolyzed mesoporous biochar in Batch and fixed-bed column reactor: Isotherm, Thermodynamics, Mass

transfer, Kinetic analysis. Surfaces and Interfaces 23, 100985. https://doi.org/10.1016/j.surfin.2021.100985

5. Das, L., Saha, N., Ganguli, A., Das, P., Bhowal, A., Bhattacharjee, C., 2021. Calcium alginate–bentonite/activated biochar composite beads for removal of dye and Biodegradation of dye-loaded composite after use: Synthesis, removal, mathematical modeling and biodegradation kinetics. Environ. Technol. Innov. https://doi.org/10.1016/j.eti.2021.101955

6. Saha, N., Das, L., Ganguli, A., Das, P., Bhowal, A., Bhattacharjee (2021), Comparative experimental and mathematical analysis on removal of dye using raw rice husk, rice husk charcoal and activated rice husk charcoal: batch, fixed-bed column, and mathematical modeling. Biomass Conversion and Biorefinery DOI:10.1007/s13399-021-01996-8

4. **List of published Book chapter:**

1. Das, Lopamudra & Das, Papita & Bhowal, Avijit & Bhattacharjee, Chiranjib. (2022). Natural Biodegradable Polymeric Bio-adsorbents for Textile Wastewater. Polymer Technology in Dye-containing Wastewater (pp.209-225). DOI:10.1007/978-981-19-0886-6_9.
2. Das, L., Saha, N., Saha, Das, P., Bhowal, A., Bhattacharya, C., (**2020)**. Application of Synthesized Nanocellulose Material for Removal of Malachite Green from Wastewater, in: Recent Trends in Waste Water Treatment and Water Resource Management. https://doi.org/10.1007/978-981-15-0706-9_2

5. **List of patents:** Nil

6. **List of conferences Presentations:**

1. Lopamudra Das, Papita Das, Avijit Bhowal: Extracted Cellulose/ Graphene Oxide nano-composite preparation and application for fluoride removal, International conference on Nanotechnology (ICNT-2019), 28-29th December, 2019 organized by Institute of Fire and Safety Engineering, Haldia, West Ben, India., Proceedings:-978-93-5361-912-1, page-69gal
2. Lopamudra Das, MS Karuna, Papita Das, Avijit Bhowal; Advances in eco-friendly approaches for Defluoridation process using Sugarcane bagasse-derivatives and composites, International conference on Chemical Engineering Enabling Transition Towards Sustainable Future (Chemtsf-2022) organized by the Department of Chemical Engineering, IIT Roorkee during September 8-10, 2022
3. Lopamudra Das, Sharwan Kumar, Varsha Singh, Uddeshya Gangwar, Sumit Gangwar, Dr. MS Karuna, Hiba Roshan Khan, Papita Das, Avijit Bhowal. Synthesis and application of agro-waste derived nanocellulose/PVA hybrid hydrogel for treatment of textile dye containing waste water: Batch and Column study, ACMS - 2022 International conference on advances in chemical and material science, organised by IIChE, held in Heritage Institute of technology on 14-16th April ,2022.

4. Lopamudra Das, Papita Das, Avijit Bhowal; Development of agro-waste derived Biopolymer grafted adsorbents for fluoride removal, 1st International Conference on Advances in Biopolymers and Composites: Health, Environment, and Energy (ABC-HEE, 2022), organized by Motilal Nehru National Institute of Technology (MNIT) Allahabad Prayagraj- 211004, India on October 20-22, 2022
5. Lopamudra Das, niladri shikhar saha, papita das, avijit bhowal, chiranjib bhattacharya. Batch adsorption studies on removal of Crystal Violet dye from aqueous solutions using raw sugarcane bagasses, International Conference on Emerging Technologies for Sustainable Development (ICETSD 19) on March 5-6, 2019 at GCELT campus, Kolkata.WB,India. , Proceedings:- 978-81-8211-146-2 , Page- 95-98
6. Lopamudra Das, niladri shikhar saha, papita das, avijit bhowal, chiranjib bhattacharya; Fixed bed column study for the removal of aqueous malachite green dye solution using raw sugarcane bagasse. 12th All India Peoples' technology congress organised by forum of scientists, engineers & technologists (FOSET-2019), 16-17th February 2019.
7. Lopamudra Das, Niladri Saha, Papita Das, Avijit Bhowal, Chiranjib Bhattacharya; Application of synthesized Nano-cellulose material for removal of malachite green from waste water, 8th International Conference on Sustainable Waste Management (8th ICON- 2018) by Acharaya Nagarjuna University, Andhra Pradesh, during November 22-24, 2018, volume-2, Page- 838 – 845

PROFORMA – 1

"Statement of Originality"

I Lopamudra Das, registered on 1st November, 2019 do hereby declare that this thesis entitled "**Development of carbonaceous and polymeric material grafted composites for remediation of pollutants from wastewater**" contains literature survey and original research work done by the undersigned candidate as part of Doctoral studies.

All information in this thesis have been obtained and presented in accordance with existing academic rules and ethical conduct.

I declare that, as required by these rules and conduct, I have fully cited and referred all materials and results that are not original to this work.

I also declare that I have checked this thesis as per the "Policy on Anti Plagiarism, Jadavpur University, 2019", and the level of similarity as checked by iThenticate software is **9%.**

Lopamudra Das.

Lopamudra Das

Date: 27/02/2023

Certified by Supervisor(s):

Avijit Bhowal

1. Dr. Avijit Bhowal

Professor

Chemical Engineering Department

Jadavpur University

Kolkata – 700032

India

Professor
CHEMICAL ENGINEERING DEPARTMENT
JADAVPUR UNIVERSITY
Kolkata-700 032

Papita Das

2. Dr. Papita Das

Professor

Chemical Engineering Department

Jadavpur University

Kolkata – 700032

India

Professor
CHEMICAL ENGINEERING DEPARTMENT
JADAVPUR UNIVERSITY
Kolkata-700 032

PROFORMA – 2

CERTIFICATE FROM THE SUPERVISORS

This is to certify that the thesis entitled "**DEVELOPMENT OF CARBONACEOUS AND POLYMERIC MATERIAL GRAFTED COMPOSITES FOR REMEDIATION OF POLLUTANTS FROM WASTEWATER**" submitted by Lopamudra Das, who got her name registered on 01.11.2019 (Index. No. D-7/ISLM/93/19, Registration No. D-7/ISLM/93/19, Class roll No. 301910305001) for the award of Ph.D. (Engineering) degree of Jadavpur University is absolutely based upon her own work under the supervision of Dr. Avijit Bhowal and Dr. Papita Das and that neither her thesis nor any part of the thesis has been submitted for any degree/diploma or any academic award anywhere before.

Dr. Avijit Bhowal
Professor
Chemical Engineering Department
Jadavpur University
Kolkata – 700032
India

Professor
CHEMICAL ENGINEERING DEPARTMENT
JADAVPUR UNIVERSITY
Kolkata-700 032

Dr. Papita Das
Professor
Chemical Engineering Department
Jadavpur University
Kolkata – 700032
India

Professor
CHEMICAL ENGINEERING DEPARTMENT
JADAVPUR UNIVERSITY
Kolkata-700 032

DEDICATED

TO

MY BELOVED

FATHER, MOTHER, AND HUSBAND

Acknowledgement

I am greatly indebted to Professors, **Dr. Avijit Bhowal and Dr. Papita Das**, my research Supervisors for their constant inspiration to me to carry over my work and giving constructive criticism and valuable suggestions throughout the course of project without their guidance I could not be able to complete my PhD work. I am also grateful to **Prof. Chiranjeb Bhattacharjee** for his enthusiasm, scholarly encouragement which helped me to complete my project work. My heartiest thanks are offered to all the Professors of Chemical Engineering department and School of Advanced Studies on Industrial Pollution Control Engineering, Jadavpur University.

I gratefully acknowledge the financial assistance received from **Dalmia Holding Groups**. I am extremely thankful to my seniors, friends, and all other fellow members, **Sandipan Bhatttacharya, Dr. Niladri Anjan Saha, Dr. Vijoyeta Chakraborty, Antara Ganguli, Dr. Dolanchapa Sikdar, Dr. Shubhalakshmi Sengupta, Dr. Suvendu Mana, Dr. Azizur Rahman, Dr. Sudipta Goswami, Dr. Sudhanya Karmakar, Mrs. Moumita Sharma, Preetha Ganguly, Rwiddhi Sarkhel, Dr. Uttariya Roy, Subhasis Ghosh, Poushali Chakraborty, Sayan Mukharjee, Akash Hossain, Sanket Roy,** deserve heartfelt appreciation for their help, cooperation, and generous advice throughout the PhD work. I am also thankful to **Sri. Jatish Das** for his association with me during the use of instrumental facilities. A special thank goes to the laboratory and library staffs for providing and supplying me necessary facilities. Special thanks to my loving sisters **(Sudipa Das Rana, Aparupa Das Kar, Gopabhadra Das, Sandipa Das)** for giving me mental support and encourage me. Last but not the least, I pay my best personal regards, gratitude and love to my parents (**Sri. Durgapada Das, and Smt. Purnima Das**) who inspired me to achieve the best in life, in the form of higher education. And also, I wish to express special regards to my husband (**Mr. Arunanshu Pal**) for his able guidance, soft heartened nature and lot of patience that encouraged me to go ahead and overcome the intricacies of my present attempt. I also thankful to my In-laws (**Smt. Pratima Kundu Pal, Sri. Dashurathi Pal**) for their support and blessing**.**

Lopamudra Das
School of Advanced Studies on Industrial Pollution Control Engineering
Jadavpur University
Kolkata-700032, West Bengal, India

Contents

List of Figures

List of Tables

Final thesisLOPA.pdf

WORD COUNT	42262	TIME SUBMITTED	22-FEB-2023 12:30PM
		PAPER ID	96882967

Chapter.1

Introduction and Background

1.1. Introduction to Dyes

Dye is a chemical substance that imparts color when applied to a substance (such as cloths, papers, leathers etc.). Dyes and dyeing products are used in numerous sectors including textile, plastic, rubber, paper & print, leather, cosmetics, and biomedical. The major application of dye nevertheless is in textile industries. Dyes are applied in textiles simultaneously both for imparting color to original raw material and to the products. They are generally used in the form of powder, paste, or liquid dispersion, and they can dissolve completely in aqueous medium (such as water). Dyes can be natural or synthetic.

Before the period of the industrial revolution with inventing technologies, textile materials were colored with natural biodegradable dyeing compounds obtained from plant/animal source, which were not ever a danger towards the Mother Nature as they were biodegradable. But by 1900, synthetic dyes accounted for approximately 90 percent of the whole dye industry market. There are many reasons which can be attributed for the diminishing utilization of natural dyes in commercial market. The industrial revolution of 1850 in Europe was one of them. This revolution created a huge surge in requirement of easily obtainable, and comparably cheap or synthetic dyes.

1.1.1. Synthetic Dyes: Classification and class:

Dyes can be classified on the basis of chemical structure (azo dye, nitro dye, etc.), nuclear structure (anionic, cationic, or nonionic), or industrial application (reactive dye, acid dye, etc.) (Nikfar & Jaberidoost, 2014). From structural perspective, the dyes can be identified by two key groups: chromophores and auxochromes. The chromophore provides color to the dye molecule and auxochromes enriches the compatibility of the products (Salleh et al., 2011). On basis of industrial usage, dyes can be classified as

Basic Dye: Basic dyes are mainly water soluble and known as cationic dye as they produce colored cations by ionization in solution. They are largely utilized in paper, medicine industry, and also used for dyeing polyacrylonitrile, silk, cotton, nylons, polyesters, etc. These dyes specifically belong to the chemical structures of diazahemicyanine, triarylmethane, cyanine, and acridine, etc. Some examples of basic dye are Methylene blue, Malachite green, Basic Red 46, Brilliant Green, etc (Nikfar & Jaberidoost, 2014).

***Acid Dye*:** Acid dyes are water soluble and known as anionic dyes as they produce colored anions by ionization in solution. These dyes are applied for coloring nylon, wool, silk, modified acrylics, paper printing, leather, food, and cosmetics. Most of these dyes are anionic type and have capability of dissolving in water. They mainly belong to the chemical structures of the

azo, azine, xanthene, and nitros, etc. Some examples of these dye are Acid Red 18, Acid Yellow 23, Acid Black 48, etc. (Banerjee et al., 2017).

***Disperse Dye*:** These water-insoluble dye is used mostly for dying polyester, cellulose, nylon, cellulose acetate, and acrylics. They are nonionic type of dyes and mainly contain chemical structures of benzodifuranones, nitro, azo, anthraquinones, etc. Some examples of these dyes are Disperse Red 1, Disperse Orange 3, Disperse Blue 35, etc. (Yang et al., 2017).

***Direct Dye*:** These dyes are used for coloring of cotton, rayon, paper, nylon, leather, etc. They dissolve in water and produce anions in solution. These dyes have chemical structure of stilbene, phthalocyanine and oxazine etc. (Salleh et al., 2011). Some examples of excessive used direct dyes are Direct Orange 34, Direct Red 23, Direct Black 38, etc.

***Reactive Dye**:* These anionic dyes largely used for coloring on cotton, wool and other cellulosic fibers etc. These dyes belong to the chemical groups including anthraquinone, azo, phthalocyanines, formazan, oxazines, etc. Some examples of these dye are Reactive Black 5, Reactive Blue 4, Reactive Red 120, and Reactive Red 2 (Bhupinderkaur & Chanchal, 2016).

Solvent Dye: They are conventionally applied for fuels, resins, plastics, lubricants, woods, and waxes and are specifically solvent-soluble but not water-soluble. They mainly contain chemical structural group of azo and anthraquinones, phthalocyanines, etc. (Puvaneswari et al., 2006). Some examples of this type of dyes are Natural Black 1, Mordant Blue 14 and Mordant Red 3.

1.1.2. Toxicity of dye

The color concentrations in the textile effluents vary from 10 to 200 mg/L^{-1} (Islam et al., 2020). Several dyes have visibility in water even at very less concentrations (1 mg/L^{-1}). Hence, dumping of untreated colored textile outflow in exposed water not only causes aesthetic problems to human being and aquatic life. Additionally, discharged contaminated water are also responsible for environmental degradation and mostly affect the aquatic ecosystem as they hamper photosynthesis process by blocking light penetration through water layer and decrease the concentration of dissolved oxygen (Stan et al., 2019).

Synthetic dyes have complex chemical structure, photolytic stability, and non-biodegradable substance (Salleh et al., 2011; Sudha & Saranya, 2014). For example, dyes which contain chemical structural class of azo group binds to an aromatic ring (Banerjee et al., 2017). These dyes can form aromatic amines, arylamines by mineralization which are considered to be hazardous (Bhupinderkaur & Chanchal, 2016). Maximum numbers of textile dyes are water-soluble and easily absorbed on living cell membrane by contact and by inhalation. This may cause a threat of cancer, splenic sarcomas, chromosomal abnormalities, nuclear anomalies,

hypersensitivity, eye-irritation, skin irritation, contact dermatitis, respiratory distress, lacrimations when inhaled or consumed (Puvaneswari et al., 2006; Sudha & Saranya, 2014).

1.2. Introduction to Fluoride

Fluorine (F) is a highly electronegative reactive chemical element with atomic number 9 and ~~it~~ is the lightest element of halogen group. It can be found in nature as pale-yellow diatomic gas as it has boiling point and melting point of -188° C -219.6° C, respectively. Fluorine has an electronegativity of 3.98 on the Pauling scale and has ionization energy of 1680.6 KJ/mol by its first ionization. It is known as powerful oxidizing agent owing to its highly reactive nature it forms a variety of compounds. Some of the extensively used fluorine-containing compounds are CaF_2 (Calcium Fluoride), NaF (Sodium Fluoride), HF (Hydrogen Fluoride), CF_2Cl_2 (Dichlorodifluoromethane) etc.

Natural sources

Fluorine is a highly reactive and abundant element on earth surface and its simplest electronegative ion is fluoride (F^-) (Sivasankar et al., 2016). It shows strong affinity to form compounds with other chemicals and hence it doesn't occur in its natural elemental state. Fluoride exists in different amounts in earth's crusts, rock-forming minerals and volcanic ash. Fluoride concentration of groundwater is subject to the chemical, physical, geographical characteristics of the underground layer of water-bearing permeable sediment rock. Huge variations of fluoride-bearing rock-forming minerals are exist in nature such as sellaite (MgF_2), fluorite (CaF_2), fluorapatite, cryolite (Na_3AlF_6), apatites, topaz, amphibole, mica, and phosphorite etc. (Datta et al., 1996; Mohapatra et al., 2009).

Naturally occurring fluoride in the human body is generally found as calcium fluoride in bones and teeth. Fluoride can enter the body with food and by drinking water. On consuming fluoride-containing food, fluoride enters the blood circulation. Most of it (99%) is then accumulated and absorbed by teeth and bones. Fluoride in very low concentration is thought to be an essential mineral for bone formation and to prevent tooth decay. Almost all the crops and vegetation contain traces of fluoride, which is mainly captivated from the soil and the sources of water (Wambu et al., 2015). Average content of naturally occurring fluoride in fresh vegetables and fruits are in very low level (in a range of 0.01 to 1 mg/L).

Fluoride can be emitted from effluents of the different manufacturing industries such as power stations, semiconductor industries, steel &aluminum industries, cosmetic industries, nickel

production, glass, plastic, cement production industries. Also, as a result of manmade activities. Hydrogen fluoride is widely employed in the production of aluminum and CFCs (chlorofluorocarbons). The effluents discharged from of numerous industrial activities affects the ecosystem and living beings by contaminating water, air, soil, crops and vegetables. Excessive usage of synthetic fertilizers including superphosphate, potash and NPK pollutes soil and fresh water by releasing significant quantities of fluoride into it. In addition, recently 'C6' short-chain fluorine-based formulations is being widely used to repel oil and water on textiles and clothing (fluorine-based durable water and oil textile repellents). Other fields where fluorine-containing compounds are utilized are electronic industries, tanning leathers, potable water fluoridation (Sodiumhexa fluorosilicate, sodium fluoride are generally used), insecticide production (example: sodium fluoride is extensively used), ceramics& fluorescent lamp industry (Calcium fluoride is widely used) (Bhatnagar et al., 2011).

1.2.1. Toxicity of fluoride

Fluoride is one of the vital harmful pollutants which pollutes underground water as well as surface water and affects heath of living beings. Fluoride enters the ground-water because of natural leaching from fluoride rich rocks and volcanic ash (such as Fluorspar, cryolite, fluorapatite and sellaite etc.) (Wambu et al., 2015). Almost all the crops and vegetation contain traces of fluoride, which is mainly captivated from the soil and the sources of water. Hydrofluorosis diseases caused by excess intake of fluoride contaminated drinking water (permissible limit 1-1.5 mg/L) have become a global issue of great concern. Intake of fluoride over permissible limits lead to fluorosis syndrome, reproductive decline and skeletal tissues damages. Damage to the thyroid, have been reported as widespread diseases. Long-lasting fluoride exposure either by way of ingesting of fluoride-contaminated potable-water or fluoride released by the industries cause dental fluorosis and skeletal fluorosis (bone deformities) in living being. In addition, non-skeletal fluorosis in soft tissues or body parts due to the fluoride endemic provinces (such as gastrointestinal discomforts, neurological disorders, and irregular reproductive cycles, genotoxic effects, allergic reactions, polyuria, polydipsia, etc., have also been reported in human being as well as in domestic cattle's (Choubisa 2012a). The excess concentration of fluoride in potable water is not only the key reason for 'fluorosis' syndrome but the total ingestion of fluoride from all sources also responsible for these health problems.

As a result of rapid industrial development, various medical ailments among industrial personnel, inhabitants and domesticated cattle are increasing at the alarming rate attributable to the excess fluoride exposure and contamination. Nearly 20 developing countries are facing

to the hydrofluorosis diseases. Developing countries in Asia including India and African countries are ferociously affected (Choubisa and Choubisa, 2016). Almost 19 states of India, mostly Rajasthan, Andhra Pradesh, Utter Pradesh, Maharashtra, Gujarat, and West Bengal are suffering from high fluoride concentrations in groundwater as well as surface water. Industrial fluorosis disease was first identified in cattle from a farm nearby to a superphosphate production industry (Choubisa and Choubisa, 2016). India was introduced to the industrial fluorosis disease for first time in Orissa, as per report domestic cattle living nearby to an aluminum factory was suffered from this disease (Rao and Pal, 1978).

1.3. Techniques for removal of pollutants from wastewater

With developing technologies, various industry discharges worrying amounts of toxic pollutants in their effluent stream which affect the ecosystem. There is a crucial necessity to treat the toxic effluents of the industries before discharging into the open waterbodies to prevent carcinogenic impacts on living body.

The conventional physical and chemical techniques designed for the treatment of contaminated water includes adsorption, ultra-filtration, coagulation, ion exchange have been discussed below. Advantages and limitations of those methods have been presented in Table 1.1.

Chemical precipitation

Chemical precipitation is the methods of conversion of a solution into separable solid substance by converting the element into insoluble form or by converting the solution to a super saturated one. This technique generally used in wastewater treatment process for remediation of dissolved toxic metals from wastewaters. Several drawbacks of this process are there such as high operation cost, high secondary sludge production, toxic pollutant loaded sludge disposal and handling problem arises, periodic investigation of initial and treated effluent is essential to estimate the accurate quantity of chemicals to be added.

Coagulation

Coagulation is one of the most conventional wastewater treatment methods. It is generally a useful technique for separation of suspended matter and colloidal type of particles. Usually, the colloids carry electro-negative charges therefore the coagulants are generally inorganic or organic electro-positive. Addition of $Al_2(SO4)_3$ (aluminum sulphate), $FeSO_4$ (ferric sulphate), $FeCl_3$ (ferric chloride) gives hydrolysable metallic ions or organic polyelectrolyte, which can remove the surface electrical charges of the colloids. Moreover, the metallic hydroxides and the organic polyelectrolytes can improve the particle aggregation into flocks, thus enhancing the sedimentation. The dissolved matter or sludge formed is separated by other physical

chemical processes. The disadvantage of this method are sludge disposal and incomplete pollutant removal process.

Membrane filtration

Membrane filtration procedure has been established as an important technique for wastewater purification process. In this method the separation process occurs through the semi permeable membrane by application of hydraulic pressure. Semipermeable membrane acts as a thin barrier in between two phases or a medium. In presence of proper driving force, the membrane permits one or more constituents to pass through one medium to another medium (Shrestha et al., 2021). There are typically three types of membrane filtration are there including Ultrafiltration, Nanofiltration and Reverse osmosis. The drawbacks of this method are imperfect remediation of pollutants, membrane fouling, high energy consumption, costly membrane requirement and low durability of the membrane, etc (Onyango et al., 2004). The membrane may get clogged with the pollutants existing in the wastewater and can be damaged as a result of extra pressure on the membrane (Onyango et al., 2004).

Ion exchange

Ion exchange technique is based on the exchange between two ions to achieve the required efficiency (Chen and Wang, 2017). The main principle behind this method is the displacement of a weakly bound ion by a stronger binding ion. This phenomenon is used to remove targeted ions from an aqueous solution. This method is applied to perform for elimination of organic and inorganic contaminants along with other toxic heavy metals from wastewater. The significant limitations of this technique are expensive process due to the costly resin, incomplete pollutant removal, each resin can be applied for limited cycle of separation process. Additionally, this method is also very sensitive to pH condition.

Ozonisation

Ozone is known as an influential oxidant and can oxidize a wide variety of organic and inorganic compounds. Organic compounds are generally transformed into organic radicals due to the withdrawal of a hydrogen atom via hydroxyl (OH) radicals. This organic radical goes through successive reactions and is ultimately mineralized to CO_2 and H_2O. Some of the important parameters for decontamination of organic compounds in wastewater with this technique include pH, dose of ozone and catalyst dose. Important drawbacks related to this method are expensive operation technology, higher electrical power consumption, expensive equipment requirement etc.

Chemical oxidation

Industrial wastewater can be treated by chemical oxidation techniques where pollutants are eliminated by using different chemicals. Hydrogen peroxide is extensively used as oxidation agent. This technique has few notable limitations including requirement of costly chemicals, possibility of emission of hazardous by-products, secondary pollutant generation, etc.

Adsorption process for wastewater treatment

In recent years, adsorption is being extensively explored for treatment of polluted water. Adsorption process on to absorbent surface generally occurs through three stages (Mohapatra et al., 2009):

(a) diffusion/transport of adsorbate (pollutant) molecule to the adsorbent's outer exterior from bulk solution across the boundary layer adjacent to the solid particle;

(b) Adsorption of adsorbate molecule on adsorbent surfaces;

(c) The adsorbed molecule about to replace with the structural elements within adsorbent which depending on the chemical characteristics of adsorbent, or transported to the internal surfaces in case of porous materials (i.e., intra particle diffusion).

Among all the wastewater treatment process (Table 1.1), adsorption is considered to be a reasonable technique because of its less operative cost, higher uptake capacity, recycle and regeneration capability of adsorbent, and shows high quality of water purification without generation of any secondary sludge.

Table 1.1: Comparative table between pollutants removal techniques

Treatment techniques	**Advantages**	**Disadvantages**	**References**
Chemical precipitation	• It is cost effective, Simple operation • Simplicity of design, construction, operation and maintenance	• Trained operator is needed for the daily operations • High secondary sludge production • Toxic pollutant loaded sludge disposal and handling problem arises • Extra operational cost required for sludge disposal • Periodic investigation of initial and treated effluent is essential to estimate the accurate quantity of chemicals to be added	Crini and Lichtfouse, 2019

Ion exchange	• High fluoride removal efficiency • Possibility in the retention of taste and color of treated water.	• Pollutant removal efficiency is decreased in occurrence of other ions • Expensive process due to the costly resin • Before final disposal, the regeneration of ion exchange resin is necessary • High cost of Regeneration • Treated water becomes acidic and may contain excess amount of chloride	Chen and Wang, 2017
Reverse osmosis and Electro dialysis	• No additional chemicals are required • Effective in wide range of pH condition • No intervention by other ions presents in feed water • Simple, automated process • Small operational space is required	• Limited lifetime before membrane fouling occurs • High operational cost due to membrane fouling • High electrical energy demand. • Maintenance cost is high as membranes are expensive and sensitive to temperature, pH • Remineralisation is necessary after treatment as it eliminates all the ions (including essential minerals for health) from feed water. • The treated water possesses very low pH	Crini and Lichtfouse, 2019
Coagulation/ Flocculation	• Simple process and low capital cost • Extensive variety of commercial chemicals are available as coagulants and flocculants • Rapid and effective process for the removal of insoluble pollutants	• Additional chemical load (coagulants, flocculants, aid chemicals) on the effluent leads to the high sludge generation • Sludge disposal cost (waste management and special treatment cost) is high • Time consuming process • Correction of pH level in effluent is necessary	Kumar et al., 2017

Adsorption	• Easy operation technique and efficient process with fast kinetics • Low Initial Capital cost and operational cost • Inexpensive adsorbent • Less time-consuming process • Percentage of regeneration is significantly high • Simple operating conditions • Effective in wide range of pH condition • Pollutant removal capacities is high	• Needs pre treatment • Separate treatment of pollutant loaded sludge is needed before discard in final effluent • Selectivity is low	Manna et al., 2018

…….##########.....

Chapter.2

Literature review

Sources of dye and fluoride and their toxicity have been discussed in Chapter 1. Among the several conventional physiochemical treatment techniques available for removal of these pollutants from wastewater adsorption process is considered to be the most efficient. In last few decades, an extensive variation of adsorbent materials and their chemical and physical modifications were experimented upon for remediation process. Investigation has been directed towards developing inexpensive, effective, eco-friendly and high-capacity adsorbent material. In this chapter we have focused on the present status of research of a few of them. The efficiency and suitability of the developed adsorbents are evaluated through adsorption isotherm, kinetic and thermodynamic study.

2.1. Adsorption Isotherm study

The well-known adsorption isotherm models including Langmuir, Freundlich, Temkin and Fritz-Schlunder (F-S) are used to evaluate the adsorption equilibrium data (Aljeboree et al., 2014). The Langmuir model assume that monolayer adsorption of adsorbate molecule takes place on the adsorbent surface with identical homogeneous binding sites (Langmuir, 1918). Empirical model equation nonlinear and linear forms of Langmuir model (Eqn. 2.1 & Eqn. 2.2) are given below:

$$q_e = \frac{q_m K C_e}{1 + K C_e} \dots\dots\dots\dots\dots\dots\dots (2.1)$$

$$C_e/q_e = 1/K_L q_m + C_e/q_m \dots\dots\dots (2.2)$$

Where, C_e (mg/L), q_e (mg/g), q_m (mg/g), and K_L (L/mg) are adsorbate concentration in the solution at equilibrium, equilibrium adsorption capacity, the maximum capacity at monolayer adsorption and maximum Langmuir constant respectively.

Freundlich model is based assuming heterogeneous distribution of binding sites on the adsorbent surface. The nonlinear and linear form of the model equation are as follows:

$$q_e = K_f C_e^{1/n} \dots\dots\dots\dots\dots\dots\dots (2.3)$$

$$\log q_e = \log k_f + \frac{1}{n} \log C_e \dots\dots\dots (2.4)$$

Where, K_f (L/mg) and n, represent the Freundlich constant and Freundlich isotherm intensity, respectively. According to the model, when 1<n<10, the adsorption system is favorable (Freundlich & Heller, 1939).

Temkin model (eqn. 2.5 or eqn. 2.6) signifies the influence of the adsorbate-adsorbent interaction on adsorption process. The model assumes the heat of the adsorption process would reduce linearly with increasing surface coverage. The model is generally valid for the exceptionally low and high value of adsorbate concentration.

$$q_e = \frac{RT}{b} log(K_T C_e) \dots\dots\dots\dots (2.5)$$

Or,

$$q_e = \frac{RT}{b} log(K_T) + \frac{RT}{b} log(C_e) \dots\dots (2.6)$$

Where, K_T (L/mg) and b (kJ/mol) are the Temkin isotherm coefficient corresponding to the equilibrium binding constant.

The F-S model (eqn. 2.7 and eqn. 2.8) is based on the three-parameter adsorption isotherm relating the Langmuir and Freundlich model (Fritz & Schlunder, 1974).

$$q_e = \frac{K_{FS} q_{mFS} C_e}{1 + K_{FS} C_e^n} \dots\dots\dots\dots (2.7)$$

Or,

$$\frac{C_e}{q_e} = \frac{1}{K_{FS} q_{mFS}} + \frac{C_e^n}{q_{mFS}} \dots\dots\dots\dots (2.8)$$

Where, K_{FS} (L/mg), and q_{mF} (mg/g) represent the Fritz-Schlunder isotherm model constant, and adsorption capacity at equilibrium condition respectively.

2.2. Adsorption Kinetics modelling

Kinetics studies provide information about equilibrium adsorption capacity and adsorption rate which depend on the availability of active binding sites, physicochemical nature of the adsorbent and specific surface area (Bhattacharyya and Sharma 2004). The mechanism of the adsorption processes often includes chemical interaction among the adsorbent and adsorbate along with mass transfer, bulk transfer, intraparticle diffusion, diffusion into micropores/macropores and diffusion through the liquid film around the solid phase surface (Kooh et al., 2016). Four models of adsorption kinetics are generally applied to correlate the experimental kinetic data and to evaluate the possible rate-controlling step. Pseudo-first and pseudo-second-order kinetic models specify that the general adsorption process is reliant on adsorbate quantity and availability of adsorptive sites on the adsorbent surface (Saha et al., 2022). Pseudo-second-order kinetics is also based on the concept of chemisorption (Aljeboree et al., 2014). The non-linear & linear empirical equations of pseudo 1st order (Eqn. 2.9 & Eqn. 2.10) and pseudo 2nd order (Eqn. 2.11 & Eqn. 2.12) models are given below (Kooh et al., 2016).

$$q_t = (1 - exp^{-k_1 t}) \dots\dots\dots (2.9)$$

$$log(q_e - q_t) = log\, q_e - tk_1/2.303 \ldots\ldots (2.10)$$

$$q_t = \frac{k_2 q_e^2 t}{1 + k_2 q_e t} \ldots\ldots\ldots\ldots (2.11)$$

$$t/q_t = 1/k_2 q_e^2 + t/q_e \ldots\ldots (2.12)$$

Where, q_t and q_e represented the quantity of adsorbate adsorbed per unit quantity of the adsorbent (mg/g) at any time't', and at equilibrium condition, respectively. k_1, and k_2, signify the corresponding rate constants (min^{-1}) of the pseudo 1st order model and pseudo 2nd order kinetic model, respectively.

In order to evaluate the intraparticle diffusion mechanism, kinetic data were analyzed using Weber and Morris model (Kooh et al., 2016). According to this model, the adsorption capacity changes almost proportionately with the $t^{1/2}$ (square root of the contact time). The explanation of this model based on a theoretical basis (if the line passes across the origin the adsorption is dictated by the intraparticle diffusion; if not, the intraparticle diffusion was not the only rate-limiting step and other transport processes might control the biosorption rate). The empirical equation of Weber-Morris intraparticle (Eqn. 2.13) kinetic model is given below (Aljeboree et al., 2014).

$$q_t = k_3 t^{1/2} + C \ldots\ldots\ldots\ldots (2.13)$$

Where, k_3 is the rate constants (min^{-1}) of the intraparticle diffusion ($mg\ g^{-1} min^{-1/2}$) and C signify to the boundary layer thickness.

2.3. Thermodynamic study

The thermodynamic parameters were estimated to describe the thermodynamic behavior of adsorption mechanism for removal of pollutant by adsorbent and to evaluate the feasibility of the removal process. The thermodynamic parameters (Gibbs free energy change (ΔG), the enthalpy change of the reaction (ΔH), entropy change (ΔS)) were estimated based on equilibrium adsorption data obtained at different temperatures and the Van't Hoff formula (Eqn. 2.17) given by

$$K_c = \frac{C_a}{C_e} \ldots\ldots\ldots\ldots (2.14)$$

$$lnK_c = -\frac{\Delta G}{RT} = -\frac{\Delta H}{RT} + \frac{\Delta S}{R} \ldots\ldots\ldots\ldots (2.15)$$

where, $K_c$and C_e denote the distribution coefficient for adsorption process and adsorbate concentration under equilibrium condition respectively, C_a represent the adsorbed mass of

adsorbate molecule per unit mass of adsorbent (mg/L), R and T denote the gas constant and absolute temperature respectively.

2.4. Introduction to the biosorbent

Researchers are focusing on agro waste as an efficient and eco-friendly adsorbent for the removal of pollutants from wastewater. A large number of agro-based industries, such as sugar, jute and cotton produce large quantities of agro-waste which puts strain on proper waste disposal management and environmental ecosystem. As a consequence, researchers are giving attention for seeking toward maximizing the efficiency of the use of raw materials and minimizing the accumulation of waste by reusing agricultural residues. The agglomeration tendency of fine or powdery material because of the small-size is one of the serious limitations as it reduces the adsorption rate. To reduce this problem, polymeric/carbonaceous materials were applied as the template to disperse the fine/powdery materials for synthesis of the composite material. The composites containing biomaterials, biopolymers, carbonaceous materials and inorganic material are getting significant attention because of their integrated benefit and their impressive advantages such as biodegradability, economically viability, non-toxicity, feasibility, and renewability.

Extensive research is focused on the synthesis of the chemically modified multi-component hybrid composite material derived by reinforcing or grafting the synthetic polymers, carbonaceous material, and metal oxide onto natural ones including starch, cellulose, chitosan/chitin, and alginate. In this section, latest advances on biosorbent development and their applications for treatment of dye and fluoride contaminated wastewater have been reviewed.

2.4.1. Natural polymers and polymer-based composites as biosorbent

Polymeric biocomposites are those in which at least one of the constituents either the polymer matrix or the reinforcement is prepared from biomaterial (Varghese et al., 2019). Polymer-based composites are the combination of polymer with some reinforcements or filers materials such as fibers, whiskers, particles for its longer stability, and higher efficiency. Cellulose, chitosan, chitin, alginate etc., are the most abundant renewable biopolymers which are very common and efficient raw materials available as template to synthesize polymeric composite for dye and fluoride adsorption process. Due to having nontoxic nature, flexibility, biodegradable capability, high uptake capacity, low density, and recyclability, natural biopolymer-derived biosorbents can be ecological alternatives in the field of wastewater treatment (Azizi Samir et al., 2005; Galiano et al., 2018).

Natural biodegradable polymer derived from animal-origin (chitin, chitosan, collagens, and nucleic acids) or from vegetable-origin (starch, cellulose and alginates) are being researched worldwide as biosorbent for decontamination of wastewater. This is because they are renewable-resources based material, decomposable, inexpensive, non-hazardous, and generate less sludge at the post-treatment process (Reddy et al., 2013; Galiano et al., 2018). Natural biopolymers comprising of several functional groups in their molecular chains; shows remarkable ability in the formation of the hybrid polymeric biosorbent by chemical modification with advantageous functional and commercial properties (Pourjavadi et al., 2007). In this perspective, natural polymers have drawn the attention of research worldwide to prepare biodegradable polymeric biosorbents by combining petroleum monomers or bio-based sources with natural polymers. Few types of biodegradable natural polymers and their composites are documented in the following section of the review literature.

Cellulose and Cellulose based polymer

Cellulose molecule is a linear, crystal-like homo-polymer consists of D-glucose linkages that are interconnected through β -1,4glycosidic bonds. They are mostly obtained from various plant sources like grasses, stalks of vegetable, wood pulps, cotton, jute, etc and consist of repeating β-(1–4) D-glucose linkages (Ganguly et al., 2020). Moreover, animals, bacteria, algae, fungi, and cellular slime molds, are also huge source for the fabrication of cellulosic fiber (Brown, 2004; Azizi Samir et al., 2005). Due to the orientation of the O-H groups in the cellulose chain, they have a tendency to stick out alongside the long chain molecules and are readily accessible for H-bonding. Cellulose materials show appreciable strength and strong resistance to the solvents due to existence of the H-bonding in the crystalline regions. Cellulose grafted polymeric composites for decolorisation of textile wastewater, synthesized by reinforcing cellulosic fibers (micro-fibers or macro-fibers) with a polymer matrix (such as PVA (poly vinyl alcohol), PAN (poly acrylonitrile), PEO (poly ethylene oxide) (Wang et al. 2014; Silva et al., 2013) or biomaterials (such as carbonaceous material (Luo & Zhang, 2009), bentonite clay (Anirudhan et al., 2016) or metal oxides (Song et al., 2016) have been reported in the literature. The blending of those materials with cellulose influences the characteristics and performance of polymeric composite in terms of flexibility, absorptivity, resistance to biofouling (Silva et al., 2013; Yin & Deng, 2015). Karim et al. (2014) described efficient remediation of Rhodamine dye by nanocellulose crystals. They suggested that negative charged nanocelluloses formed a stable bond with cationic dyes which enhanced the adsorption efficiency. Wang et al. (2014) reported removal efficiency of 99.8% using MnO_2 coated

cellulose biopolymer biosorbent for decolorizing methylene blue containing wastewater. Zhao & Wang (2012) reported the grafting of carboxy methylcellulose with montmorillonite to prepare composites for removal of Congo red dye. Activated carbon reinforced magnetic cellulose biosorbents were developed by applying external magnetic field and were employed for organic dye adsorption from colored water (Luo & Zhang, 2009). Yang et al. (2017) prepared polyacrylamide/cellulose hydrogels and discussed their utilization in decolorisation process for removal of methylene blue dye. Ammavasi and Mariappan (2018) developed and examined the fluoride removal efficiency of magnetic iron oxide fabricated cellulose-based composite for drinking water purification. Sankararamakrishnan et al. (2019) reported the extraction of cellulose fibers from sugarcane bagasse, and prepared Zerovalent-iron/Zirconium doped cellulose fibers. The fluoride uptake capacity was found to be 35.70 mg/g.

Starch and Starch based polymer

Starch is one of the greatest abundant and accessible natural biopolymers in the world. Crystalline starch is produced through hydrolysis of the crystal-like part of the starch (Le Corre et al., 2010; Nasrollahzadeh et al., 2020). To attain precise biosorption efficiency, chemical modifications of starch are frequently required (Zou et al., 2011; Zhou et al., 2019). A well-known operative method for preparing modified starch by chemical reformation is graft copolymerization with definite biological monomers, synthetic monomers or carbonaceous material. Grafted starch showed remarkable improved functional properties such as increase in fractal dimension and high biosorption efficiency (Meimoun et al., 2018; Du et al., 2018). Gong et al. (2015), characterized and evaluate the adsorption efficiency of magnetic carboxy methyl starch (CMS)/PVA for removal of methylene blue dye. Zhou et al. (2019) reported adsorption behavior of polyaluminum ferric chloride-starch graft polymeric composite for the treatment of textile wastewater. Bhattacharyya et al. (2018) developed graphene oxide/potato starch composite. Li et al (2020) reported the adsorption study of multiple cationic dyes by applying Silica-sand/anionized-starch polymeric composite. Sen et al. (2011) studied the preparation, characterization and utilization of polyacrylamide grafted carboxymethyl starch for the treatment of colored textile industrial wastewater. Preparation and characterization of Starch/Fe_3O_4 was studied by Stan et al. (2019). They reported dye adsorption efficiency of more than 70% for removal of Optilan Blue. Li et al. (2021) reported the synthesis of magnetic starch-based composite and their removal potential for methylene blue dye. Xia et al. (2020) reported adsorption potential of modified Starch/PVA biopolymer for the treatment of textile wastewater. Azman et al. (2015) focused on the synthesis and operational efficiency evaluation

of Starch-grafted polyacrylamide hybrid hydrogels. Preparation and decolourization efficiency of chitosan-starch based polymeric composite for adsorption of congo red dye was discussed by Sami et al. (2017).

Alginate and Alginate based composites

Alginate is one type of natural polysaccharide derived from cell-wall of brown algae and consist of two uronic acid units (1–4)-β-D-mannuronic acid and (1–4)-α-L-guluronic acid residues (Russo et al., 2021). It is another exceptionally significant natural polymer that scientists are paying attention in the field of water purification technology, biomedical engineering and biotechnology (Wu et al., 2012; Li et al., 2013). Moreover, alginate have been found to be cost-effective natural biopolymer for the synthesis of the polymeric biosorbent (Parlayici, 2019). Alginates have been chemically modified by applying graft copolymerization method to enhance its functional properties. In the last few years, studies have emphasized on applications of alginate-based polymeric composites in water purification process for removal of pollutants because of their nontoxicity, mechanical-stability and biocompatibility (Li et al., 2013; Wu et al., 2012; Kuang et al., 2015). Alginates can be chemically modified or grafted through several approaches especially through polycondensation and radical polymerization (Sonawane et al., 2009). Presence of divalent cations (for example calcium ion) helps to form alginates gel by crosslinking them. Asadi et al. (2018) suggested calcium alginate grafted polymeric beads for treatment of methyl violet dye containing wastewater. Pourjavadi et al. (2007) reported preparation method of chemically modified alginate-based composite. Composite was synthesized using sodium alginate and kaolin and was crosslinked by methylene biscrylamide. Raghav and Kumar (2019) obtained fluoride uptake values of 200 mg/g in defluoridation process using alginate based polymeric composite named Fe-Al-Ni/alginate. Wu et al. (2016) prepared sodium alginate/carboxymethyl cellulose composite impregnated with calcium and aluminum. The maximum fluoride removal capacity obtained was 35.98. mg/g at pH 2 and 298 K.

Chitin and Chitosan based composites

Another abundant natural biodegradable polysaccharide is chitin. It largely originates in the external skeletons of crustaceans and other invertebrates and as well as in the specific fungi cell-wall (Martel et al. 2001). Chitin molecule consist of linear β-1,4-linked polymer of N-acetyl-D-glucosamine. Chitosan is fundamentally a derived form of chitin produced by enzymatic N-deacetylation and can be synthesized chemically from native chitin (Yang et al.,

2008). Chitosan is structurally categorized as the amino-polysaccharide of glucosamine and is less crystalline compared to chitin because of the definite antiparallel chains in their structure and their cross linking. Chitin is insoluble but chitosan is water-soluble. On account of having higher degree of hydration, chitosan exhibited high biosorption efficiency, significant reactivity, considerable selectivity which assists the biosorption of pollutants (Chatterjee et al., 2007; Kardam et al., 2014). Chitosan biopolymer is a possible source of base material for synthesis of the chitosan-based polymeric composites for decolorization of textile contaminated water due to their nano-scale size, high specific surface area, and nonexistence of diffusion limitations (Rosa et al., 2008; Kardam et al., 2014). A great number of chitosan-grafted polymeric biosorbents have been investigated for their dye uptake capacity under different operational conditions. Manna et al. (2018) studied multiple dye adsorptions by GO coated chitin and obtained adsorption efficiency more than 75 %. Banerjee et al. (2017) showed adsorption of acid yellow and acid blue dye using chitosan-GO nanocomposite. GO and PVA reinforced chitosan showed effective biosorption capability for the removal of Congo red dye from colored wastewater. Amir et al. (2016) focused on the synthesis process of polymer composite by combining chitosan polymer with TiO_2 nanoparticles for encapsulation and photodegradation of Methyl Orange. Modified chitosan-ethyl acrylate was synthesized by Sadeghi-Kiakhani et al (2013). They reported that biosorption ability for adsorption of Basic dyes (Blue 41 and Basic Red 18) was remarkably enhanced after introducing carboxyl (COOH) groups into the chitosan structure. Zhou et al. (2011) investigated the removal of acid dyes using modified magnetic chitosan composite and concluded that the dye adsorption improved due to the strong electrostatic interaction among anionic dye and protonated amino groups present in chitosan structure. Hussaini Jagaba et al. (2018) developed modified chitosan-based composites by combining with other materials including polyacrylamide and bentonite clay. They obtained high adsorption efficiency (99%) using those adsorbents for removal of direct dye under low pH condition. Sairam Sundaram et al. (2008) developed bioorganic composite, nano-hydroxyapatite /chitosan and reported that the prepared composite was effective for fluoride adsorption. Sundaram et al. (2009) investigated the defluodation of contaminated water using magnesia/chitosan polymeric composite. Zhang et al. (2015) reported fluoride remediation process using Fe-impregnated chitosan. The fluoride uptake capacity was 1.97 mg/g for 10 mg/L of initial fluoride concentration. Valdez-Alegria et al. (2020) fabricated biopolymers grafted composites, chitosan-polyvinyl alcohol and investigated their capacity in fluoride remediation from aqueous solution.

2.4.2. Carbonaceous materials and their composites as biosorbent

Carbon-derivatives such as activated carbon, graphene, graphene oxide and their derivatives have notable contribution in advanced techniques for wastewater treatment in industrial scale due to their high specific surface area, high adsorption efficiency (Saha et al., 2022). Despite having many appreciable properties (Fernandez et al., 2014), commercial activated carbon has limited application on pollutant elimination as they are very expensive. Activated carbon prepared from low-cost agro-waste is an alternative for economically feasible, and environment-friendly adsorption (Deniz and Karaman 2011; Fernandez et al. 2014). The raw materials utilized to derive activated carbon include woods, charcoal, seeds, coal, petroleum residues, synthetic polymers and also low-priced agro-waste materials such as sugarcane bagasses, rice-husk, sawdust, coconut shell, tea waste, fruit waste/ peels, etc. The application and effectiveness of carbonaceous material-based composites are increasing with advances in surface modification technologies (Nekouei et al., 2015). The adsorption efficiency of the activated biochar is significantly dependent on the chemical and physical properties of the forerunner substance, activating agent, the carbonization time among others utilized during the activation process (Li et al., 2020). Employing oxidation methods, experts prepared negative-charged surface of by acid treatments on the surface of activated carbons (Ma et al., 2018; Li et al., 2020). By alkali treatment electro-positive charges on carbon surface increases which helps in the adsorption of anionic pollutants. The addition of functional groups such as -COOH, -OH, and –COO etc. on carbon surface modifies adsorptive pores by changing the dimensions and form, which enhances adsorption efficiency (Ndazi et al., 2007). Extensive investigations are being performed for modernization of innovative carbonaceous material-based biosorbents for water purification process (Deniz and Karaman 2011). Various effective activating chemical agents such as phosphoric Acid (Varil et al., 2017), Sulphonic acid (Zhang, et al., 2015), NaOH (Linares-Solano et al., 2012), KOH (Njoku et al., 2014), and ZnCl2 (Nekouei et al., 2015), etc. have been used so far by the researchers to synthesis efficient agro-waste based activated biochar. Alkali treatment enhanced structural stability, ion-exchange ability, and reactive quality of cellulose-containing agro-waste (Ndazi et al., 2007). Karthikeyan and Elango (2008) noted that efficiency of over 90% was obtained with graphite for fluoride removal from its aqueous solution. Tchomgui-Kamga et al. (2010) utilized $CaCl_2$ (calcium chloride) impregnated wood charcoal prepared by carbonization at different temperatures (500 ^oC, 650 ^oC, 900 ^oC) for defluoridation process in batch system. They reported fluoride removal efficiency >92% at neutral pH using adsorbent dosage of 4g/L for initial F^- concentration of 10 mg/L. Li et al. (2011) investigated and reported on the fluoride remediation by graphene as

adsorbent in batch reactor. They achieved maximum uptake capacity of adsorbent as 17.65 mg/g for 0.0025 g/L of the initial concentration of fluoride solution at 25°C temperature. Zhu et al. (2011) prepared $AlCl_3$ modified cattle bone char and investigated its application in the defluoridation of water. They found fluoride removal efficiency to be 97% and adsorption capacity of 6.8 mg/g at neutral pH. Yadav et al. (2013) evaluated fluoride adsorption potential of the wheat straw, sawdust, and activated carbon derived from sugarcane bagasse. They found the maximum fluoride uptake capacity as 1.15 mg/g. Getachew et al. (2015) developed activated biosorbents by thermal activation using banana peel and coffee husk as raw materials and utilized them for the treatment of fluoride-contaminated water. They found that the maximum fluoride removal efficiency of banana peel and coffee husk was 85% and 86% respectively for initial fluoride concentration of 10 mg/L at pH 2. Because of high surface area and hydrophobic surface property, carbonaceous material of fine size requires balance out in composite synthesis to reduce agglomeration tendency. Tang et al. (2018) developed composite containing hydroxyapatite coated with carbon-nanotube and examined their application in the defluoridation process for treatment of wastewater. They achieved maximum biosorption capacity of 11.05 mg/g. Roy et al. (2017b) obtained removal efficiency of 94.22%. using 10g/L of reduced graphene oxide for treatment of fluoride containing solution for initial adsorbate concentration of 50 mg/L while contact time and agitation speed was 100 min and 150 RPM respectively. Zhang et al. (2017) developed zirconium-chitosan/graphene oxide composite and employed these adsorbents for fluoride biosorption from aqueous solution. Jin et al. (2015) examined defluoridation of water onto amorphous alumina-modified expanded graphite. The achieved adsorption capacity was 1.18 mg/g and found highest biosorption efficiency to be 94.4%. Chitosan doped graphite composite showed fluoride uptake capacity of 37.9 mg/g at pH 6.5 (Dongre, 2018) and also showed excellent regeneration capacity of the adsorbent.

2.4.3. Magnetic nano-particle based biosorbent

Xu et al. (2016) synthesized Al_2O_3-Fe_3O_4-expanded graphite nano-sandwich adsorbent and reported the maximum fluoride uptake capacity to be 3.35 mg/g. Dhillon et al. (2015) produced hydrous hybrid Fe-Ca-Zr oxide biosorbent and investigated their applications in fluoride remediation. The estimated adsorption capacity for fluoride removal was 250 mg/g. Abo Markeb et al. (2017) prepared Ce–Ti@Fe_3O_4 nano-composite and reported that fluoride uptake capacity of 91.04 mg/g could be achieved at neutral pH. Zhao et al. (2010) reported that Fe_3O_4-$Al(OH)_3$ nano-adsorbent shows significant adsorption of fluoride due to the combined advantages of magnetic separation and aluminum oxide ($Al(OH)_3$). Zhang et al. (2016) synthesized Fe-Ti bimetallic oxide coated Fe_3O_4 magnetic nanoparticle. The Fluoride

adsorption capacity was 57.22mg/g. Mohseni-Bandpi et al. (2015) fabricated chitosan impregnated Fe_3O_4 nano-adsorbents and evaluated the defluoridation of wastewater. They reported the higher fluoride bioorption proficiency of modified magnetic nano-adsorbent to be 9.43mg/g. Ma et al. (2007) produced and investigated the characteristics of adsorption equilibrium of defluoridation study using magnetic-chitosan as nano-adsorbent material. They reported that the estimated fluoride removal capacity was 20.93-23.98mg/g.

2.4.4. Other novel biosorbent

Hafshejani et al. (2017) prepared Al_2O_3 nanoparticles and examined their ability in defluoridation process as adsorbent. The adsorbent exhibited maximum removal capacity of 13.70 mg/g. Dhillon et al. (2018) investigated the fluoride remediation study using Ca-Ce composite as adsorbent and determined fluoride uptake capacity to be 83.33 mg/g. Mukherjee et al. (2020) developed ferrihydrite composite grafted with cellulose nanofiber-polyaniline and examined the fluoride adsorption efficiency of this prepared composite. Maximum uptake capacity achieved was 50.80 mg/g. Kumari et al. (2022) synthesized Aluminium fumarate-based polymeric composite using chitosan coated PVA support polymer matrix and examined fluoride adsorption efficiency of prepared composite from ground water. They reported that 9 g of composite material kept in pouch-like tea bag can reduce fluoride concentration in 1 L groundwater from 10-30 mg/L to 1-1.5 mg/L after 100 min. Zare et al. (2022) noted that uptake capacity of modified alginate beads for fluoride was 51.02 mg/g.

142

Srivastava et al. (2004) reviewed malachite green (MG) is a widely used textile dye. It is also used in food, leather, pharmaceutical, and other industries. They summarized the toxicity of Malachite green dye (MG) on human being, different fish species and animals. They reported that the toxicity of MG rises with dye concentration, contact time, and temperature. In their study, toxic effects of MG dye including carcinogenicity, mutagenesis multi-organ tissue injury, chromosomal fractures have been reviewed. They reported that notable changes arise in biochemical parameters of blood in various MG exposed fish species. Moreover, malachite green dye was found in their several body parts such as serum, liver, kidney, muscles and also in eggs.

Tahir et al. (2016) evaluated the performance of modified sugar cane bagasse (SB) and carbonaceous materials derived from SB for treatment of Malachite green dye (MG) containing wastewater. Carbonaceous bagasse (C-SB) was prepared by chemical treatment of SB using formaldehyde and sulfuric acid. In their study, the influence of dye concentrations, adsorbent dose, time interval and system temperature were investigated in a batch process. The adsorption

isotherm process was well explained by Langmuir model for the dye concentration in the range of 1×10^{-5} M to 1×10^{-4} M. The adsorption efficiency was 89% for carbonaceous materials derived from SB. They reported that malachite green dye adsorption efficiency was higher in the modified sugarcane bagasse (89.60%) than in SB (78%). Thermodynamic study suggested the spontaneous nature of the decolorization process.

Kerrou et al. (2021) reported the efficiency of Sugarcane bagasse in remediation of methylene blue dye. They examined the effect of variation of experimental conditions including initial dye concentration, contact time, dosage, pH, and temperature by evaluating batch kinetic and isotherm experimental data. The dye adsorption equilibrium and kinetics was found to be well explained by Langmuir isotherm equation and pseudo-second-order kinetics respectively. They reported that the monolayer adsorption capacity was 49.261 mg/g. The thermodynamic parameters were as follows: ΔG°: −4.35 kJ/mol; ΔH°: −31.062 kJ/mol; ΔS°: −0.084 J·mol/K. These results pointed towards the spontaneous and exothermic reaction of the adsorption process. They observed that dye adsorption efficiency increased from 80.27% to 98.49% as adsorbent dosage increased from 0.5 g/L to 5 g/L. The maximum uptake efficiency was obtained at pH 10. Removal efficiency was found to be decrease at higher temperature.

Singh et al. (2015) examined defluoridation of aqueous solution using sugarcane bagasse in a batch process. They observed the influence of different operational variables including pH, adsorbent dose, contact time, initial fluoride concentration, and temperature on fluoride removal efficiency of sugar cane bagasse. The value of the point of zero charge for the adsorbent was 6.3. Approximately 45% removal efficiency was achieved within 60 min at initial concentration of 4 mg/L and adsorbent dosage of 1 g/L. Maximum adsorption capacity was 1.82 mg/g at an initial adsorbate concentration of 4 mg/L which increased to 4.12 mg/g on increasing concentration to 8mg/L. Isotherm of fluoride adsorption study was described by evaluating various isotherm models including Langmuir, Freundlich, Temkin and Redlich-Peterson. The kinetics of defluoridation process could be suitably described by following pseudo second-order kinetics.

Yadav et al. (2012) proposed an economically viable and efficient approach to eliminate fluoride especially for rural areas. They examined the viability of low-priced adsorbents (activated bagasse carbon, sawdust raw, and wheat straw raw) derived from agro-biomass vis-a-vis commercially purchased activated carbon. They reported the adsorption efficiency of these adsorbents for an initial fluoride concentration of 5mg/L at neutral pH after 60 min of contact time and 4g/L of adsorbent dosage to be as the following: activated carbon: 57.6%; activated bagasse carbon: 56.4%; sawdust raw: 49.8%; wheat straw raw: 40.2%. The fluoride

adsorption equilibrium followed Freundlich isotherm, whereas the surface biosorption and intra-particle diffusion phenomena equally contributed towards the rate limiting step.

Mohan et al. (2012) investigated the potential of biochar derived from pine bark for fluoride removal. Pine bark was pyrolyzed at 400 °C and 450 °C. Batch experiments of removal process were observed under various experimental conditions such as system temperatures, time, pH etc. The highest uptake efficiency was obtained under acidic condition (pH 2). The rate of fluoride removal was found to be reduced on increasing system temperature signifying the exothermic nature of the system. The performance proficiency of pine bark char was estimated by following the Langmuir, Freundlich, Temkin among other isotherm models equations. They found maximum monolayer uptake capacity in accordance with the Langmuir model for pine bark char as 9.77mg/g at temperature of 25 °C. Defluoridation process was in accordance with pseudo-second-order kinetics.

Aziz et al. (2019) prepared sodium alginate-based composites for cadmium adsorption using batch and continuous flow adsorption system. Among three type of prepared alginate-based composite beads (SA-Clay, SA-Phosphate and alginate-Activated Charcoal beads), better result was found with sodium alginate-Activated Charcoal (SA-Ch) beads. The maximum uptake capacity for cadmium adsorption onto SA-Ch was 137 mg/g for initial adsorbate concentration of 1000 mg/L. The equilibrium data could be fitted with Langmuir isotherm model. Rate of adsorption could be suitably described using pseudo second-order model equation. They also performed continuous column study. The maximum breakthrough time for sodium alginate-Activated Charcoal beads was 48 h for initial feed concentration of 500 mg/L at flow rate of 2 mL/min with 150g of adsorbents beads of 2.5mm average ID. By analyzing XRD, SEM, BET and FTIR characterization of prepared composites, they confirmed change in surface functional groups due to specific chemical interactions.

Verma et al. (2020) developed ecofriendly Sodium alginate/graphite hybrid hydrogel and investigated its potential for removal of malachite green dye. Hydrogel beads were reinforced using graphite powder to improve its uptake capacity. They prepared hydrogel by free radical polymerization of sodium alginate, and graphite powder in hot air oven and hydrogel was cross-linked using acrylic acid. The highest dye uptake capacity as 628.93 mg/g. The equilibrium data of dye adsorption system were notably fitted by Langmuir model and the rate of removal followed pseudo-second-order kinetics. The prepared alginate-based composite displayed excellent uptake efficiency (about 91%) even after third successive cycle.

Mandal and Chakrabarty (2011) extracted cellulose from sugarcane bagasse. During cellulose isolation process, they used sodium chlorite ($NaClO_2$) for beaching the raw bagasse,

and Sodium sulfite (Na_2SO_3) to eliminate the lignin (entirely) and hemicellulose (partly). Sodium hydroxide (NaOH) was utilized to eradicate the hemicellulose completely from residue. To prepare nanocellulose, isolated cellulose was acid hydrolyzed by refluxing with 60% (w/v) H_2SO_4 and agitating for 5 h at 50 ◦C. Deionized water was added to the solution and cooled to normal room temperature. After washing, the mixture was centrifuged and then sonicated for 5 min in an ice bath. Resulting suspension was freeze-dried. Thermo-gravimetric graph of isolated cellulose and nanocellulose suggested that the degradation temperature of nanocellulose was lower than sugarcane bagasse. Differential Scanning Calorimetry analysis showed that moisture content of adsorbent was different for each respective adsorbent.

Tavakolian et al. (2020) evaluated the performance of nanocrystalline cellulose and alginate-nanocrystalline cellulose composite beads (ALG-ENCC) for remediation of methylene blue-a cationic dye in batch adsorption studies. Electrosterically stabilized nanocrystalline cellulose was extracted from wood pulp via two step oxidation by periodate (an anion composed of iodine and oxygen) and chlorite. Wood pulp was oxidized by periodate by combining pulp, NaCl, and NaIO4 and water. The reaction was stopped by addition ethylene glycol (10 mL) and oxidized pulp (named as dialdehyde modified cellulose) was washed with deionized water and filtered using nylon cloth. Modified cellulose was then oxidized by chlorite by combining with NaCl, $NaClO_2$, and H_2O_2 and water. Mixture was continuously stirred and centrifuged to separate fibers from the solution (pH was adjusted in between 4.8-5.2). They combined nanocrystalline cellulose with alginate beads to enhance the uptake capacity of individual components in wastewater treatment process and to reduce the loss of nanocrystalline cellulose during filtration process. Maximum dye adsorption capacity for alginate-based nanocrystalline cellulose (ALG-ENCC) was found to be 1250 mg/g. Dye adsorption efficiency decreased under acidic condition. Their synthesized adsorbents have efficient potential for remediation of cationic dye as well as the heavy metals.

Wahyuningsih et al. (2016) isolated cellulose from pineapple leaf and fabricated cellulose reinforced PVA (Poly vinyl alcohol) polymeric composite to enhance thermal stability and physical stability. Cellulose derived from pineapple leaf by removing lignin using NaCl and then resulting mixture was hydrolysed using 64% w/w acid sulfate solution under stirring condition for 90 min at 45 °C. After washing with deionized water and suspension was centrifuged. Separated fibers suspension was freeze-dried and stored. They prepared nanocellulose from the cellulose fiber by ultrafine Grinder and developed polymeric film by adding nanocellulose fiber (10-50%) and glycerol (0-1%) in PVA solution. They examined the impact of fibrillation of extracted cellulose via chemical-mechanical treatments and observed

the influence of reinforcement on nanocellulose density in PVA medium. On addition of nanocellulose, PVA-film density decreased significantly by 4 to 8 times. With addition of nanocellulose, thickness of PVA composite increased from 0.02 mm to 0.03 mm and without nanocellulose addition, the film thickness was 0.11±0.069 mm. Changing the concentration of nanocellulose in film showed significant effect on properties of composite. The rate of water vapor transmission of composite film was found to be improved by increase in glycerol addition though the physical stability was reduced.

2.5. Fixed bed

2.5.1. Theory of Breakthrough curves

Fixed adsorbent bed are generally used in industries for continuous removal of pollutants. The wastewater flows either up or down the column packed with adsorbents. The dynamic behavior of the fixed-bed column is evaluated using breakthrough curve. The breakthrough curve of fixed bed study is obtained by plotting C_t/C_0 vs. time, where C_t was the adsorbate concentration in the effluent, and C_0 was the adsorbate concentration in feed. The shape of C_t/C_0 vs. time plot of breakthrough curve is useful for process design. The breakthrough time (t_b) and the nature of curves are very significant aspects to analyze the performance of the fixed-bed column.

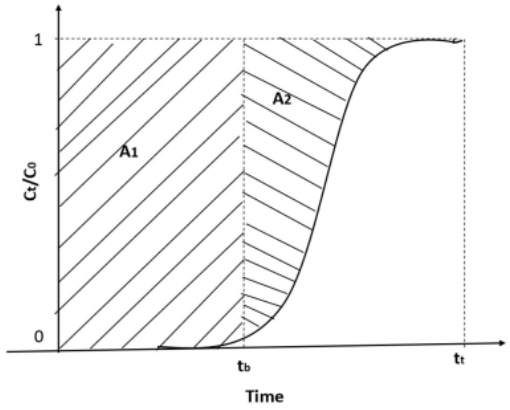

Fig. 2.1: Typical breakthrough curve

A set of parameters quantifying the characteristics of the breakthrough curve are estimated using the following equations (Equ. 2.18- 2.24).

The total time or stoichiometric capacity:

$$t_t = \int_{t=0}^{t=\infty} \left(1 - \frac{C_t}{C_0}\right) dt \ldots\ldots\ldots\ldots (2.18)$$

Time Equivalent to usable capacity:

$$t_b \approx t_u = \int_{t=0}^{t=t_b} \left(1 - \frac{C_t}{C_0}\right) dt \ldots\ldots\ldots\ldots (2.19)$$

Total adsorbed mass of adsorbate:

$$S_{tot} = Q C_0 t_t \ldots\ldots\ldots\ldots\ldots\ldots\ldots (2.20)$$

Adsorbed mass of adsorbate corresponding to the breakpoint:

$$S_b = Q C_0 t_u \ldots\ldots\ldots\ldots\ldots\ldots\ldots (2.21)$$

Where Q was indicated as the volumetric feed flow rate

The total mass of adsorbate injected in the column:

$$M_{tot} = Q C_0 t_f \ldots\ldots\ldots\ldots\ldots (2.22)$$

Where t_f was denoted as the final or total time of the column experiment

Adsorbate Removal efficiency:

$$R = \frac{S_{tot}}{M_{tot}} \ldots\ldots\ldots\ldots (2.23)$$

Equilibrium adsorbate adsorption capacity:

$$S_{eq} = {}^{S_{tot}}/_{m_s} \ldots\ldots\ldots\ldots\ldots (2.24)$$

Where m_s represented the mass of adsorbent (g).

2.5.2. Mathematical Modelling of column experiment

The efficiency of the fixed bed adsorbent-column is evaluated using the theory of the breakthrough characteristics. Some of the mathematical models to predict breakthrough behavior and estimate of the influence of experimental parameters on fixed-bed adsorption are

Yoon-Nelson model

Relatively less complicated, Yoon and Nelson model was used for analyzing breakthrough curve. The model assumes the rate of decrease in the probability of adsorption is proportional to the probability of adsorbate adsorption and breakthrough. The nonlinear and linear form of the Yoon and Nelson model equation are (Aksu & Gonen, 2004):

$$\frac{C_t}{C_0} = 1/(1 + \exp\ (k_{YN}\tau - k_{YN}t)) \ldots\ldots\ldots\ldots\ldots (2.25)$$

$$\ln\left(\frac{C_0}{C_t} - 1\right) = k_{YN}\tau - k_{YN}t \text{---------} (2.26)$$

where, τ denote the time required for 50% breakthrough (min) of the solute, t represent the contact time (min), and k_{YN} is the rate constant of adsorption process (Bulgariu & Bulgariu, 2013). The value of k_{YN} (L/min) and τ (min) can be obtained from $\ln\left(\frac{C_0}{C_t} - 1\right)$vs.$t$ plot.

Thomas model

Another extensively used model for analyzing breakthrough curve is the Thomas model (Chen et. al., 2012). Thomas model establishes the relationship between the influencing parametres and bed capacity. It assumes the addsorption process to be limited by mass transfer at the interface, while considering external and internal diffusion limitations are absent. Linear and nonlinear form of Thomas model was as follows:

$$C_t/C_0 = \frac{1}{1 + exp(\frac{m\,k_{Th}q_0}{Q} - k_{Th}C_0t)} \dots\dots\dots\dots (2.27)$$

$$\ln\left(C_0/C_t - 1\right) = \frac{m\,k_{Th}q_0}{Q} - k_{Th}C_0t \text{--------} (2.28)$$

where, t, k_{Th} and Q denote the total flow time (min), Thomas kinetic coefficient (mL/min mg), and volumetric flow rate respectively, m (g) and q_0 (mg/g) represent the adsorbent mass and MG removal capacity of bed (Chen et al., 2012). The magnitude of the parameters k_{Th} and q_0 are obtained from the slope and intercept of the plot between $\ln\left(C_0/C_t - 1\right)$ vs. t.

BDST (Bed Depth Service Time) model

The model assumes that the adsorption rate is controlled by the surface reaction in between the adsorbate material and the unused capacity of the adsorbents (Saha et al., 2012). Breakthrough time determined at different bed heights are required to predic the service time of the column using this model. Nonlinear and Linear form of BDST model are:

$$C_t/C_0 = \exp\left(C_0K_{BDST}t - N_0K_{BDST}\frac{Z}{U_0}\right) \dots\dots\dots (2.29)$$

$$\ln\left(C_0/C_t - 1\right) = N_0K_{BDST}\frac{Z}{U_0} - C_0K_{BDST}t \dots\dots (2.30)$$

$$t = \frac{Z}{C_0U_0}N_0 - \frac{1}{C_0K_{BDST}}\ln\left(C_0/C_t - 1\right) \dots\dots (2.31)$$

Where, K_{BDST}, Z and N_0 indicated the BDST model constant (L/mg min), bed height (cm) and maximum volumetric adsorption capacity (mg/L) respectively. U_0 denoted the superficial velocity (cm/min) of the fixed-bed column.

2.5.3. Review on relevant literature and experimental studies

Somasekhara Reddy and Nirmala (2014) examined the continuous removal of direct dye, Congo red (CR) using seed husk of Bengal gram (*Cicer arietinum*) (SHBG) in fixed bed. The influence of operational variables including pH (5.6, 7.02, 9.1), column bed height (3.5, 7, 10, 12.5 cm), initial dye concentration (25-100 mg/L), adsorbent particle size (53-150 µm) on

breakthrough curve was investigated. The capacity of adsorbent column was obtained as 6.572 mg/g at inlet flowrate of 0.67 mL/min for an initial concentration of CR dye of 50 mg/L. They apply BDST (bed depth service time analysis) model in order to predict the breakthrough curves of column adsorption process.

Mohammed et al. (2016) studied the potential of cellulose nanocrystal-alginate (CNC-ALG) hydrogel beads for adsorption of Methylene blue dye (MB) by in a fixed-bed system under various experimental conditions. They evaluated the influence of different column operating parameters such as initial MB dye concentration in feed solution (50-250 mg/L), adsorbent bed height (22-66 cm) and flow rate (1.17-4.40 mL/min) on the breakthrough curves. The maximum adsorption capacity of the fixed-bed column was 255.5 mg/g (for initial MB dye concentration= 50 mg/L, bed height=22cm, flowrate=4.40 mL/min). The effectiveness of the adsorbent bed was higher at low flowrate as large residence time helped to improve the degree of adsorption.

Manna et al. (2018) studied the characteristics of fixed bed for adsorption of Fluoride using lignocellulosic bio-sorbents. They reported that the neem oil phenolic resin treated adsorbent could reduce fluoride content both from fluoride containing synthetic and groundwater. the found that adsorption bed performance was better at higher bed height, lower flow rate and lowest initial fluoride concentration in feed solution. They verified column experimental data by applying theoretical modelling such as BDST model to predict the performance of adsorbent column for removal of fluoride using their prepared biosorbent. In addition, they revealed that the bio-sorbents used in their study were regenerable and reusable for more than five cycles.

Ramesh et al. (2012) reported batch and continuous fixed-bed studies for fluoride adsorption using Bottom ash as adsorbent. They performed continuous column study in a glass column (2.5 cm ID and 20 cm column height). The effect of different adsorbent bed height (10-20 cm) was observed for a constant initial concentration of fluoride solutions (10 mg/L) under a constant flow rate of 10 mL/min at 33°C temperature. Column study data were fitted with BDST model, Thomas model, and Yoon-Nelson model. The results showed that with increasing adsorbent bed height fluoride adsorption capacity increased because of an increase in availability of adsorptive binding sites and the contact time between adsorbate and adsorbent. Thomas model predicted maximum adsorption capacity to be 0.3714 mg/g.

Different polymeric biosorbents and their adsorption capacity for textile dye removal are reviewed and presented in the following table (table 2.1).

Table 2.1: Potential of polymeric composites in dye removal

Dye	Polymeric biosorbent	Adsorption capacity (mg/g)	Reference
Acid blue 25	Chitosan/cyclodextrin Material	77.4	Martel et al. 2001
Malachite green	Poly (vinyl alcohol)/chitosan composite	380.65	Jeon et al., 2008
Reactive orange 16	Chitosan/sepioliteclay	190.965	Marrakchi et al., 2016
Malachite Green	NiO NPs/Chitin beads	370.37	Raval et al., 2016
Methylene Blue	Chitosan based graphene oxide (GO) gels	1100	Cheng et al., 2013
Acid Yellow 36	Chitosan-GO nanocomposite	68.86	Banerjee et al., 2017
Acid Red 2	Magnetic chitosan nanocomposites	90.06	Kadam & Lee, 2015
Methylene Blue	Magnetic chitosan- GO composite	180.83	Fan et al., 2012
Methylene Blue	Chitosan/organic rectorite-Fe3O4	24.690	Zeng et al., 2015
Malachite green	Native cellulosic polymers	2.422	Sekhar et al., 2009
Methyl orange	Natural carbohydrate polymeric biosorbents of rice flour	173.24	Md. Munjur et al., 2020
Rhodamine B	Carbohydrate polymeric adsorbent of wheat flour	142.26	Hasan et al., 2018
Methylene Blue	GO reinforced PVA/Carboxymethyl cellulose	172.14	Dai et al., 2018
Methylene Blue	MnO_2 coated cellulose nanofibers	Not reported	Wang et al., 2014
Brillint green	Phosphate cellulose integrated with chloroethyl phosphate	114.2	De Castro Silva et al., 2016
Malachite green	Graphene oxide /cellulose bead	30.09	Zhang et al., 2015
Reactive red dye	Aminoethanethiol modified cellulose surface	78.00	Silva et al., 2013
disperse dyes	Polyacrylamide Grafted Cellulose	25.84	Yang et al., 2017
Reactive Brilliant Red	Magnetic amine/Fe_3O_4-resin	101.0	Song et al., 2016
Malachite green	Alginate/poly aspartate composite hydrogel beads	300-350	Sonawane et al., 2009

Malachite Green	Super paramagnetic sodium alginate-coated Fe_3O_4	47.84	Mohammadi et al., 2014
Methylene blue	Alginate grafted poly-acrylonitrile beads	03.51	Salisu et al. 2015
Methylene blue	Sodium alginate-coated perlite beads	74.6	Parlayici, 2019
Methylene Blue	GO/Calcium alginate	181.81	Y. Li et al., 2013
Crystal violet	hybrid sodium alginate-PVA -silica oxide	1756.2	Lin et al., 2019
Methylene Blue	Activated organo-bentonite /sodium alginate	414.1	Belhouchat et al., 2017
Acid green 25	Sodium alginate/titania	151.5	Mahmoodi et al., 2011
Methylene Blue	Graphene oxide/potato starch composite	500	Bhattacharyya et al., 2018
Reactive Orange 131	modified starch/polyvinyl alcohol composite	539	Xia et al., 2020
Crystal violet	Silica-sand/anionized-starch	1246.40	Li et al., 2020
Crystal violet	MCNCs/starch-g-(AMPS-co-AA)	2500	Moharrami & Motamedi, 2020
Optilan Blue	Starch/Fe_3O_4	74.58	Stan et al., 2019
Malachite green	polyacrylamide/bentonite composite	243.11	Anirudhan & Suchithra, 2009

Different biosorbents and their adsorption capacity for fluoride removal are reviewed and presented in the following table (table 2.2).

Table 2.2: Potential of various composites in fluoride removal

Adsorbents	Adsorbent capacity (mg/g)	References
Iron Oxide-Hydroxide Nanoparticles	16.7	Raul et al., 2012
Cellulose@HAPnanocomposites	2.76	Yu et al., 2003
Zirconium–Cerium/polyvinyl alcohol	8.07	Sai et al., 2020
Zirconium–Lanthanum/polyvinyl alcohol	8.35	Sai et al., 2020
nano-hydroxyapatite/chitosan (n-HApC)	1.56	Sairam et al., 2008a
Chitosan-based mesoporous alumina	8.264	Jagtap et al., 2011
Activated alumina	2.41	Ghorai and Pant, 2005
Bleaching powder	0.2	Kagne et al., 2009
carboxylated chitosan beads	1.664	Viswanathan et al., 2009

Fe/Zr)-alginate microparticles	0.981	Swain et al., 2013
Hydrous ferric oxide doped alginate beads	8.9	Sujana et al., 2013
La-Ce-modified chitosan	3.72	Liang et al., 2013
neodymium-modified chitosan	22.38	Yao et al., 2009
Fe(III)-loaded ligand exchange cotton cellulose	18.6	Zhao et al., 2008
ceramic-based adsorbent	2.16	Chen et al., 2010

…….########…….

Chapter.3

Aim and Objectives

3.1. Aim and objectives

Pure water accessibility is one of the crucial and basic needs in most of the countries in world. With advancement of technology and industrial activity, demand for uncontaminated water for daily use is increasing. Major parts of the contaminants are coming from different industry containing heavy metals, hazardous dye, radioactive pollutants, toxic chemicals, fluoride etc. The water pollution associated with the inappropriate or unlawful untreated effluents discharged from industrial, farming, and domestic unwanted water contains an extensive variety of harmful carcinogenic chemical products.

Dye is used in several sectors like textile, cosmetic, plastic, paper, leather, and pigment industries. The effluent of those industries heavily pollutes the surface and groundwater, thereby, making it unhealthy for consumption and unfit for agricultural purposes. The toxicity of dyes can range from irritants for eyes and skin, to having carcinogenic and mutagenic effects if allowed to remain in the body at high doses for a long time. Additionally, the color water obstructs the penetration of sunlight on water bodies. This prevents the growth of marine lives by preventing photosynthesis and reducing the concentration of dissolved oxygen.

Malachite Green (MG), which is a common textile dye, that can cause carcinogenic effects and organ damage in animals if consumed for a long time, is used as an adsorbate in the project research work. MG dye is the most popular cationic dye used for dyeing cotton, wool, leather, nylon, and silk. MG dye is also being used in significant quantities in the aquaculture industries where it is illegally used as low-cost topical antifungal and parasiticide. Due to its carcinogenic and mutagenic nature, industrial effluent containing MG dye is very much harmful to marine life. According to the U.S. FDA (Food & Drug Administration) sample testing protocols, MG dye residue must be below 1 mg/g (USA Today, 2017).

Manmade sources of Fluoride contamination are effluent discharged from various industrial activities such as coal-burning stations, steel production, aluminum, phosphorus, production of bricks, glass, plastic, cement, and HF production plant. Another source of fluoride pollution in potable water and surface water is because of the excessive use of fertilizers (superphosphate, NPK, potash etc.) which also contain notable amount of fluoride. WHO (world health organization) recommended permissible limit of fluoride as 1.5 mg/L. Almost 19 states of India, including Rajasthan, Andhra Pradesh, Uttar Pradesh, Maharashtra, West Bengal, and Gujarat are suffering from high fluoride concentrations in groundwater as well as surface water (Ayoob and

Gupta 2006; Amalraj and Pius 2013). Fluoride affects the ecosystem and living beings by contaminating water, air, soil, crops and vegetables. Intake of fluoride lead to the fluorosis syndrome, reproductive decline, skeletal tissues damages, and damage to the thyroid.

A wide range of approaches has been developed for ensuing the adequacy and proficiency of the wastewater treatment. Several advanced physicochemical techniques such as electrodialysis, precipitation, reverse osmosis, ion exchange process, and adsorption have been projected to remove pollutant from their aqueous solution. The limitations of many of these procedures are complex, highly expensive, and produce poisonous carcinogenic secondary pollutant. Of late, researchers are focusing on environmental-friendly, economical, and low energy-consuming treatment technology. Adsorption is accepted as the most efficient process for decolorization and defluoridation process due to advantages such as ease of operation, low operating cost, insensitivity to toxic substances, viability etc.

India is one of the agricultural countries in the world. A large number of agro-based industries, such as jute, cotton, and sugar produce large quantities of agro-waste which hamper in proper waste disposal management and environmental ecosystem. According to the Press Information Bureau, India generates 62 million tons of waste (mixed waste containing both recyclable and non-recyclable waste) every year, with an average annual growth rate of 4%. In recent years, researchers are paying attention to efficient use of agricultural residues to minimize the accumulation of waste. Agricultural wastes are affluent in organic substances due to presence of various functional groups which help to bind the electro-positive ions and electro-negative ions. Despite of having many appreciable properties, commercial adsorbents (such as activated carbon) that are most used on industries are very expensive and non-biodegradable. Researchers are therefore investigating agro-waste and their derivatives as an efficient and eco-friendly adsorbent for treatment of industrial effluent water due to its favorable properties, including abundance, biocompatibility, biodegradability, cost-effectivity, and non-toxicity. Agro-waste derived biosorbent material can offer an alternate purification process to substitute the commercial adsorbent (Matei et al., 2001).

The uptake rate of pollutants by adsorbents depend on the intraparticle and continuous phase mass transfer resistances. Decreasing the particle size enhances the removal rate of pollutants leading to reduced equipment size and more efficient use of the adsorbents. Limitations of application of fine, granular adsorbent include reactor cleaning, difficulty in separation of adsorbent from treated

solution and clogging. They could be easily released in effluent discharge resulting in underutilization of their removal capacity by regeneration. The complexity accomplished in recovering the powdery adsorbents from treated solutions post adsorption makes these undesirable for the large-scale application. Beads or hydrogel film form of those granular adsorbents reduces these drawbacks. Composite production by inserting agro-waste derived activated biochar and biopolymer within an inflexible polymer has become a new appreciable technique.

Research Gap: The more the quantity and toxicity of the pollutants, the greater the obstacles to design a suitable efficient, cost-effective wastewater treatment technique. Feasible application of agro-waste derived adsorbents in the wastewater treatment process was explored in many research papers (Chowdhury et al., 2011; Sing et al., 2011; Madhusudana Rao et al., 2013;). However, the application of the proposed agro-waste derived carbonaceous and bio polymeric materials grafted composite beads and hydrogel films for dye and fluoride removal process is still a not much researched area. Biodegradation of pollutant loaded adsorbent is essential before disposing/discarding to reduce its adverse effect on the environment (Wagner et al., 1996; Premraj and Doble, 2005). Though there is huge volume of work on the biodegradation of pollutants from wastewater (such as Bacillus sp. used to biodegrade 2, 4, 6-TNT (Lin et al., 2013), Pseudomonas sp used for bioremediation of Reactive Red 2 (Kalyani et al., 2009; Banerjee et al., 2017)), there has been only a limited research on use of micro-organism for degradation of pollutant loaded adsorbent.

Sugarcane is widely cultivated in tropical and subtropical countries such as India, Sri Lanka, Pakistan, Bangladesh, Malaysia, Philippines Hawaii, Australia, and Indonesia. Bagasse is the by-product obtained after crushing the sugar cane stalks and is fibrous in nature. Burning as fuel and landfilling are extensively used method in many states of India to discard the crop residue. Landfilling of the waste sugarcane bagasse produces a large amount of leachate which causes hazardous contamination to the open water body as well as groundwater. The recycling of the sugarcane bagasse into biosorbent is an efficient alternative to the conventional process for minimizing the solid-waste handling problems and produce inexpensive, ecofriendly biodegradable adsorbent for wastewater treatment. Sugarcane bagasse contains about 40–55% of cellulose, hemicellulose as much as 26–35% (Wulandari et al. 2016; Mandal and Chakrabarty 2011). Hence, it is a potential resource of readily available low-cost raw material for cellulose

extraction, activated biochar production and surface modified biosorbent preparation for wastewater treatment process.

The objective of this research work is to synthesis carbonaceous and polymeric material grafted biodegradable composites derived from abundantly available low-cost agro-waste sugar cane bagasse and to investigate the application of these biodegradable adsorbents for decolorization of MG dye contaminated wastewater and defluoridation of water. The focus has also been on reutilization of dye and fluoride-loaded adsorbents obtained post-adsorption and biodegradation of pollutant loaded adsorbents by isolated microorganism before final disposal of the biosorbents into the environment.

The following was done within the framework of the present research work

- Preparation of activated charcoal and extraction of cellulose from sugarcane bagasse
- Synthesis of different types of carbonaceous material and biopolymer-based composites.
- Physiochemical characteristics of prepared adsorbents were analyzed using FTIR, SEM, TGA, and BET. FTIR was conducted to analyze the characteristic functional groups on the surface of adsorbents. Surface morphology of adsorbent was evaluated by SEM characterization. The estimate of adsorbent surface area which is important for fixed bed was obtained using BET analysis.
- Investigation on the adsorption efficiency of synthesized biosorbent for removal of MG dye and Fluoride separately both in batch process and continuous removal in fixed bed.
- Investigation of the effects of various operational parameters (factors) on removal efficiency of the prepared adsorbents.
- Estimation of adsorption isotherms, kinetic and thermodynamic parameters from experimental data. Adsorption isotherm was determined to explain the adsorption mechanism and the interactive behavior between the distribution of the adsorbate molecule within the solution and on the adsorbent surface. The adsorption capacity under equilibrium condition and the rate constants of contact time-dependent adsorption process were estimated by applying kinetic model. Kinetic study was performed to understand the mass transfer mechanism dictating uptake rate required for designing suitable contactors. Thermodynamic study was conducted to describe the thermodynamic behavior of adsorption process.

- Evaluation of the dynamic behavior and performance of the adsorbent column in terms of the breakthrough curve at various investigational conditions (such as feed flow rate, feed concentration, adsorbent-bed height, solution pH).
- Investigation on the Recycle potential (Regeneration study) and Biodegradation study of the pollutant-loaded composites. Pollutant elimination by biosorption process becomes less expensive and beneficial if the pollutant-loaded biosorbent can be regenerated.

3.2. Complete Work Flow

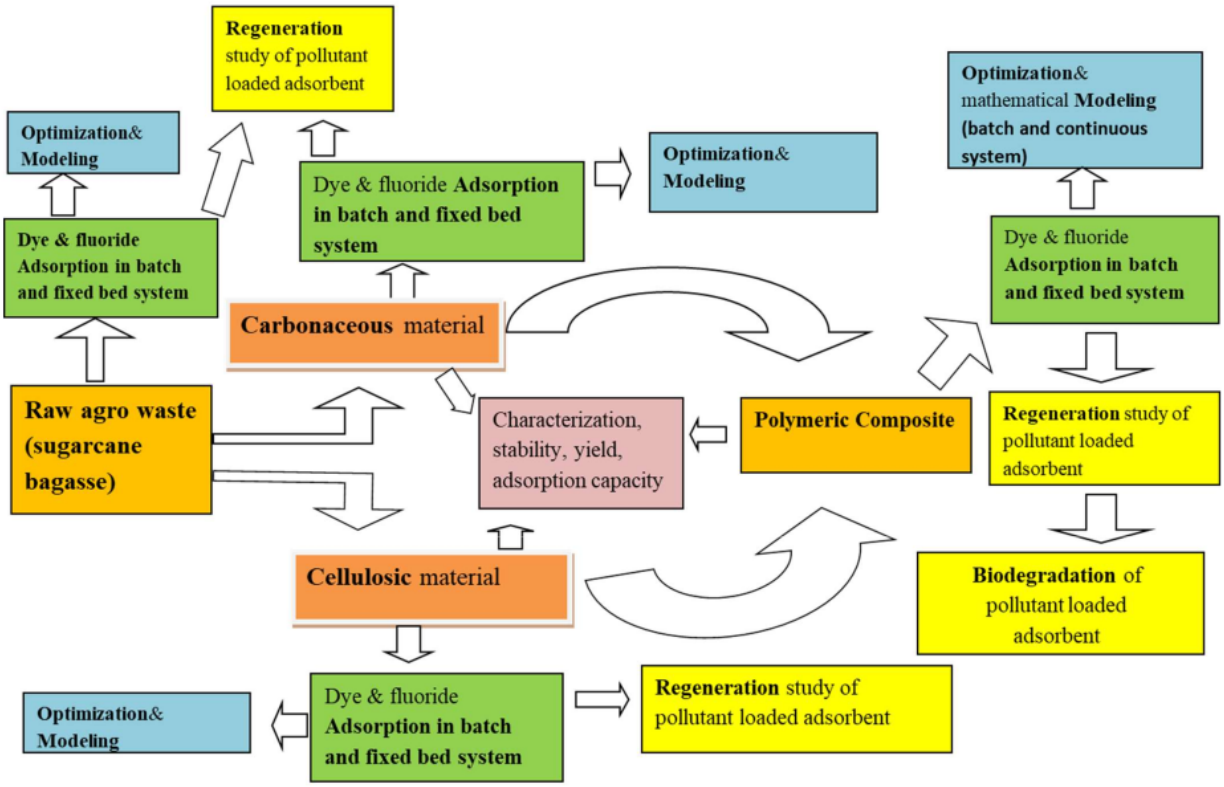

Chapter.4

Materials and methods

4.1. Chemicals and Instruments used

Malachite green dye (99.99% purity) (Loba Chemie), Sodium hypohlorite (NaClO) (Merck Life Science Pvt. Ltd.), sodium fluoride (NaF) (Merck Life Science Pvt. Ltd.), sodium hydrogen sulfite ($NaHSO_3$) (Merck Life Science Pvt. Ltd.), sodium hydroxide (NaOH) (Merck Life Science Pvt. Ltd.), hydrochloric acid (HCl) (Merck Life Science Pvt. Ltd.), H_2SO_4 (Merck Life Science Pvt. Ltd.), Nitric acid(69%) (Merck Life Science Pvt. Ltd.), Ethanol (ChangshuHongsheng Fine Chemicals Co. Ltd.), total ionic strength adjustment buffer (TISAB), fluoride ISE meter (ORION STAR A214). Sodium Alginate was provided by HiMedia. Polyvinylalcohol (PVA) was supplied by LOBA Chemie., Acetic Acid was supplied by Merck life science Private ltd, UV–Vis Spectrophotometer (Perkin Elmer Lambda 365), BOD shaker (G.B. Enterprises, India), Centrifuge (Remi RM – 12C), Glasswares (Borosil), pH meter (Eutech Instrument), Vacuum Filter (Rivotek, Riveria glass Pvt. Ltd.), Vacuum oven drier (G B Enterprises) Weighing Machine (BSA224S – CW, Satorius), deionized water (DI).

4.2. Adsorbent preparation

4.2.1. Production activated biochar using Sugar cane bagasse

Sugarcane bagasse (SB) collected from local markets in Kolkata, India was washed to remove dust and other foreign particles and dried overnight in the electrical drier. The bagasse fibers were then cut into small pieces crushed in a mixer-grinder and sieved. The sieved fines (80 - 100 µm) were collected in a porcelain bowl and pyrolyzed in a muffle oven for 2 hr at a temperature of 800˚C in an inert atmosphere (N_2 air purging). After 2 hr, the carbonized material was allowed to cool. The carbonized black, amorphous sample obtained is known as Sugarcane Bagasse biochar.

An aqueous solution of NaOH (Merck life science Pvt ltd) was prepared of strength 15 wt % (w/v) NaOH. Each gram of prepared biochar sample was mixed with 10 ml of aqueous NaOH solution and stirred for 24 hr in a glass beaker at 50 °C. After 12 hr, the stirring was stopped and the suspension filtered. The solid particles were then dried in an electric oven at 105˚C for 4 hr and then subjected to a second round of thermal activation in a muffle oven for 2 hr at 800˚C. Carbonized biochar was repeatedly washed with 10% HCl solution followed by distilled water to make it neutral (pH≈7). After washing, chemically activated samples were dried at 105˚C. The resultant product, Sugarcane Bagasse activated biochar (SBAC) was utilized for the MG removal process.

4.2.2. Synthesis of Sodium alginate-bentonite/SBAC composite beads

To prepare sodium alginate beads, 2 g amount of sodium alginate was taken and dissolved in 100 ml demineralized water under mechanical agitation by a magnetic stirrer for about 1 hour. Then, 1g of sugarcane bagasse activated charcoal (SBAC) and bentonite clay (2g) were added to the solution. The mixing process was further carried out overnight to ensure that the solution is homogenous. This solution was added dropwise to Calcium chloride solution of 4% (w/v) concentration by burette to get beads (named as Alginate-bentonite/SBAC). The beads were stored in deionized water and separated by filtration using Whatman filter paper.

4.2.3. Nanocellulose/PVA composite synthesis

For each gram of raw grinded (80-100 µm) Sugarcane Bagasse (SB), 50ml of 0.4%, NaClO solution was used to bleach and the mixture was continuously stirred for 2 hr at 50°C. After filtering and washing five times with deionized water (to reduce excess NaClO and to make solution pH neutral), the treated mass was added to 1.7% $NaHSO_3$ solution for 30 min. Filtration was followed by washing. Hemicellulose was eliminated from the dried mass by treating with 17.5 % NaOH for 1 hr under continuous stirring. Lastly, this treated mass was strained and washed several times with DI water till the pH level of the solution reached neutral value. Synthesized cellulose was used to prepare nano-cellulose using sulfuric acid (50%H_2SO_4) by acid hydrolyzation technique. After freeze drying, powdered formed nano-cellulose ware stored in an airtight container.

Poly vinyl alcohol (PVA) powder (4 g) was diluted with 50 ml of distilled water and heated to 85 °C in a hot water bath for 5h. After cooling the PVA solution to room temperature, 0.5g of nano-cellulose was added to it and the mixture was stirred at 600 rpm for 3 hr at 60 °C until it was dissolved completely. Final polymeric suspensions were poured into a petri-dish and left to dry at 40 °C. After drying, the composite films were cut into designated small sizes (~ 40 mm and 30mg weight) and stored in an airtight container.

4.2.4. Alginate-Nanocellulose composite beads synthesis

Sodium-alginate solution was prepared by adding sodium-alginate powder with deionized water in a ratio of 1:50 and stirred for 1 hr. Then, 2g of bentonite and 1g of extracted cellulose were added to the solution. To develop uniform size beads, this solution was poured drop by drop in 4% (w/v) calcium chloride solution from burette at continuous stirring condition. The beads were kept in deionized water. After separation, these beads were dried (dehumidified) at 40-50 °C in electric oven and stored for future study.

4.3. Characterization of prepared adsorbents

Functional groups on the surface of synthesized adsorbents were characterized by analyzing FTIR spectra (Perkin Elmer FT-IR). The sample was dried overnight to remove any water retained. Before preparing translucent sample disk, sample was dried overnight and then encapsulated into dry KBr (potassium bromide) disk. FTIR spectra of the material were recorded at wavenumber range of 450 to 4000 cm^{-1} with 4 cm^{-1} resolution. Surface topography of the synthesized adsorbent surface was identified by the SEM technique (carried out by CARL ZEISS).

Surface area, pore diameter, and total pore volume of prepared adsorbent material were derived from the N_2 adsorption/desorption data on BET analyser (Brunauer Emmet Teller). Surface analyzer (Quantachrome® ASiQwin) was used to obtain N_2 adsorption data under 77.35 K temperature and relative pressure in the range of 0.100583 to 0.02985. The t-plot method was applied to determine the micropore volume of adsorbent particle.

For Point zero charge characterization (PZC) of the prepared adsorbent, 0.1 g of adsorbent material was added to 45 mL of KNO_3 solutions (0.1 N) and sealed. The pH of the solution was varied from 2.0 to 12.0 by adding HNO_3 (0.1 N) or NaOH (0.1 N) solution. The slurry was shaken at 150 rpm for 24 h to attain the equilibrium condition. The initial and final pH were recorded after shaking. The difference between the value of final and initial pH (ΔpH) vs. initial pH value was plotted. The Point of zero charge (PZC) is a point of the plotted curve at which ΔpH = 0.

4.4. Batch adsorption study

Batch study of MG dye removal efficiency of various biosorbents was performed by adding specified amount of the adsorbents to 100 ml of MG dye stock solution. The experiments were carried out in a BOD-shaker at 140 rpm. The influence of investigational condition were observed by varying solution pH (2, 4, 6 and 8), initial adsorbate concentration (MG dye: 5-20 mg/L; Fluoride: 2-10 mg/L), amount of adsorbent (1, 2, 4 and 6 g/L) and temperature (30, 35, 40 and 45°C). The basic pH value was adjusted by adding 0.1 NaOH and acid condition using HCl (0.1N). After 24 hr, the solution sample was separated from adsorbent by centrifuged (REMI RM-12C) at 10000 rpm for 10 min. The MG dye concentration in residual solution was measured using UV-Vis Spectrophotometer at wavelength 617 nm. The concentration of fluoride ion was measured with a fluoride-ion meter (ORION STAR A214). The adsorbate uptake capacity at t time, q_t (mg/g) and adsorbate uptake capacity at adsorption equilibrium condition, q_e (mg/g) was calculated using the equations given below:

$$q_t = (C_0 - C_t) \times \frac{V}{W} \ldots\ldots\ldots\ldots (4.1)$$

$$q_e = (C_0 - C_e) \times \frac{V}{W} \ldots\ldots\ldots\ldots\ldots (4.2)$$

Where, C_0 (mg/L) is initial pollutant concentrations, whereas C_e (mg/L) is the concentration at equilibrium concentrations, and C_t (mg/L) is concentration at time t. V (L) is the experimental solution volume, and W was the weight of the adsorbent mass used for adsorption measured in grams. The adsorption efficiency (%R) ware derived according to the equation (eqn. 4.3):

$$\%R = (C_0 - C_e) \times \frac{100}{C_0} \ldots\ldots\ldots (4.3)$$

Equilibrium concentration obtained from batch study under various adsorbate concentration were fitted to the isotherm model equation (Langmuir, Freundlich Temkin model). The rate constants of the kinetic models (pseudo first, pseudo second order and intraparticle diffusion) were obtained by fitting the model to the experimental batch concentration versus time data.

4.2.5. RSM modelling

The central composite design (CCD) was done by "Design-Expert" software (version 7.0, Stat-Ease, Inc. USA). A standard RSM design (CCD) was used to categorize the relationship between the response function and the system variables. The response surface contour plots were analyzed to identify the relations between the various independent variables and their influences on the adsorption system response. Process factors, pH, contact time, adsorbent dose have significant effects on the removal efficiency of prepared adsorbent. To predict the optimal point of the system response (% removal of MG dye and fluoride) a quadratic model was used. twenty experiments were carried out to determine the removal efficacy using RSM design (central composite design).

The empirical relationship between the three selected independent variables and statistically the probable optimum condition was determined by the quadratic equation given below:

$$Y = \beta_0 + \sum_{i=1}^{k=3} \beta_i x_i + \sum_{i=1}^{k=3} \beta_{ii} x_{i^2} + \sum_{i=1}^{k=3} \sum_{j=i+1}^{k=3} \beta_{ij} x_i x_j + \varepsilon \ldots\ldots\ldots\ldots (4.4)$$

where, Y = response (dependent variable), $\beta_i = \beta_{ii} = \beta_{ij}$ = coefficients of linear, quadratic and interaction effect, β_0 = constant coefficient, xi and x_j = factors (independent variables). And ε = error. In this study Y is the removal efficiency (%R) and x is independent variables (pH, Time, adsorbent dose). The optimized condition of independent variables for removal process were estimated using regression equation and by analyzing the contour plots. The quadratic

model and coefficient of correlation were followed to predict the interaction between the various factors in a specific range. To obtain maximum removal efficiency, contact time, pH and adsorbent dose were fixed within ranges of 30-120min, 2-8, and 0.5–1 g/L, respectively.

4.5. Fixed bed column study

A glass column of 50 cm length and internal diameter of 3 cm was used to carry out the fixed-bed column experiment for MG dye and fluoride removal study using prepared adsorbent. Wire mesh (1 cm height) were placed at the inlet and outlet of the adsorbent column. A peristaltic pump was used to introduce the solution at top of the fixed bed. The solution flowed down the column under the gravity. The experiment was performed by varying feed concentration (MG dye:50-200 mg/L; Fluoride: 8-12mg/L), feed flowrate (10, 13, 16 mL/min), adsorbent bed depth (5 cm, 7 cm, 9 cm), and pH of inlet solution (4, 6, 7, 8) at 30°C. Samples from the effluent solutions were collected at certain time interval and the concentration of the pollutants measured. Operation of the adsorbent bed was stopped when the concentration in the effluent reached that of the feed. The equations proposed by Yoon-Nelson, and Thomas kinetics were used to predict the breakthrough curve.

4.6. Continuous adsorption experiments in fluidized bed

The schematic of the experimental set up used for fluidized bed experiments is shown in Fig. 4.1. A glass cylinder (4 cm dia. and 30 cm height) was utilized as the fluidized-bed reactor. The solid composite beads were loaded into the fluidized-bed adsorption column. The feed solution was forced up the fluidized bed by means of peristaltic pump. Samples of the effluent was collected at time interval from the sample collection pipe (outlet pipe ID=0.75cm) and its concentration measured using UV-Vis. spectrophotometer (for MG dye) or fluoride-ion meter (for fluoride). The effects of operational factors such as feed concentration, feed flowrate, adsorbent-bed mass and composite bead diameter on the process efficiency was studied. Beads of different diameter was prepared by Beads of different diameter was prepared by using burette and dropper. Screw Gauge was used for measuring size of the composite bead particle.

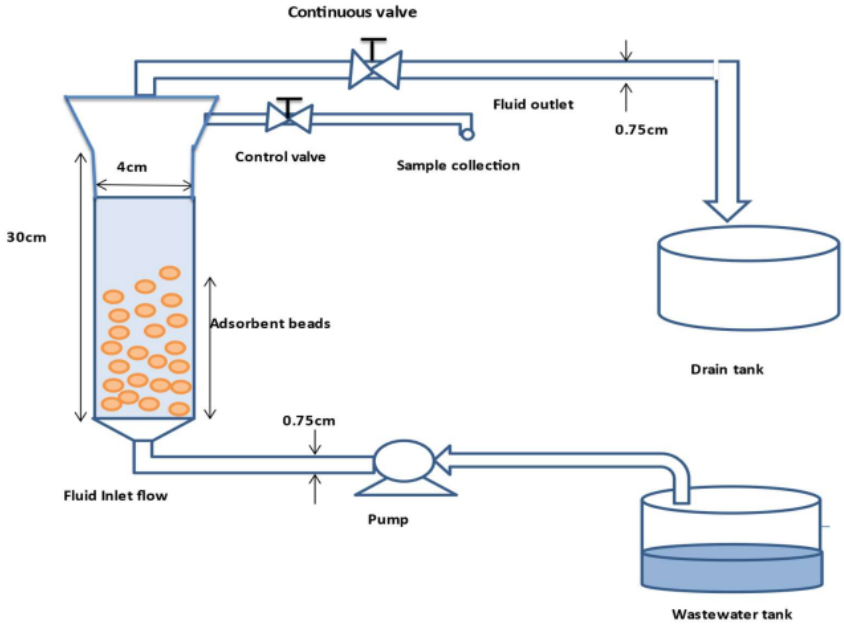

Fig. 4.1: Experimental setup for Continuous adsorption experiments in fluidized bed

Chaper.5

Evaluation of Dye removal study using carbonaceous and polymeric material grafted composites

5.1. Introduction

Gramineae Saccharum officinarum L., popularly known as Sugarcane are widely cultivated crop in tropical and subtropical country (like India, Sri Lanka, Pakistan, Bangladesh). Sugarcane Bagasse are by-product after crushing the sugar cane stalk which is fibrous in nature and contains large amount of cellulose, hemicelluloses, lignin, protein, humic substances. sugarcane, bagasse are capable in adsorption of pollutants due to presence of adsorptive sites such as hydroxyl groups, carboxylic, carbonyl and amine groups (Davila Jimenez et al., 2005). The converting the sugarcane bagasse into activated biochar is an efficient alternative for minimizing the solid-waste handling problems and produce inexpensive, eco-friendly biosorbent for malachite green (MG) dye removal.

Not all the discrete features of chemically activated biochar, bentonite clay, and sodium-alginate are favorable for removal of every pollutant, Therefor the indication of combining them into the beads form to develop an efficient polymeric composite was hypothesized. In this research work, Sodium alginate was used as a supporting polymer with the NaOH treated sugarcane bagasse activated biochar (SBAC) as this polymer is biodegradable, inexpensive, and suitable as rigid encapsulated support material (Scott et al., 1989).

Among all the natural biopolymers, cellulose seem to be the utmost attractive polymer owing to its biodegradability, high specific surface area, biocompatibility, high thermal stability, non-toxicity, high water solubility, renewability, abundant availability and they are relatively inexpensive (Wang et al., 2016). Cellulose nanocrystals derived from agro-waste, in comparison to conventional cellulose, show an excellent potential in wastewater treatment because the structures of agro-waste derived fibers constitute of hemicellulose, lignin, sterols, starch, and proteins (Noor et al., 2017). Though, the utilization of nanocellulose in water purification process is still inadequate due to their agglomeration tendency because of nano-scale size and the high specific surface area. To enhance the biosorption efficiency and overcome the drawbacks, nanocellulose can be custom-made using the binding polymer material such as PVA (Polyvinyl alcohol) and Alginate.

The present chapter describes the experimental studies carried out to evaluate the performance of carbonaceous materials-based composite and polymer grafted composites in dye removal. The investigation was carried out in batch process and fixed bed adsorption column. To this end, removal efficiency at different experimental conditions were obtained by varying operational parameters ranges. The synthesized adsorbents were characterized by analysing Fourier transfer infrared spectroscopy (FTIR), BET, and scanning electronic microscope

(SEM). The removal efficiencies were studied in a comparative batch study at various experimental conditions. The optimization of batch process parameters by designing response surface methodology (RSM) was also established. Continuous removal of dye was also studied in a fixed bed. Dynamic study data was evaluated using column adsorption kinetic models. Thomas model and Yoon-nelson model were well fitted with the experimental data for this process.

5.2. Results and discussions

5.2.1. Characterization

(i) FTIR

This technique provides a spectrum containing a large number of absorption bands from which information can be derived about the structure of an organic compound. that, many functional groups were present on the adsorbent surface. These functional groups are the potential sites for adsorption. FTIR absorption bands and corresponding possible groups of prepared adsorbents are tabulated in table 5.1(a, b, c & d).

(a) FTIR of SB, SBC, SBAC

Table 5.1(a): IR absorption bands and corresponding possible groups of SB, SBC and SBAC

Wavenumbers (cm^{-1})			**Functional groups**
SB	**SBC**	**SBAC**	
3332.64	3409.41	3421.79	O–H stretching vibration
2898.75	-	-	C–H stretching vibration
1728.37	1705.11	-	aromatic carbonyl or carboxyl C=O stretching
1603.51	1602.94	1591.52	O-N asymmetric stretching due to the presence of nitrogen compounds
1514.39	-	-	C=C stretching vibration
-		1384.22-1420.22	C-H aliphatic bending
1242.56	-	-	C–O stretching vibration
1035.57	-	1046.81	C-H stretching vibration
-	771.58	-	SiO_2 stretching vibration

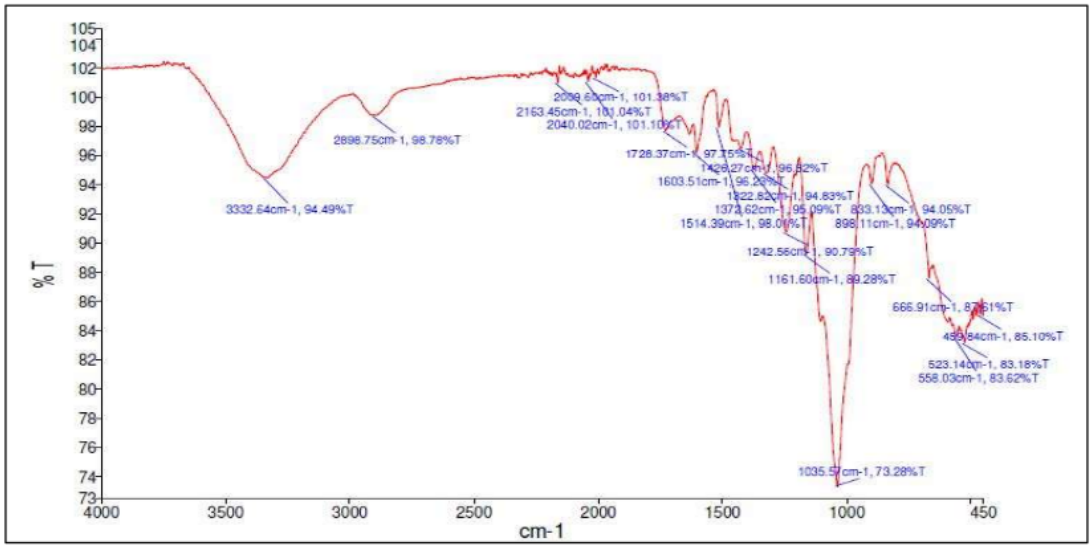

Fig. 5.1(a): FTIR spectra of raw sugarcane bagasse

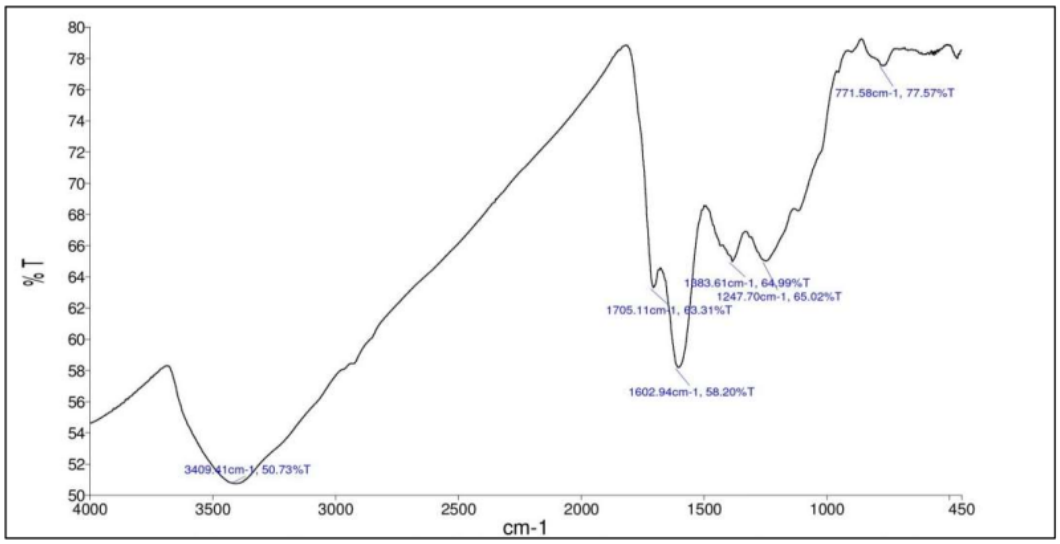

Fig. 5.1(b): FTIR spectra of SBC (SB biochar)

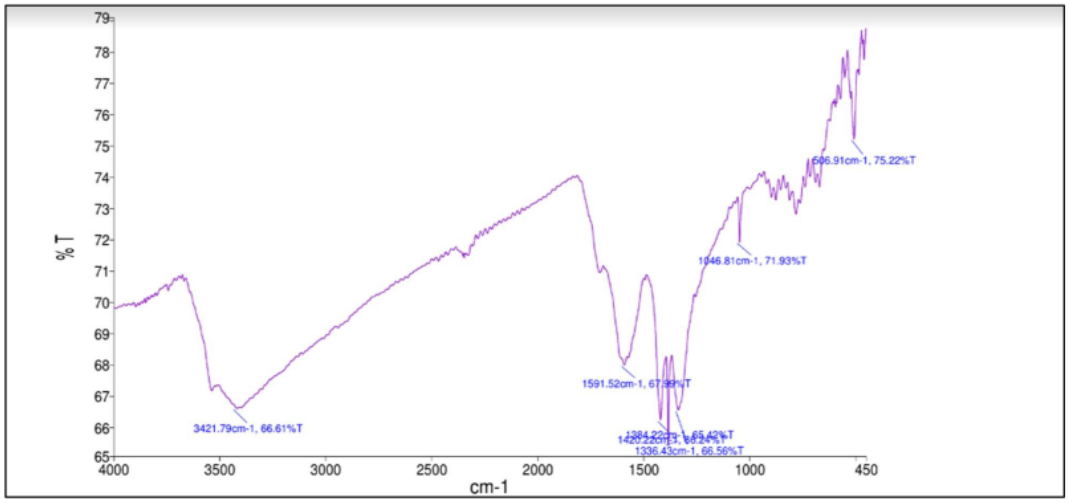

Fig. 5.1(c): FTIR spectra of SBAC (activated SB biochar)

(b) FTIR of Alginate, bentonite and Alginate-bentonite/SBAC

Table 5.1(b): IR absorption bands and corresponding possible groups of Alginate, bentonite and Alginate-bentonite/SBAC

Wavenumbers (cm^{-1})			**Functional groups**
Alginate	***Bentonite***	***Alginate-bentonite/SBAC***	
-	3696.95, 3621.73	-	Al-OH-Al stretching vibration
3429.61	3440.73	3334.95, 3257.44 and 3263.72	O–H stretching vibration
1630.34	1638.30	1599.79, 1417.09	symmetric and asymmetric stretching of the COO-
1024.70	-	-	C-O starching of carboxylic acid
1035.57	1031.82, 912.92	1046.81	Si-O stretching
-	-	1004.19	polysaccharide structure of alginate
-	771.58	-	SiO_2 stretching vibration
-	527.22	-	Al-O-Si stretching vibration
-	468.03	-	deformation of Si-O-Si

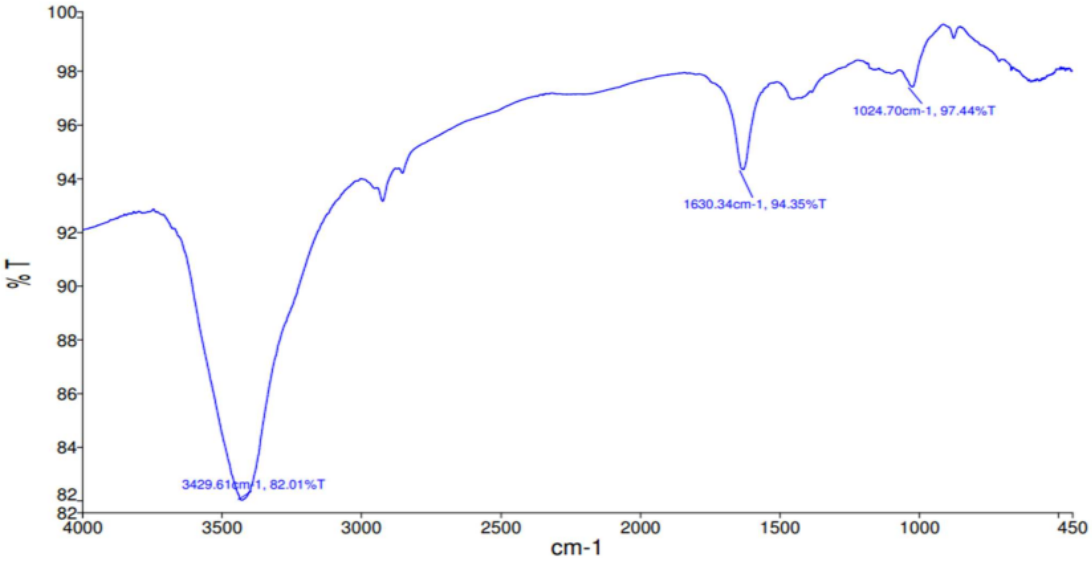

Fig. 5.1(d): FTIR image of Alginate

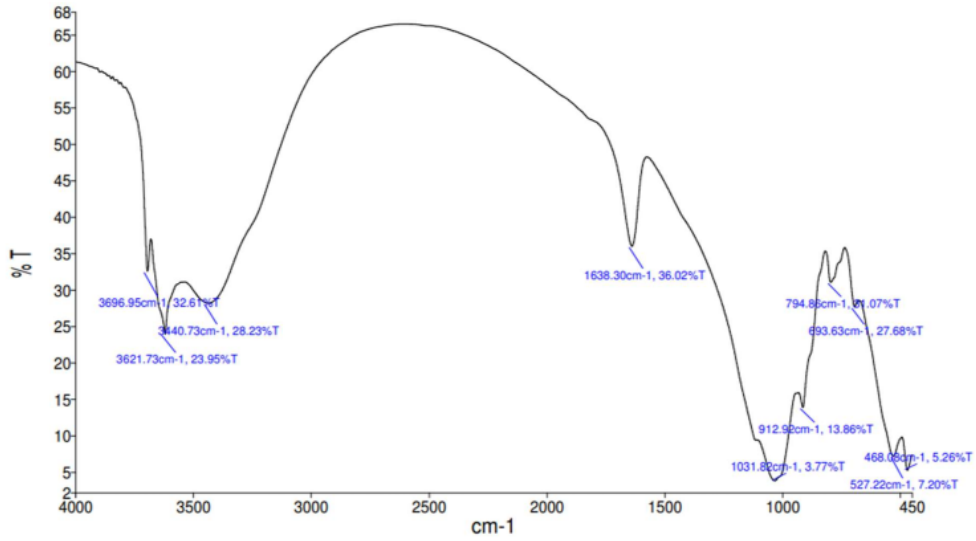

Fig.5.1(e): FTIR image of Bentonite

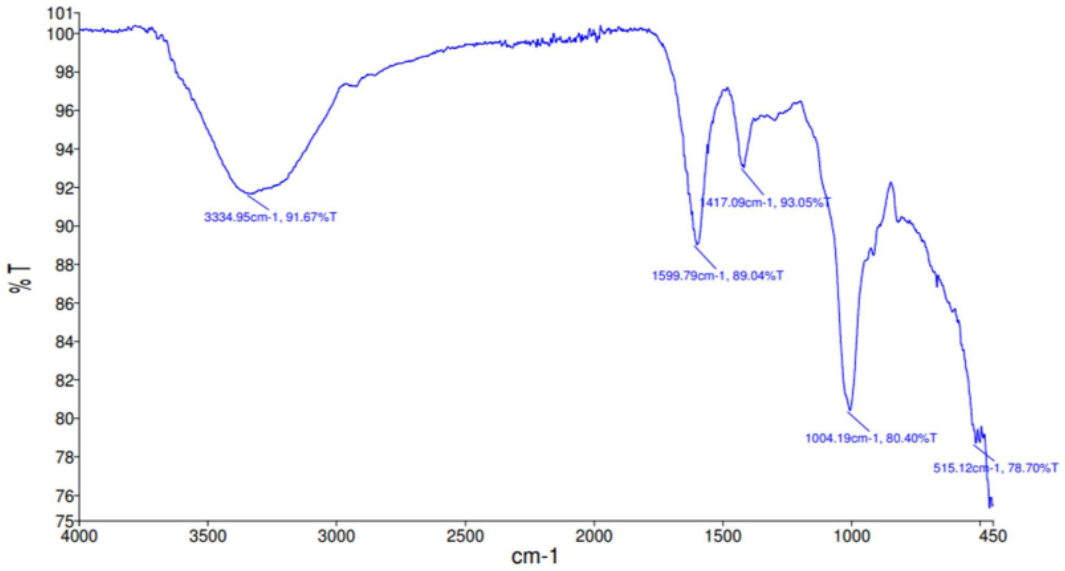

Fig. 5.1(f): FTIR image of Alginate-bentonite/SBAC beads

(c) FTIR of cellulose, PVA and Nanocellulose/PVA

Table 5.1(c): IR absorption bands and corresponding possible groups of cellulose, PVA and Nanocellulose/PVA

Wavenumbers (cm^{-1})			**Functional groups**
Nanocellulose	**PVA**	**Nanocellulose/PVA**	
3328.63	3431.25	3500-3100	OH stretching vibration
2987.63, 2901	-	2938.91	C-H stretching vibration
-	1632.18	1645.89	C-O stretching vibration
-	-	1411	CH_2 vibration
-	-	1377.33	CH_2 deformation vibration
1157.83	-	1167-900	$C-O-C$ and $C-O$ bending vibrations of the β-glycosidic linkages
-	-	1141.95, 1083.54	acetyl linkage
1056.5	1032.73	-	C-O-C stretching vibration
893.31	-	835.58	C-O-C stretching

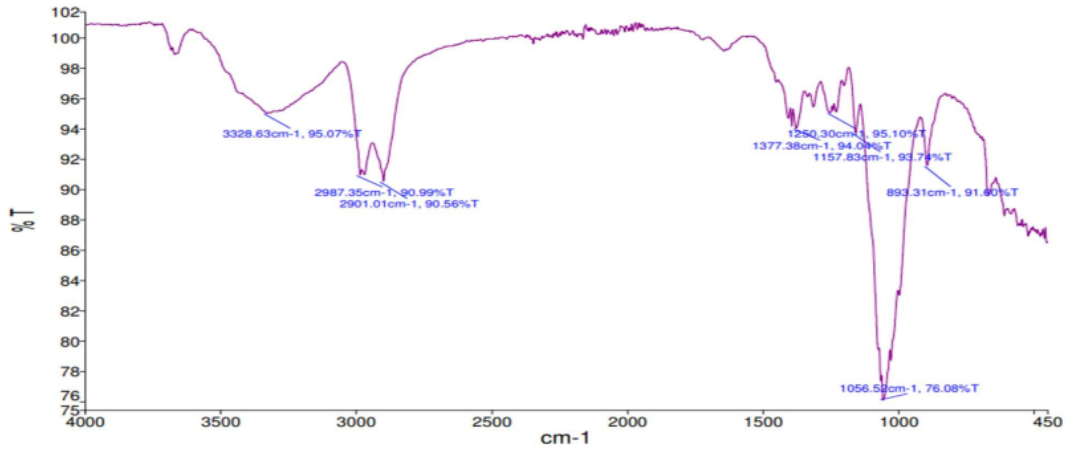

Fig. 5.2(a): FTIR spectra of Nanocellulose

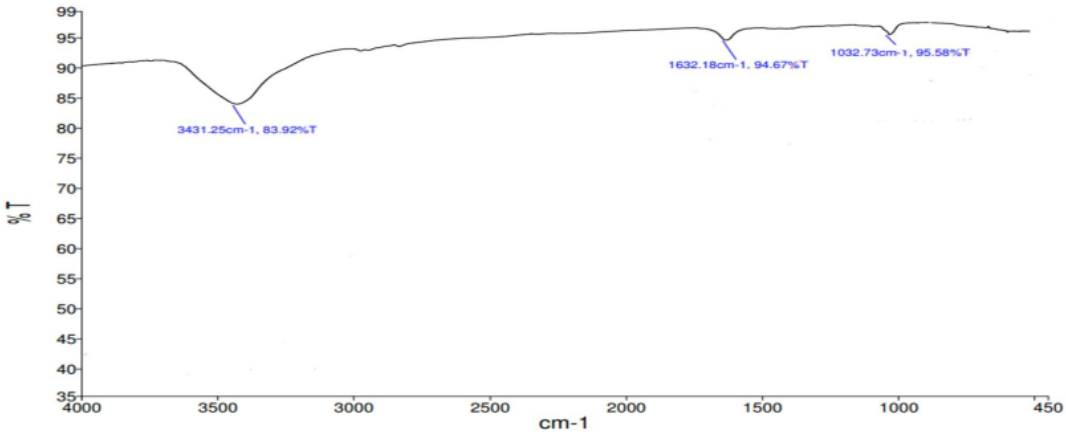

Fig. 5.2(b): FTIR spectra of PVA (Poly Vinyl Alcohol)

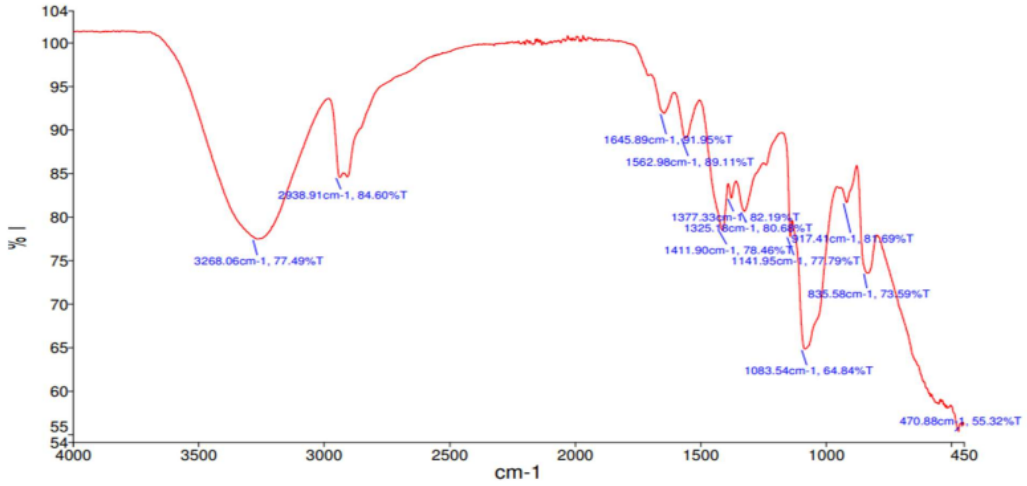

Fig. 5.2(c): FTIR spectra of nanocellulose/PVA composite hydrogel

(d) FTIR of Alginate-Nanocellulose beads

Table 5.1(d): IR absorption bands and corresponding possible groups of Alginate-Nanocellulose beads

Wavenumbers (cm^{-1})	Functional groups
Alginate-Nanocellulose beads	
3349.78	O-H group
1602.74	C-O-O stretching vibration
1006.63	C-O vibration vibration
513.77	Si-O stretching
2107.55	C-H stretching vibration
1427.95	CH_2 vibration
1303.19-913.90	C – O – C and C – O bending starching
813.99	C-H stretching

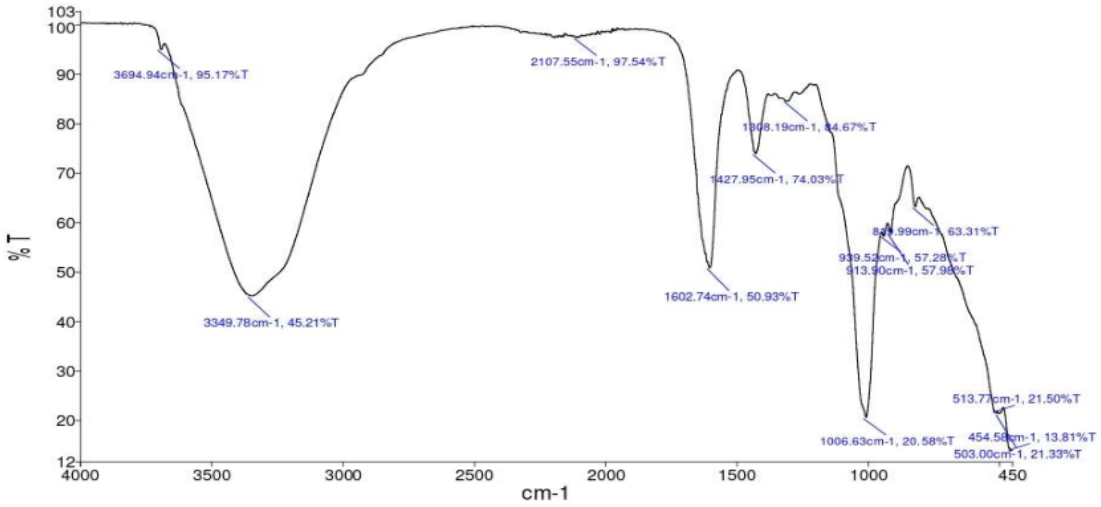

Fig. 5.3: FTIR spectra of Alginate-Nanocellulose composite beads

(ii) BET analysis results

BET results indicated that with increase in the relative pressure, the adsorbed volume of nitrogen by SBAC increased which signified the existence of micropores and mesopores on the surface of prepared adsorbent. From the BET analysis, the surface area of activated biochar (SBAC) was determined as 51.76 m^2/g; the derived value of total pore volume was

2.324×10^{-02} cc/g for pores smaller than 7.8 Å (Radius) at a relative pressure of 0.10058 and micropore volume was 0.0130 cc/g for 44.41% of mesoporosity.

Synthesized Alginate-bentonite/SBAC composite beads possess pore size of 7.8 Å (radius), BET surface area of 82.23 m^2/g, total pore volume of 0.0253 cm^3/g at P/Po = 0.10058 and micropore volume=0.01286 cm^3/g with mesoporosity (%) of 42.17.

(iii) SEM image of prepared composites

(a) SEM image of SB and Activated SB biochar:

The SEM image showed the highly adsorptive features of activated biochar with full of hollow space and deep cracks (Fig. 5.4(b)) compared to untreated raw SB powder (fig. 5.4(a)). The surface topography of the prepared chemically activated biochar is a significant point for adsorption. The micro and mesopores present in activated biochar acts as adsorptive active binding sites for the adsorption process. The thermal and chemical activation of biochar increased the numbers of these pores. Activating agent NaOH increases the mesopores in biochar.

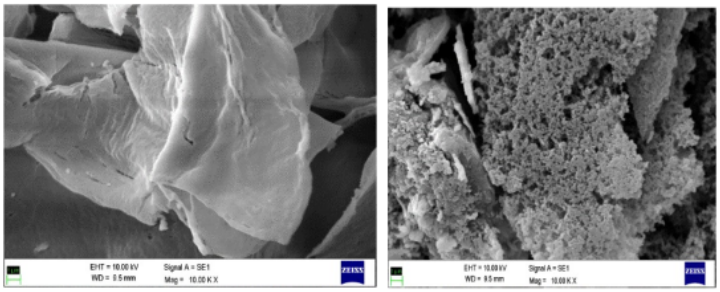

Fig. 5.4: SEM image of SB (a) and SEM image of Activated SB biochar (b)

(b) SEM image of Alginate-bentonite /SBAC beads:

Scanning electron microscopic analysis was conducted to demonstrate the surface topography of the Alginate-bentonite/SBAC composite bead. The SEM image (Fig. 5.5 (b)) of the prepared composite confirmed the successful formation, homogeneous dispersion of the component and porous structure on the composite surface.

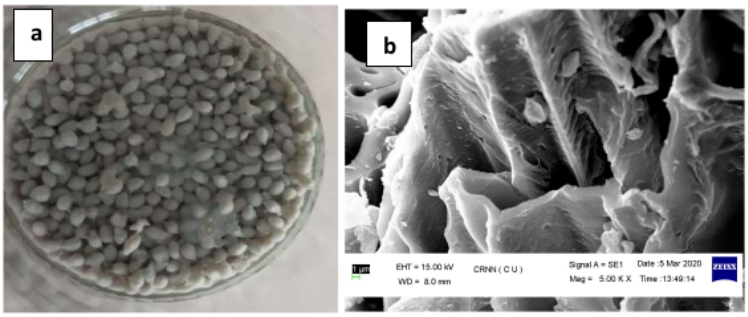

Fig. 5.5: Image of Alginate-bentonite/SBAC beads (a), SEM image of Alginate-bentonite /SBAC beads (b)

(c) *SEM image of nanocellulose/PVA composite*:

SEM image (Fig. 5.7(a)) of the cellulose nanocrystal (Nanocellulose) obtained from sugarcane bagasse indicated that there was a decrease in the size of fibrillar structure and irregular breakdown in fibril structure. SEM image (Fig. 5.7(b)) of polymer composite suggested that the nanocelluloses were dispersed uniformly in the polymeric composites. The rough surface on the nanocellulose/PVA polymer composite was due to the restriction of the spread of crack by the existence of better interaction between nanocellulose and PVA. Overall, The SEM image of nano-cellulose/PVA ensured the successful developmentof thepolymeric composite and adsorptive porous structure on the composite surface that facilitated to improve adsorption efficiency.

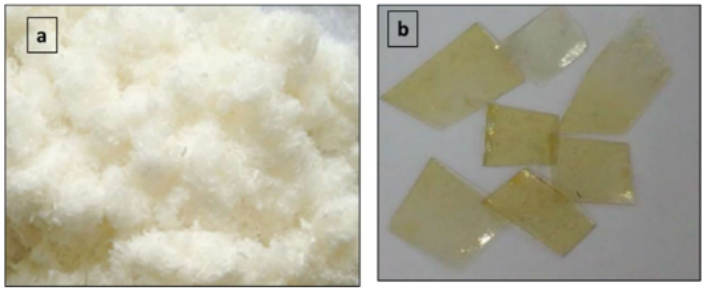

Fig. 5.6: Image of extracted cellulose (a), and prepared nano-cellulose/PVA hydrogel film

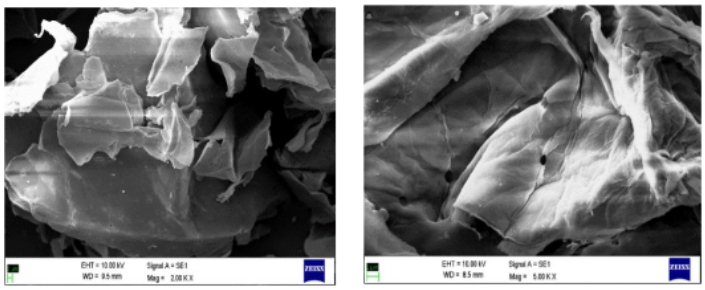

Fig. 5.7: SEM image, of cellulose nanofiber (a), nanocellulose/PVA composite (b)

***(d) SEM image of* Alginate-Nanocellulose composite:**

SEM image of derived Alginate-Nanocellulose composite has been presented Fig. 5.8(b). Characterized surface topography of the prepared composite indicate that adsorbent has porous structure in nature which helps to increase adsorption capability (Abdelrahman & Hegazey, 2019).

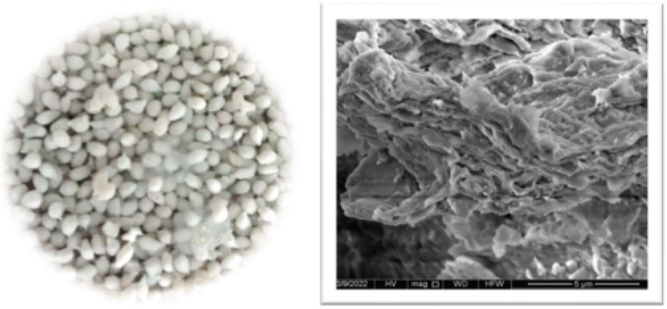

Fig. 5.8: Image of Alginate-Nanocellulose beads (a) SEM image of Alginate-Nanocellulose composite (b)

(iv) TGA analysis

(a) TGA Thermogram of Alginate-Bentonite/SBAC:

TGA thermogram curves of synthesized Alginate-Bentonite/SBAC composite beads are shown in Fig. 5.9(a). The analysis indicate that dehydration of sample mass started at 350- 400° C. At a temperature range of 400 - 550 °C major degradation took place in composites. This suggest that synthesized composite beads has high thermal stability.

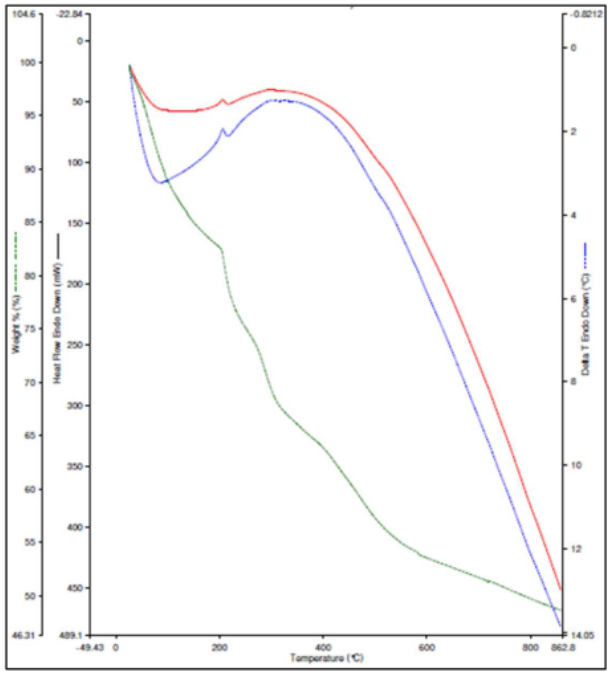

Fig. 5.9(a): TGA Thermogram of alginate-bentonite/SBAC beads

(b) TGA Thermogram of cellulose, PVA and Nanocellulose/PVA composite:

Thermogravimetric analysis (TGA) was analyzed to investigate the characteristic properties of PVA (Fig. 5.9(b)), extracted cellulose (Fig. 5.9(c)), and synthesized nano-cellulose/PVA polymer composite (Fig. 5.9(d)). In order to estimate the thermal stability and the intermolecular interaction between nano-cellulose and PVA in polymers composite, TGA analysis was conducted by measuring weight loss with time at definite temperature ranges. Fig. 5.9(d) showed that in the initial degradation was started from 80 °C. 2nd stage started from 220°C and from this point nanocellulose/PVA polymeric composites showed a higher percentage weight loss. Similar results have been noted by Ibrahim et al., (2010) and Ching et al., (2015). At the third stage of the degradation in the thermograms curve (TGA) (Beyond 480°C) nanocellulose/PVA were found to be more thermally stable compare to cellulose and PVA. On account of the inclusion of nanocellulose, thermal stability of nanocellulose/PVA composites increased. TGA curve of composite showed that the final degradation achieved at 480 °C which suggested that the thermal stability of prepared polymer composite was relatively higher than precursor components (i.e., PVA and cellulose)(Ng et al., 2015).

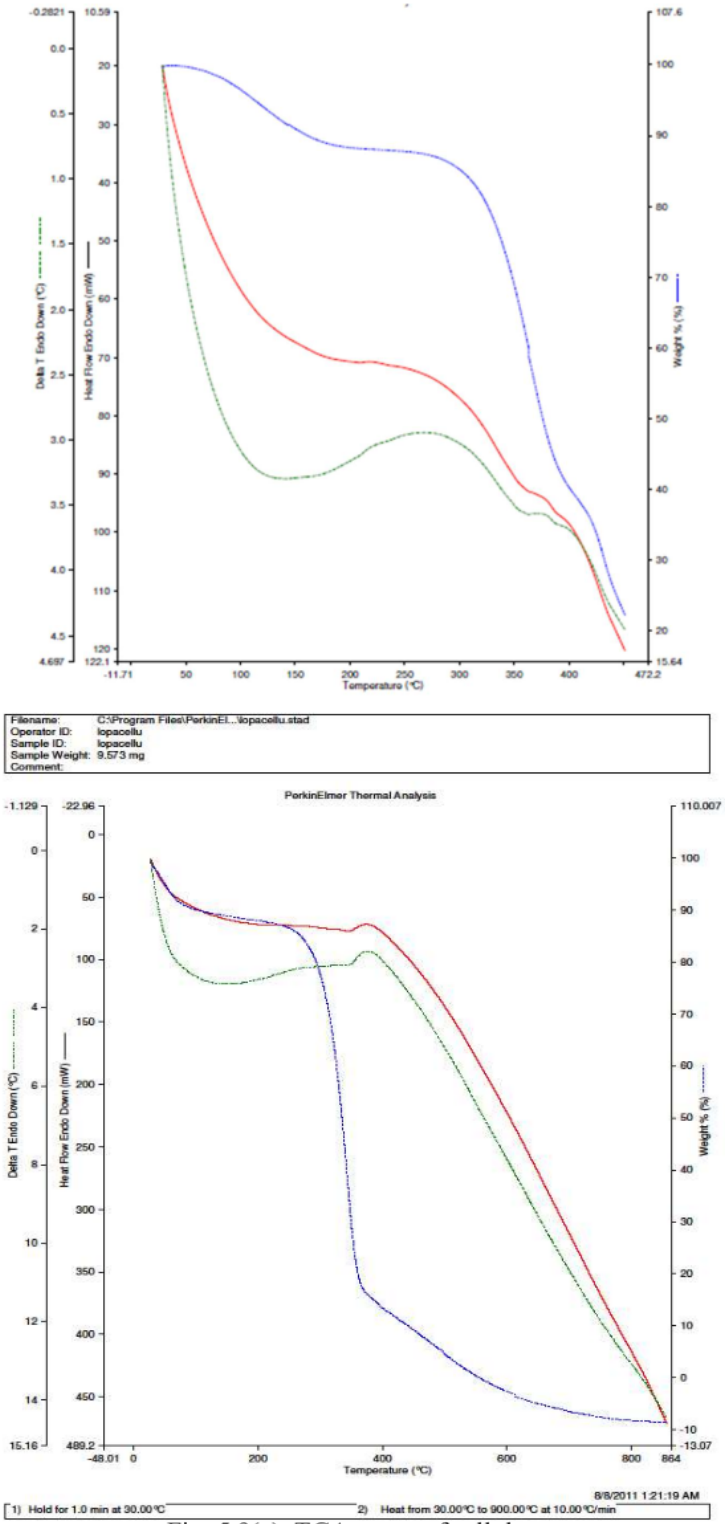

Fig. 5.9(c): TGA curve of cellulose

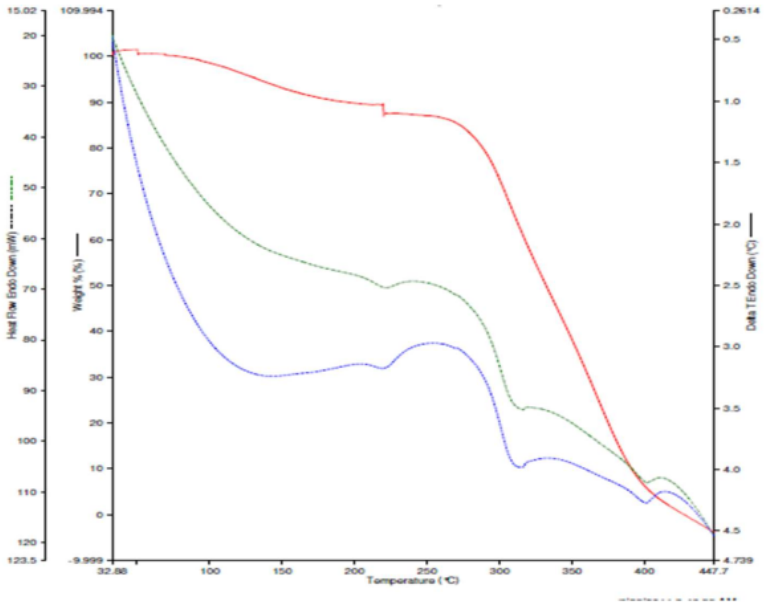

Fig. 5.9(d): TGA curve of nanocellulose/PVA

(c) TGA Thermogram of Alginate-nanocellulose composite:

TGA graph of alginate-nanocellulose composite as shown in Fig. 5.9(e) indicated that initial decomposition phase started after 150 ^{o}C temperature and at 350 ^{o}C temperature the final degradation state reached. This revealed that the high thermal stability of synthesized alginate-nanocellulose beads.

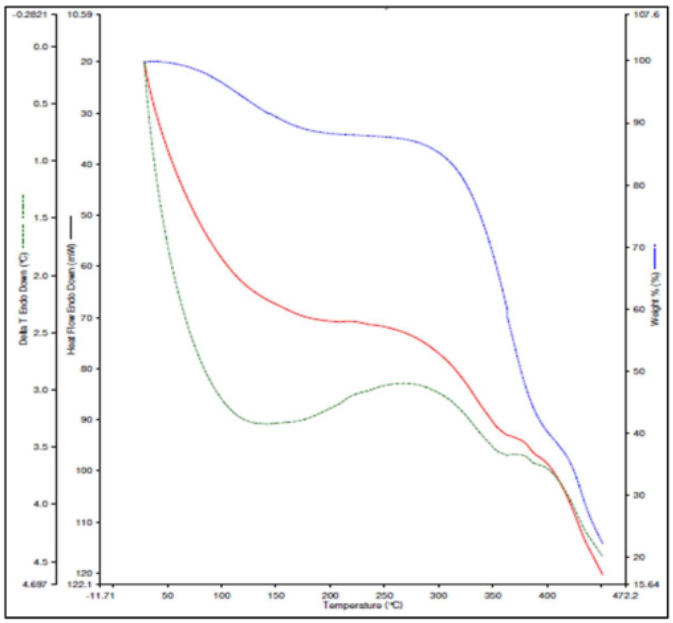

Fig. 5.9(e): TGA graph of Alginate-Nanocellulose composite

(iv) PZC results

(a) PZC curve of SB and SBAC:

PZC (Point zero charge characterization) of an adsorbent signifies the pH at which density of electrical charges on the composite surface becomes zero. PZC of SB (Fig. 5.10(a)) and SBAC (Fig. 5.10(b)) were found to be 6.5 and 7.5, respectively. At higher solution pH (pH>PZC) adsorbent surface become negative charged whereas, for pH<PZC the adsorbent surface become positive charged.

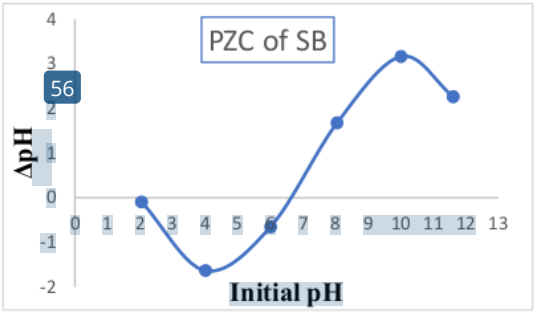

Fig. 5.10 (a): PZC graph of SB

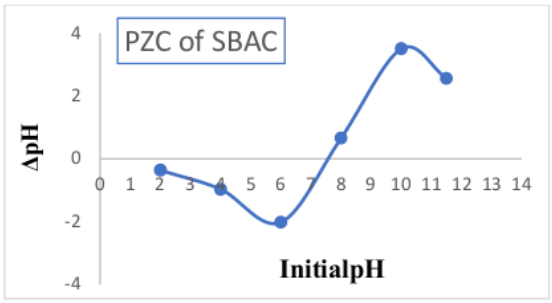

Fig. 5.10 (b): PZC graph of SBAC (activated biochar)

(b) PZC curve of Alginate-bentonite/SBAC beads:

The ΔpH vs. $pH_{initial}$ curve for Alginate-Bentonite/SBAC is shown in Fig. 5.10(c). PZC of Alginate-bentonite/SBAC composite is 6.37.

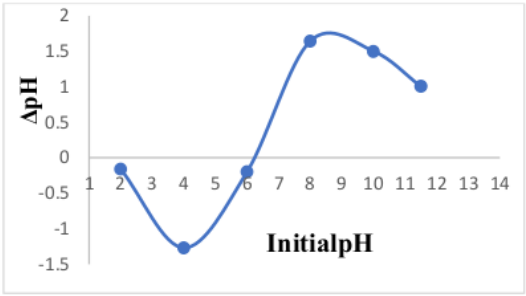

Fig. 5.10 (c): PZC curve of Alginate-bentonite/SBAC beads

(c) PZC curve of nanocellulose/PVA:

PZC characterization of prepared nanocellulose/PVA polymeric composite was determined to evaluate the nature of the charges present on the surface of the nanocellulose/PVA polymeric composite. From the Fig. 5.10(d), it was observed that the PZC value of nanocellulose/PVA was at pH 6.8.

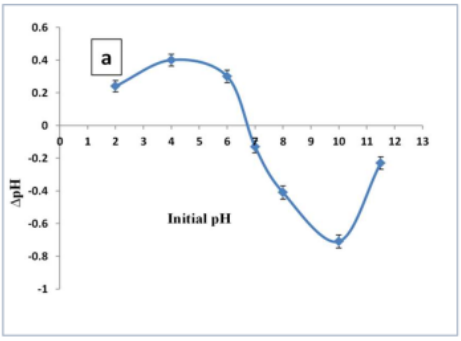

Fig. 5.10 (d): PZC curve of the nano-cellulose/PVA composite

(d) PZC curve of Alginate-nanocellulose beads:

It is noted from Fig. 5.10(e) that the point zero charge value of Alginate-nanocellulose composite beads was attained at pH 6.5.

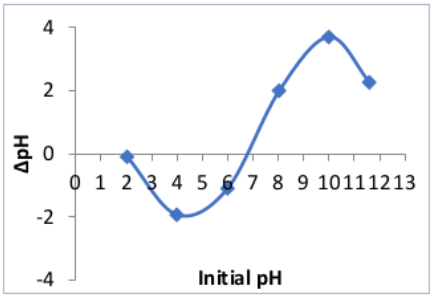

Fig. 5.10(e): PZC curve of Alginate-nanocellulose beads

5.2.2. Batch study results for MG dye adsorption onto prepared biosorbents

5.2.2.1. Comparative batch study using prepared biosorbents

Removal efficiency of prepared biosorbents at various experimental conditions are presented graphically in Fig. 5.11, Fig. 5.12, Fig.5.13, Fig.5.14 and Fig. 5.15. The effectiveness of prepared composite for MG dye removal was evaluated by comparing the results with individual components/ base materials of the composite under various operational conditions. The equilibrium concentration of dye in the solution are illustrated in Fig. 5.16-5.22. It is seen that under all experimental conditions Alginate-Nanocellulose composite beads showed better result for dye removal as compared to the base material of the composite and other composites. Fluoride removal efficiency and adsorption capacity of Alginate-Nanocellulose composite found to be higher than the other biosorbents (raw SB, SBAC, Alginate-bentonite/SBAC and Nanocellulose/PVA) under all experimental conditions.

Influence of pH

The influence of pH level on dye removal efficiency was observed using prepared adsorbents by contacting adsorbent dosage of 1g/L with 100 mol of dye solution of initial concentration of 20 mg/L at a specified solution pH and 30°C temperature for 24 hr. With SBAC, the removal efficiency was least at pH=2.0 (82.184%) and maximum at pH=8 (95.656 %) (Fig. 5.11(a)). The residual concentration of MG decreased from 3.563 to 0.8688 mg/L with increasing pH from 2 to 8.0. The adsorption efficiency of Alginate-bentonite/SBAC increased with pH. Under acidic condition (pH<7) MG removal efficiency of this composite beads was 86.85%. Adsorption efficiency increased to ≈99% at pH=8 (Fig. 5.11(b)). The corresponding concentration of dye in the solution at pH 2.0 and 8.0 was 2.63 mg/L and 0.12 mg/L respectively. At pH 2, dye adsorption efficiency of Nanocellulose/PVA was 87.35% and at higher pH (pH=8) dye removal efficiency improved to 99.07% (Fig. 5.11(c)). At basic media (pH 8), MG dye adsorption efficiency onto Alginate-nanocellulose composite obtained was 99.45 %, whereas at acidic condition (pH=2) this value reduced to 88.54% (Fig. 5.11(d)).

At pH=7, MG dye adsorption efficiency onto Alginate-nanocellulose composite, Cellulose, and Alginate were obtained as 99.13 %, 91.4%, and 57.95 %, respectively. Results suggested that Alginate-nanocellulose composite beads gave better performance than individual components of the composite.

At acidic conditions, due to the presence of a large amount of H^+ ions protonation increases which restricted the adsorption of positively charged dye molecule to the adsorbent surface resulting in a decrease in adsorption ability of adsorbent (Chowdhury and Saha, 2010).When

pH of dye solution was lower than the value of pH_{PZC}, decreasing trend of the biosorption efficiency for cationic MG dye removal was noticed as the adsorbent surface become electropositive at pH< pH_{PZC}, while at higher pH (pH > pH_{PZC}) adsorbent surface become predominantly negative charged that lead to increase in the cationic dye adsorption efficiency.

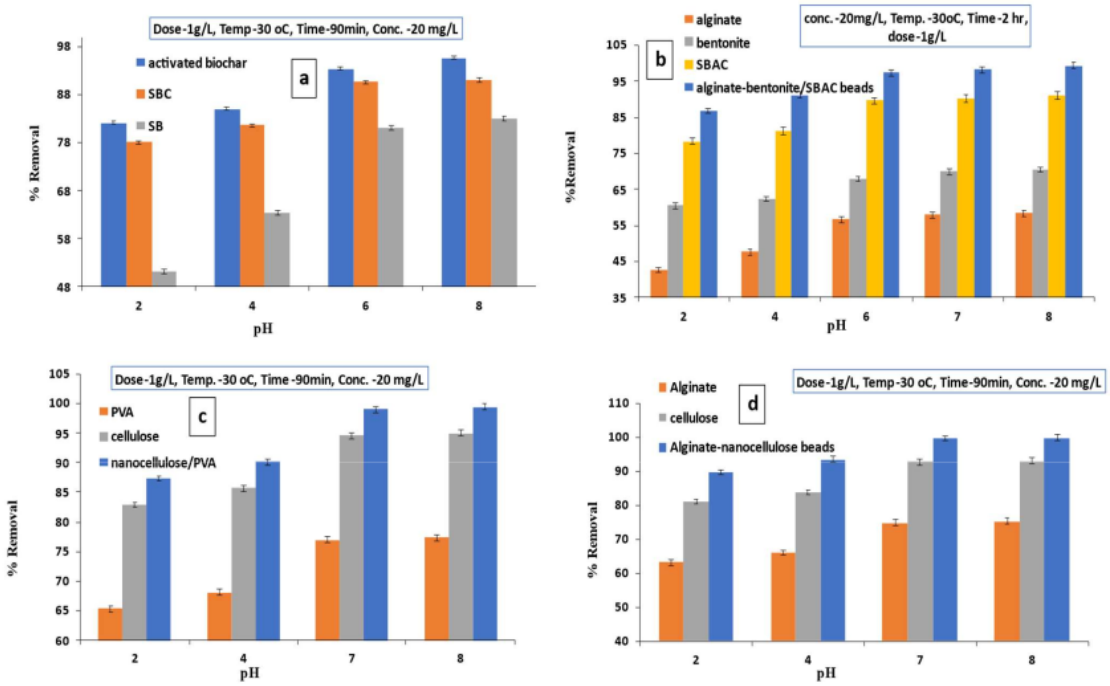

Fig.5.11: Effects of solution pH on MG dye removal efficiency of activated biochar (a), Alginate-bentonite/SBAC beads (b), Nanocellulose/PVA composite (c) and Alginate-nanocellulose beads (d)

Influence of contact time

MG dye adsorption experiment was carried out at different time interval by contacting 1g/L of adsorbent dose to the adsorbate solution (initial dye concentration of 20 mg/L) at pH 6 in a BOD shaker at 30°C under shaking speed of 140 rpm. Samples were taken out at specified time intervals. Most of the adsorption of dye took place within the first 45 min (Fig. 5.12) for all adsorbents. With increasing the contact time, dye removal efficiency of SB was increased from 58.47% to 83.05% and in case of SBAC that increased from 74.21 to 93.45% (Fig. 5.12(a). similarly, using Alginate-bentonite/SBAC composite beads as adsorbent, the dye removal efficiency increased from 78.41% to 97.75% MG dye removal efficiency of nanocellulose/PVA was found to be increased from 86.43% to 99.07% (Fig. 5.12(c)). The

decolorization efficiency Alginate-nanocellulose increased from 87.62% to 99.47 % (Fig. 5.13(d)).

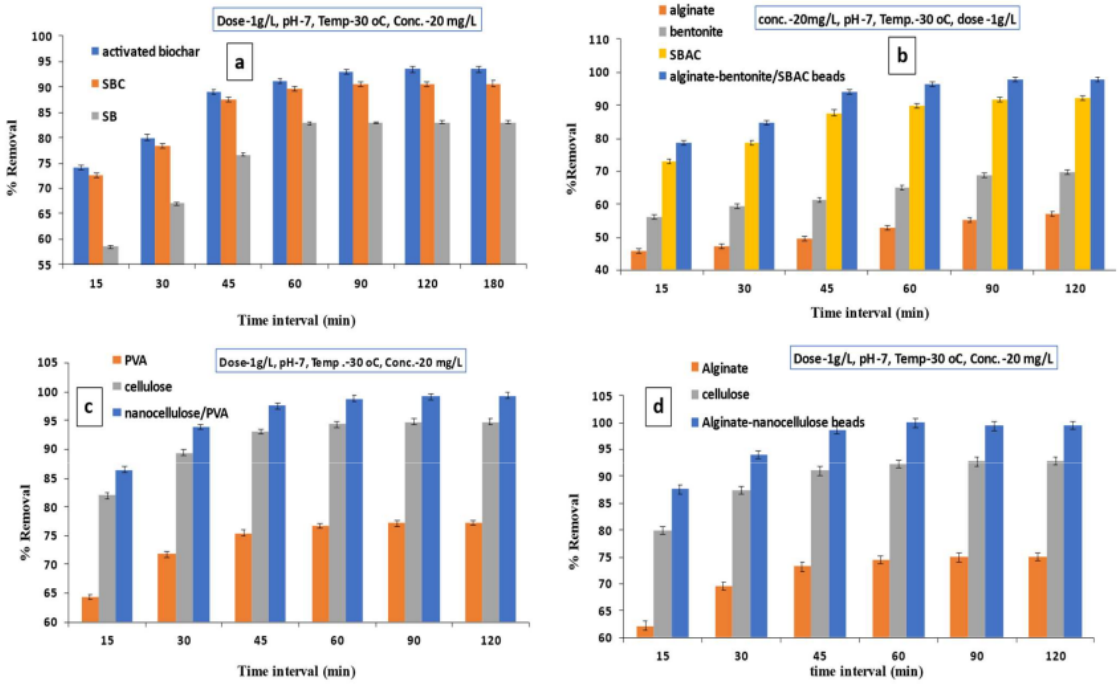

Fig. 5.12: Effects of contact time on MG dye removal efficiency of activated biochar (a), Alginate-bentonite/SBAC beads (b), Nanocellulose/PVA composite (c) and Alginate-nanocellulose beads (d)

Influence of adsorbent dosage

The adsorbent dosage is another significant parameter for the MG dye adsorption process. To investigate the adsorption response behaviour at different adsorbent doses (0.5g/L-2g/L), batch experiment was performed in a BOD shaker for 24 hr while the other parameters were constant (such as temperature=30°C, initial concentration =20 mg/L, pH=6). It was noticed that as the amount of synthesized adsorbent mass increased from 0.5g/L to 2g/L, % removal of MG dye on SBAC increased from 87.32 to 93.87% (Fig. 5.13(a)). On increasing mass of Alginate-bentonite/SBAC composite beads from 0.25g/L to 1g/L, the removal percentage of MG dye increased from 88.05 to 98.01% (Fig. 5.13(b)). With increasing adsorbent dose from 0.25 g/L to 1 g/L, dye adsorption efficiency of nanocellulose/PVA composite increased from 93.16% to 99.07% (Fig. 5.13(c)) and equilibrium concentration in residual solution decreased from 1.368 to 0.186 mg/L. With increasing dosage of Alginate-nanocellulose from 0.25 g/L to 1 g/L, dye adsorption efficiency increased from 93.16% to 99.07% (Fig. 5.13(d)) and equilibrium

concentration decreased from 1.368 to 0.186 mg/L. This is because initially, when we increase the amount of adsorbent, for the same solution concentration, the number of active sites available per unit molecule of adsorbate increases, resulting in a higher rate of adsorption (Jaman et al., 2009; Hameed, 2009).

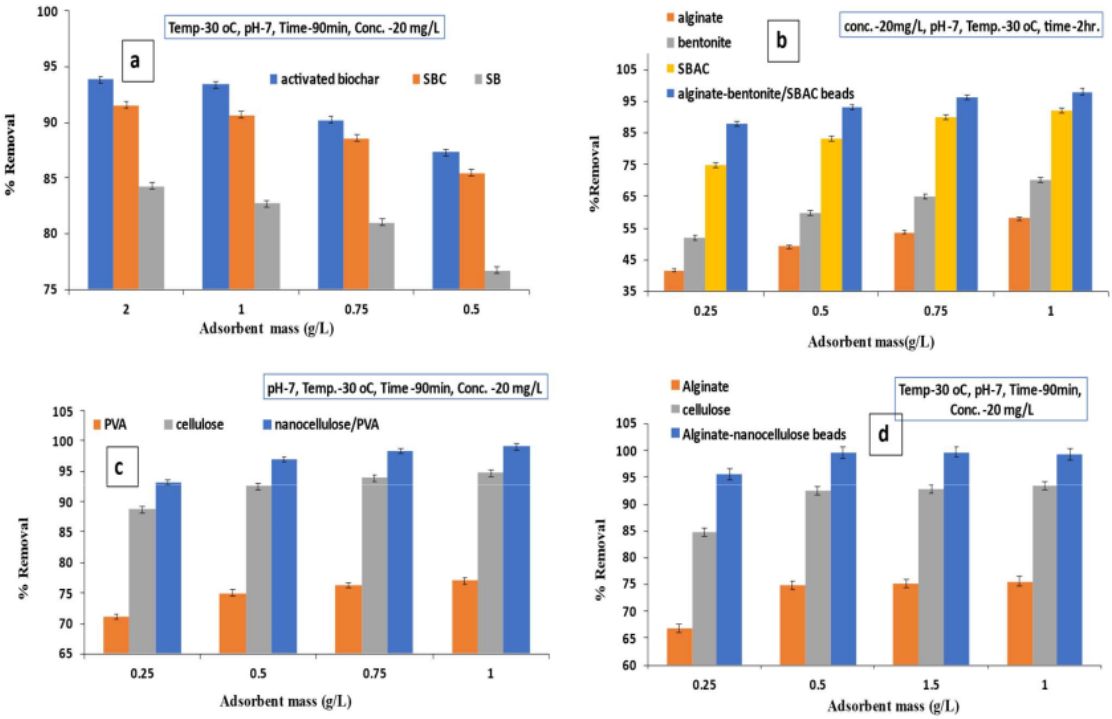

Fig. 5.13: Effects of Adsorbent dosage on MG dye removal efficiency of activated biochar (a), Alginate-bentonite/SBAC beads (b), Nanocellulose/PVA composite (c) and Alginate-nanocellulose beads (d)

Influence of adsorbate concentration

This set of experiments were carried out by contacting adsorbent dosage of 1 g/L with adsorbate solution at pH 7 in a BOD shaker for 24 hr at 30 °C. When initial MG concentration increased from 5mg/L to 20mg/L, MG dye uptake efficiency of SBAC reduced from 94.2% to 93.45% (Fig. 14(a)). Fig. 14(b) suggest that Alginate-bentonite/SBAC beads show higher MG dye uptake efficiency (97.6829% at 20 mg/L of initial concentration in MG dye solution) compared to Alginate, bentonite and SBAC. Similarly, with increase in initial MG concentration in solution from 15 mg/L to 50 mg/L removal efficiency of nanocellulose/PVA composite decreased from 99.45% to 94.87% ((Fig. 5.14(c)) and equilibrium dye concentration in solution increased from 0.084 mg/L to 2.565 mg/L. Fig. 5.14(d) showed that with varying concentration

from 15 to 50 g/L, percentage of MG dye adsorption reduced from 99.78 % to 90.081 % using Alginate-nanocellulose composite as adsorbent. With increasing dye concentration, competition for active adsorptive sites increased which reduces the removal efficiency due to the unchanged number of active adsorptive sites. With an increase in initial concentration (keeping all other parameters constant), the number of competing molecules for each vacant site is more. Hence the adsorption rate is lower.

Results suggested that under all experimental conditions Alginate-Nanocellulose composite beads showed better result for MG dye removal as compared to other prepared composites.

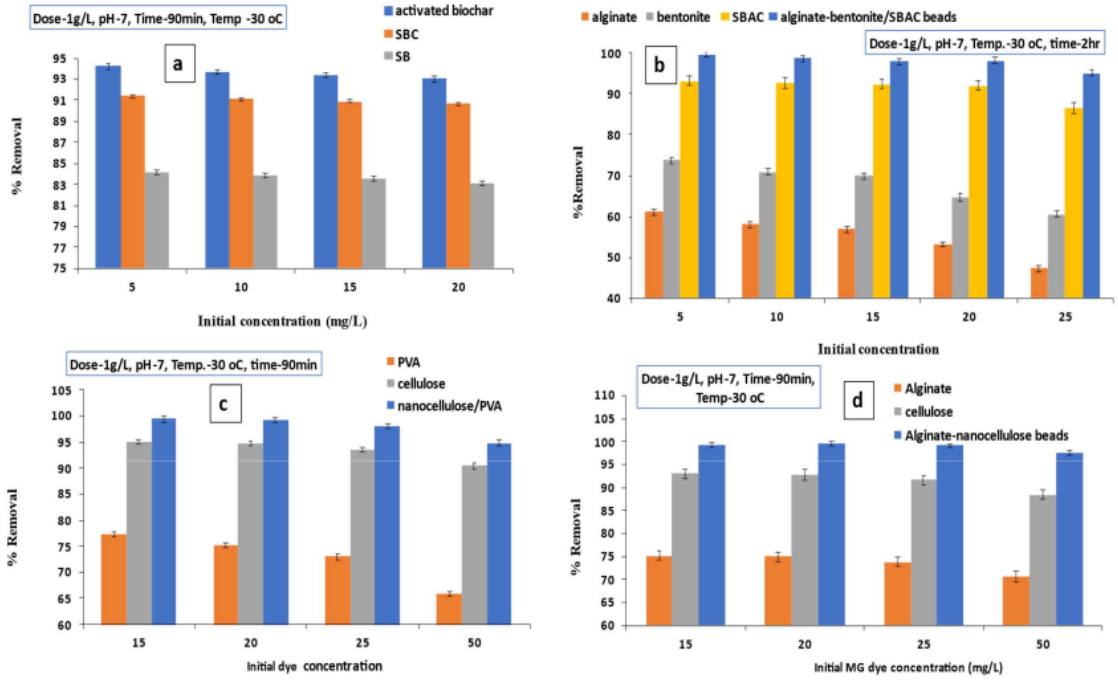

Fig. 5.14: Effect of initial adsorbate concentration on MG dye removal efficiency of activated biochar (a), Alginate-bentonite/SBAC beads (b), Nanocellulose/PVA composite (c) and Alginate-nanocellulose beads (d)

Influence of temperature

In these batch experiments, the temperature was varied from 30 to 45°C while other parameters kept constant (initial concentration of 20 mg/L, pH 6 and adsorbent dose of 1g/L, agitation speed of 140 RPM). Results (fig. 5.15(a) after 24 hr contact between adsorbent and adsorbate solution suggested that while system temperature increased from 30 °C to 45°C MG dye uptake efficiency of SBAC decreased from 93.45% to 90.13% and the equilibrium concentration of MG in the solution increased from 1.316 to 2.16 mg/L. Fig. 5.15(b) indicates that in case of

Alginate-bentonite/SBAC composite beads, dye uptake efficiency decreased (98.01% to 85%) on increasing system temperature from 30 °C to 45°C. For the same range in variation of temperature MG dye uptake efficiency of nanocellulose/PVA composite decreased from 99.07% to 90.69% (Fig. 5.15(c)) and the equilibrium concentration in the dye solution increased from 0.186 to 1.862 mg/L. Fig. 5.15(d) illustrated that as the temperature of system increased (30 °C to 45 °C), % removal of MG dye decreased (from 99.23% to 93.01% and 92.87 % to 85.4 % for Alginate-nanocellulose composite and cellulose, respectively). It is well known that the mobility of MG dye molecules is enhanced on increasing the system temperature. While the active sites on the adsorbent surface is reduces. High temperature (>40°C) facilitates the desorption process which reduces the adsorption efficiency and demote the interaction between the adsorbate and the binding sites at the bio-adsorbent surface (Chowdhury and Saha, 2010).

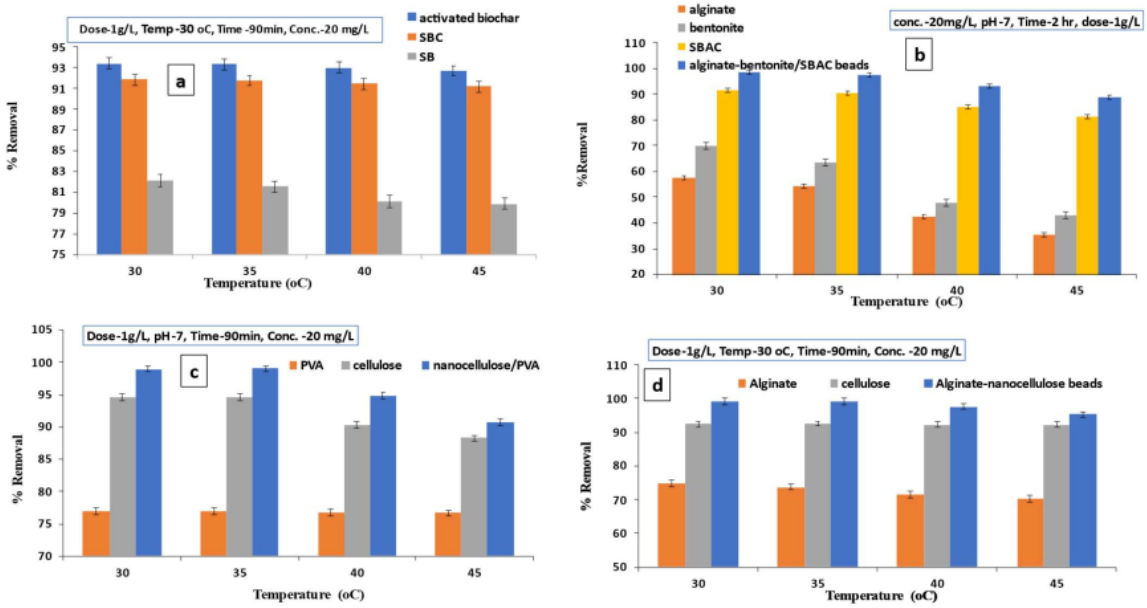

Fig. 5.15: Effect of initial adsorbate concentration on MG dye removal efficiency of activated biochar (a), Alginate-bentonite/SBAC beads (b), Nanocellulose/PVA composite (c) and Alginate-nanocellulose beads (d)

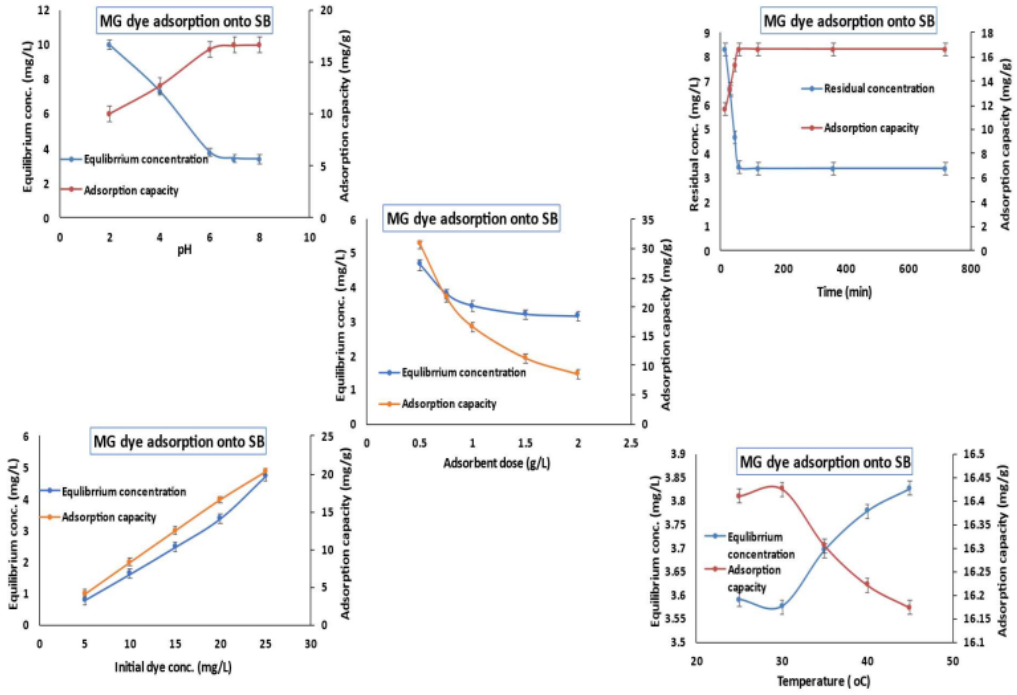

Fig. 5.16: Equilibrium concentration and MG dye adsorption capacity of raw SB at different experimental conditions

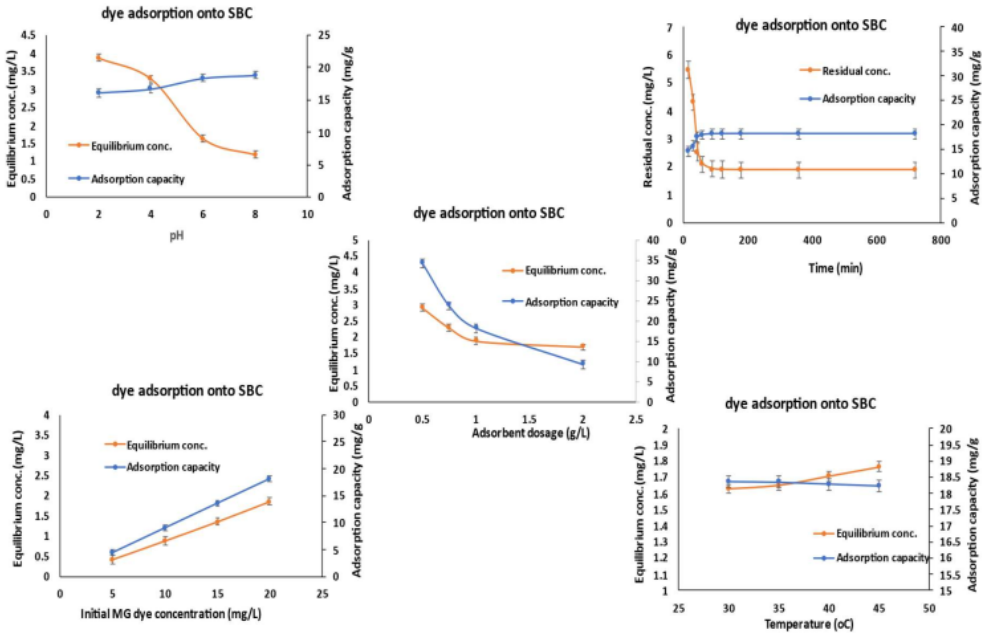

Fig. 5.17: Equilibrium concentration and MG dye adsorption capacity of SBC at different experimental conditions

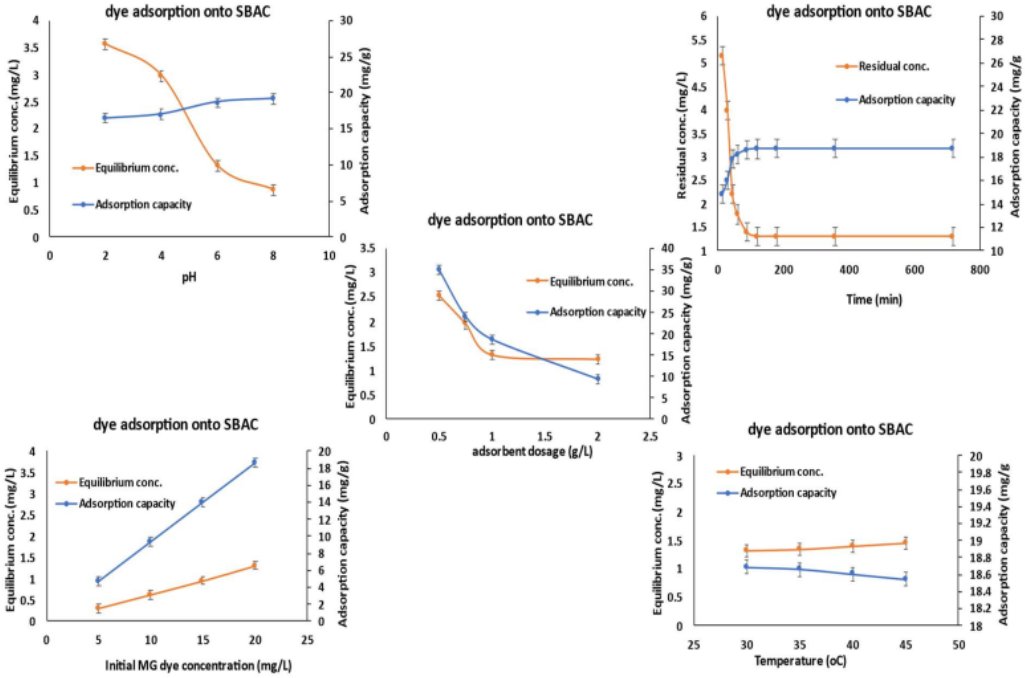

Fig. 5.18: Equilibrium concentration and MG dye adsorption capacity of SBAC at different experimental conditions

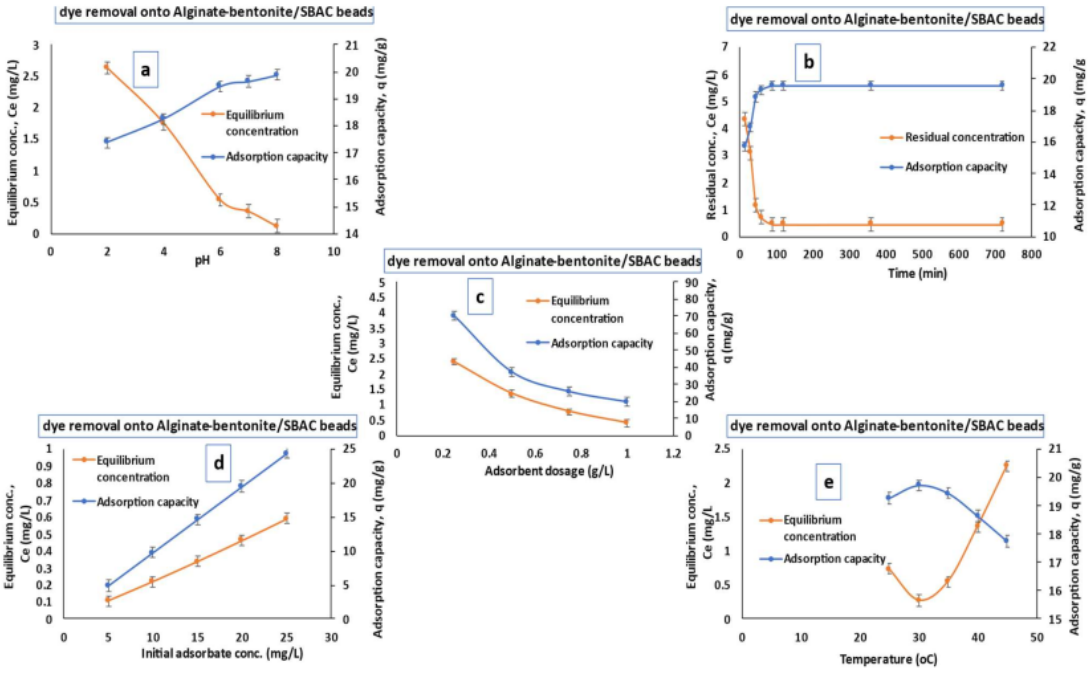

Fig. 5.19: Equilibrium concentration and MG dye adsorption capacity of Alginate-bentonite/SBAC at different experimental conditions

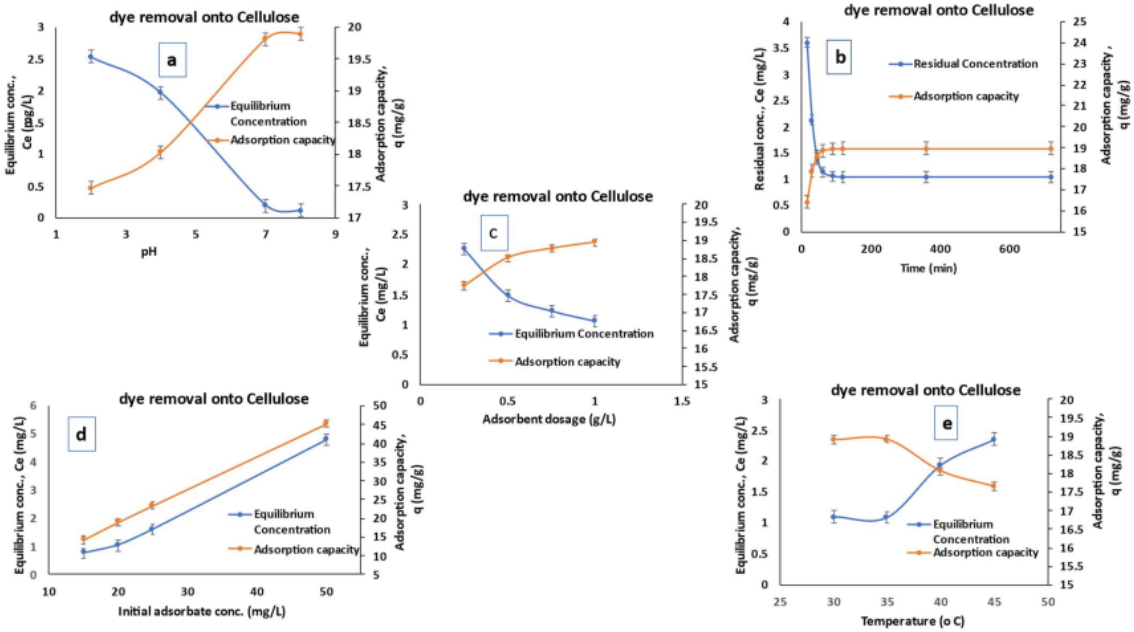

Fig. 5.20: Equilibrium concentration and MG dye adsorption capacity of cellulose at different experimental conditions

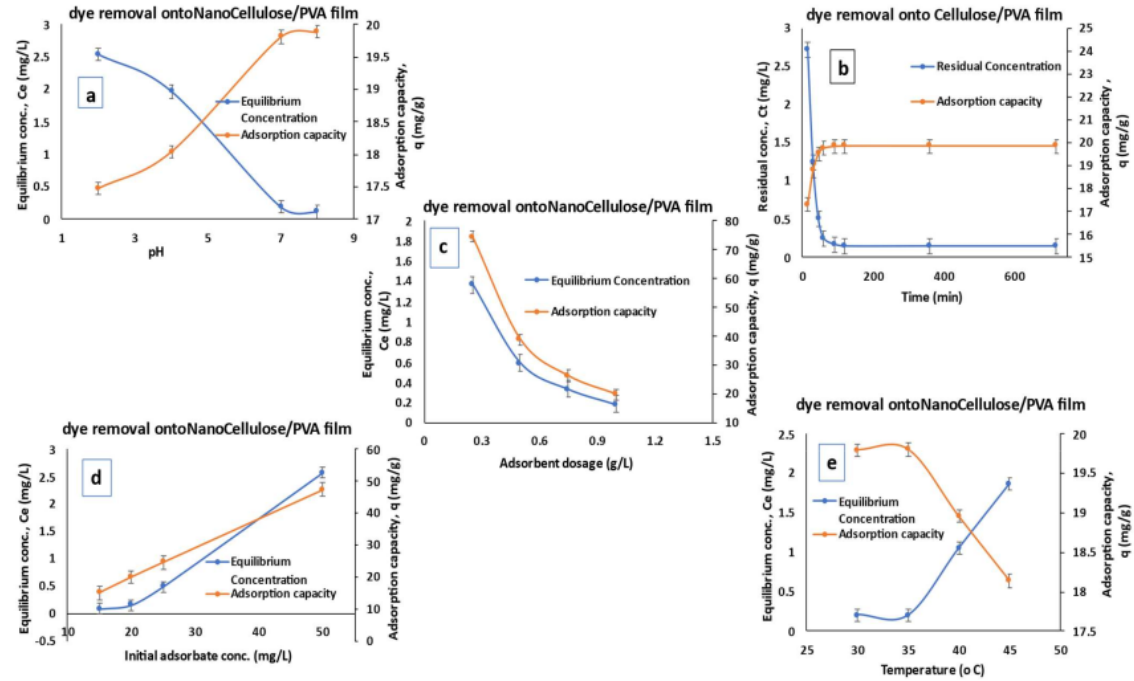

Fig. 5.21: Equilibrium concentration and MG dye adsorption capacity of Nano-cellulose/PVA hydrogel film at different experimental conditions

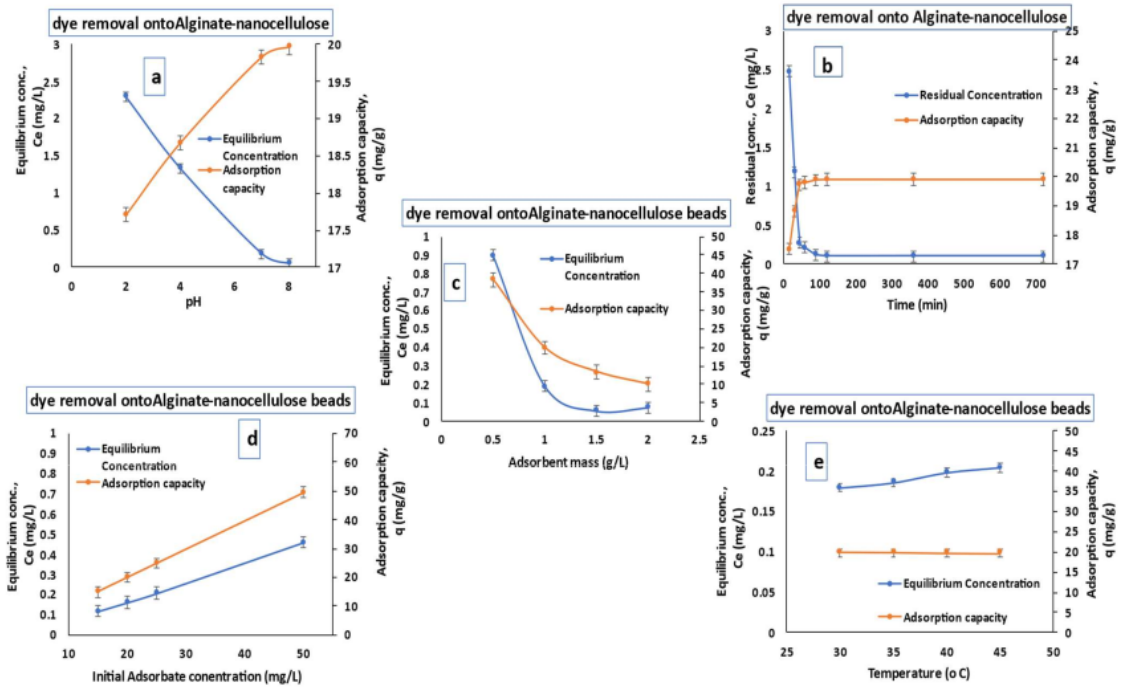

Fig. 5.22: Equilibrium concentration and MG dye adsorption capacity of cellulose at different experimental conditions

5.2.2.2. Results of Adsorption Isotherm Study

The fitting of equilibrium data to the adsorption isotherm models (Langmuir, Freundlich, and Temkin model) and corresponding graphs are presented in Fig. 5.24 to Fig. 5.27. The estimated values of Langmuir isotherm, Freundlich isotherm and Temkin model constants are presented in Table 5.2, Table 5.3 and Table 5.4, respectively. Initial adsorbate concentration ranges from 5 to 25 mg/L, while other parameters were kept constant (pH=7, adsorbent mass=1g/L, Temperature=30 °C). The result suggests that in general the Freundlich isotherm model (R^2>0.99) provided the best fit to the equilibrium adsorption data for all the adsorbents compared to the Langmuir isotherm (R^2≥0.98) or Temkin model (≥0.96). This signifies to the heterogeneous distribution of binding pores on the sorbent surface (Soleimani and Kaghazchi, 2007).

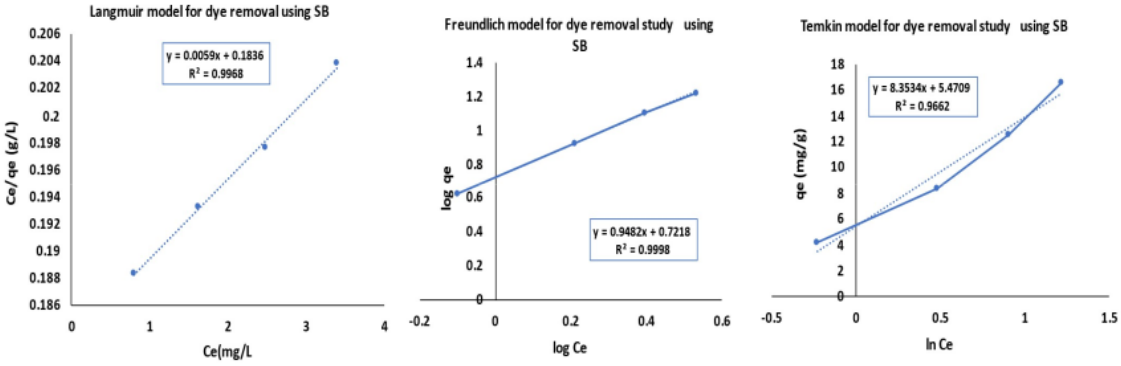

Fig. 5.23: Graphical presentation of Isotherm models for batch adsorption of MG dye onto raw SB

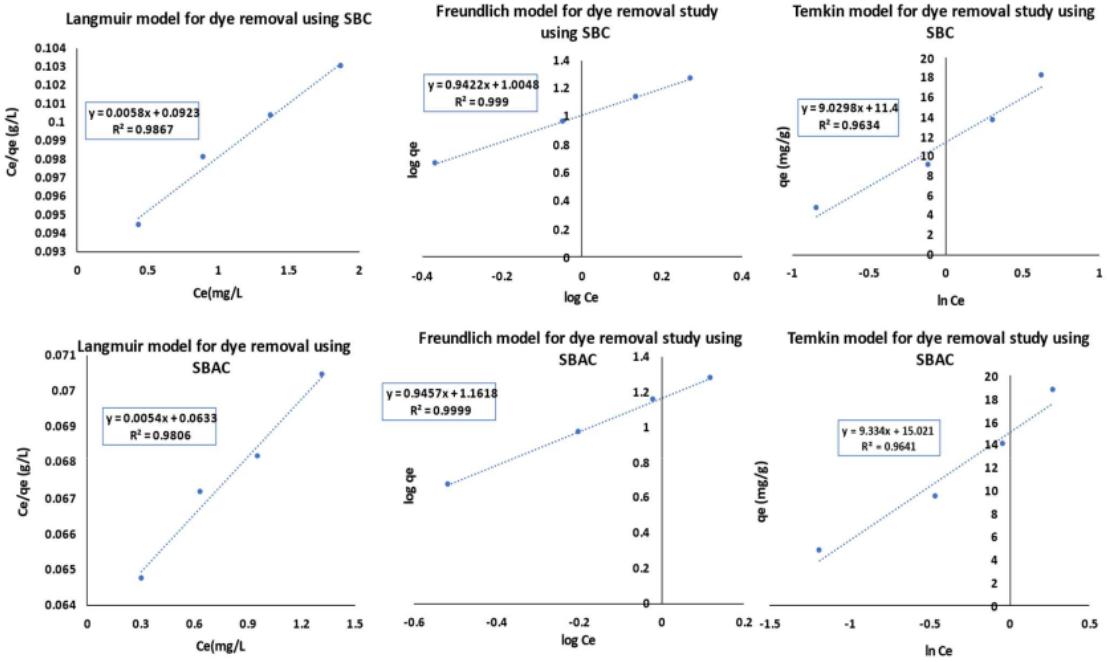

Fig. 5.24: Graphical presentation of Isotherm for batch adsorption of MG dye onto SBC and SBAC

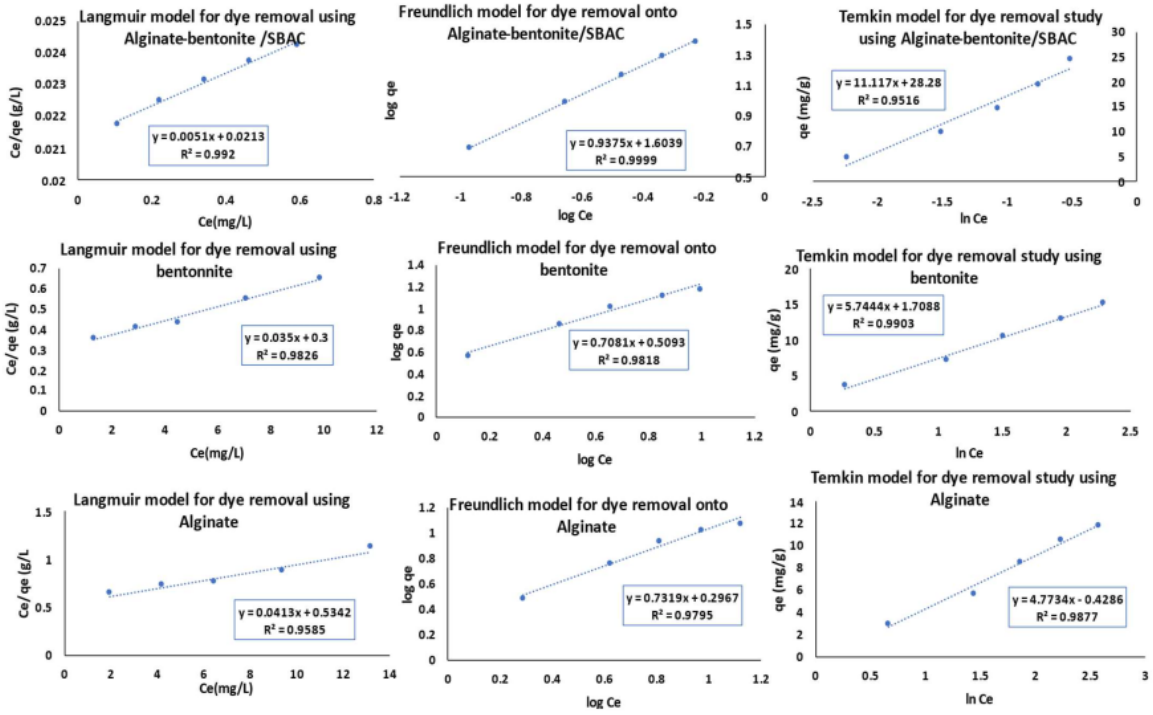

Fig. 5.25: Graphical presentation of Isotherm models for batch adsorption of MG dye onto Alginate-bentonite/SBAC beads

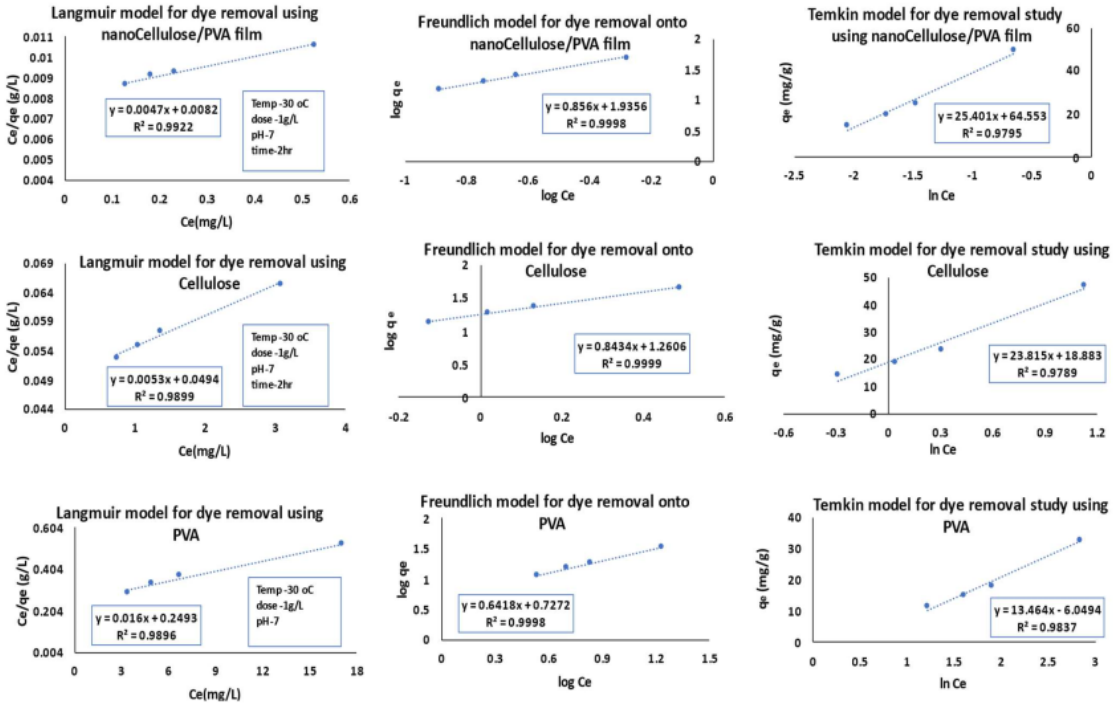

Fig. 5.26: Graphical presentation of Isotherm models for batch adsorption of MG dye onto Nanocellulose/PVA composite film, cellulose and PVA

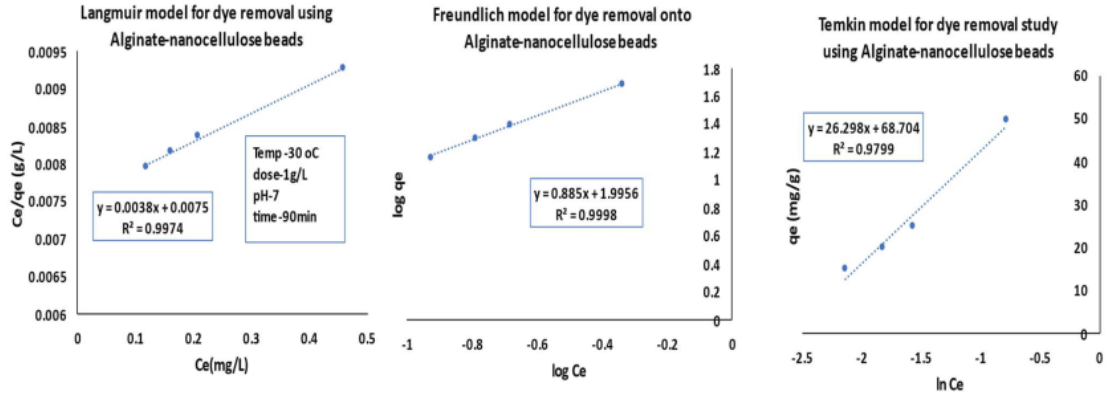

Fig. 5.27: Graphical presentation of Isotherm model for MG dye removal study using Alginate-nanocellulose beads

Table 5.2(a): Langmuir isotherm Parameters for MG dye removal on SB, SBC, and SBAC

Adsorbent	k (L/g)	q_m(mg/g)	R_L	R^2
SB	0.032	169.49	0.609	0.997
SBC	0.0617	172.414	0.448	0.987
SBAC	0.0853	185.185	0.369	0.9806

Table 5.2(b): Langmuir isotherm parameters for MG dye adsorption onto Alginate, bentonite, SBAC and Alginate-bentonite/SBAC

Adsorbent	K_l (L/gram)	q_m(mg/gram)	R_L	R^2
Alginate	0.0773	24.213	0.393	0.958
Bentonite	0.1167	28.571	0.300	0.982
SBAC	0.0853	185.185	0.369	0.981
Alginate-bentonite/SBAC	0.2394	196.078	0.173	0.992

Table 5.2(c): Langmuir isotherm parameters for MG dye adsorption onto nano-cellulose/PVA, Cellulose and PVA

Adsorbent	K_l (L/gram)	q_m(mg/gram)	R_L	R^2
PVA	0.064	62.5	0.438	0.989
Cellulose	0.107	188.68	0.318	0.989
nano-cellulose/PVA	0.573	212.76	0.080	0.992

Table 5.2(d): Langmuir Isotherm models parameters for batch adsorption of MG dye onto Alginate-nanocellulose beads

Adsorbent	K_l (L/gram)	q_m(mg/gram)	R_L	R^2
Alginate	0.0773	24.213	0.393	0.958
Cellulose	0.107	188.68	0.318	0.989
Alginate-nanocellulose beads	0.653	263.158	0.071	0.997

Table 5.3(a): Freundlich isotherm Parameters for MG dye removal on SB, SBC, and SBAC

Adsorbent	K_f(L/mg)	n	R^2
SB	5.27	1.055	0.999
SBC	10.111	1.0613	0.999
SBAC	14.514	1.057	0.999

Table 5.3(b): Freundlich isotherm parameters for MG dye adsorption onto Alginate, bentonite, Alginate-bentonite/SBAC

Adsorbent	K_F(L/mg)	n	R^2
Alginate	0.505	1.366	0.979
Bentonite	3.231	1.412	0.9818
Alginate-bentonite/SBAC	40.169	1.067	0.994

Table 5.3(c): Freundlich isotherm parameters for MG dye adsorption onto nano-cellulose/PVA, Cellulose and PVA

Adsorbent	K_F(L/mg)	n	R^2
PVA	5.336	1.558	0.999
Cellulose	18.222	1.186	0.999
nano-cellulose/PVA	86.218	1.168	0.999

Table 5.3(d): Freundlich isotherm parameters for batch adsorption of MG dye onto Alginate-nanocellulose beads

Adsorbent	K_F(L/mg)	n	R^2
Alginate	0.505	1.366	0.979
Cellulose	18.22	1.186	0.999
Alginate-nanocellulose beads	98.99	1.129	0.999

Table 5.4 (a): Temkin model Parameters for MG dye removal on SB, SBC, and SBAC

Adsorbent	Conc(mg/L)	K_T	B_T	R^2
SB	20	1.925	8.353	0.966
SBC	20	3.534	9.029	0.963
SBAC	20	4.999	9.334	0.964

Table 5.4(b): Temkin model parameters for MG dye adsorption onto Alginate, bentonite, Alginate-bentonite/SBAC

Adsorbent	Conc(mg/L)	K_T	B_T	R^2
Alginate	20	0.914	4.773	0.988
Bentonite	20	1.347	5.74	0.990
Alginate-bentonite/SBAC	20	12.729	11.117	0.952

Table 5.4(c): Temkin model parameters for MG dye adsorption onto nano-cellulose/PVA, Cellulose and PVA

Adsorbent	Conc(mg/L)	K_T	B_T	R^2
PVA	20	0.638	13.464	0.984
Cellulose		2.209	23.815	0.979
nano-cellulose/PVA		0.979	25.401	0.979

Table 5.4(d): Temkin model parameters for batch adsorption of MG dye onto Alginate-nanocellulose beads

Adsorbent	K_T	B_T	R^2
Alginate	0.914	4.773	0.988
Cellulose	2.209	23.815	0.979
Alginate-nanocellulose beads	13.633	26.298	0.979

5.2.2.3. Results of Adsorption Kinetic Study

Fig. 5.28 to 5.31 shows the fitting of the kinetic model to the experimental data. The kinetic model parameters obtained by fitting the pseudo-first-order, pseudo-second-order, and Intra-particle diffusion model to the experimental data are presented in Table 5.5, Table 5.6 and Table 5.7 respectively. Results show that the calculated q_e and that obtained for pseudo second order model are nearly same. This indicate that the adsorption kinetics of MG removal onto prepared adsorbents could be comparatively better explained by the Pseudo-second-order model (Chowdhury et al., 2011). This also signifiy that the dye removal was controlled by chemisorption by adsorbate–biosorbent interaction. Moreover, it can be said that the biosorption process was subjected to the adsorbate mass and availability of adsorptive binding sites on the adsorbent surface.

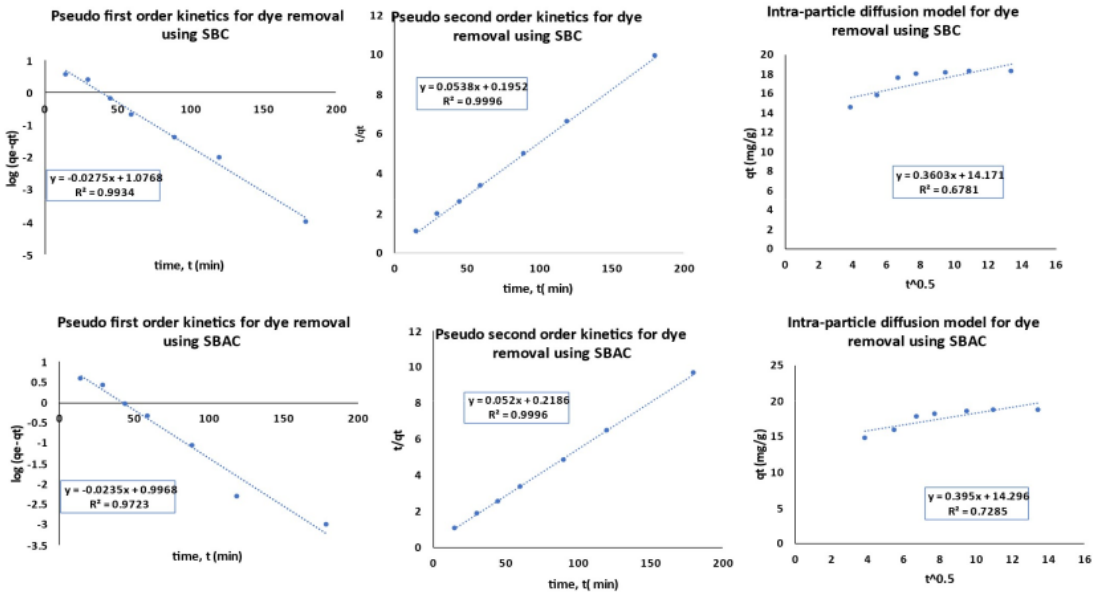

Fig. 5.28: Graphical presentation of adsorption kinetics for batch adsorption of MG dye onto SBC and SBAC

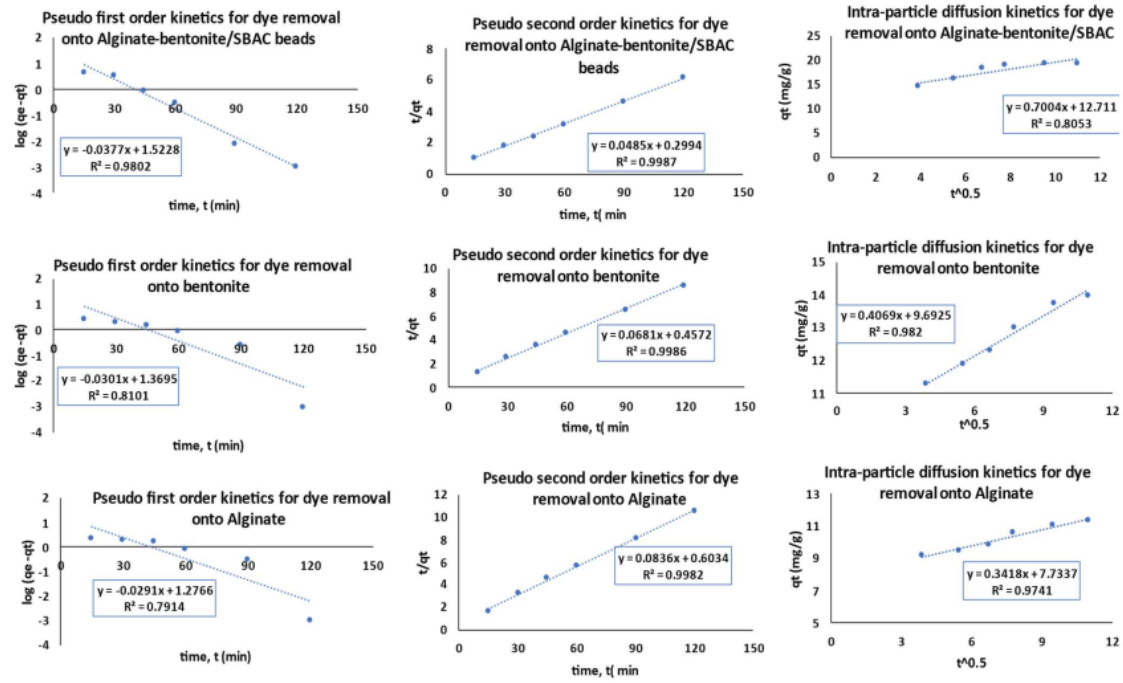

Fig. 5.29: Graphical presentation of adsorption kinetics for batch adsorption of MG dye onto Alginate-bentonite/SBAC beads

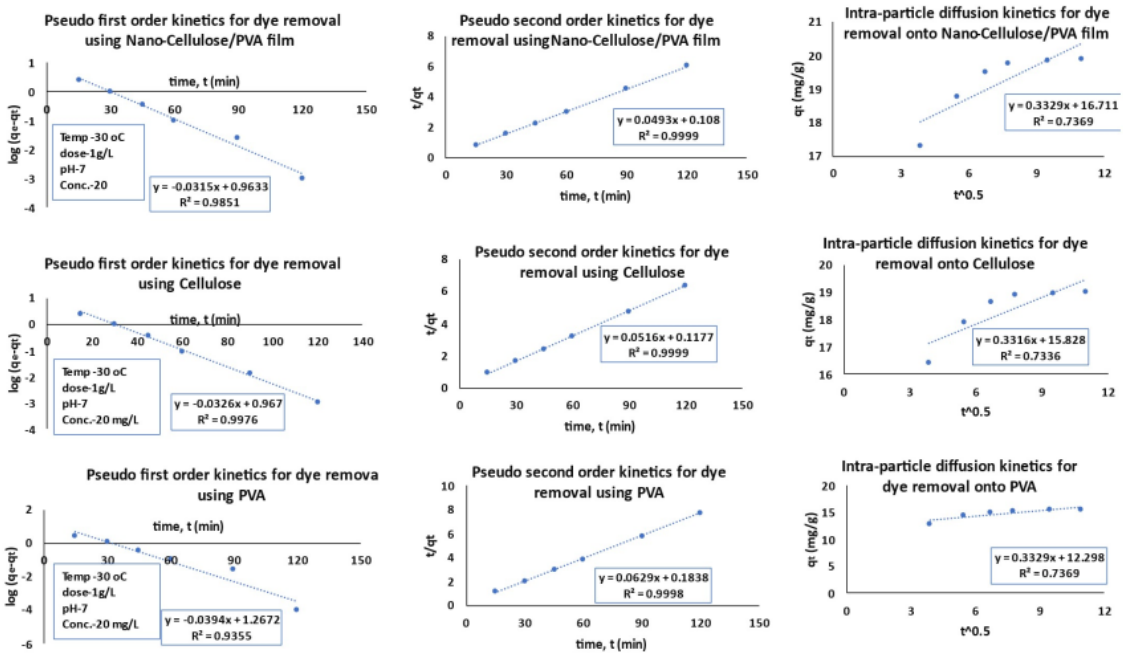

Fig. 5.30: Graphical presentation of kinetic model for batch adsorption of MG dye onto Nanocellulose/PVA composite film, cellulose and PVA

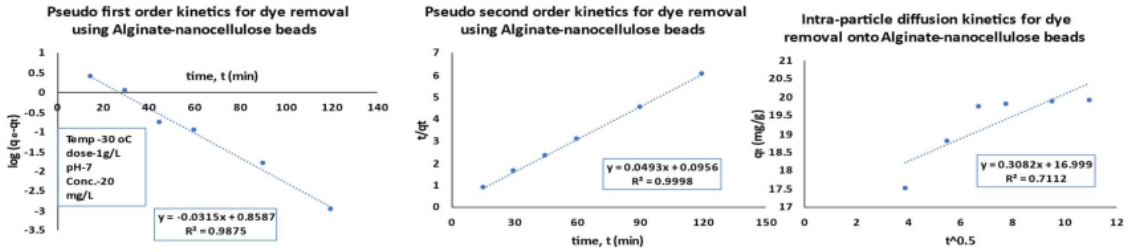

Fig. 5.31: Graphical presentation of Kinetic model for MG dye removal study using Alginate-nanocellulose beads

Table 5.5(a): Pseudo first order sorption kinetic data of MG dye adsorption on SB, SBC, and SBAC

Adsorbent	q_e(exp)	k_1(1/min)	q_e(cal)	R^2
SB	16.609	0.086	26.109	0.952
SBC	18.690	0.0541	9.926	0.972
SBAC	18.690	0.0541	9.926	0.972

Table 5.5(b): Pseudo-First-Order model parameters for MG dye adsorption onto Alginate, bentonite, Alginate-bentonite/SBAC

Adsorbent	q_e(exp)	k_1(1/min)	q_e(cal)	R^2
Alginate	11.377	0.067	18.90	0.791
Bentonite	13.983	0.069	23.415	0.81
Alginate-bentonite/SBAC	19.433	0.087	33.327	0.980

Table 5.5(c): Pseudo-First-Order model parameters for MG dye adsorption onto nano-cellulose/PVA, Cellulose and PVA

Adsorbent	q_e(exp.)	K_1(min^{-1})	q_e(cal.)	R^2
PVA	15.445	0.091	18.50	0.935
Cellulose	18.957	0.075	9.268	0.998
nano-cellulose/PVA	19.859	0.073	9.189	0.985

Table 5.5(d): Parameters of seudo-First-Order model for dye adsorption using Alginate-nanocellulose beads, Cellulose and Alginate

Adsorbent	q_e(exp.)	K_1(min^{-1})	q_e(cal.)	R^2
Alginate	11.377	0.067	18.90	0.791
Cellulose	18.957	0.075	9.268	0.998
Alginate-nanocellulose beads	19.895	0.073	7.223	0.987

Table 5.6(a): Pseudo-Second-Order sorption kinetic data of MG dye on Sb, SBC and SBAC

Adsorbent	q_e(exp)	K_2(1/min)	q_e(cal)	R^2
SB	16.609	0.0073	17.825	0.998
SBC	18.129	0.0148	18.587	0.999
SBAC	18.690	0.0124	19.231	0.999

15

Table 5.6(b): Pseudo-Second-Order model parameters for MG dye adsorption onto Alginate, bentonite, Alginate-bentonite/SBAC

Adsorbent	q_e(exp.)	K_2(min^{-1})	q_e(cal.)	R^2
Alginate	11.377	0.0115	11.962	0.998
Bentonite	13.983	0.0101	14.684	0.998
sodium alginate/SBAC beads	19.433	0.0078	20.618	0.998

Table 5.6(c): Pseudo-Second-Order model parameters for MG dye adsorption onto nano-cellulose/PVA, Cellulose and PVA

Adsorbent	q_e(exp.)	K_2(min^{-1})	q_e(cal.)	R^2
PVA	15.445	0.021	15.898	0.998
Cellulose	18.957	0.023	19.380	0.999
nano-cellulose/PVA	19.859	0.022	20.284	0.999

Table 5.6(d): Parameters of Pseudo-Second-Order model for dye adsorption using Alginate-nanocellulose beads, Cellulose and Alginate

Adsorbent	q_e(exp.)	K_2(min^{-1})	q_e(cal.)	R^2
Alginate	11.377	0.0115	11.962	0.998
Cellulose	18.957	0.023	19.380	0.999
Alginate-nanocellulose beads	19.895	0.002	20.284	0.999

Table 5.7(a): Intra-particle diffusion kinetic model data of MG dye on Sb, SBC and SBAC

Adsorbent	Conc(mg/L)	K_{int} ($min^{0.5}$)	C	R^2
SB	20	0.709	9.709	0.784
SBC	20	0.3603	14.171	0.678
SBAC	20	0.395	14.296	0.729

Table 5.7(b): Intra-particle diffusion kinetic model parameters for MG dye adsorption onto Alginate, bentonite, Alginate-bentonite/SBAC

Adsorbent	Conc. (mg/L)	K_{int} ($min^{0.5}$)	C	R^2
Alginate	20	0.342	7.733	0.974
Bentonite	20	0.407	9.69	0.982
Alginate-bentonite/SBAC	20	0.700	12.711	0.805

Table 5.7(c): Intra-particle diffusion kinetic model parameters for MG dye adsorption onto nano-cellulose/PVA, Cellulose and PVA

Adsorbent	Conc(mg/L)	K_{int} ($min^{0.5}$)	C	R^2
PVA	20	0.333	12.298	0.736
Cellulose	20	0.3316	15.83	0.734
nano-cellulose/PVA	20	0.332	16.711	0.737

Table 5.7(d): Parameters of Intra-particle diffusion kinetic model for dye adsorption using Alginate-nanocellulose beads, Cellulose and Alginate

Adsorbent	Conc(mg/L)	K_{int} ($min^{0.5}$)	C	Conc(mg/L)
Alginate	20	0.342	7.733	0.974
Cellulose	20	0.3316	15.83	0.734
Alginate-nanocellulose beads	20	0.3082	16.99	0.711

5.2.2.4. Thermodynamic study

K_c was calculated using the eqn. 2.14. Fig. 5.32 to Fig. 7.35 depicts the K_c vs. 1/T data of various biosorbents. The calculated values of Thermodynamic parameters from the above figure are listed in Table 5.8. The recorded value of ΔG was negative which suggested that the reactions were spontaneous (Saha et al., 2012). The negative value of enthalpy change obtained from the thermodynamic study indicated that the reactions involved in MG dye adsorption was exothermic. The positive value of entropy changes (ΔS) signified to the randomness of MG dye molecules on the surface of composite beads (Chowdhury and Saha, 2010).

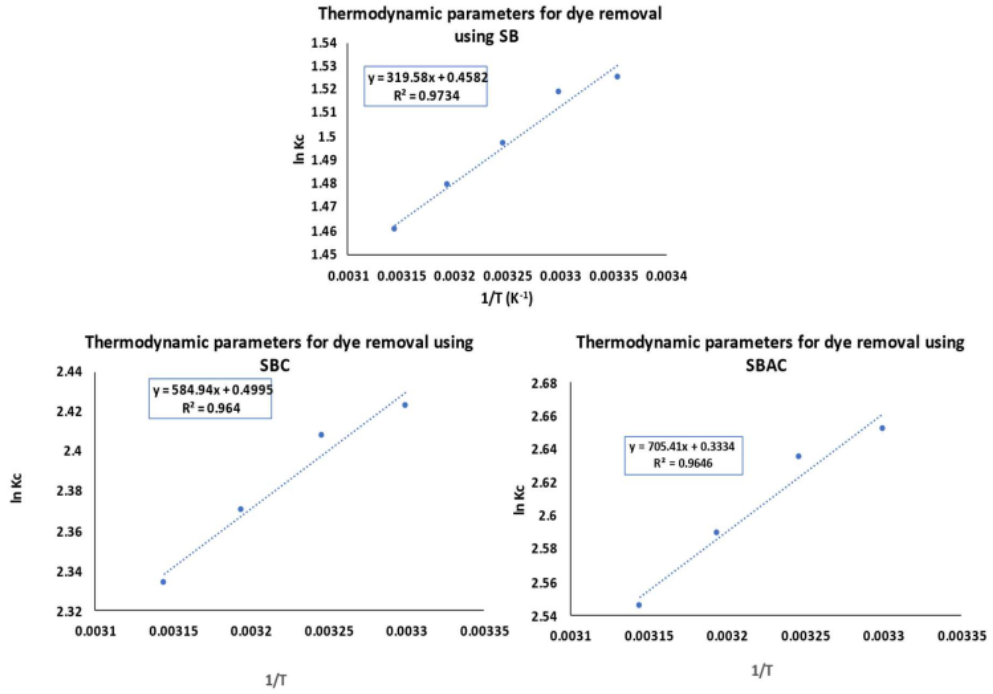

Fig. 5.32: Graphical presentation of thermodynamics study for batch adsorption of MG dye onto SB, SBC and SBAC

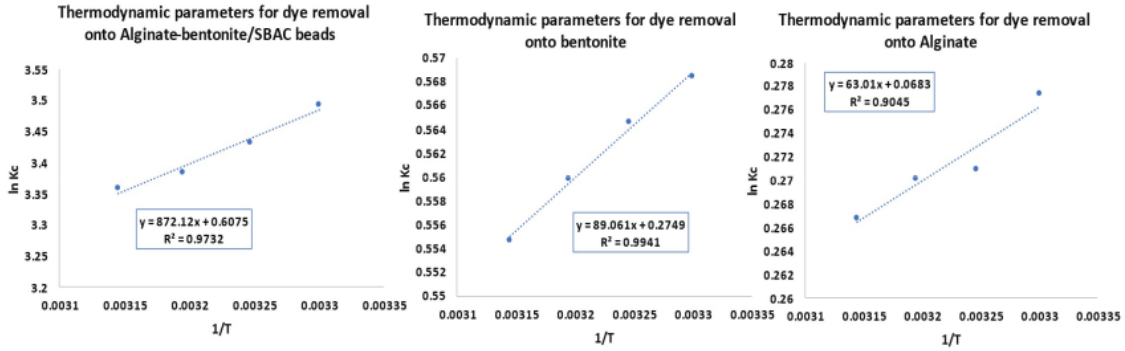

Fig.5.33: Graphical presentation of thermodynamic study for batch adsorption of MG dye onto Alginate-bentonite/SBAC beads, Bentonite and Alginate

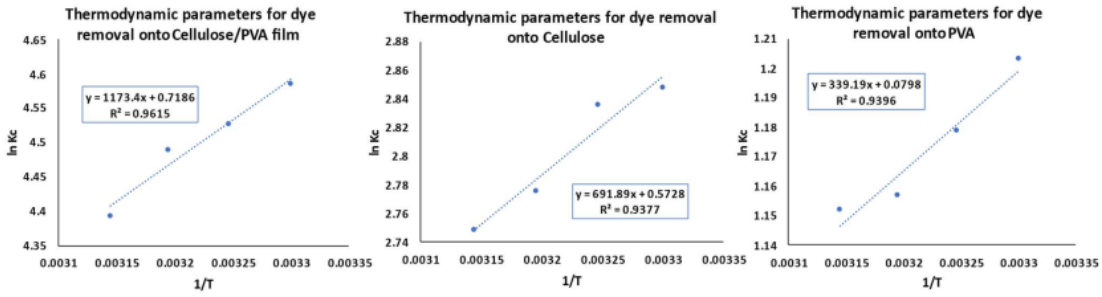

Fig. 5.34: Graphical presentation of thermodynamic study for batch adsorption of MG dye onto nano-cellulose/PVA, Cellulose and PVA

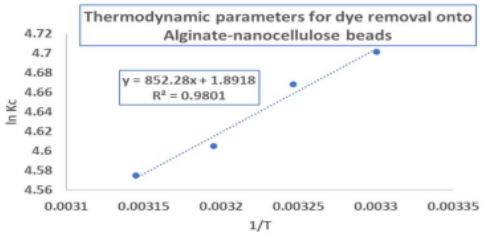

Fig. 5.35: Thermodynamic parameters for MG dye removal study using Alginate-nanocellulose beads

Table 5.8(a): Thermodynamic parameters of MG dye adsorption onto SB, SBC, and SBAC

Adsorbent	Temperature(K)	ΔG(J/mol)	ΔH(J/mol)	ΔS(J/mol k)
SB	303	-3826.727	-2656.98	3.809
	308	-3834.643		
	313	-3850.127		

	318	-3861.188		
SBC	303	-6103.732	-4863.19	4.153
	308	-6167.029		
	313	-6169.044		
	318	-6170.946		
SBAC	303	-6683.462	-5864.779	2.7769
	308	-6748.279		
	313	-6739.300		
	318	-6731.077		

Table 5.8(b): Calculate value of thermodynamic parameters MG dye adsorption onto Alginate, bentonite, Alginate-bentonite/SBAC

Adsorbent	Temperature(K)	ΔG(J/mol)	ΔH(kJ/mol)	ΔS(J/mol k)
Alginate	303	-698.721	-523.865	0.568
	308	-693.552		
	313	-702.691		
	318	-705.303		
Bentonite	303	-1431.947	-740.453	2.285
	308	-1445.598		
	313	-1456.687		
	318	-1466.256		
SBAC	303	-6683.462	-5864.779	2.7769
	308	-6748.279		
	313	-6739.300		
	318	-6731.077		
Alginate-bentonite/SBAC	303	-8800.423	-7250.805	5.0507
	308	-8789.226		
	313	-8806.061		
	318	-8880.835		

Table 5.8(c): Calculate value of thermodynamic parameters MG dye adsorption onto nano-cellulose/PVA, Cellulose and PVA

Adsorbent	Temperature(K)	ΔG(kJ/mol)	ΔH(J/mol)	ΔS(J/mol k)
PVA	303	-3.030	-2820.026	0.664
	308	-3.018		
	313	-3.009		
	318	-3.045		
Cellulose	303	-7.174	-5752.37	4.7622
	308	-7.263		
	313	-7.222		
	318	-7.266		
Nanocellulose/PVA	303	-11.550	-9755.65	5.974
	308	-11.592		
	313	-11.683		
	318	-11.617		

Table 5.8(d): Derived values of thermodynamic functions of MG dye biosorption onto Alginate-nanocellulose beads

Adsorbent	Temperature(K)	ΔG(J/mol)	ΔH(J/mol)	ΔS(J/mol k)
Alginate	303	-698.721	-523.865	0.568
	308	-693.552		
	313	-702.691		
	318	-705.303		
Cellulose	303	-7173.777	-5752.37	4.7622
	308	-7262.645		
	313	-7221.811		
	318	-7265.759		
Alginate-nanocellulose beads	303	-11843.720	-7094.17	15.728
	308	-11954.421		
	313	-11984.214		
	318	-12095.927		

5.2.2.5. RSM study results for MG dye removal onto prepared biosorbents

The ranges and levels of process variables (for Malachite green) examined in this research were, weight of bio-adsorbent, pH, and contact time given in Table 5.9. Consistent with this design, a total of 20 experiments were carried out for MG dye removal using prepared biosorbents (Table 5.10).

Table 5.9: Experimental range and levels of independent variables for MG dye removal process using raw SB and SBAC

Independent variables	Range and levels (coded)					
	Units	-1	0	+1	-alpha	+alpha
pH		4	6	8	2.63641	9.36359
Dose	g/L	0.5	1.375	1.5	0.159104	1.8409
Time	min	40	80	120	12.7283	147.272

(a) RSM study using SB, SBAC

Experimental design and statistical analysis:

An empirical relationship between the response and the independent variables has been expressed by the following quadratic models. Final Equation in Terms of Actual Factors:

*MG Dye Removal efficiency of raw **SB***:

$R1 = +31.54169 + 10.27227 \times pH + 12.55305 \times dose + 0.082256 \times time - 0.41000 \times pH \times dose - 3.87500E\text{-}003 \times pH \times time - 6.15000E\text{-}003 \times dose \times time - 0.58697 \times pH^2 - 3.17746 \times dose^2 - 2.27777E\text{-}004 \times time^2$ ..... (5.1)

*MG Dye Removal efficiency of activated biochar (**SBAC**)*:

R1 = +40.33516+10.41171× pH+14.17132 × Dose +0.096449 × Time-0.45250 × pH × Dose-3.15625E-003 × pH ×Time-9.87500E-003 ×Dose × Time-0.61306 × pH^2-3.73498 × Dose-3.14891E-004×$Time^2$……(5.2)

Results obtained from quadratic model implied that RSM model analysis was highly significant as model F-value was 125.60 h Values of "Prob > F″ less than 0.0500 (a 0.01% chance that a "Model F-Value" this large could occur due to noise), the R^2 value was high (0.9745), Adj R-Squared value for both adsorbents were obtained as 0.9516 (SBAC) and 0.9833 (SB). The value of Pred R-Squared for both adsorbents were 0.8074 (SBAC) and 0.9335 (SB) with a low value of CV (0.81).

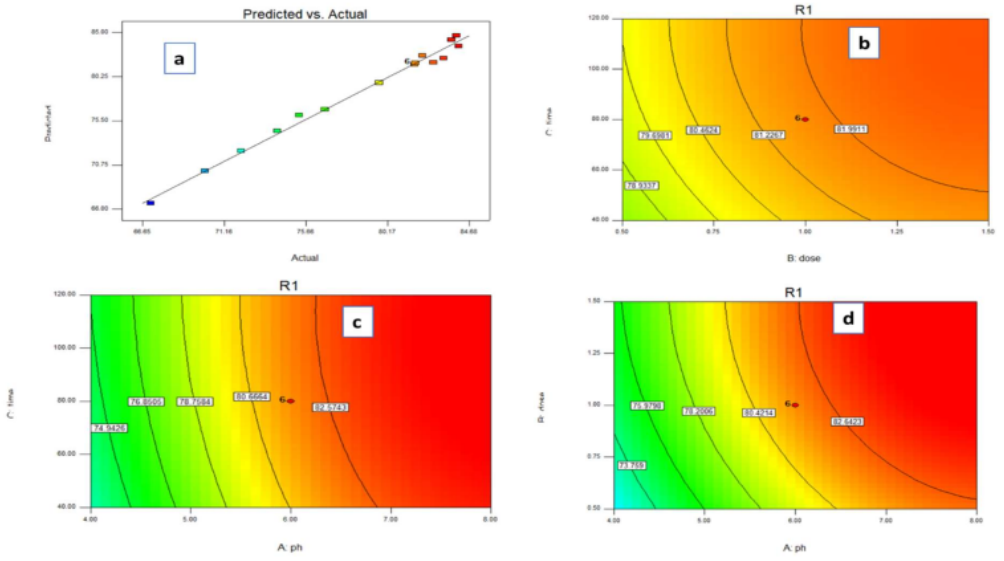

Fig. 5.36. Actual vs. predicted values of MG dye removal using raw SB (a), 2D contour plots on combine effect of time and adsorbent dose (a), combine effect of contact time and pH (b), and combine effect of pH and adsorbent dose on MG removal efficiency(c).

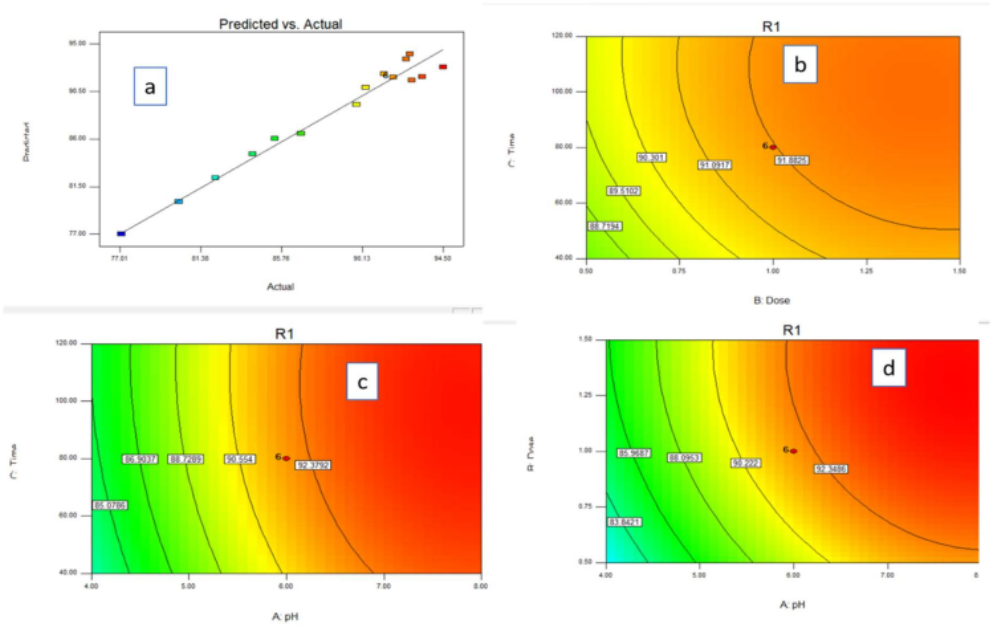

Fig. 5.37. Actual vs. predicted values of MG dye removal on SBAC(a), 2D contour plots on combine effect of time and adsorbent dose (a), combine effect of contact time and pH (b), and combine effect of pH and adsorbent dose on MG removal efficiency(c).

From Fig. 5.36(a) and 5.37(a), it was observed that experimental removal efficiency was close to the predicted values for selected MG dye removal experiment.

from RSM model the optimized conditions for MG dye removal study using raw SB was observed as pH: 6.81, dose: 1.06 g/L and contact time: 114.93 min. The removal efficiency at this experimental parameter removal efficiency at was found as 83.71%. The removal efficiency at optimized conditions for MG dye removal study using SBAC (pH: 7.08, dose: 1.08 g/L and contact time: 77.95 min) was found as 93.833%.

The combined effect of time and dosage (when pH was constant) is shown in Fig. 5.36(b) and 5.37(b). The removal efficiency improved with agitation time and adsorbent masses. The optimum conditions were found to be 1.08 g/L and 77.95 min for adsorbent dose and contact time, respectively. The removal efficiency was 93.833% at this optimum condition in case of SBAC, the optimized conditions for MG dye removal study using raw SB was pH: 6.81, dose: 1.06 g/L and contact time: 114.93 min and at this condition removal efficiency was found as 83.71%.

Combine effect of independent process variables contact time and solution pH on removal efficiency of MG dye using raw SB and SBAC had described in terms of 2D contour plot in

Fig. 5.36(c) and 5.37(c). The maximum adsorption efficiency obtained was 93.833% at pH value of 7.08 after 77.95 min contact time in case of SBAC.

The Surface plot (Fig. 5.36(d) and 5.37(d)) showed that the removal efficiency of MG onto SB and SBAC was increased with pH. The optimized conditions for MG dye removal study using raw SB were observed as pH=6.81, dose=1.06 g/L and contact time=114.93 min. The removal efficiency obtained at this condition was 83.71%. The maximum adsorption of 93.833% was achieved at the optimum conditions for the adsorbent dose 1.08 g/L and pH 7.08 in case of SBAC.

***(b) RSM study* using Alginate-bentonite/SBAC beads**

Final Equation in Terms of Actual Factors:

*% Removal for MG dye adsoption onto **Alginate-bentonite/SBAC** beads:*

$$R1 = +46.22169 + 10.27227 \times pH + 12.55305 \times dose + 0.082256 \times time - 0.41000 \times pH \times dose - 3.87500E\text{-}003 \times pH \times time - 6.15000E\text{-}003 \times dose \times time - 0.58697 \times pH^2 - 3.17746 \times dose^2 - 2.27777E\text{-}004 \times time^2 \quad \ldots\ldots\ldots\ldots\ldots\ldots\ldots\ldots\ldots\ldots (5.3)$$

Results obtained from quadratic model implied that RSM model analysis was highly significant as model F-value was 121.96 with Values of "Prob > F" less than 0.0001, the R^2 value was high (0.9783), Adj R-Squared value was obtained as .9833 and the value of Pred R-Squared was 0.9335 with a low value of CV (0.69).

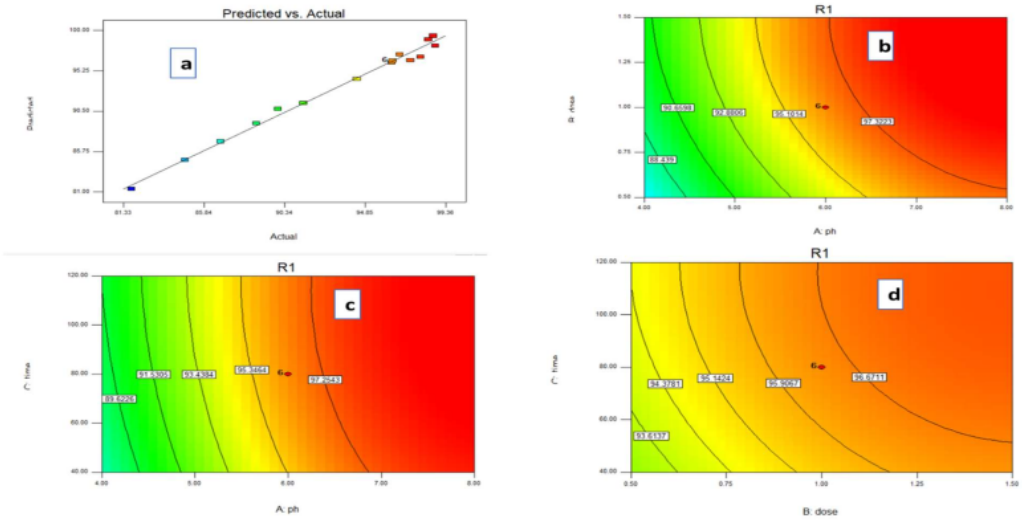

Fig. 5.38. Actual vs. predicted values of MG dye removal on Alginate-bentonite/SBAC beads (a), 2D contour plots on combine effect of pH and adsorbent dose (a), combine effect of contact time and pH (b), and combine effect of time and adsorbent dose on MG removal efficiency(c).

The 2D contour plot (Fig. 5.38(b)) showed that the removal efficiency of MG on prepared composite beads was increased with increasing pH. The maximum adsorption of 98.06% was achieved at a pH of 6.98. The optimum conditions were found to be 0.99 g/L, pH 6.98 for the adsorbent dose and pH of the solution respectively. The combined effect of time and dosage was shown in fig. 5.38(c). The removal efficiency was improved with rising agitation time and adsorbent masses comparatively. The optimum conditions were found to be 0.99 g/L, 66.14 min for adsorbent dose and contact time respectively with 98.06% removal efficiency.

Combine effect of independent process variables contact time and pH of the system on elimination efficiency of MG dye using Alginate-bentonite/SBAC composite beads had described in terms of 2D contour plot in fig. 5.38(d). From the 2D contour plot, maximum adsorption efficiency was obtained as 98.06% at a pH value of 6.98 after 66.14 min contact time.

(c) RSM study using cellulose and NanoCellulose/PVA composite

A quadratic model corresponding to the empirical relationship between the response and the independent parameters has been stated as follows:

Final Equation in Terms of Actual Factors:

MG dye Removal efficiency of ***cellulose****:*

$R1=+43.30536+10.39270\times pH+13.12933 \times Dose+0.067049 \times Time-0.55250\times pH \times Dose-2.53125E-003 \times pH \times Time+9.75000E-004\times Dose \times Time-0.59122\times pH^2-3.24548\times Dose^2-2.38406E-004 \times Time^2$……..(5.4)

MG dye Removal efficiency of ***nanocellulose/PVA****:*

$R1 = +47.09169+10.27227\times pH+12.55305\times Dose+0.082256\times Time-0.41000\times pH \times Dose-3.87500E-003\times pH \times Time-6.15000E-003 \times Dose \times Time-0.58697\times pH^2-3.17746\times Dose^2-2.27777E-004 \times Time^2$……(5.5)

The Model F-value of 125.60 implies the model is significant and the R^2 value was high (0.9912 for composite and 0.9904 for cellulose). The "Pred R-Squared" of 0.9272 is in reasonable agreement with the "Adj R-Squared" of 0.9817 for cellulose with CV of 0.75. Whereas, in case of nanocellulose/PVA hydrogel composite, value of the "Pred R-Squared" was 0.9335 and "Adj R-Squared" was 0.9833 with a low value of CV (0.68).

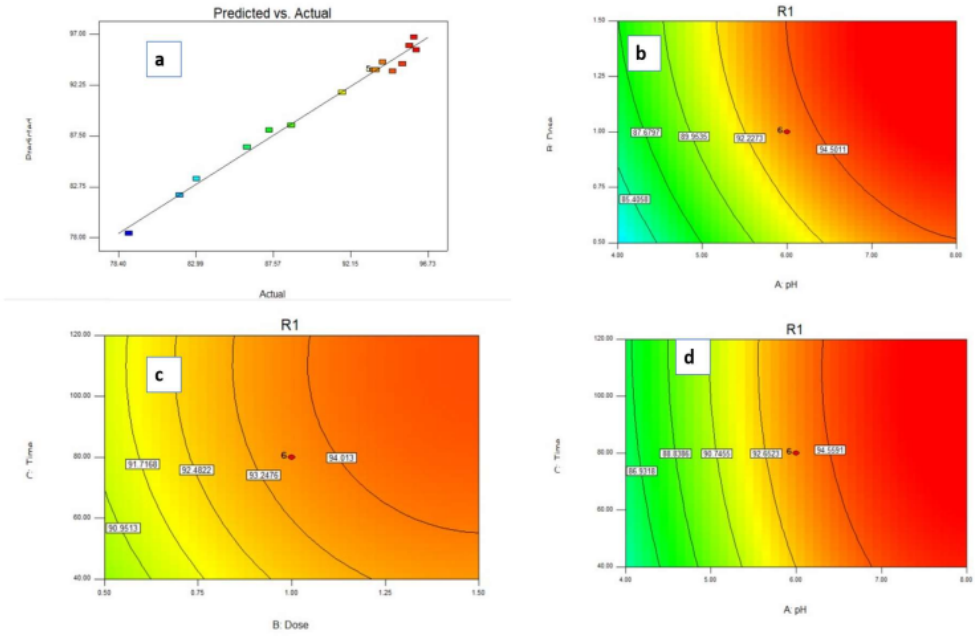

Fig. 5.39. Actual vs. predicted values of MG dye removal onto Cellulose (a), 2D contour plots on combined effect of pH and adsorbent dose (a), combined effect of contact time and pH (b), and combined effect of time and adsorbent dose on MG removal efficiency(c).

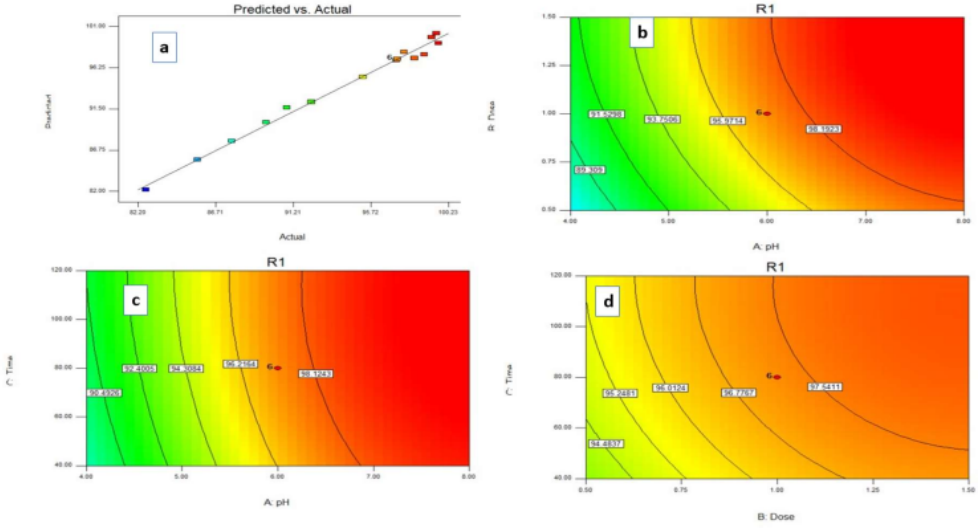

Fig. 5.40. Actual vs. predicted values of MG dye removal onto NanoCellulose/PVA (a), 2D contour plots on combine effect of pH and adsorbent dose (a), combine effect of contact time and pH (b), and combine effect of time and adsorbent dose on MG removal efficiency(c).

The 2D contour plot (Fig. 5.39 (b) and Fig. 5.40(b)) showed that the optimized conditions for MG dye removal study using cellulose were observed as pH: 6.75, dose: 0.96 g/L and contact time: 49.89 min and at this condition removal efficiency was found as 94.502%. The maximum adsorption of 98.97 % was achieved at the optimum conditions for the adsorbent dose 1 g/L and pH 6.71 in case of nanocellulose/PVA.

The combined effect of time and dosage was shown in 2D contour plot (Fig. 5.39 (c) and Fig. 5.40(c)). In case of nanocellulose/PVA, the optimum conditions were found to be 1g/L, 118.54 min for adsorbent dose and contact time, respectively and at this condition removal efficiency was found as 98.97 %. the optimized conditions for MG dye removal study using cellulose were observed as pH: 6.75, dose: 0.96 g/L and contact time: 49.89 min and at this condition removal efficiency was found as 94.502 %. Combined effect of independent process variables; contact time and pH of the system on elimination efficiency of MG dye using extracted cellulose and nanocellulose/PVA had described in terms of 2D contour plot in Fig. 5.39 (d) and Fig. 5.40(d).

(d) RSM study using Alginate-nanocellulose composite beads

Final Equation in Terms of Actual Factors:

MG Dye Removal efficiency of ***Alginate-nanocellulose*** *beads:*

R1 =+45.68320+11.02308×pH+16.33040×Dose+0.078104×Time-0.86525× pH ×Dose-2.78437E-003× pH × Time-0.016012× Dose × Time-0.63694× pH2-3.48765 × Dose2-2.00010E-004 ×Time2……(5.6)

Results obtained from quadratic model implied that RSM model analysis for Alginate-nanocellulose beads was highly significant as model F-value was 121.96 with Values of "Prob > F" less than 0.001, the R2 value was high (0.9910), Adj R-Squared value was obtained as 0.9828 and the value of Pred R-Squared was 0.9307 with a low value of CV (0.65).

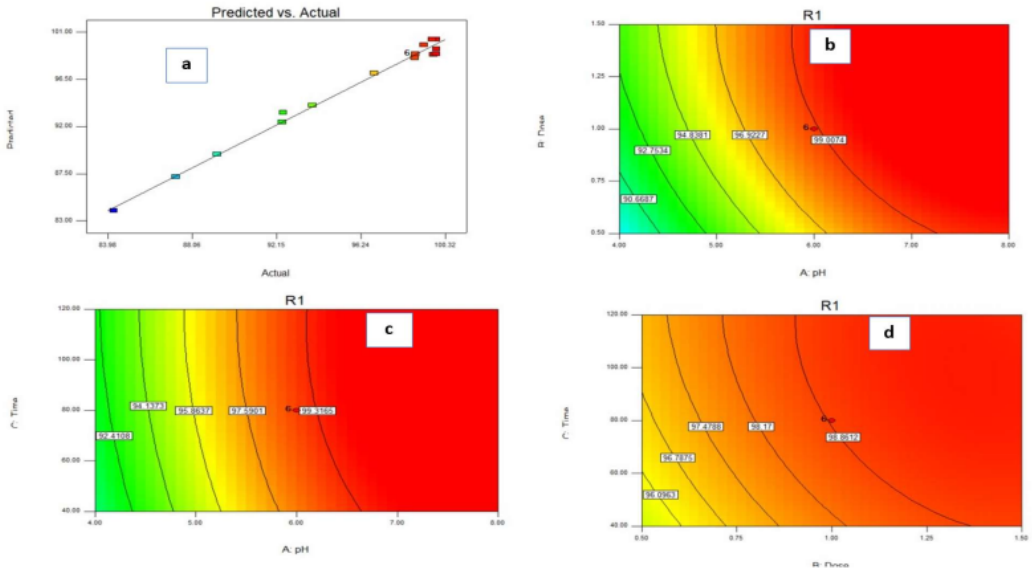

Fig. 5.41: Predicted vs. Actual values for MG dye adsorption onto Alginate-nanocellulose (a), 2D contour plots on combine effect of pH and dose (b), combine effect of contact time and pH (c), and combine effect of contact time and adsorbent dose (d) on dye removal efficiency

Fig. 5.41(b) represented the 2D surface plots for combined impacts of biosorbent dose and pH on MG dye uptake rate.

Combined influences of solution pH and time upon decolorization efficiency have been displayed in Fig. 5.42(c). Fig. 5.41 (d) represented the 2D surface plots for combined impacts of biosorbent dosage and contact time on dye elimination efficiency. The optimized condition for MG dye adsorption experiment was observed from RSM model was pH-6.46, dose 0.98 g/L and time 64.42 min and removal was found as 99.52%.

Table 5.10: Experimental result data of RSM study for dye removal using raw SB, SBAC, Cellulose, Alginate-bentonite/SBAC, nano-cellulose/PVA and Alginate-nanocellulose

Run	pH	Dose (g/L)	Time (min)	%R of MG dye removal (raw SB)	%R of MG dye removal (SBAC)	%R of MG removal (Cellulose)	%R of MG dye removal (Alginate-bentonite/SBAC)	%R of MG removal (nano-cellulose/PVA)	%R of MG removal (Alginate-nanocellulose)
1	4	0.5	40	70.082	78.082	82.01	84.762	85.63	87.26
2	6	1	80	81.702	89.702	93.63	96.382	97.25	98.87
3	6	1	12.7	79.702	87.702	91.63	94.382	95.25	96.87

4	4	0.5	120	72.082	80.082	84.01	86.762	87.64	89.25
5	4	1.5	40	74.082	82.082	86.01	88.762	89.63	92.42
6	2.6	1	80	67.082	75.082	79.01	81.762	82.63	84.25
7	6	1	80	81.702	89.702	93.63	96.382	97.25	98.87
8	6	1	80	81.702	89.702	93.63	96.382	97.25	98.87
9	6	1	80	81.702	89.702	93.63	96.382	97.25	98.87
10	8	1.5	120	83.97	91.97	95.9	98.65	99.53	99.69
11	6	1	147.27	82.702	90.702	94.63	97.382	98.25	99.87
12	9.36	1	80	84.102	92.102	96.03	98.782	99.65	99.89
13	6	1	80	81.702	89.702	93.63	96.382	97.25	98.87
14	6	1.84	80	83.27	91.27	95.2	97.95	98.82	99.75
15	8	1.5	40	83.702	91.702	95.63	98.382	99.25	99.87
16	8	0.5	120	82.102	90.102	94.03	96.782	97.66	99.27
17	4	1.5	120	75.282	83.282	87.21	89.962	90.84	92.45
18	6	1	80	81.702	89.702	93.63	96.382	97.25	98.87
19	6	0.16	80	76.702	84.702	88.63	91.382	92.25	93.87
20	8	0.5	40	81.65	89.65	93.58	96.33	97.21	98.85

5.2.3. Fixed bed study results of MG dye removal using prepared biosorbents

Continuous fixed bed study of MG dye removal using raw SB, SBAC, Alginate-bentonite/SBAC beads and Nanocellulose/PVA composite were investigated. The result of breakthrough in continuous fixed bed adsorption study was examined by varying fixed-bed height, feed flowrate and feed concentration. The results are presented in Fig. 5.42, Fig. 5.43, Fig. 5.44 and Fig. 5.45 in terms of C_t/C_0 vs time plot. and performance behaviour at various operational conditions. In all cases Alginate-bentonite/SBAC composite beads shows better results in comparison with raw SB, SBAC, Nanocellulose/PVA composite.

Influence of pH

Effect of pH on MG adsorption was examined by varying feed pH from 4 to 8 at a feed flow rate of 10mL/min for C_0=50 mg/L. The breakthrough characteristics curves for SB, SBAC Alginate-bentonite/SBAC beads and Nanocellulose/PVA are depicted in presented in Fig. 5.42(a), Fig. 5.43(a), Fig. 5.44(a) and Fig. 5.45(a), respectively. The breakthrough parameters are presented in Table 5.11(a, b, c & d). According to the results obtained from the column study, the breakthrough time increased with increasing pH which indicate the higher adsorption capacity of the adsorbent bed and removal efficiency.

Influence of bed height

The hight of the adsorbent column is an important monitoring parameter for evaluating the performance of the adsorbent column and adsorption efficiency. The breakthrough curves (Fig. 5.42(b), Fig. 5.43(b), Fig. 5.44(b) and Fig. 5.45(b)) were obtained by varying the bed height

(5,7, 9 cm) at constant feed flowrate of 10mL/min and feed concentration of 50 mg/L. Amount of adsorbent for 5 cm bed hight of fixed-bed column containing Raw SB=3.9g, using SBAC=3.1g, for Alginate-bentonite/SBAC beads=3.3g and for Nanocellulose/PVA=3.53g. Adsorbent amount in 7 cm bed hight are 7.4 g, 4.2g, 5.6g and 4.1g using SB, SBAC, Alginate-bentonite/SBAC and Nanocellulose/PVA respectively. Adsorbent mass in 9 cm height of adsorbent column is 8.25g, 4.9g, 6.1g and 4.78g using SB, SBAC, Alginate-bentonite/SBAC and Nanocellulose/PVA respectively. The breakthrough time increased from 220 min to 525 min with increase in adsorbent bed height from 5 to 10 cm containing raw SB (Table 5.11(a)). With SBAC as adsorbent, the breakthrough time increased from 260 min to 580 min with an increase of column height from 5 to 9 cm (Table 5.11(b)). Table 5.11(c) indicate that on increasing column bed height from 5 to 9 cm, the breakthrough time raised from 290 min to 600 min using Alginate-bentonite/SBAC beads as adsorbent. Result showed that breakthrough time increased from 275 min to 585 min with increase of column height from 5 to 9 cm using Nanocellulose/PVA as adsorbent (Table 5.11(d)). This is due to the fact that with increasing adsorbent loading the interaction time between MG molecules and the surface of adsorbent increased as well as the number of vacant active sites (Chowdhury et al., 2013). Alginate-bentonite/SBAC composite beads shows better results in comparison with raw SB, SBAC, Nanocellulose/PVA composite.

Influence of feed flow rate

Influence of the feed flowrate on the dynamic behaviour of continuous flow column was investigated by varying the feed flow rate of dye solution (5, 10, 16 mL/min) at feed concentration of 50 mg/L and at adsorbent bed height of 5cm (Raw SB=3.9g, using SBAC=3.1g, for Alginate-bentonite/SBAC beads=3.3g and for Nanocellulose/PVA=3.53g). The breakthrough curves for dye removal using raw SB, SBAC, Alginate-bentonite/SBAC beads and Nanocellulose/PVA composite at this condition shown in Fig. 5.42(c), Fig. 5.43(c), Fig. 5.44(c) and Fig. 5.45(c), respectively. The increase of feed flowrate from 10 to 16 mL/min led to decrease of breakthrough time from 260 min to 160 min for SBAC, from 290 min to 175 min for Alginate-bentonite/SBAC and from 275 min to 165 min for Nanocellulose/PVA as adsorbent. The increase in adsorption capacity of adsorbent bed at constant column bed height with decreasing inlet flow rate may be attributed to the longer contact time between MG dye molecules and adsorbent which facilitated the enhancement of amount of solute transfer to the adsorbent bed thereby increasing biosorption of MG dye (Saha et al., 2012).

Influence of feed concentration

The effect of initial dye concentration on the breakthrough curve was examined by varying the initial concentration of MG dye solution (50mg/L, 100mg/L, 200 mg/L) for adsorbent bed height of 5cm at a feed flowrate of 10mL/min. The significant influence of feed concentration on breakthrough characteristics for dye removal using raw SB, SBAC, Alginate-bentonite/SBAC beads and Nanocellulose/PVA composite at this condition is seen Fig. 5.42(d), Fig. 5.43(d), Fig. 5.44(d) and Fig. 5.45(d) respectively. It is observed that with raw SB as adsorbent breakthrough time decreased from 220 to65 min with an increase in feed concentration (from 50-200mg/L) resulting in the sharpness of breakthrough curves. similarly, with SBAC as adsorbent breakthrough time decreased from 260 to110 min with an increase in feed concentration. The breakthrough time for fixed-bed containing Alginate-bentonite/SBAC beads decreased from 290 min to 130 min with an increase in feed concentration (200mg/L) (Table 5.11(c)). Result shows that with an increase in feed concentration (from 50-200mg/L) breakthrough time decreased (from 275 to 115) using Nanocellulose/PVA as adsorbent (Table 5.11(d)).

Table 5.11(a): Parameters of the breakthrough curves for MG dye adoption onto **Raw SB**

Q(ml/min)	C_0 (mg/L)	pH	L_b(cm)	t_b	t_t (min)	M_{tot} (mg)	S_{tot}	S_b/S_{tot}	R (%)	S_{eq}(mg/mg)
10	50	6	5	220	420.32	340	210.16	0.523	61.81	56.8
10	50	6	7	485	685.11	545	342.555	0.708	62.85	46.291
10	50	6	9	525	725.04	575	362.52	0.7241	63.05	39.191
10	100	6	5	130	230.5	350	230.5	0.564	65.86	62.297
10	200	6	5	65	165.31	520	330.62	0.393	63.58	89.356
16	50	6	5	120	320.55	432	256.44	0.374	59.36	69.308
5	50	6	5	430	630.05	205	157.5125	0.682	76.83	42.570
10	50	4	5	110	190.11	140	95.055	0.579	67.89	25.690
10	50	7	5	240	433.52	370	216.76	0.554	58.58	58.583
10	50	8	5	340	540.31	395	270.155	0.629	68.39	73.014

Table 5.11(b): Parameters of the breakthrough curves for MG dye adoption onto **SBAC**

Q(ml/min)	C_0 (mg/L)	pH	L_b(cm)	t_b	t_t (min)	M_{tot} (mg)	S_{tot}	S_b/S_{tot}	R (%)	S_{eq}(mg/mg)
10	50	6	5	260	481.875	355	240.937	0.5396	67.87	86.049
13	50	6	5	210	403.207	390	262.0845	0.5208	67.20	93.602

16	50	6	5	160	371.954	464	297.563	0.4302	64.13	106.273
10	100	6	5	165	273.061	385	273.061	0.6043	70.92	97.522
10	200	6	5	110	206.379	610	412.758	0.533	67.66	147.414
10	50	4	5	125	208.397	147.5	104.198	0.599	70.64	37.214
10	50	7	5	270	502.975	370	251.488	0.5368	67.97	89.817
10	50	8	5	435	638.823	427.5	319.411	0.6809	74.72	114.075
10	50	6	7	525	821.171	565	410.585	0.6393	72.67	105.278
10	50	6	9	575	884.73	600	442.365	0.6499	73.73	91.022

Table 5.11(c): Parameters of the breakthrough curves for MG dye adsorption onto **Alginate-bentonite/SBAC**

Q(ml/min)	C_0 (mg/L)	pH	L_b(cm)	t_b	t_t (min)	M_{tot} (mg)	S_{tot}	S_b/S_{tot}	R (%)	S_{eq}(mg/mg)
10	50	6	5	290	516.0331	387.5	258.0165	0.56198	66.584	78.1868
13	50	6	5	240	445.2756	403	289.4291	0.538992	71.818	87.7058
16	50	6	5	175	368.3551	476	294.6841	0.475085	61.908	89.2982
10	100	6	5	190	278.3202	415	278.3202	0.682667	67.065	84.3394
10	200	6	5	130	230.6889	680	461.3779	0.563529	67.849	139.811
10	50	4	5	145	225.5457	155	112.7729	0.642885	72.756	34.1735
10	50	8	5	455	659.4792	435	329.7396	0.689938	75.802	99.9210
10	50	6	7	550	757.2362	570	378.6181	0.726326	66.424	67.6103
10	50	6	9	600	947.2973	632.5	473.6486	0.633381	74.885	63.1531

Table 5.11(d): Parameters of the breakthrough curves for MG dye adsorption onto **nano-cellulose/PVA**

Q(ml/min)	C_0 (mg/L)	pH	L_b(cm)	t_b	t_t (min)	M_{tot} (mg)	S_{tot}	S_b/S_{tot}	R (%)	S_{eq}(mg/mg)
10	50	6	5	275	521.3278	367.5	260.6639	0.527499	70.928	93.09425
13	50	6	5	225	406.2898	386.75	264.0883	0.553792	68.283	94.31726
16	50	6	5	165	370.7209	456	296.5767	0.445079	65.038	105.9203
10	100	6	5	175	274.897	395	274.897	0.636602	69.594	98.1775
10	200	6	5	115	207.8571	620	415.7143	0.553265	67.050	148.4694

10	50	4	5	125	208.7731	142.5	104.3865	0.598736	73.253	37.28091
10	50	8	5	425	682.2897	425	341.1449	0.622903	80.269	121.8375
10	50	6	7	535	744.5198	567.5	372.2599	0.718584	65.596	100.6108
10	50	6	9	585	861.9255	605	430.9627	0.678713	71.233	92.68016

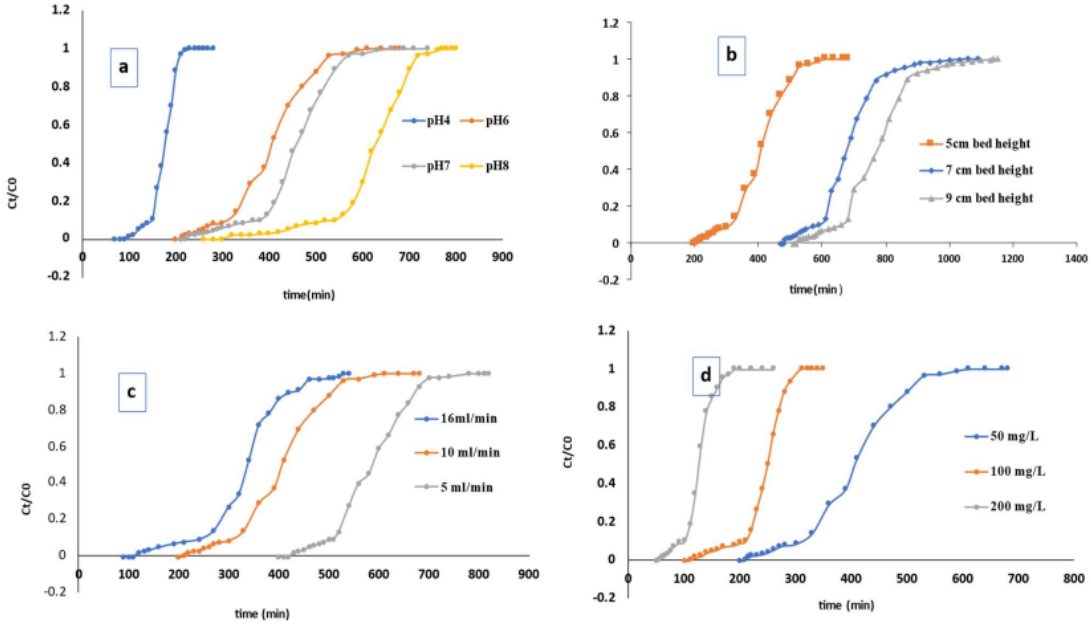

Fig. 5.42: Effect of various operational conditions on breakthrough curve for fluoride adsorption in fixed-bed containing raw SB

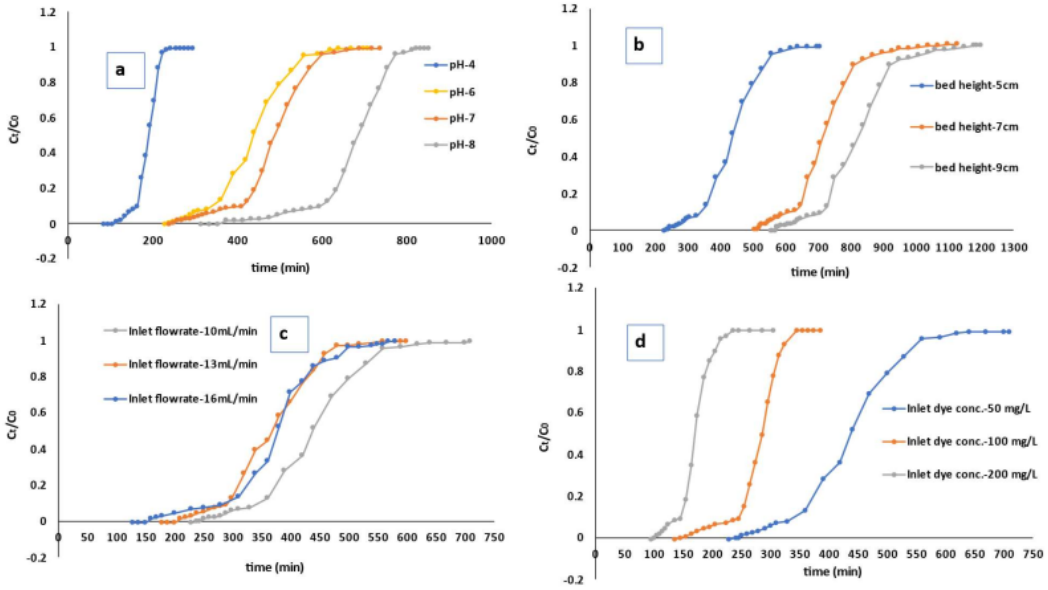

Fig. 5.43: Effect of various operational conditions on breakthrough curve for fluoride adsorption in fixed-bed containing raw SBAC

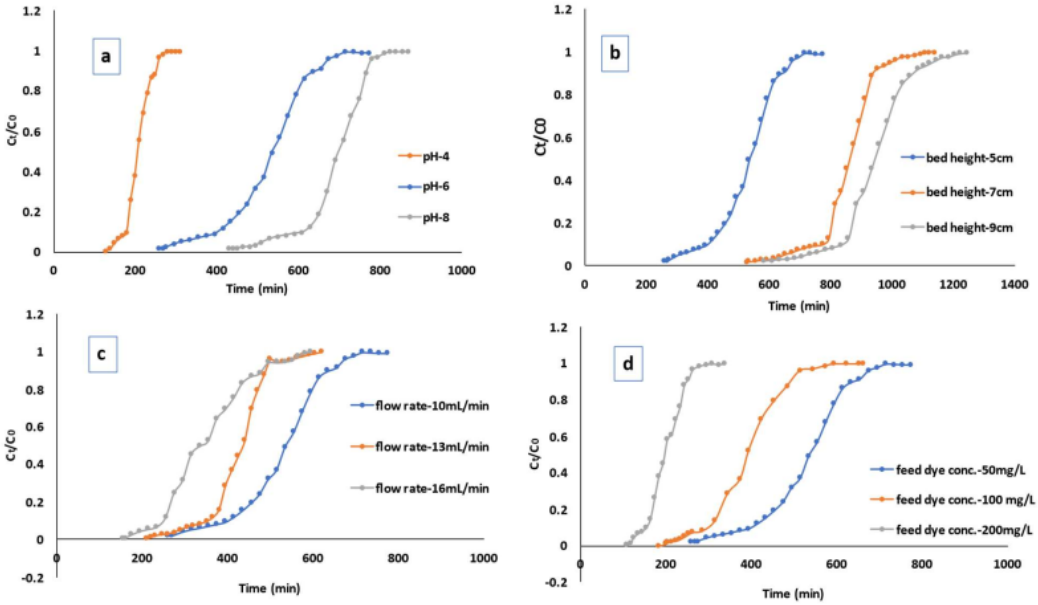

Fig. 5.44. Effect of various experimental conditions (at different pH (a), at different bed height (b), at various feed flow rate (c) and at different MG dye concentrations (d)) on breakthrough curve for MG dye adsorption onto Alginate-bentonite/SBAC

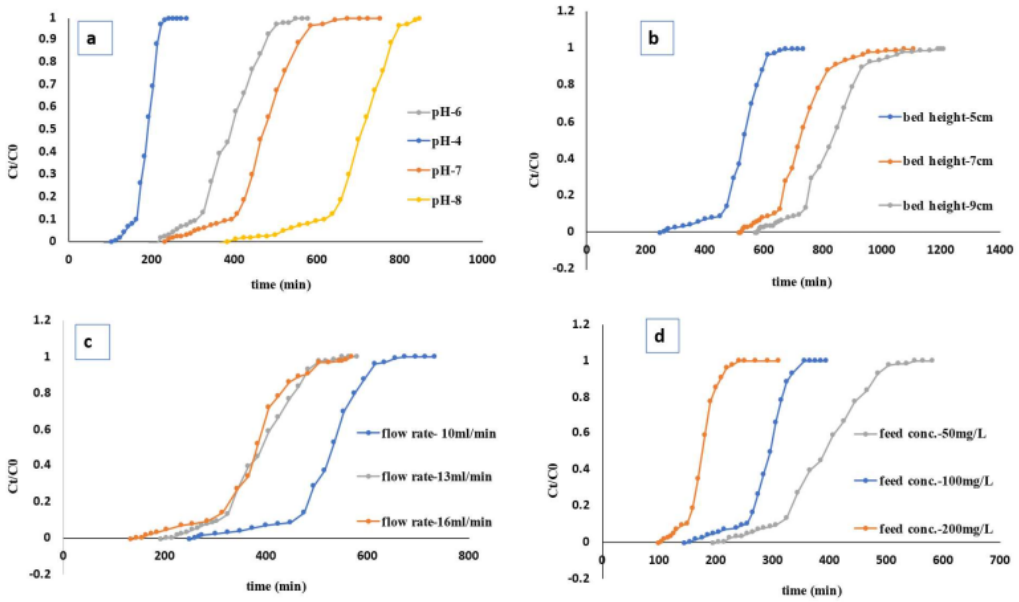

Fig. 5.45: Effect of various operational conditions on breakthrough curve for dye removal using nanocellulose/PVA composite (at different pH (a), at different bed height (b), at different inlet flow rate (c), at various inlet concentrations (d))

Kinetic Modelling data of fixed-bed column adsorption of MG dye

Calculated values of Yoon-Nelson model parameters (k_{YN} and τ) and Thomas model parameters (k_{Th} and q_0) along with corelation coefficients (R^2) are shown in Table 5.12 (a, b, c &d) for raw SB, SBAC, Alginate-bentonite/SBAC beads and Nanocellulose/PVA composite, respectively. Results showed that the model parameter k_{YN} increased with concentration of feed solution and the value of τ decreased. On the other hand, with increase in flow rate of feed solution and pH, the estimated value of k_{YN} and τ is reduced. It was noted that k_{Th} decreased with increasing both the adsorbent bed height and the flow rate of the feed solution, whereas q_0 increased for such conditions. The value of q_0 increased with increasing both the feed concentration and pH of dye solution. Results showed that the correlation coefficient are in the range of 0.95 to 0.99. Results suggests that experimental data obtained from fixed-bed column study were well established by Thomas model as well as Yoon-Nelson model.

Table 5.12(a): Derived Parameters of column kinetic models for MG dye adsorption on **raw SB** at different experimental conditions

Operational parameters				Thomas model			Yoon-Nelson model		
F(ml/min)	C_0(mg/L)	Z(cm)	pH	k_{TH} ($\times10^{-3}$ L/mg min)	q_0($\times10^2$ mg/g)	R^2	k_{YN} (L/min)	τ (min)	R^2
10	50	4	6	0.5116	541.266	0.978	0.02558	405.400	0.978
10	50	8	6	0.3432	477.4661	0.995	0.01716	694.032	0.995
10	50	10	6	0.307	416.1653	0.996	0.01535	781.960	0.996
16	50	4	6	0.4104	686.2342	0.981	0.02052	328.413	0.981
5	50	4	6	0.546	391.8407	0.995	0.02733	579.923	0.995
10	100	4	6	0.524	619.754	0.960	0.05245	229.09	0.960
10	200	4	6	0.328	693.308	0.962	0.06578	127.911	0.962
10	50	4	4	0.1505	231.047	0.977	0.07528	170.913	0.977
10	50	4	7	0.463	596.702	0.980	0.02315	441.56	0.980
10	50	4	8	0.500	783.095	0.9527	0.02297	578.985	0.9527

Table 5.12(b): Derived Parameters of column kinetic models for MG dye adsorption on **SBAC** at different experimental conditions

Experimental conditions				Yoon Nelson model			Thomas model		
F(ml/min)	C_0 (mg/L)	Z (cm)	pH	k_{YN} (L/min)	τ (min)	R^2	k_{TH} ($\times10^{-3}$ L/mg min)	q_0 ($\times10^2$ mg/g)	R^2
10	50	5	6	0.0232	451.234	0.962	0.464	805.775	0.962
13	50	5	6	0.0262	363.44	0.983	0.524	843.7	0.983
16	50	5	6	0.0222	362.994	0.987	0.444	1037.126	0.987
10	100	5	6	0.0462	268.947	0.988	0.462	960.525	0.988
10	200	5	6	0.0572	170.637	0.950	0.286	1218.836	0.950
10	50	7	6	0.0192	763.058	0.978	0.384	978.2795	0.978
10	50	9	6	0.0162	839.61	0.998	0.324	863.7963	0.998
10	50	5	4	0.0632	186.409	0.961	1.264	332.8732	0.961
10	50	5	7	0.0222	477.423	0.986	0.444	852.541	0.986
10	50	5	8	0.0222	639.804	0.937	0.444	1142.507	0.937

Table 5.12(c): Derived parameters of column kinetic models for MG dye adsorption onto **Alginate-bentonite/SBAC** at different experimental conditions

Experimental conditions				Yoon Nelson model			Thomas model		
F(ml/min)	C_0 (mg/L)	pH	Z (cm)	k_{YN} (L/min)	τ (min)	R^2	$k_{TH}\times10^{-2}$ (L/mg min)	$q_0\times10^2$ (mg/g)	R^2

10	50	6	5	0.0242	486.033	0.970	0.0484	736.4137	0.970
13	50	6	5	0.0254	415.275	0.971	0.0508	817.9671	0.971
16	50	6	5	0.0214	361.355	0.956	0.0428	17.52025	0.956
10	50	6	7	0.0199	747.236	0.961	0.0398	667.1752	0.961
10	50	6	9	0.0148	917.297	0.971	0.0296	611.5315	0.971
10	50	4	5	0.0678	205.545	0.982	0.1356	311.4329	0.982
10	50	8	5	0.0231	660.779	0.950	0.0462	1001.181	0.950
10	100	6	5	0.0455	277.780	0.974	0.0455	841.7582	0.974
10	200	6	5	0.0479	200.688	0.985	0.02395	1216.297	0.985

Table 5.12(d): Derived parameters of column kinetic models for MG dye adsorption onto **nano-cellulose/PVA** at different experimental conditions

Experimental conditions				**Yoon Nelson model**			**Thomas model**		
F(ml/min)	**C_0 (mg/L)**	**pH**	**Z (cm)**	**k_{YN} (L/min)**	**τ (min)**	**R^2**	**$k_{TH}\times 10^{-2}$ (L/mg min)**	**$q_0\times 10^2$ (mg/g)**	**R^2**
10	50	6	5	0.0241	491.327	0.93	0.0482	1169.83	0.93
13	50	6	5	0.0283	376.289	0.971	0.0566	447.964	0.97
16	50	6	5	0.0215	363.720	0.97	0.0430	1385.60	0.97
10	100	6	5	0.0521	274.357	0.93	0.0521	1306.46	0.93
10	200	6	5	0.0658	177.857	0.93	0.0329	1693.87	0.93
10	50	4	5	0.0758	188.773	0.96	0.1516	449.459	0.96
10	50	8	5	0.0195	683.589	0.97	0.039	1627.59	0.97
10	50	6	7	0.0177	734.519	0.99	0.0354	1748.85	0.99
10	50	6	9	0.0161	831.925	0.99	0.0322	1980.77	0.99

5.3. Summery

In this present work, the applicability of raw SB, SBAC, Alginate-bentonite/SBAC beads for the biosorption of MG dye and fluoride was investigated in the batch, and the continuous flow fixed-bed column mode. Taking into consideration the obtained results from the present study following conclusions were made:

- Isotherm study suggested that the Freundlich isotherm model (R^2 =0.999) provided the best fit to the equilibrium adsorption data of the batch experiment and the biosorption capacity.

- Dye adsorption Isotherm showed that the estimated value of monolayer adsorption capacity 169.49, 172.414, 185.185, 196.078, 188.68, 212.76, and 263.158 mg/g for SB powder, SBC, SBAC, Alginate-Bentonite/SBAC beads, Cellulose, NanoCellulose/PVA, Alginate-Nanocellulose beads respectively.
- Adsorption kinetic study indicated that the adsorption system using the biosorbent was directed by the Pseudo-Second-order model.
- From the thermodynamic point of view, the negative value of ΔG (Gibbs free energy) and ΔH (Enthalpy change) at all temperatures signified that the reactions involved in biosorption process were spontaneous and exothermic, respectively. the positive value of ΔS signified the randomness of adsorbate molecules on the biosorbent surface
- RSM modeling showed that optimization was effectively correlated with batch experimental data.
- Fixed-bed column study revealed that the Breakthrough time decreased with increasing both initial feed concentration and feed flow rate. Whereas it was increased with the pH of the feed solution. Adsorbent bed capacity and breakthrough time improved with increasing bed height.
- Fixed bed study for MG dye removal indicated that Alginate-bentonite/SBAC composite beads shows better results in comparison with raw SB, SBAC, Nanocellulose/PVA composite as adsorbent.
- Thomas model and Yoon–Nelson model satisfactorily described the adsorption of MG dye onto prepared biosorbents in a fixed-bed column system

Results indicated that NaOH treated activated biochar (SBAC) derived from sugarcane bagasse, Alginate-bentonite/SBAC and Nanocellulose/PVA exhibited a very good adsorption capacity towards aqueous Malachite Green (MG) remediation and possibly will be used as an efficient and economically feasible adsorbent substance for the exclusion of pollutants from contaminated water.

Chapter.6

Evaluation of Fluoride removal study using carbonaceous and polymeric material grafted composites

6.1. Introduction

In this present chapter, the application carbonaceous and polymeric material grafted composites in Fluoride removal process in in batch and fixed-bed systems has been discussed. The effects of key operational parameters (pH, composite dosages, and initial concentration of fluoride in solution) on the adsorption ability were examined. Bio-sorption isotherm study, kinetics study, and thermodynamic analysis of the remediation process has been reported. The optimized condition of independent variables for removal process were estimated using regression equation and by analyzing the contour plots obtained from RSM study. Fixed bed study data was evaluated using column adsorption kinetic models (Thomas and Yoon-Nelson).

6.2. Results and discussion

6.2.1. Comparative batch study using prepared biosorbents

Fluoride removal efficiency of prepared biosorbents at various experimental parameters are presented graphically in Fig. 6.1, Fig. 6.2, Fig. 6.3, Fig. 6.4 and Fig. 6.5. Graphical presentation of equilibrium concentration and fluoride adsorption capacity of those biosorbents under optimum conditions were illustrated in Fig. 6.6-6.12. Fluoride removal efficiency and adsorption capacity of nanocellulose/PVA found to be higher than the other biosorbents (raw SB, SBAC, Alginate-bentonite/SBAC and Alginate-nanocellulose) under all experimental conditions. The results suggest that the fluoride removal efficiency of nanocellulose/PVA for all the experimental conditions showed better result as compared to other prepared biosorbents.

Influence of pH

The influence of pH level on defluoridation efficiency was observed using raw SB, SBC and SBAC as adsorbents at various pH (2, 4, 6, 7, 8) by contacting 2g/L of adsorbent mass to fluoride solution of specified pH for 24 hr in BOD shaker while other parameters were kept constant (initial fluoride concentration=6 mg/L temperature= 30°C, agitation speed=140 RPM). With SBAC, defluoridation efficiency at pH = 2.0 was 64.7577 % and 54.35% at pH = 8.0. Defluoridation efficiency of Alginate-bentonite/SBAC was 80.334 % at pH = 2.0 which decreased to 65.31% at pH 8.0 (Fig. 6.1(b)). The corresponding fluoride concentration in the residual solution was 1.179 mg/L and 1.961 mg/L respectively. At pH 2.0, % removal of Fluoride by Nanocellulose/PVA was obtained to be 87.72 % (Fig. 6.1 (c)) and the value of equilibrium concentration of fluoride in the solution was 0.737 mg/L whereas at higher pH (pH 8.0) equilibrium concentration of fluoride solution decreased to 1.98 mg/L and removal efficiency was 67.04%. Similarly, at high acidic media (pH 2.0), Fluoride adsorption efficiency

onto Alginate-nanocellulose composite and cellulose, were 86.28% and 78.39%, respectively, whereas at basic condition (pH = 8.0) this value reduced to 73.23% and 56.43% respectively (Fig. 6.1(d)). at pH 7 defluoridation efficiencies of Nanocellulose/PVA polymeric composite, cellulose and PVA were 83.14%,75.95% and 55.06% respectively. Results suggested that Nanocellulose/PVA composite gave better performance than individual components of the composite.

At basic condition (>7), adsorption efficiency significantly depended on the competition capability of OH^- ion with fluoride anions for active binding sites on the biosorbent surface (Stipp 1999; Munagapati et al. 2010). PZC results indicated that once pH of fluoride was lower than the value of pH_{PZC}, higher biosorption efficiency for anionic fluoride removal was noted as the adsorbent surface become electropositive at pH< pH_{PZC}. At higher pH (pH > pH_{PZC}) adsorbent surface become predominantly negative charged resulting in low adsorption efficiency. Further experiments were carried out at pH 6. The cause is the cost saving benefit and a possibility to search the minimum requirement in order to employ the biosorbent in the rural areas, where pH maintains might not be a desirable solution.

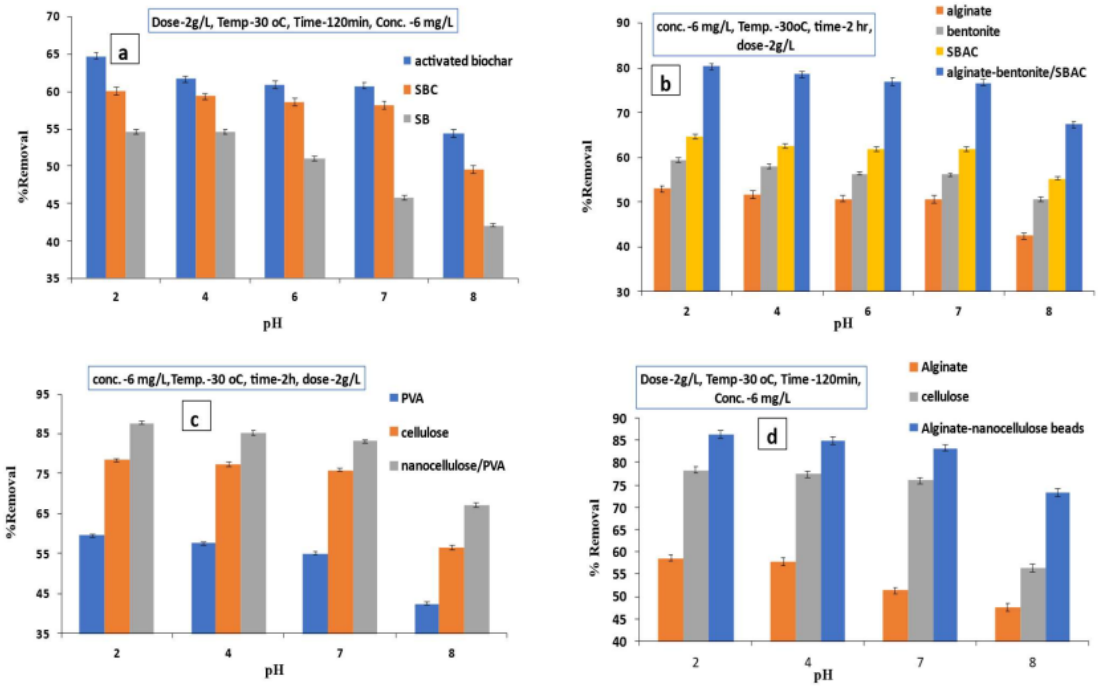

Fig. 6.1: Effects of solution pH on Fluoride removal efficiency of activated biochar (a), Alginate-bentonite/SBAC beads (b), Nanocellulose/PVA composite (c) and Alginate-nanocellulose beads (d)

Influence of contact time

The fluoride adsorption experiment was carried out at different time interval at constant initial fluoride concentration (6mg/L), system temperature (30 ^{o}C), adsorbent dose (2 g/L) and pH (6.0). It was noted that most of the the defluoridation process took place within first 30 min (Fig. 6.2). Similarly, with increasing contact time, fluoride adsorption capacity increased and residual concentration of fluoride in solution decreased (Fig. 6.6- Fig. 6.12). It was observed that with increasing the contact time fluoride removal efficiency of SB and SBAC increased and maximum efficiency was 54.6% and 60.944% respectively (Fig. 6.2(a)). With increasing contact time Fluoride remediation efficiency of Alginate-bentonite/SBAC composite beads was increased and maximum efficiency obtained was 76.93% (Fig. 6.2(b). With increasing contact time, the fluoride removal efficiency improved from 71.05% to 83.11% (Fig. 6.2(c)). Similarly with Alginate-nanocellulose composite as adsorbent with increasing contact time defluoridation efficiency increased and maximum defluoridation efficiency found to be 83.72% (Fig. 6.2(d)).

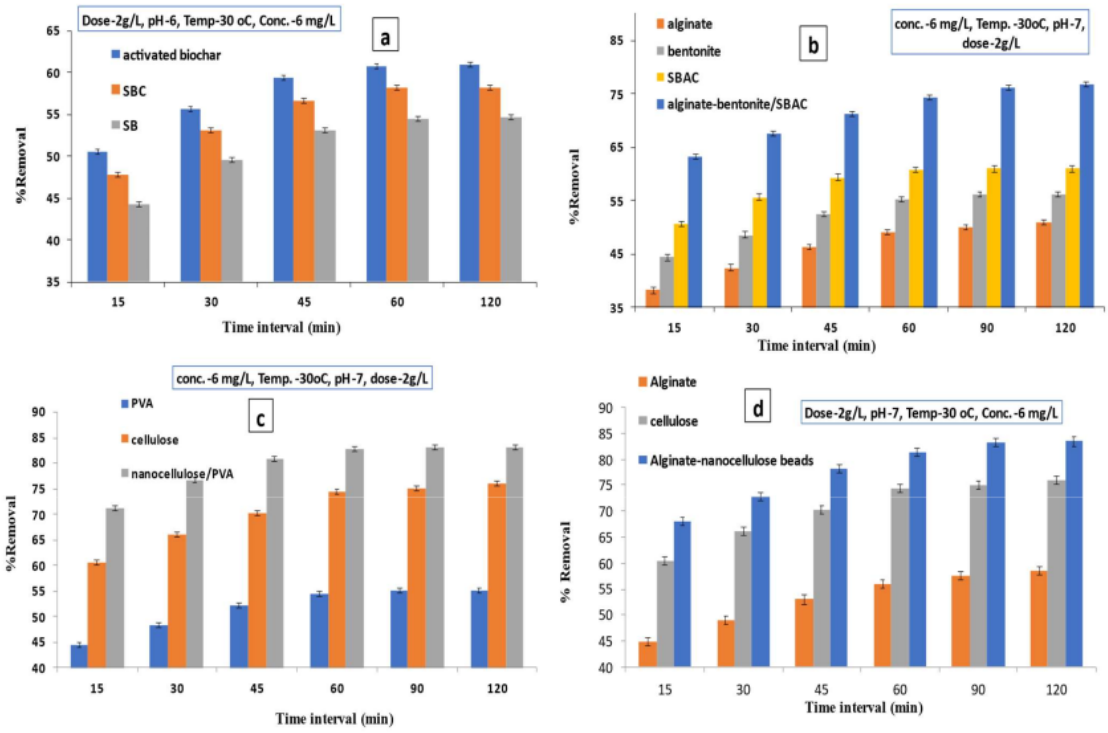

Fig. 6.2: Effects of contact time on Fluoride removal efficiency of activated biochar (a), Alginate-bentonite/SBAC beads (b), Nanocellulose/PVA composite (c) and Alginate-nanocellulose beads (d)

Influence of adsorbent dosage

To investigate the influence of adsorbent dosage on defluoridation efficiency, batch experiment was conducted at various dosages of adsorbent (0.5, 0.75, 1, and 2g/L) in a BOD shaker for 24 hr keeping initial concentration of fluoride solution (6 mg/L) at pH (6), temperature (30°C), agitation speed (140 RPM) constant. It was noticed that as the amount of adsorbent mass increased, percentage of fluoride removal decreased (Fig. 6.3) on increasing adsorbent dose from 0.5g/L to 2g/L, % removal of fluoride on SBAC increased from 59.56 to 60.99% (Fig. 6.3(a)). Percentage of fluoride removal by Alginate-bentonite/SBAC beads increased from 68.01 to 76.93 % (Fig. 6.3(b)) for the same variation of adsorbent dose (Fig. 6.3(b)). Results indicate that on increasing nanocellulose/PVA polymeric composite dosages from 0.5 to 2 g/L, percentage of fluoride removal improved from 76.82 to 83.21% and equilibrium fluoride concentration decreased as of 1.391 to 1.01 mg/L (Fig. 6.3(c)). Similarly, it has been noticed that at higher mass of adsorbents (2g/L) lead to greater percentage removal of fluoride (83.72 % and 76.11% for Alginate-nanocellulose composite and cellulose respectively (Fig. 6.3(d)).

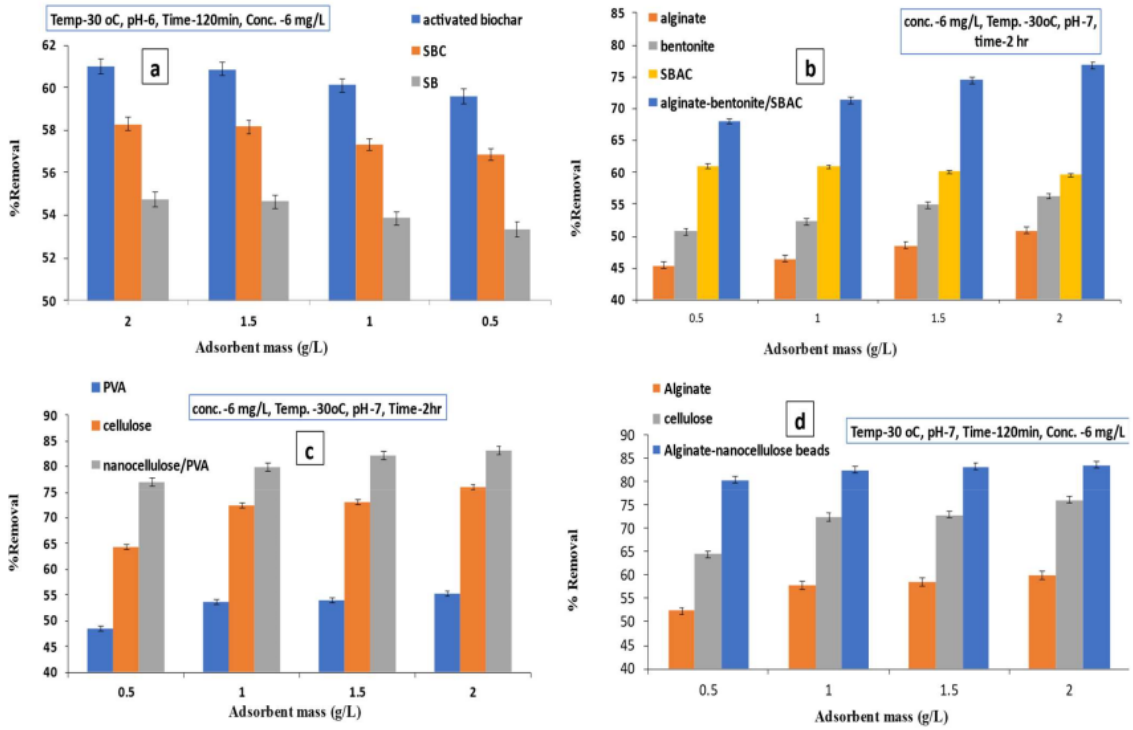

Fig. 6.3: Effects of adsorbent dosage on Fluoride removal efficiency of activated biochar (a), Alginate-bentonite/SBAC beads (b), Nanocellulose/PVA composite (c) and Alginate-nanocellulose beads (d)

Influence of adsorbate concentration

To study the influence of adsorbate concentration on the fluoride adsorption efficiency, 24 hr batch experiments were performed in a BOD incubator at 30°C temperature by varying the fluoride concentration (2-10 mg/L) and contacting fixed amount of adsorbent dose (2 g/L) with the adsorbate solution of specified concentration at pH 6 under a constant agitation speed (140 RPM). As shown in Fig. 6.4(a), when initial fluoride concentration increased from 2mg/L to 10mg/L, fluoride uptake efficiency of SBAC reduced from 62.11 to 59.22%. with increasing initial concentration of fluoride solution from 2mg/L to 8 mg/L, fluoride uptake efficiency of Alginate-bentonite/SBAC beads reduced from 81.78% to 72.3% (Fig. 6.4(b)). With Nanocellulose-PVA as adsorbent (Fig. 6.4(c)) the removal efficiency decreased from 85.4% to 74.06% when initial concentration increased as of 4 mg/L to 10 mg/L and the equilibrium concentration of residual fluoride solution was lowest (0.584 mg/L) at the lowest initial adsorbate concentration (4 mg/L). similarly, Fig. 6.4(d) showed that with changing concentration from 4 to10 g/L, percentage of fluoride adsorption was reduced from 85.87 % to 79%, 76.65% to 68.4%, and 61.03% to 54.9% in case of Alginate-nanocellulose composite, cellulose, and alginate, respectively.

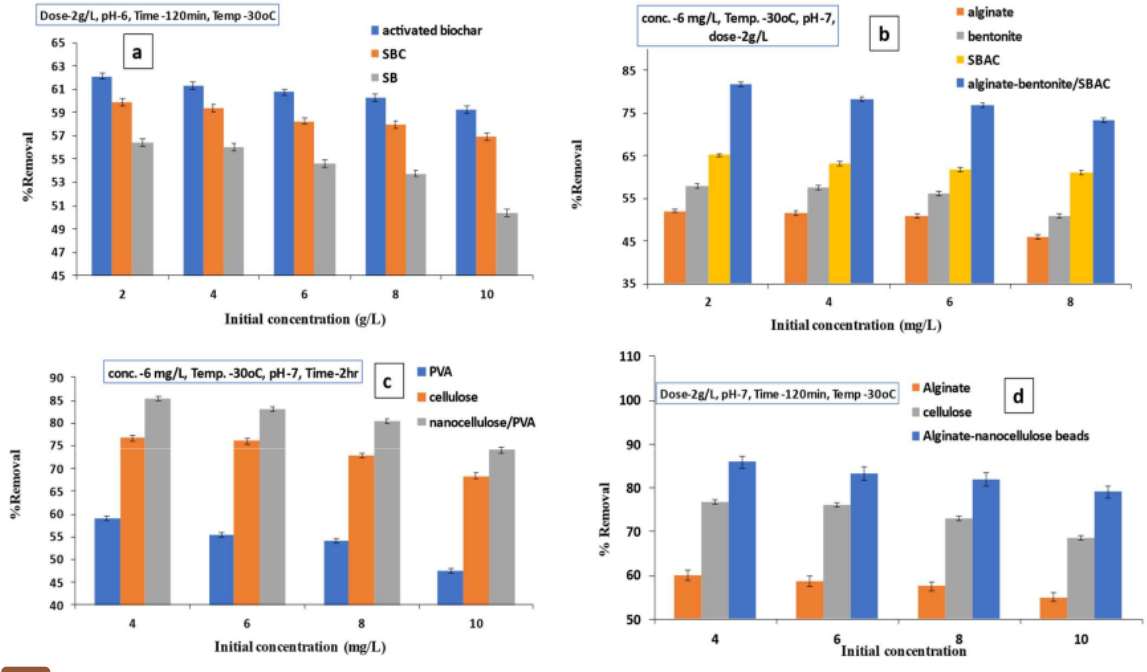

Fig. 6.4: Effects of initial adsorbate concentration on Fluoride removal efficiency of activated biochar (a), Alginate-bentonite/SBAC beads (b), Nanocellulose/PVA composite (c) and Alginate-nanocellulose beads (d)

Influence of system temperature

To investigate the influence of temperature on the fluoride removal efficiency of SB, SBC and SBAC, batch experiments were performed with initial fluoride concentration of 6 mg/L at pH 6.0 using adsorbent dose of 2g/L in a BOD shaker for 24 hr. Fig. 6.5(a) show that while system temperature increased from 25°C to 45°C fluoride uptake efficiency of SBAC decreased from 60.78% to 54.8% and equilibrium concentration was raised from 2.353 to 2.703 mg/L. Similarly, on increasing temperature from 25°C to 45°C fluoride uptake efficiency of Alginate-bentonite/SBAC composite beads reduced from 76.53% to 67.31% (Fig. 6.5(b)) and the equilibrium concentration was increased from 1.17 mg/L to1.96 mg/L. the fluoride removal efficiency of Nanocellulose/PVA was decreased from 83.23% to 60.95% (Fig. 6.5(c)) for the same variation in temperature and the equilibrium concentration of fluoride solution was lowest (1.0122 mg/L) at 25°C. Fig. 6.5(d) illustrated that as the temperature of system increased from 30 °C to 45 °C, % removal of fluoride decreased from 83.72% to 79.01% for Alginate-nanocellulose composite.

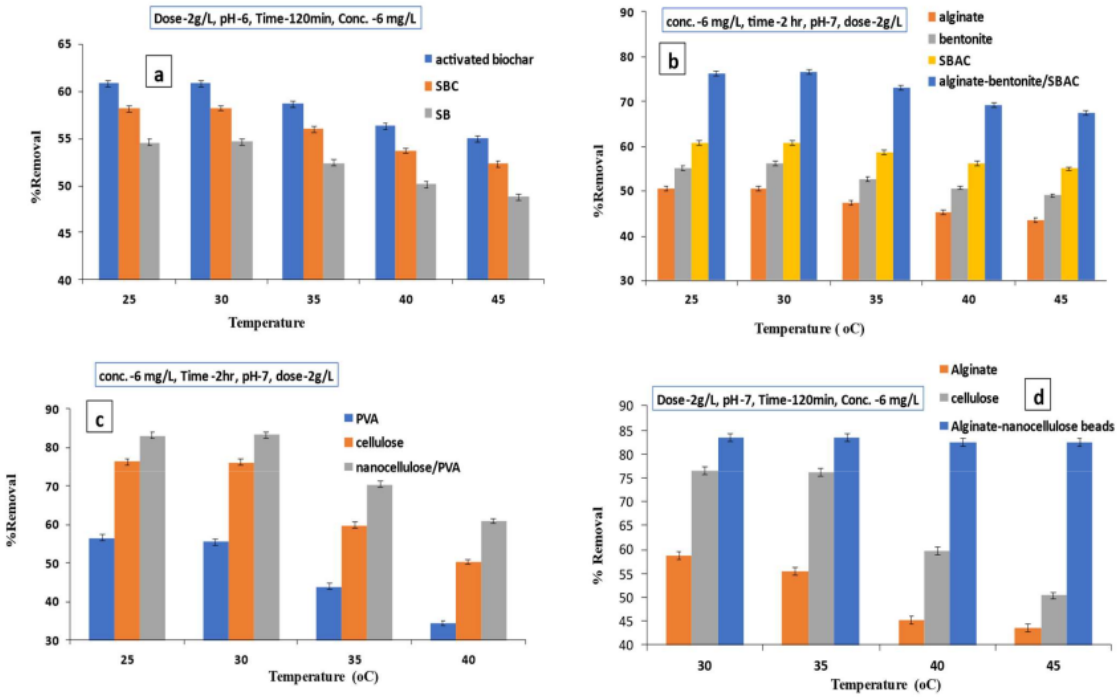

Fig. 6.5: Effects of Temperature on Fluoride removal efficiency of activated biochar (a), Alginate-bentonite/SBAC beads (b), Nanocellulose/PVA composite (c) and Alginate-nanocellulose beads (d)

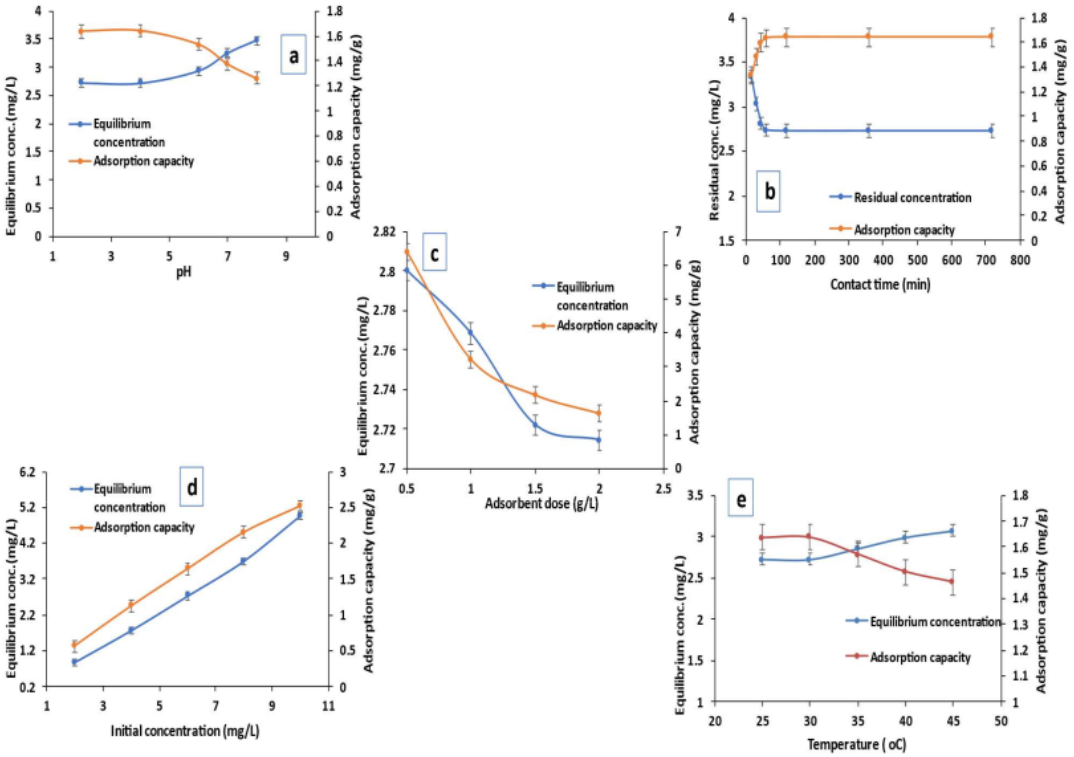

Fig. 6.6: Equilibrium concentration and Fluoride adsorption capacity of raw SB at different experimental conditions

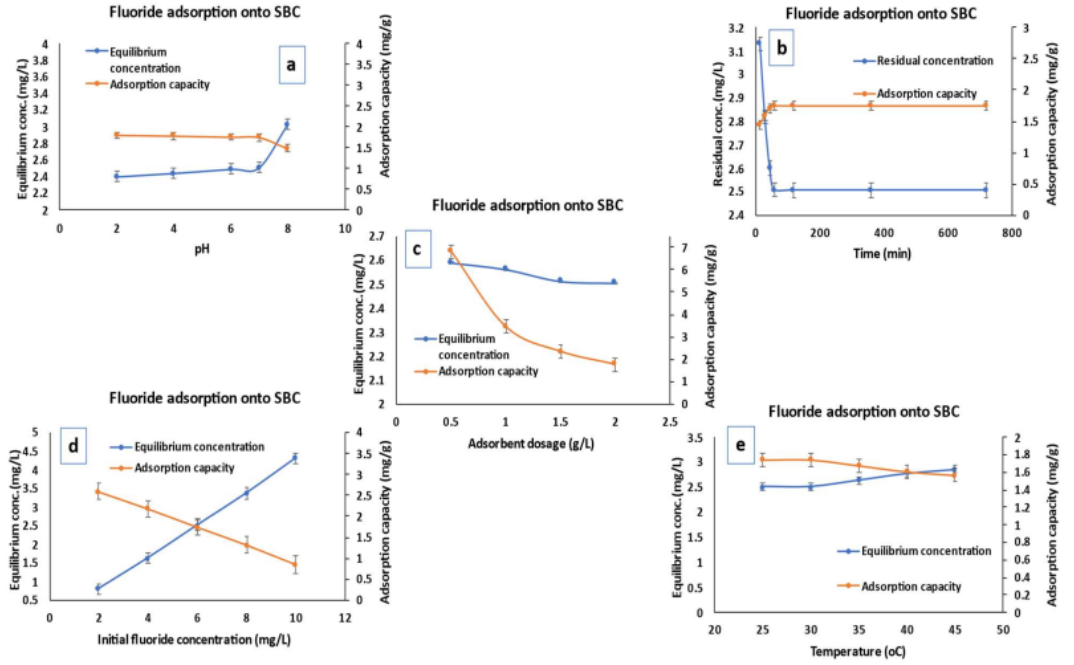

Fig. 6.7: Equilibrium concentration and fluoride adsorption capacity of SBC at different experimental conditions

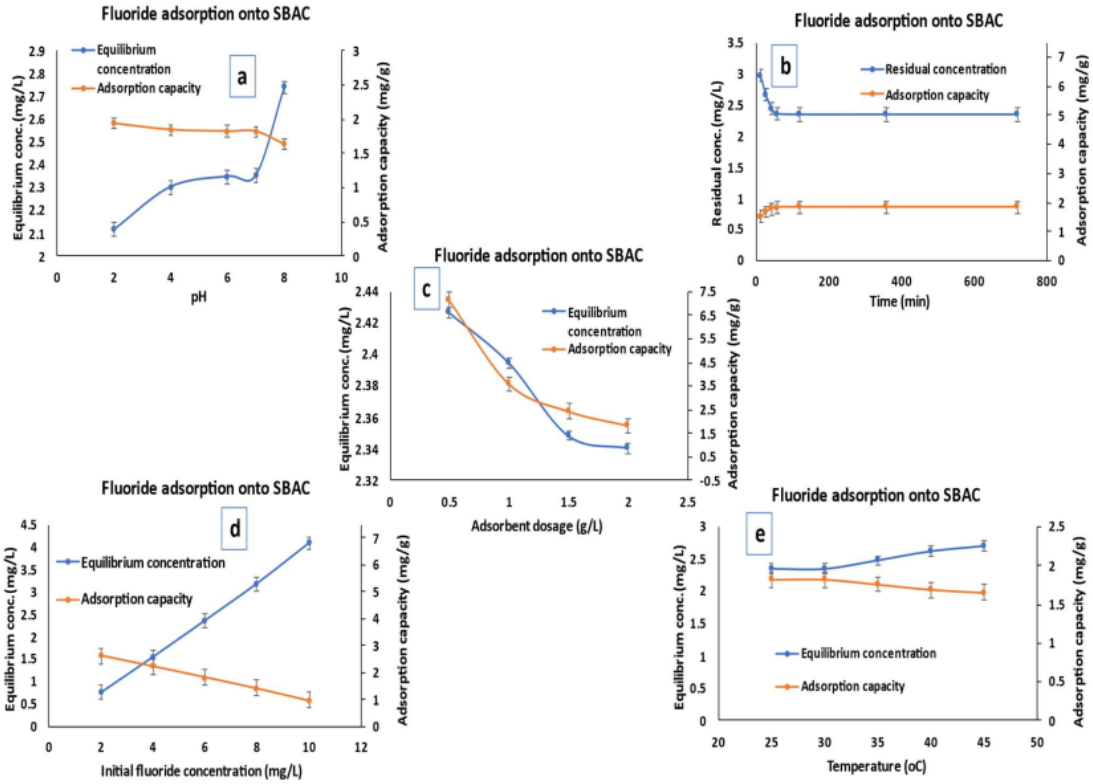

Fig. 6.8: Equilibrium concentration and fluoride adsorption capacity of SBAC at different experimental conditions

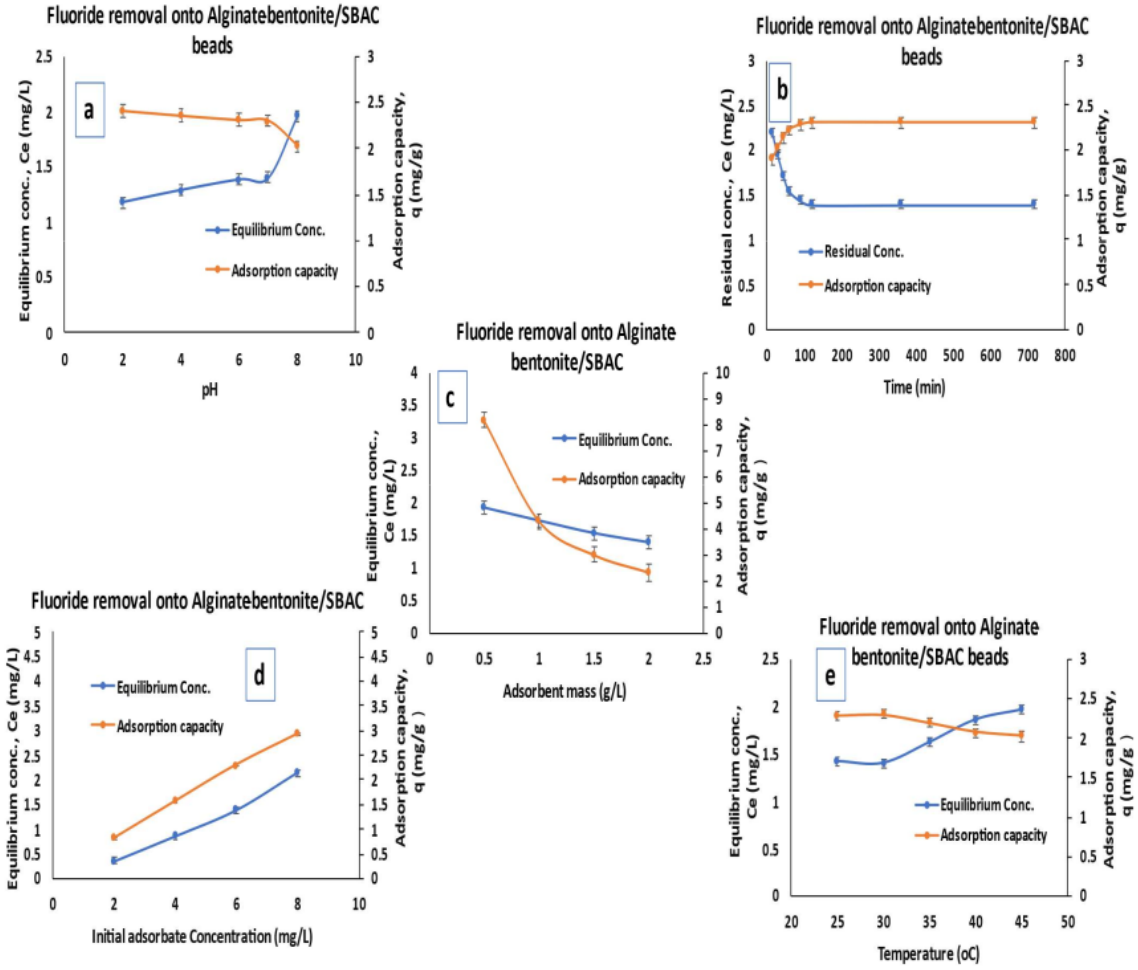

Fig. 6.9: Equilibrium concentration and Fluoride adsorption capacity of Alginate-bentonite/SBAC composite at different experimental conditions

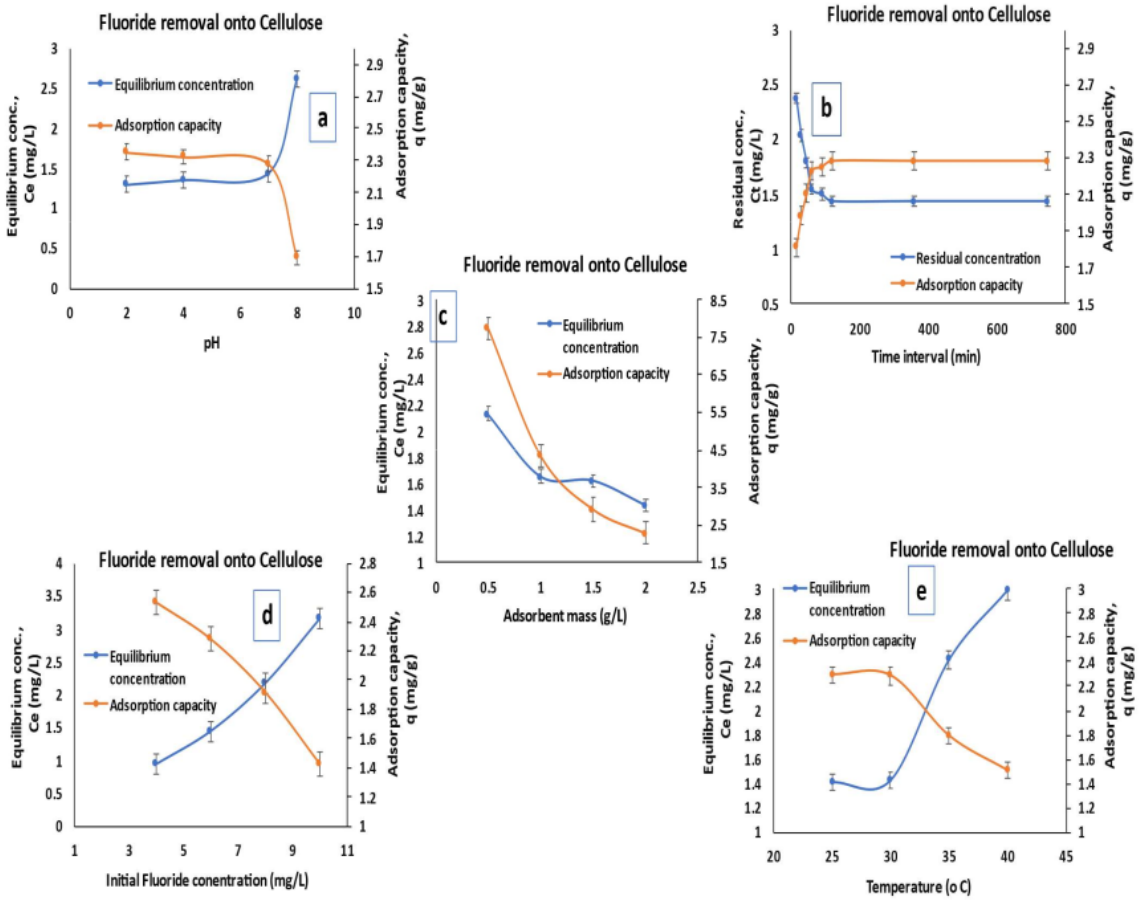

Fig. 6.10: Equilibrium concentration and Fluoride adsorption capacity of Cellulose at different experimental conditions

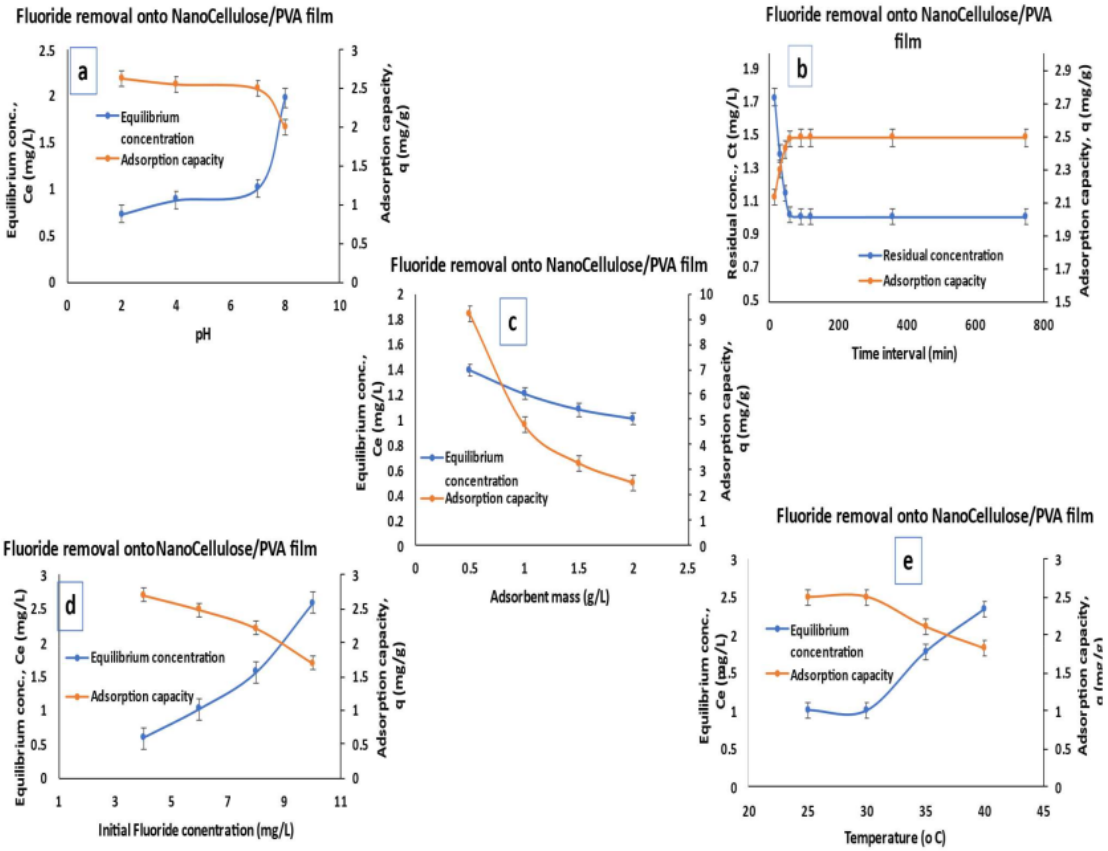

Fig. 6.11: Equilibrium concentration and Fluoride adsorption capacity of nanocellulose/PVA at different experimental conditions

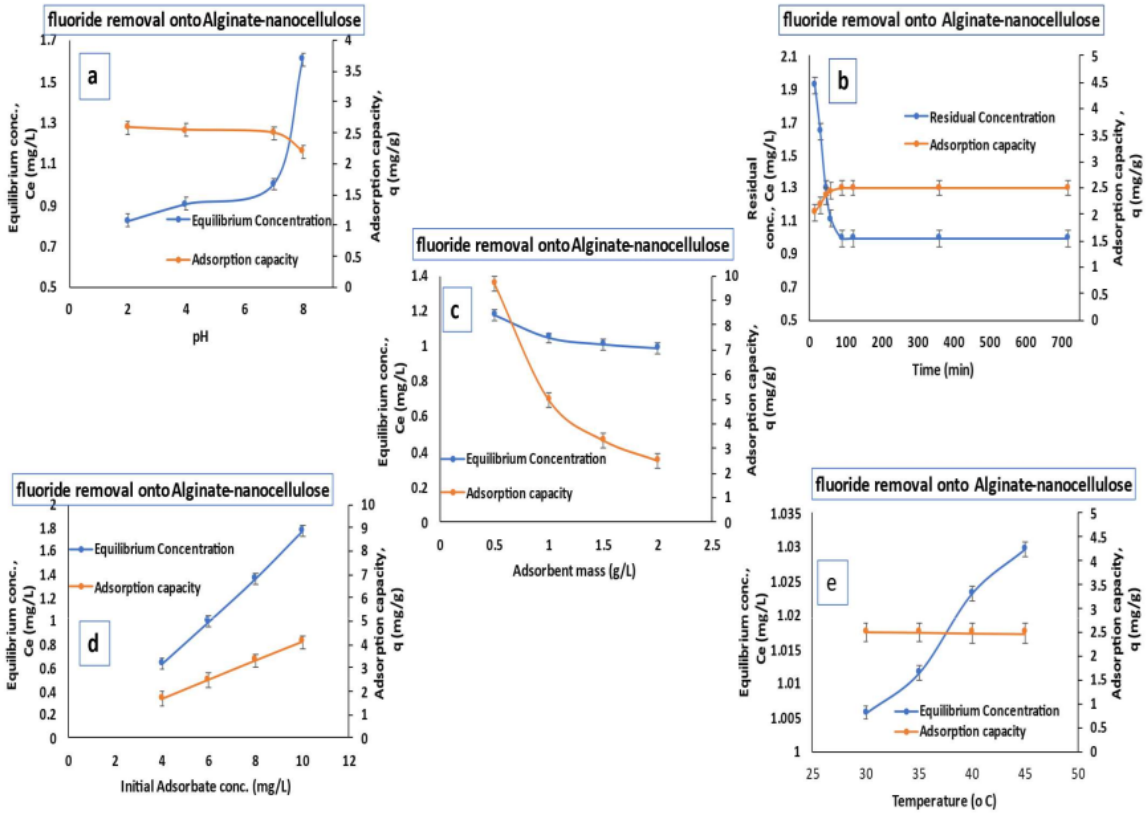

Fig. 6.12: Equilibrium concentration and fluoride adsorption capacity of Alginate-Nanocellulose at different experimental conditions

Fluoride adsorption Isotherm study

The fitting of equilibrium data to the adsorption isotherm models (Langmuir, Freundlich, and Temkin model) and corresponding graphs are presented in Fig. 6.13 to Fig. 6.17. Values of all the derived parameters are listed in the Table 6.1, Table 6.2, and Table 6.3. In general, the experimental equilibrium data was fitted well by the Freundlich model equation ($R^2 > 0.99$).

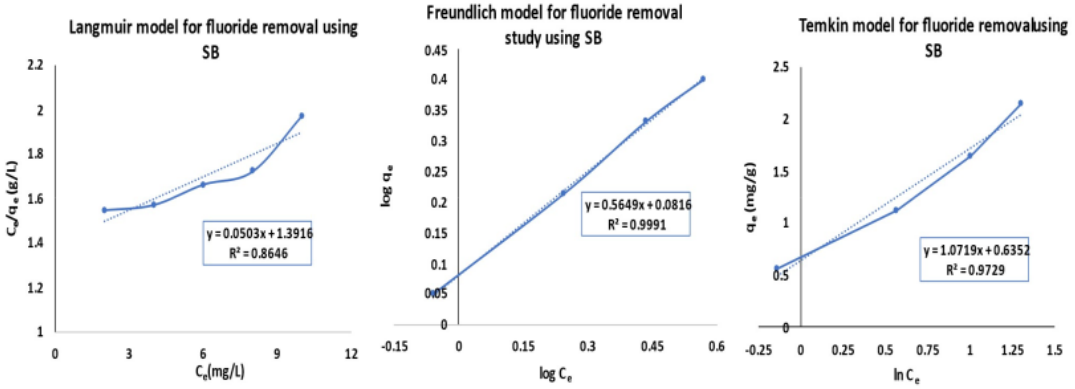

Fig. 6.13: Graphical presentation of Isotherm models for batch adsorption of Fluoride using raw SB

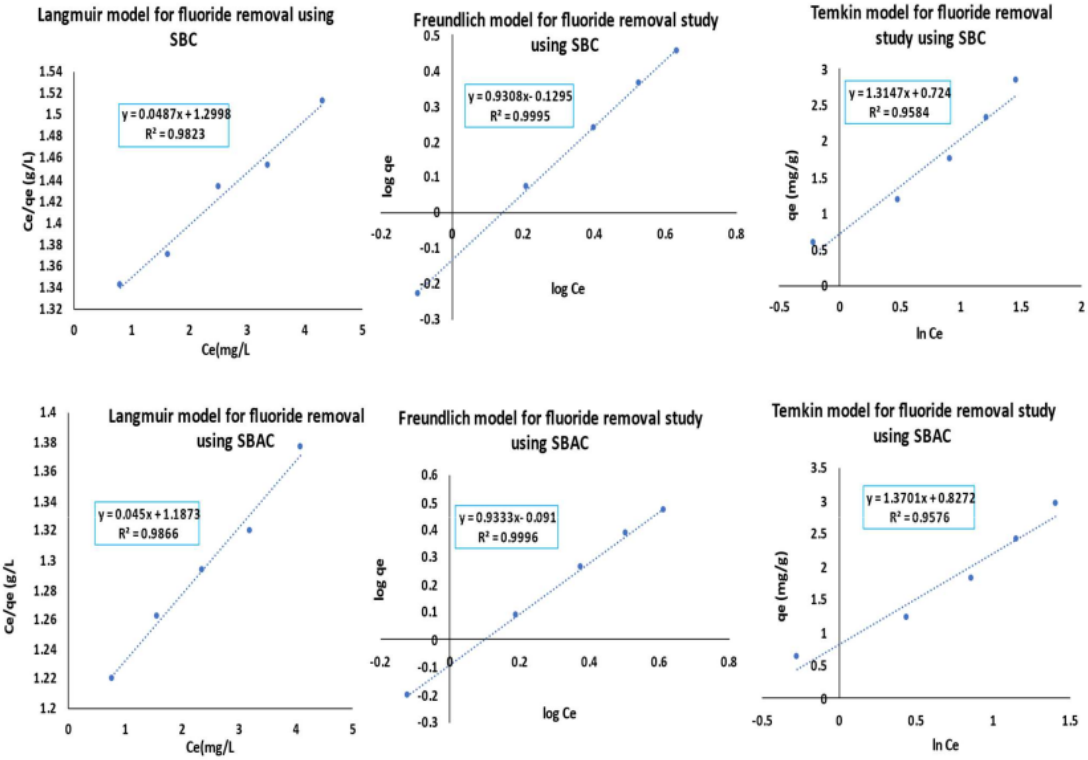

Fig. 6.14: Graphical presentation of adsorption Isotherm for batch adsorption of fluoride using SBC and SBAC

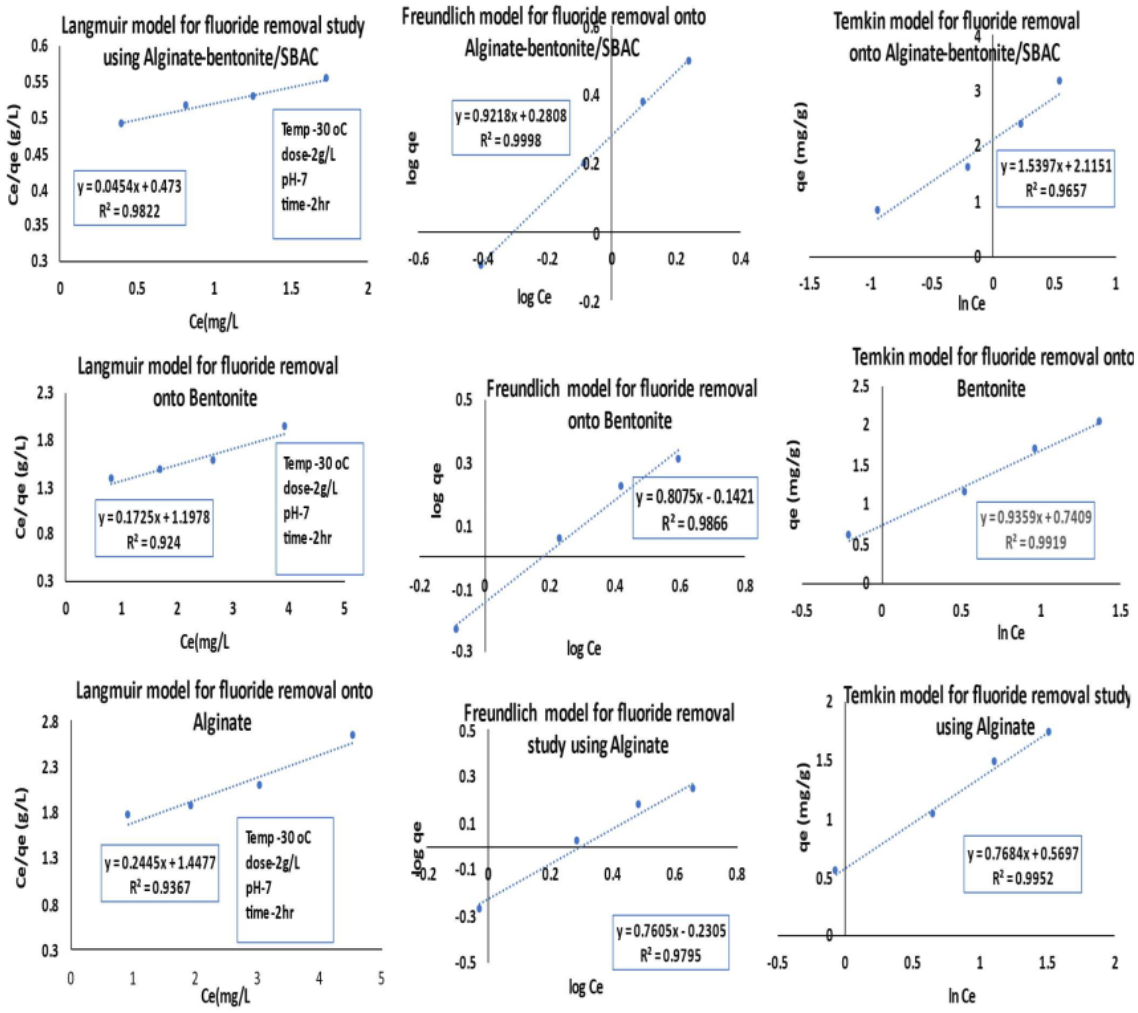

Fig. 6.15: Graphical presentation of Isotherm models for batch adsorption of Fluoride using Alginate-bentonite/SBAC, bentonite and Alginate

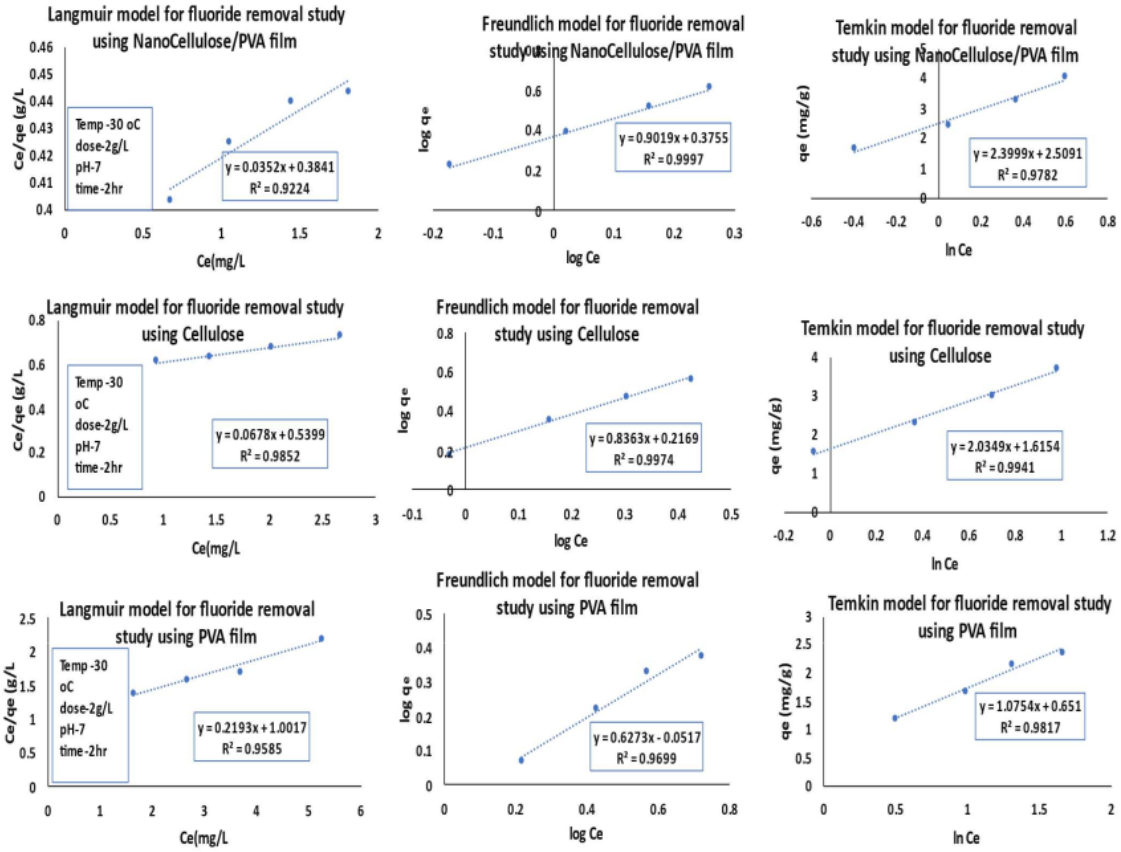

Fig. 6.16: Graphical presentation of Isotherm models for batch adsorption of Fluoride using nano-cellulose/PVA, Cellulose and PVA

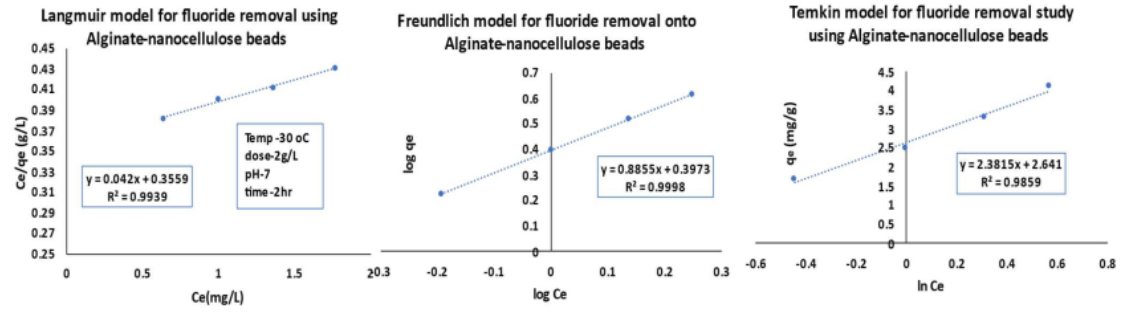

Fig. 6.17: Adsorption Isotherm study graph for batch adsorption of fluoride onto Alginate-nanocellulose

Table 6.1(a): Langmuir isotherm parameters for fluoride adsorption onto SB, SBC and SBAC

Adsorbent	k_L (L/g)	q_m(mg/g)	R_L	R^2
SB	0.0361	19.88	0.8217	0.865
SBC	0.0374	20.53	0.816	0.982
SBAC	0.0379	22.22	0.814	0.987

Table 6.1(b): Langmuir isotherm parameters for fluoride adsorption onto Alginate, bentonite, SBAC and Alginate-bentonite/SBAC

Adsorbent	K_l (L/gram)	q_m(mg/gram)	R_L	R^2
Alginate	0.169	4.089	0.497	0.9367
Bentonite	0.144	5.797	0.536	0.924
Alginate-bentonite/SBAC	0.096	24.6	0.816	0.982

Table 6.1(c): Langmuir isotherm parameters for Fluoride adsorption onto nano-cellulose/PVA, Cellulose and PVA

Adsorbent	K_l (L/gram)	q_m(mg/gram)	R_L	R^2
PVA	0.219	4.56	0.4321	0.958
Cellulose	0.126	14.75	0.570	0.985
nano-cellulose/PVA	0.092	28.41	0.645	0.922

Table 6.1(d): Derived parameters of Langmuir Isotherm models for batch adsorption of fluoride onto Alginate-nanocellulose, Cellulose and Alginate

Adsorbent	K_l (L/gram)	q_m(mg/gram)	R_L	R^2
Alginate	0.169	4.089	0.497	0.936
Cellulose	0.126	14.75	0.570	0.985
Alginate-nanocellulose beads	0.118	23.809	0.585	0.993

Table 6.2(a): Freundlich isotherm Parameters for fluoride removal using SB, SBC, and SBAC

Adsorbent	K_f (L/mg)	n	R^2
SB	0.670	1.143	0.994
SBC	0.742	1.0743	0.999
SBAC	0.814	1.191	0.999

Table 6.2(b): Freundlich isotherm parameters for fluoride adsorption onto Alginate, bentonite, and Alginate-bentonite/SBAC

Adsorbent	K_F(L/mg)	n	R^2
Alginate	0.588	1.315	0.979
Bentonite	0.721	1.24	0.987
Alginate-bentonite/SBAC	1.909	1.085	0.999

Table 6.2(c): Freundlich isotherm parameters for Fluoride adsorption onto nano-cellulose/PVA, Cellulose and PVA

Adsorbent	K_F(L/mg)	n	R^2
PVA	0.888	1.594	0.969
Cellulose	1.648	1.195	0.997
nano-cellulose/PVA	2.374	1.109	0.999

Table 6.2(d): Freundlich isotherm parameters for fluoride adsorption onto Alginate-nanocellulose, Cellulose and Alginate

Adsorbent	K_F(L/mg)	n	R^2
Alginate	0.588	1.315	0.979
Cellulose	1.648	1.195	0.997
Alginate-nanocellulose beads	2.496	1.129	0.999

Table 6.3(a): Temkin model Parameters for fluoride removal using SB, SBC and SBAC

Adsorbent	Conc(mg/L)	K_T	B_T	R^2
SB	6	1.808	1.072	0.973
SBC	6	1.734	1.315	0.958
SBAC	6	1.829	1.37	0.957

Table 6.3(b): Temkin model parameters for fluoride adsorption onto Alginate, bentonite, and Alginate-bentonite/SBAC

Adsorbent	Conc(mg/L)	K_T	B_T	R^2
Alginate	6	2.099	0.7684	0.995
Bentonite	6	2.207	0.9359	0.992
Alginate-bentonite/SBAC	6	3.95	1.5397	0.9657

Table 6.3(c): Temkin model parameters for Fluoride adsorption onto nano-cellulose/PVA, Cellulose and PVA

Adsorbent	Conc(mg/L)	K_T	B_T	R^2
PVA	6	2.212	2.035	0.994
Cellulose	6	1.832	1.075	0.982
nano-cellulose/PVA	6	1.169	2.399	0.978

Table 6.3(d): Temkin model parameters for fluoride adsorption onto Alginate-nanocellulose, Cellulose and Alginate

Adsorbent	K_T	B_T	R^2
Alginate	2.099	0.7684	0.995
Cellulose	1.832	1.075	0.982
Alginate-nanocellulose beads	2.883	2.494	0.986

Fluoride adsorption Kinetics study

Fig. 6.18 to 6.22 shows the fitting of the kinetic models to the experimental data. The magnitude of the parameters of the kinetic model are listed in Table 6.4, Table 6.5 and Table 6.6. By comparing the experimental q_e value and theoretical q_e value for both kinetic models, it was noticed that q_e obtained from Pseudo-second-order kinetics was nearly equal to that of its experimental value.

Results suggested that fluoride adsorption onto biosorbents might be better explicated by following pseudo-second-order kinetic equation ($R^2 > 0.99$).

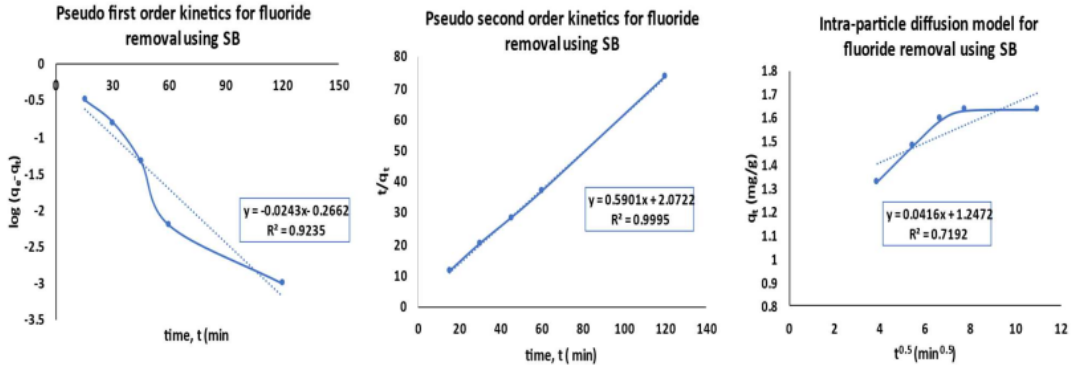

Fig. 6.18: Graphical presentation of kinetic models for batch adsorption of Fluoride using raw SB

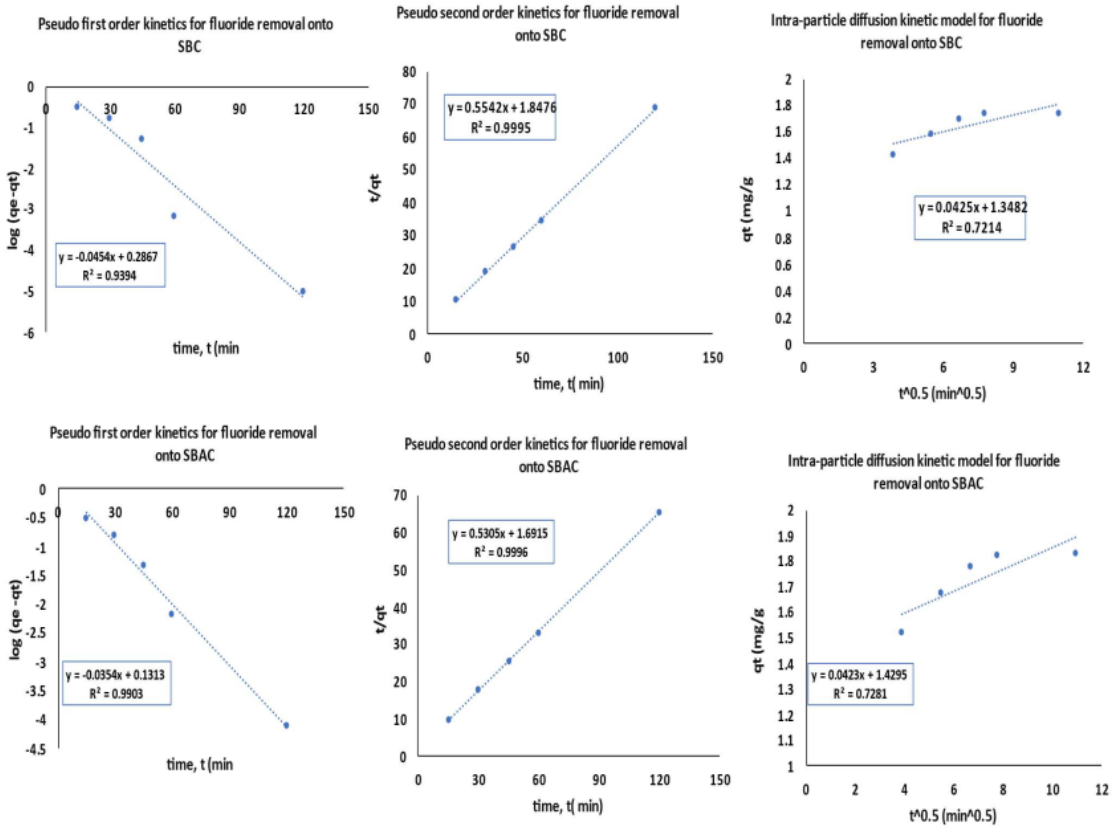

Fig. 6.19: Graphical presentation of adsorption kinetics for batch adsorption of fluoride using SBC and SBAC

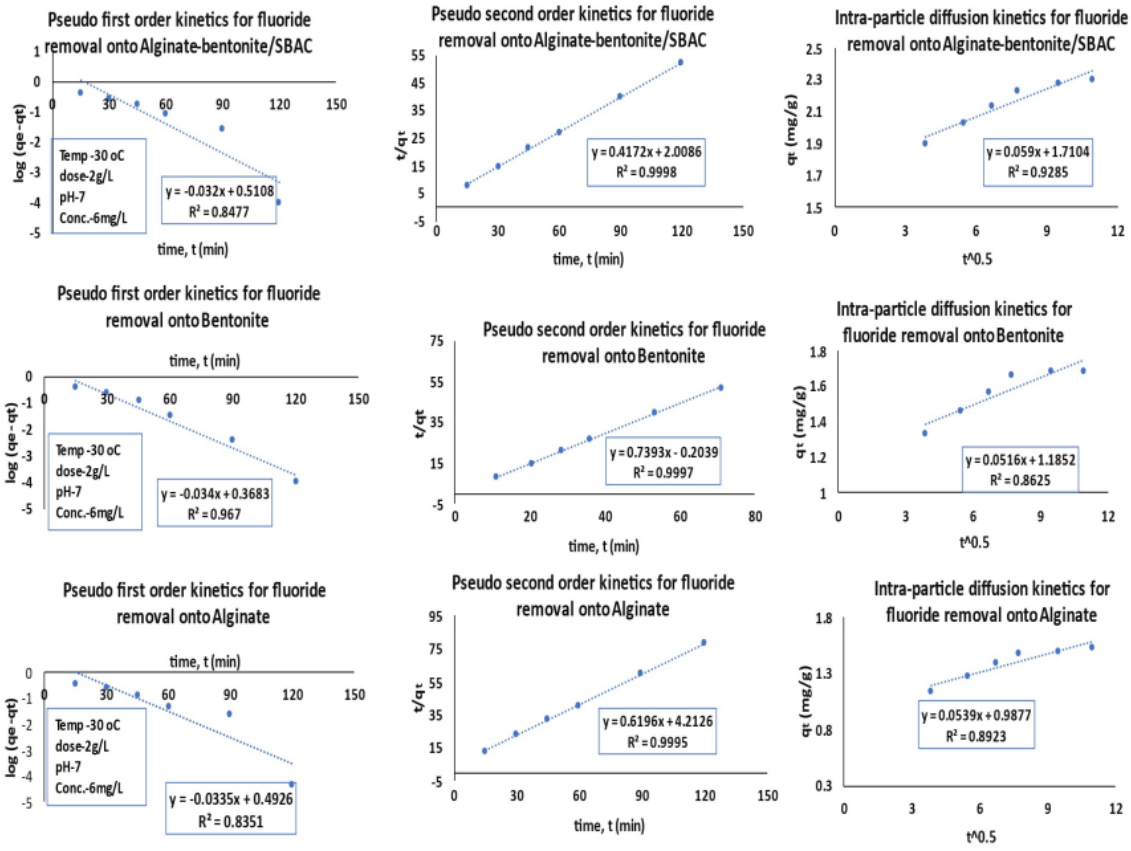

Fig. 6.20: Graphical presentation of kinetic models for batch adsorption of Fluoride using Alginate-bentonite/SBAC, bentonite and Alginate

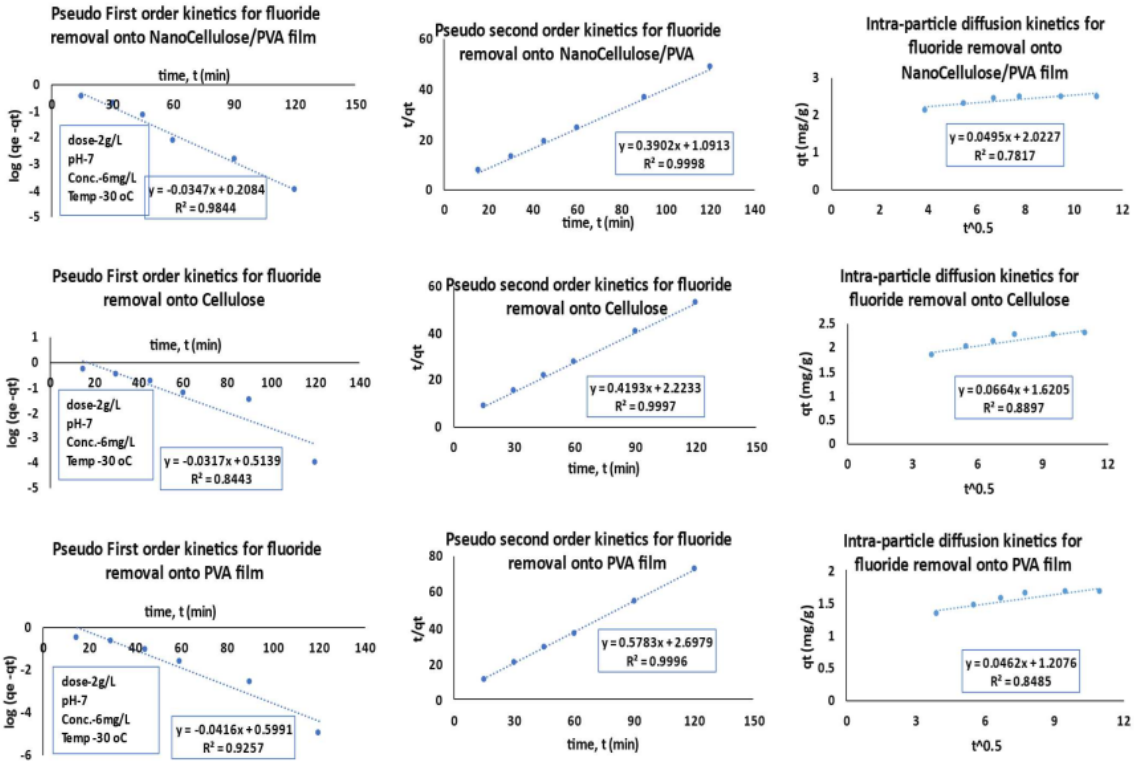

Fig. 6.21: Graphical presentation of kinetic models for batch adsorption of Fluoride using nano-cellulose/PVA, Cellulose and PVA

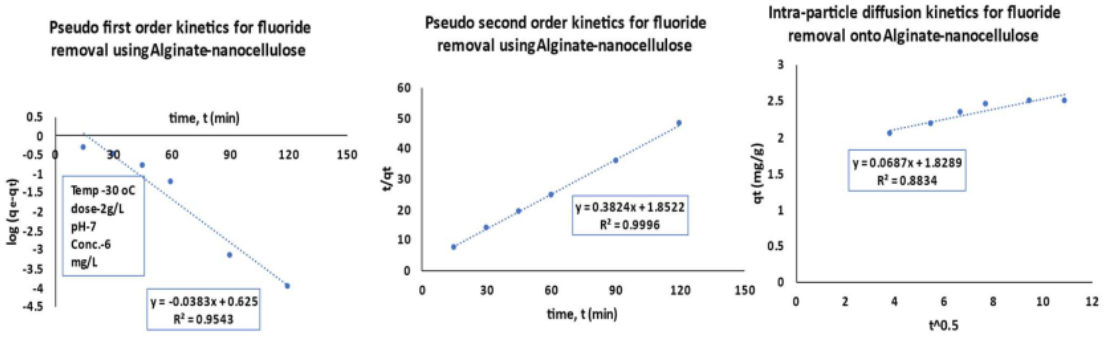

Fig. 6.22: Adsorption Kinetics study graph for batch adsorption of fluoride onto Alginate-nanocellulose

Table 6.4(a): Pseudo-first-order kinetic parameters for fluoride adsorption onto SB, SBC and SBAC

Adsorbent	q_e(exp)	k_1(1/min)	q_e(cal)	R^2
SB	1.639	0.056	0.542	0.9235
SBC	1.83	0.0815	1.353	0.990
SBAC	1.83	0.0815	1.353	0.990

Table 6.4(b): Pseudo-First-Order model parameters for fluoride adsorption onto Alginate, bentonite, and Alginate-bentonite/SBAC

Adsorbent	q_e(exp.)	K_1(min^{-1})	q_e(cal.)	R^2
Alginate	1.525	0.077	3.108	0.8351
Bentonite	1.682	0.078	2.335	0.967
Alginate-bentonite/SBAC	2.3055	0.074	3.242	0.848

Table 6.4(c): Pseudo-First-Order model parameters for fluoride adsorption onto nano-cellulose/PVA, Cellulose and PVA

Adsorbent	q_e(exp.)	K_1(min^{-1})	q_e(cal.)	R^2
PVA	1.656	0.095	3.972	0.925
Cellulose	2.283	0.073	3.265	0.844
nano-cellulose/PVA	2.50	0.079	1.615	0.984

Table 6.4(d): Parameters of Pseudo-First-Order model for fluoride adsorption onto Alginate-nanocellulose, Cellulose and Alginate

Adsorbent	q_e(exp.)	K_1(min^{-1})	q_e(cal.)	R^2
Alginate	1.525	0.077	3.108	0.835
Cellulose	2.283	0.073	3.265	0.844
Alginate-nanocellulose beads	2.502	0.088	4.217	0.954

Table 6.5(a): Pseudo second order sorption kinetics parameters for fluoride adsorption onto SB, SBC and SBAC

Adsorbent	q_e(exp)	K_2(1/min)	q_e(cal)	R^2
SB	0.7852	1.639	1.694	0.999
SBC	1.747	0.1662	1.804	0.999
SBAC	1.83	0.1663	1.885	0.999

Table 6.5(b): Parameters of Pseudo-Second- Order model for fluoride adsorption onto Alginate, bentonite, and Alginate-bentonite/SBAC

Adsorbent	q_e(exp.)	K_2(min^{-1})	q_e(cal.)	R^2
Alginate	1.525	0.091	1.6139	0.999
Bentonite	1.682	0.0867	2.397	0.999
Alginate-bentonite/SBAC	2.3055	0.0866	2.396	0.999

Table 6.5(c): Pseudo-Second-Order model parameters for Fluoride adsorption onto nano-cellulose/PVA, Cellulose and PVA

Adsorbent	q_e(exp.)	K_2(min^{-1})	q_e(cal.)	R^2
PVA	1.656	0.124	1.72	0.999
Cellulose	2.283	0.079	2.38	0.998
nano-cellulose/PVA	2.50	0.139	3.44	0.999

Table 6.5(d): Pseudo-Second-Order model parameters for fluoride adsorption onto Alginate-nanocellulose, Cellulose and Alginate

Adsorbent	q_e(exp.)	K_2(min^{-1})	q_e(cal.)	R^2
Alginate	1.525	0.091	1.6139	0.999
Cellulose	2.283	0.079	2.38	0.998
Alginate-nanocellulose beads	2.502	0.079	2.615	0.999

Table 6.6(a): Intra-particle diffusion kinetic model parameters for fluoride adsorption onto SB, SBC and SBAC

Adsorbent	Conc(mg/L)	K_{int} ($min^{0.5}$)	C	R^2
SB	6	0.0416	1.247	0.7192
SBC	6	0.0425	1.348	0.721
SBAC	6	0.0423	1.429	0.728

Table 6.6(b): Intra-particle diffusion kinetic model Parameters for fluoride adsorption onto Alginate, bentonite, and Alginate-bentonite/SBAC

Adsorbent	Conc(mg/L)	K_{int} ($min^{0.5}$)	C	Conc(mg/L)
Alginate	6	0.0539	0.9877	0.892
Bentonite	6	0.0516	1.1852	0.862
Alginate-bentonite/SBAC	6	0.059	1.71	0.928

Table 6.6(c): Intra-particle diffusion kinetic model parameters for fluoride adsorption onto nano-cellulose/PVA, Cellulose and PVA

Adsorbent	K_{int} ($min^{0.5}$)	C	Conc(mg/L)
PVA	0.046	0.0664	0.849
Cellulose	0.066	0.16205	0.889
nano-cellulose/PVA	0.049	2.0227	0.782

Table 6.6(d): Parameters of Intra-particle diffusion kinetic model for fluoride adsorption onto Alginate-nanocellulose, Cellulose and Alginate

Adsorbent	Conc(mg/L)	K_{int} ($min^{0.5}$)	C	Conc(mg/L)
Alginate	6	0.0539	0.9877	0.892
Cellulose	6	0.066	0.162	0.889
Alginate-nanocellulose beads	6	0.069	1.829	0.883

Thermodynamic study

The magnitude of K_c was calculated using the eqn. 2.14. Fig. 6.23 to Fig. 6.26 depicts the K_c vs. 1/T data of various biosorbents. The magnitude as for ΔG, ΔH, and ΔS obtained from the plots based on eqn. 2.14. and eqn. 2.15 are presented in the Table 6.7. The negative value of ΔG suggest that the fluoride removal process using prepared biosorbents was spontaneous and the negative value of ΔH suggested that F^- adsorption was associated with the exothermic reaction. The positive value of ΔS signify that the fluoride adsorption system was random.

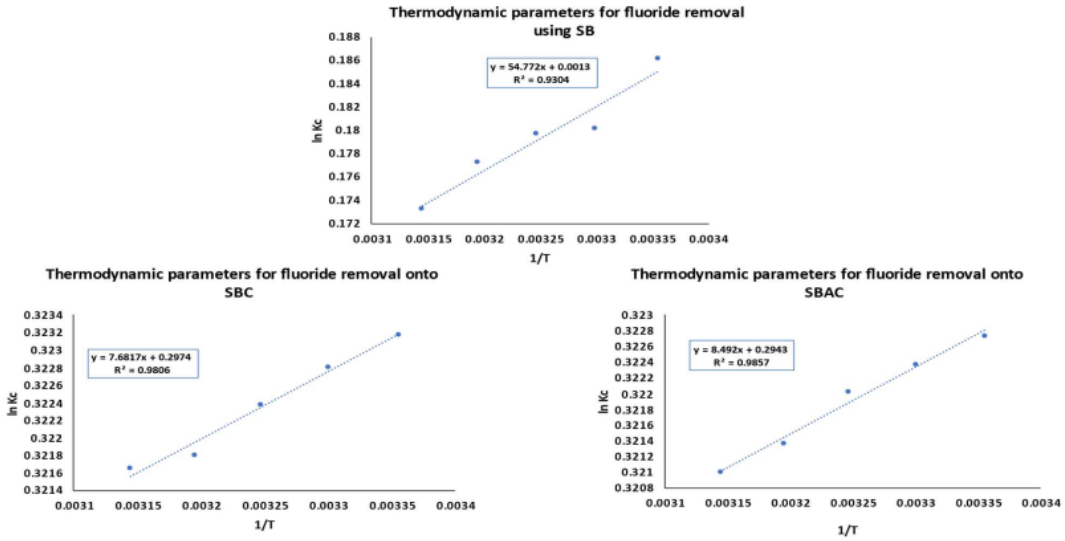

Fig. 6.23: graphical presentation of thermodynamics study for batch adsorption of fluoride using SB, SBC and SBAC

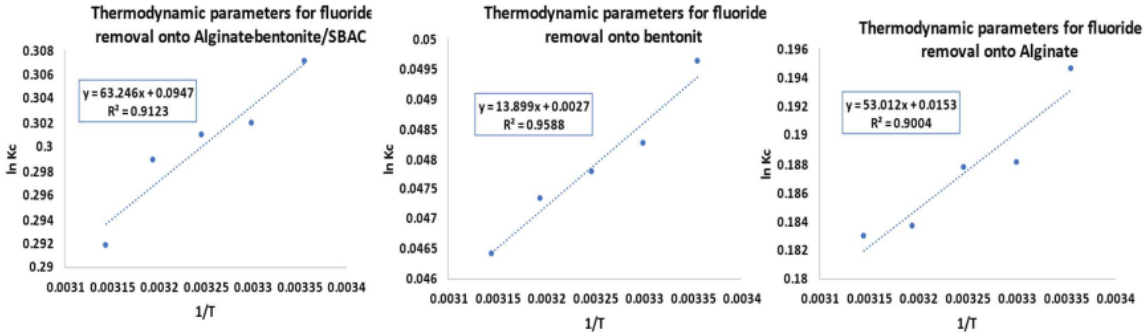

Fig. 6.24: Graphical presentation of thermodynamics study for batch adsorption of fluoride using Alginate-bentonite/SBAC, Bentonite and Alginate

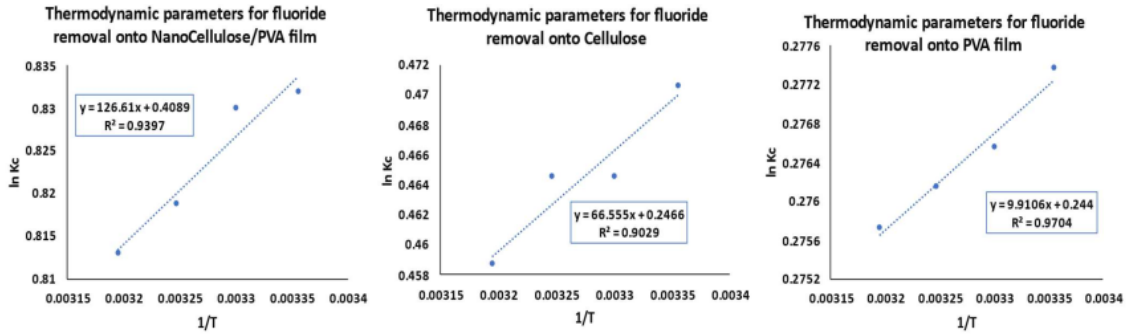

Fig. 6.25: Graphical presentation of thermodynamics study for batch adsorption of fluoride using nano-cellulose/PVA, Cellulose and PVA

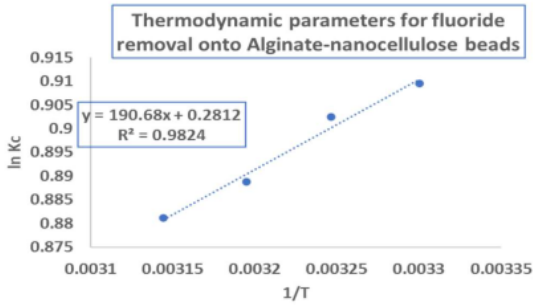

Fig. 6.26: Graphical presentation of thermodynamic parameters for batch adsorption of fluoride onto Alginate-nanocellulose

Table 6.7(a): Thermodynamic parameters of fluoride adsorption onto SB, SBC, and SBAC

Adsorbent	Temperature(K)	ΔG(J/mol)	ΔH(J/mol)	ΔS (J/mol k)
SB	298	-466.869	-455.374	0.0108
	303	-412.653		
	308	-412.019		
	313	-383.500		
	318	-466.869		
SBC	298	-800.676	-63.865	2.472
	303	-813.198		
	308	-825.505		
	313	-837.416		
	318	-848.6657		
SBAC	298	-799.600	-70.602	2.447
	303	-812.104		
	308	-824.577		
	313	-836.284		
	318	-848.6657		

Table 6.7(b): Calculate value of thermodynamic parameters for fluoride adsorption onto Alginate, bentonite, SBAC and Alginate-bentonite/SBAC

Adsorbent	Temperature(K)	ΔG(J/mol)	ΔH(kJ/mol)	ΔS (J/mol k)
Alginate	298	-482.365	-440.742	0.127
	303	-473.984		
	308	-480.772		
	313	-478.078		
	318	-483.795		
Bentonite	298	-122.929	-115.556	0.0224
	303	-121.533		
	308	-122.367		
	313	-123.164		
	318	-122.713		
Alginate-bentonite/SBAC	298	-760.772	-525.827	0.787
	303	-760.737		
	308	-770.692		
	313	-777.926		
	318	-771.626		

Table 6.7(c): Thermodynamic parameters for Fluoride adsorption onto nano-cellulose/PVA, Cellulose and PVA

Adsorbent	Temperature(K)	ΔG(J/mol)	ΔH(kJ/mol)	ΔS (J/mol k)
PVA	298	-687.190	-82.397	2.029
	303	-696.666		
	308	-707.119		
	313	-717.537		
Cellulose	298	-1165.769	-553.296	2.050
	303	-1170.212		
	308	-1189.381		
	313	-1193.550		
Nanocellulose/PVA	298	-2061.421	-1052.635	3.399
	303	-2090.863		
	308	-2096.890		
	313	-2115.839		

Table 6.7(d): Estimated values of thermodynamic state parameters for fluoride removal using Alginate-nanocellulose, Cellulose and Alginate

Adsorbent	Temperature(K)	ΔG(J/mol)	ΔH(J/mol)	ΔS (J/mol k)
Alginate	298	-482.365	-440.742	0.127
	303	-473.984		
	308	-480.772		
	313	-478.078		
Cellulose	298	-1165.769	-553.296	2.050
	303	-1170.212		
	308	-1189.381		
	313	-1193.550		
Alginate-nanocellulose beads	303	-2291.195	-1585.313	2.343
	308	-2311.058		
	313	-2312.722		
	318	-2329.530		

RSM analysis for Fluoride removal study using prepared biosorbents

The ranges and levels of process variables (for Fluoride) examined in this research were, weight of bio-adsorbent, pH, and contact time given in Table 6.8. Consistent with this design, a total of twenty runs were carried out for fluoride removal study using raw SB, SBAC, Alginate-bentonite/SBAC, Nanocellulose/PVA and Alginate-nanocellulose composite beads (Table 6.9).

Table 6.8: Experimental range and levels of independent variables for fluoride removal process using raw SB and SBAC

Independent variables	**Range and levels (coded)**					
	Units	-1	0	+1	-alpha	+alpha
pH		2	4.5	7	0.295518	8.70448
Dose	g/L	0.75	1.375	2	0.323879	2.42612
Time	min	60	90	120	39.5462	140.454

(a) RSM study using SB and SBAC

Experimental design and statistical analysis:

From Fig. 6.27 (a) and 6.28 (b), it was observed that actual removal efficiency values were close to the predicted values for selected defluoridation experiment. An empirical relationship between the response and the independent variables has been expressed by the following quadratic models. Final Equation in Terms of Actual Factors:

*Fluoride Removal efficiency of **raw SB** (%R):* R1 =+52.58909-0.51058×pH+4.82164× Dose+0.029596× Time+0.068800× pH × Dose-6.33333E-004 × pH × Time+0.013067× Dose × Time-0.040205×pH^2-1.58005 ×$Dose^2$-1.45634E-004 × $Time^2$……. (6.1)

*Removal efficiency of **SBAC** (%R):*

R1=+58.58909-0.51058×pH+4.82164×Dose+0.029596×Time+0.068800×pH×Dose-6.33333E-004×pH×Time+0.013067×Dose×Time-0.040205×pH^2-1.58005×$Dose^2$-1.45634E-004×$Time^2$……..(6.2)

F-value obtained from the model was118.68 which suggested the model was significant. There is only a 0.01% chance that a "Model F-Value" this large could occurred because of noise. Values of "Prob > F" <0.0500 indicated model terms were significant. The "Pred R-Squared"

for both adsorbent 0.9213 (SBAC) and of 0.9213 (SB) is in functional agreement with the "Adj R-Squared" of 0.9824 (SBAC) and 0.9824 (SB) with low CV value (0.52).

The estimated error in between the predicted and the actual data of fluoride removal experiment was very less (Fig. 6.27(a) and Fig. 6.28(a)). Combined influences of solution pH and time upon defluoridation efficiency of SB and SBAC have been displayed in Fig. 6.27(b) and Fig. 6.28(b). The maximum defluoridation efficiency of SBAC was obtained as 60.98 % at a pH value of 6.36 after 75.55 min contact time. Whereas, in case of SB it was 57% at a pH value of 5.0 after 114.44 min. Fig. 6.27(c) and Fig. 6.28(c) represented the 2D contour plots for combined impacts of biosorbent dose and pH on fluoride uptake rate using SB and SBAC as adsorbent material. Based on the plot, % removal of fluoride increased as dosage increased simultaneously it was decreased with increasing pH, afterward a steady drop was observed. The maximum adsorption of fluoride onto SBAC was achieved as 60.98 % at the optimum conditions for the adsorbent dose of 1.9 g/L and pH 6.36. Whereas, in case of SB it was 57% at a dose of 1.96 g/L at pH 5.0. Fig. 6.27(d) and Fig. 6.28(d) represented the 2D contour plots for combined impacts of biosorbent dosage and contact time on fluoride elimination efficiency. The optimized condition for fluoride adsorption experiment using SBAC was observed from RSM model was pH-6.36, dose 1.9 g/L and time 75.55 min and removal was found as 60.98 %. Whereas, in case of SB it was 57% at a dose of 1.96 g/L after 114.44 min.

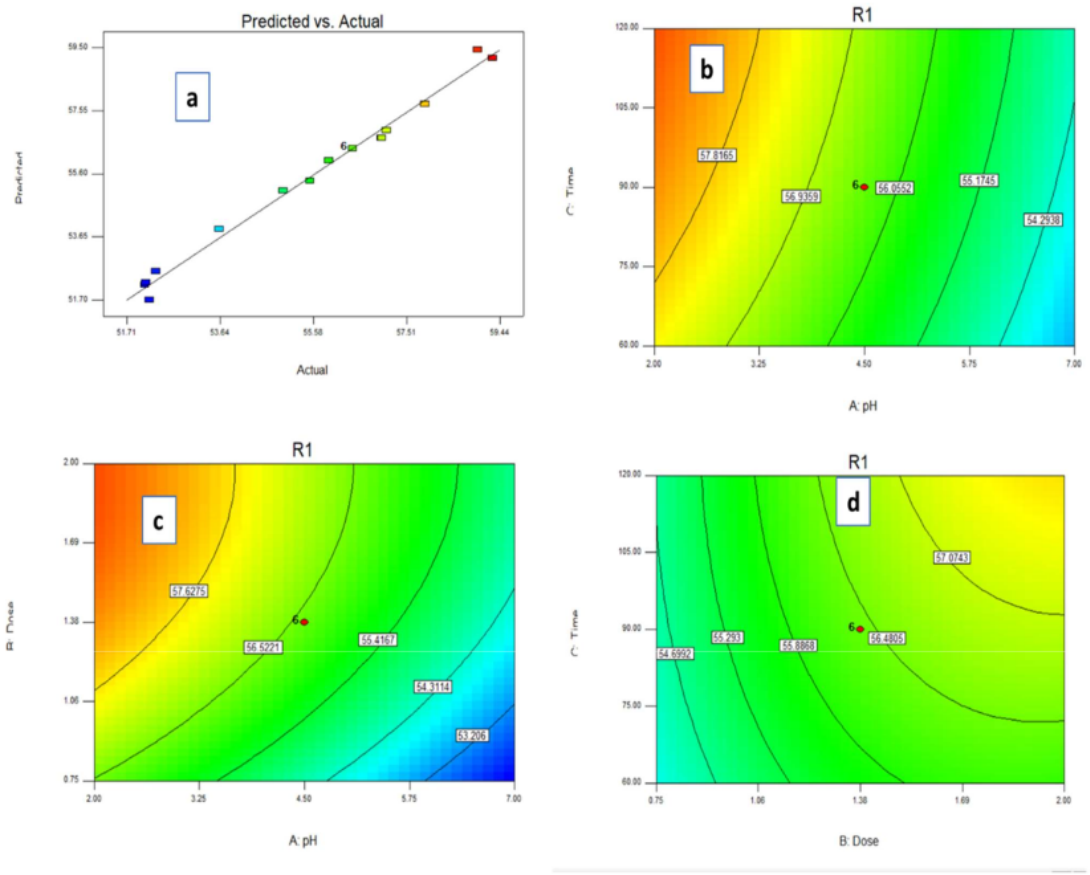

Fig. 4.27: Simulated vs. experimental values for Fluoride adsorption onto raw SB (a), 2D contour plots on combine effect of pH and contact time (b), combine effect of pH and adsorbent dose (c) and combine effect of contact time and adsorbent dose on fluoride removal efficiency(d)

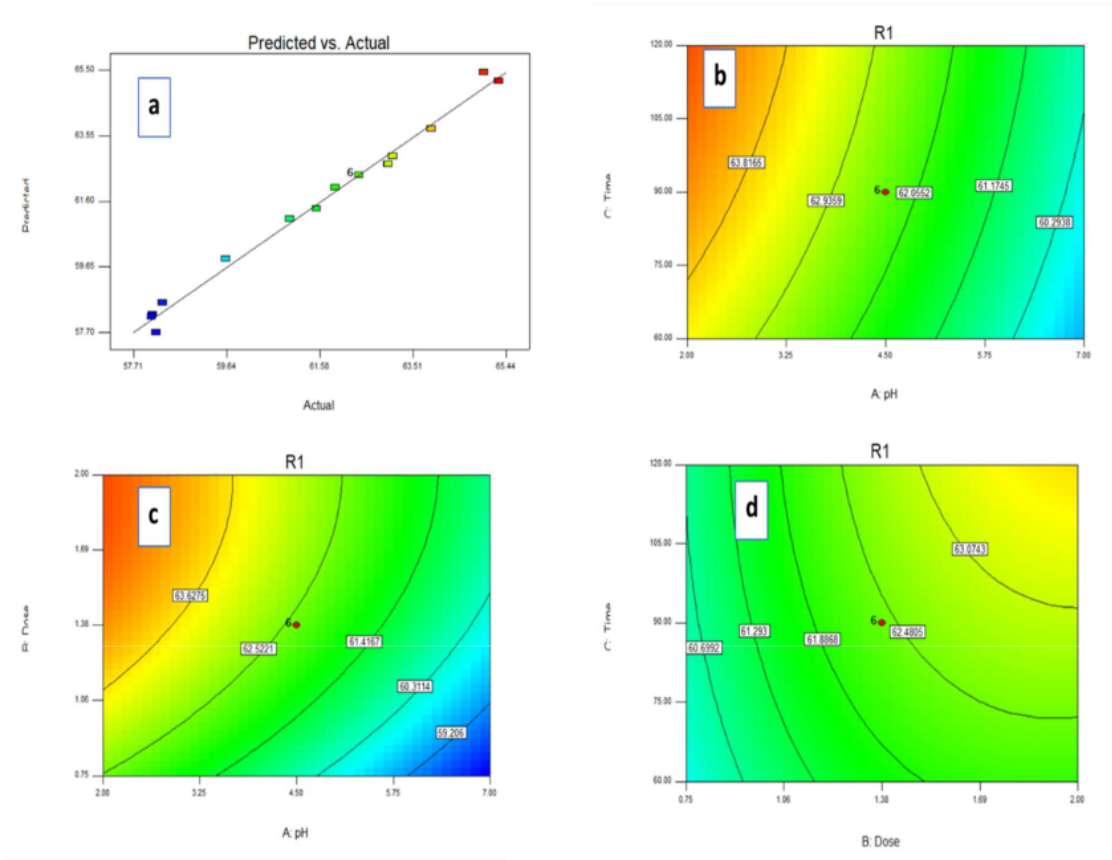

Fig. 4.28: Simulated vs. experimental values for Fluoride adsorption onto SBAC (a), 2D contour plots on combine effect of pH and contact time (b), combine effect of pH and adsorbent dose (c) and combine effect of contact time and adsorbent dose on fluoride removal efficiency(d)

(b) RSM study using Alginate-bentonite/SBAC

Final Equation in Terms of Actual Factors:

%Removal for fluoride adsorption onto **Alginate-bentonite/SBAC**,

R1=+74.34909-0.51058×pH+4.82164×Dose+0.029596×Time+0.068800×pH×Dose-6.33333E-004×pH× Time+0.013067× Dose×Time-0.040205× pH^2-1.58005×$Dose^2$-1.45634E-004× $Time^2$……..(6.3)

Results obtained from quadratic model implied that RSM model analysis was highly significant as model F-value was 118.68 with values of "Prob > F" less than 0.0001, the R^2 value was high (0.9907), Adj R-Squared value was obtained as 0.9824 and the value of Pred R-Squared was 0.9213 with a low value of CV (0.38).

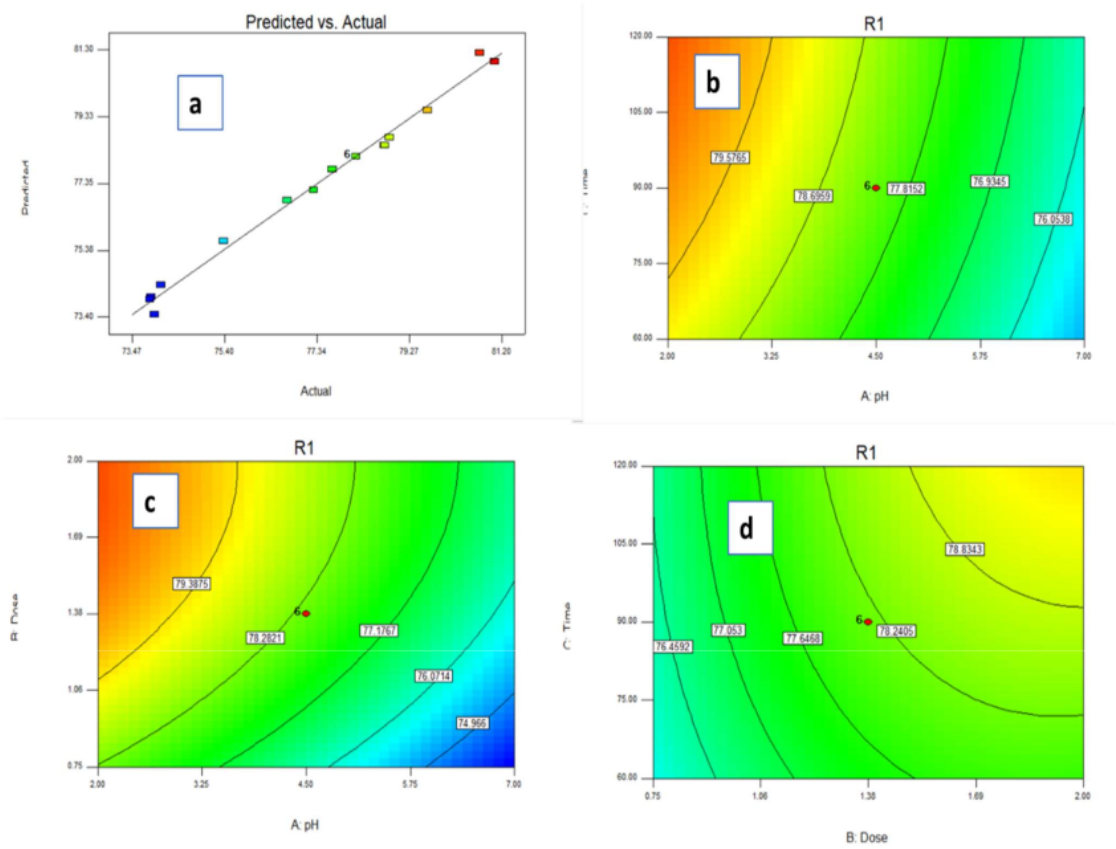

Fig. 6.29: Simulated vs. experimental values for Fluoride adsorption onto Alginate-bentonite/SBAC (a), 2D contour plots on combine effect of pH and contact time (b), combine effect of pH and adsorbent dose (c) and combine effect of contact time and adsorbent dose (d) on fluoride removal efficiency

The estimated error in between the predicted and the actual data of fluoride removal experiment was very less (Fig. 6.29(a)). Combined influences of solution pH and time upon defluoridation efficiency have been displayed in Fig. 6.29 (b). The maximum adsorption of fluoride onto Alginate-bentonite/SBAC composite beads was achieved as 77.32 % at the optimum conditions for the contact time of 80.63 min and pH 5.84

Fig. 6.29 (c) represented the 2D surface plots for combined impacts of biosorbent dose and pH on fluoride uptake rate. Based on the plot, % removal of fluoride increased as dosage increased simultaneously it was decreased with increasing pH, afterward a steady drop was observed. The optimized condition for fluoride adsorption experiment using Alginate-bentonite/SBAC

composite beads was observed from RSM model was pH-5.84, dose 1.82 g/L removal was found as 60.98 %.

Fig. 6.29 (d) represented the 2D surface plots for combined impacts of biosorbent dosage and contact time on fluoride elimination efficiency. It was observed that at a higher biosorbent dosage accessibility of adsorptive sites increased which led to higher defluoridation efficiency. The optimized condition for fluoride adsorption experiment was observed from RSM model was pH-5.84, dose 1.82 g/L and time 80.63 min and removal was found as 77.32 % (Sinha et al., 2013).

(c) *RSM study using Cellulose and Nanocellulose/PVA*

Final Equation in Terms of Actual Factors:

Fluoride removal efficiency of ***Cellulose*****,** R1 =+71.18703+0.35923×pH+4.93842×Dose-5.70112E-003×Time-0.27200× pH ×Dose-8.90000E-003× pH×Time+0.039200×Dose×Time-0.018259×pH^2-1.68146×$Dose^2$+1.22654E-004 × $Time^2$……..(6.4)

Fluoride removal efficiency of ***Nanocellulose/PVA***, R1=+81.29170-0.70524× pH+5.85287×Dose+0.020492×Time-0.045600×pH×Dose+6.16667E-004×pH×Time+ 3.53333E-003×Dose × Time-5.13668E-003× pH^2-1.51677× $Dose^2$-5.13849E-005× $Time^2$……..(6.5)

Results obtained from quadratic model implied that RSM model analysis was highly significant as model F-value was 86.7 with Values of "Prob > F" less than 0.0500, the R^2 value was high (0.9873), Adj R-Squared value was obtained as 0.9760 and the value of Pred R-Squared was 0.9033 with a low value of CV (0.37).

Fig. 6.30(b) and 6.31 (b) represented the 2D surface plots for combined impacts of biosorbent dose and pH on fluoride uptake rate for cellulose and composite, respectively. Based on the plot, % removal of fluoride increased as dosage increased simultaneously it was decreased with increasing pH, afterward a steady drop was observed. The maximum adsorption of fluoride onto cellulose was achieved as 74.9% at the optimum conditions for the adsorbent dose of 1.78 g/L and pH 6.30. Whereas, in case of nanocellulose/PVA it was 84.89% at a dose of 1.93 g/L at pH 5.41.

Fig. 6.30(c) and 6.31(c) represented the 2D surface plots for combined impacts of biosorbent dosage and contact time on fluoride elimination efficiency of cellulose and composite, respectively. The optimized condition for fluoride adsorption experiment using cellulose was observed from RSM model was pH-6.30, dose 1.78 g/L and time 91.83 min and removal was

found as 74.9 % (Sinha et al., 2013). Whereas, in case of nanocellulose/PVA it was 84.89 % at a dose of 1.93 g/L after 92.80 min.

Combined influences of solution pH and time upon defluoridation efficiency have been displayed in Fig. 6.30(d) and 6.31(d) for cellulose and composite, respectively. The maximum defluoridation efficiency of cellulose was obtained as 74.9 % at a pH value of 6.30 after 91.83 min contact time. Whereas, in case of composite it was 84.89 % at a pH value of 5.41 after 92.80 min.

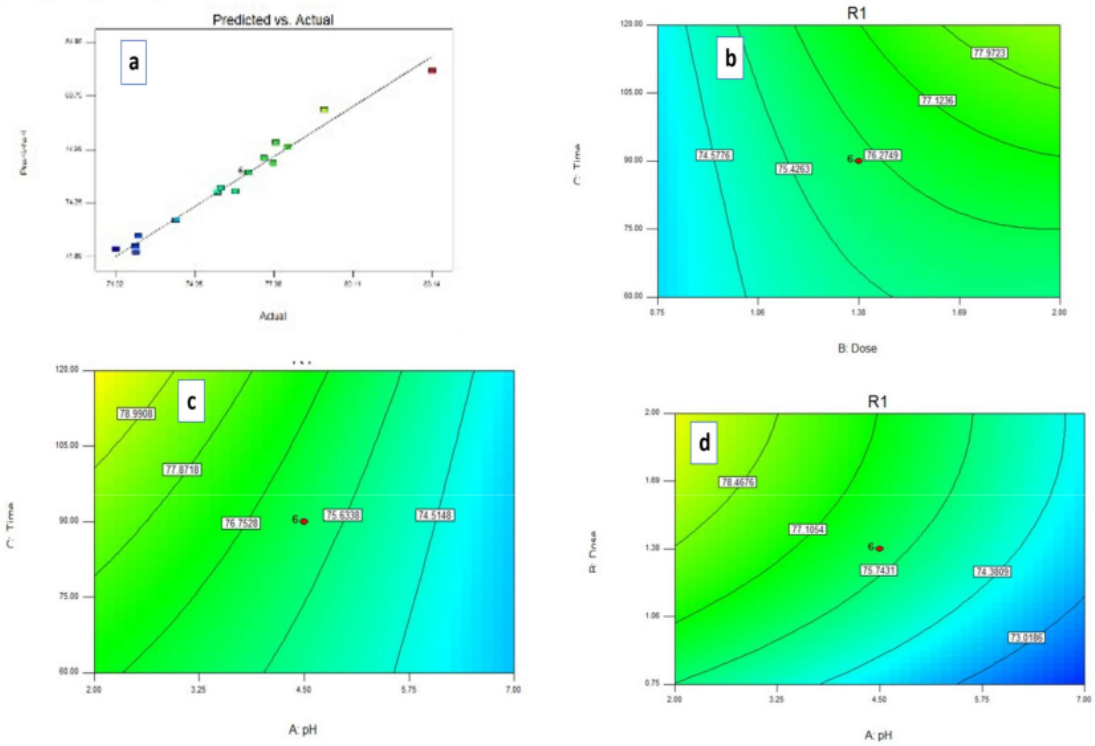

Fig. 6.30: Simulated vs. experimental values for Fluoride adsorption onto Cellulose (a), 2D contour plots on combined effect of pH and time (b), combined effect of contact time and pH (c) and combined effect of dose and pH (d) on fluoride removal efficiency

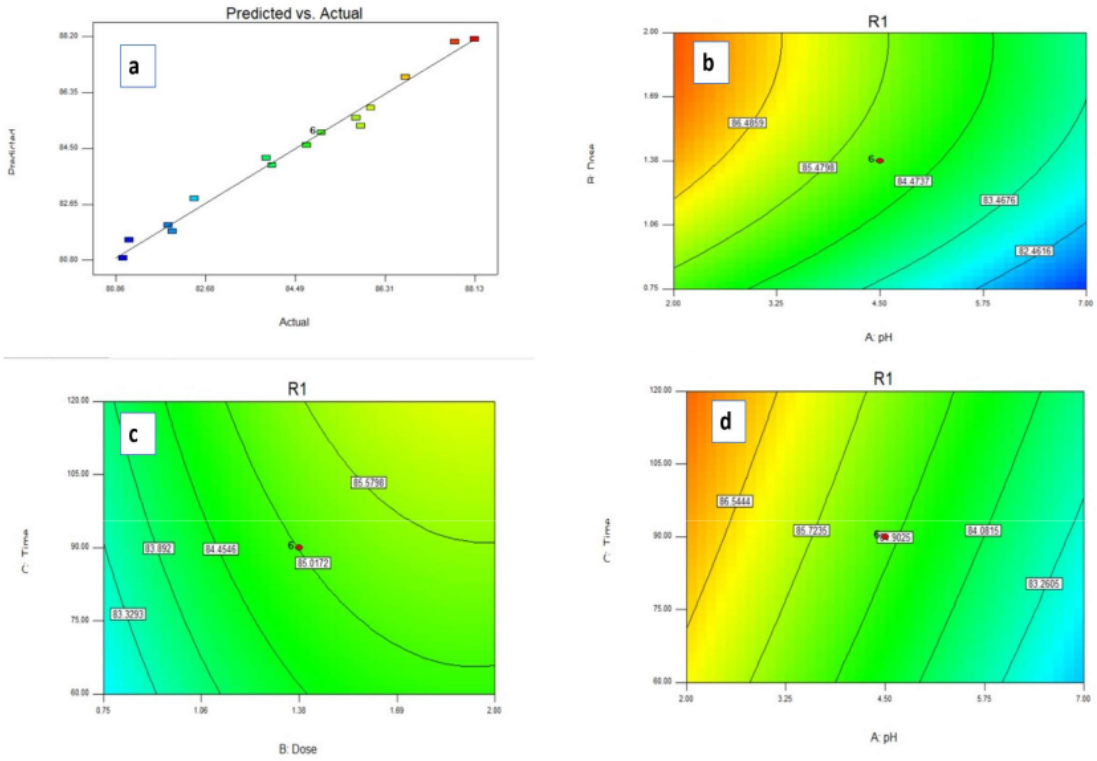

Fig. 6.31**:** Simulated vs. experimental values for Fluoride adsorption onto Nanocellulose/PVA (a), 2D contour plots on combined effect of pH and dose (b), combined effect of contact time and adsorbent dose (c) and combined effect of contact time and pH (d) on fluoride removal efficiency

(d) ***RSM study using Alginate-nanocellulose composite***

Final Equation in Terms of Actual Factors:

% removal of fluoride using ***Alginate-nanocellulose****:*

R1= +71.18703+0.35923×pH+4.93842×Dose-5.70112E-003×Time-0.27200×pH×Dose-8.90000E-003×pH×Time+0.039200×Dose×Time-0.018259×pH^2 1.68146×$Dose^2$+1.22654E-004×$Time^2$……..(6.6)

Results obtained from quadratic model implied that RSM model analysis was highly significant as model F-value was 124.05 with Values of "Prob > F" less than 0.0500, the R^2 value was high

(0.9911), Adj R-Squared value was obtained as 0.9831 and the value of Pred R-Squared was 0.9275 with a low value of CV (0.34).

The estimated error in between the predicted and the actual data of fluoride removal experiment was very less (Fig. 6.32(a)). Combined influences of solution pH and time upon defluoridation efficiency have been displayed in Fig. 6.32(b). Fig. 6.32(c) represented the 2D surface plots for combined impacts of biosorbent dose and pH on fluoride uptake rate. Based on the plot, % removal of fluoride increased as dosage increased simultaneously it was decreased with increasing pH, afterward a steady drop was observed. Fig. 6.32(d) represented the 2D surface plots for combined impacts of biosorbent dosage and contact time on fluoride elimination efficiency. The optimized condition for fluoride adsorption experiment was observed from RSM model was pH-5.67, dose 1.89 g/L and time 85.71 min and removal was found as 82.79 % (Sinha et al., 2013).

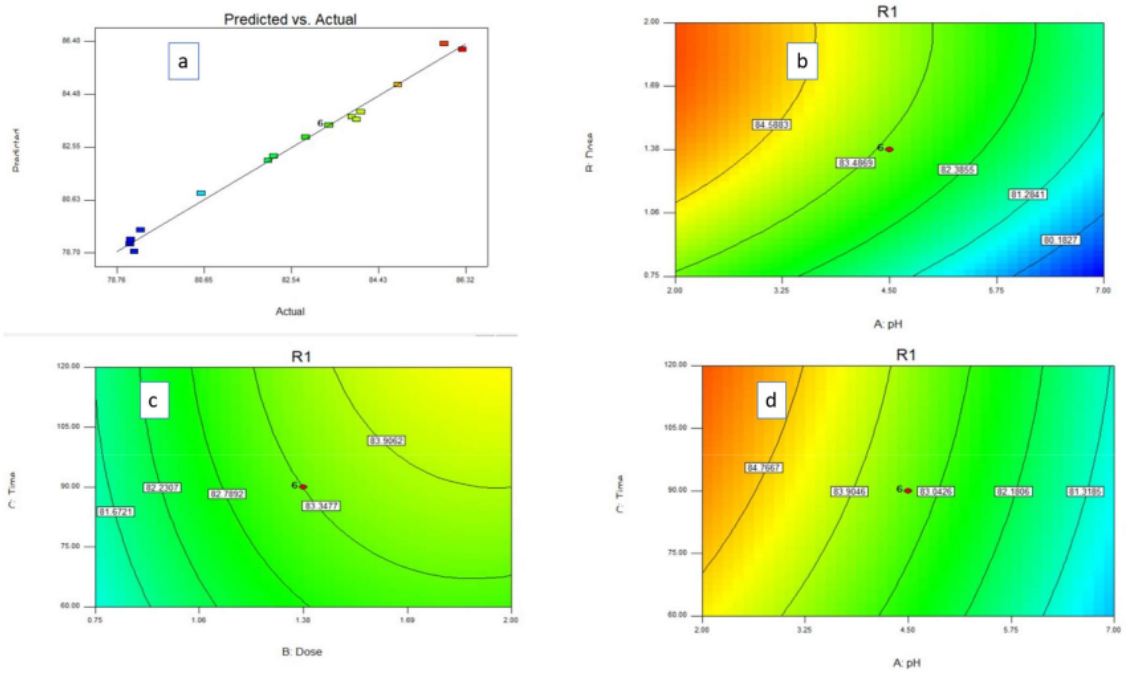

Fig. 6.32: Simulated vs. experimental values for Fluoride adsorption onto Alginate-nanocellulose (a), 2D contour plots on combine effect of pH and dose (b), combine effect of contact time and adsorbent dose (c) and combine effect of contact time and pH (d) on fluoride removal efficiency.

Table 6.9: Experimental results of RSM study using raw SB and SBAC for Fluoride removal

Run	pH	Dose (g/L)	Time (min)	%R of Fluoride removal (SBAC)	%R of Fluoride removal (SB)	%R of Fluoride removal (Alginate-bentonite/SBAC)	%R of Fluoride removal (nanocellulose/ PVA)	%R of Fluoride removal (Alginate-nanocellulose)	%R of Fluoride removal (Cellulose)
1	8.70	1.375	90	58.07	52.07	73.83	79.03	76.63	71.79
2	4.5	1.375	90	62.39	56.39	78.15	83.35	80.95	76.11
3	4.5	2.43	90	62.99	56.99	78.75	83.95	81.55	76.71
4	7	0.75	60	58.17	52.17	73.93	79.13	76.73	71.89
5	4.5	1.375	90	62.39	56.39	78.15	83.35	80.95	76.11
6	2	0.75	120	62.98	56.98	78.74	83.85	81.45	77.05
7	4.5	1.375	90	62.39	56.39	78.15	83.35	80.95	76.11
8	2	0.75	60	61.89	55.89	77.65	82.85	80.45	75.61
9	2	2	60	63.89	57.89	79.65	84.85	82.45	77.61
10	4.5	0.32	90	58.3	52.3	74.06	79.26	76.86	71.02
11	7	2	60	59.62	53.62	75.38	80.58	78.18	73.34
12	4.5	1.375	90	62.39	56.39	78.15	83.35	80.95	76.11
13	7	2	120	61.5	55.5	77.26	82.03	79.63	75.05
14	4.5	1.375	90	62.39	56.39	78.15	83.35	80.95	76.11
15	4.5	1.375	140.45	63.09	57.09	78.85	84.05	81.65	77.16
16	0.295	1.375	90	65.29	59.29	81.05	86.25	83.85	79.01
17	4.5	1.375	90	62.39	56.39	78.15	83.35	80.95	76.11
18	4.5	1.375	39.55	60.95	54.95	76.71	82.15	79.75	74.91
19	2	2	120	64.98	58.98	80.74	85.85	83.45	83.14
20	7	0.75	120	58.09	52.09	73.85	79.05	76.65	71.81

6.2.2. Results of Fluoride adsorption study in Fixed-bed Column using prepared biosorbents

Fluoride adsorption efficiency of raw SB, SBAC, Alginate-bentonite/SBAC and Nanocellulose/PVA was also obtained in fixed-bed adsorption system at different bed height (4am, 8cm, 10 cm), pH (4.0, 6.0, 8.0), feed flow rate (5.0, 10.0, 13.0 mL/min) and feed concentration (8.0, 10.0, 12.0 mg/L). Effect of operational parameters on breakthrough curve were found similar to that obtain in column study of dye adsorption. Under all experimental condition Nanocellulose/PVA composite beads shows better results in comparison with raw SB, SBAC, Alginate-bentonite/SBAC composite.

Influence of pH

To determine the influence of pH on the breakthrough curve, experiment was investigated at different pH (4 to 8) keeping initial fluoride concentration, flow rate and bed height constant at 10 mg/L, 5 mL/min, and 4 cm, respectively using raw SB, SBAC, Alginate-bentonite/SBAC and Nanocellulose/PVA as biosorbent for individual study. It was observed that on increasing the pH of the feed solution, the breakthrough time decreased which indicates that fluoride removal efficiency and adsorption capacity was lower. Breakthrough time at pH = 4.0 for fluoride adsorption in fixed bed using raw SB as adsorbent was 65 min and at pH = 8.0 it was 25 min (Fig. 6.33(a)). With SBAC as adsorbent, the breakthrough was achieved after 115min at pH = 2.0 and at pH = 8.0 it was 80min (Fig. 6.34(a)). With Alginate-bentonite/SBAC beads, breakthrough time at pH=4 and pH = 8.0 was 240 min and145 min respectively (Fig. 6.35(a)). On increasing the value of solution pH from 4.0 to 8.0, the time required to reach breakthrough condition decreased from 225 min to 110 min for Nanocellulose/PVA composite (Fig. 6.36(a)).

Influence of bed height

Influence of bed height on the breakthrough time for fluoride removal study in the fixed-bed column containing prepared biosorbents were investigated by varying the height (4.0 cm-8.0 cm). Amount of adsorbent for 4 cm bed hight of fixed-bed column containing Raw SB=3.7g, using SBAC=2.8g, for Alginate-bentonite/SBAC beads=3.1g and for Nanocellulose/PVA=2.1g. Adsorbent amount in 6 cm bed hight are 5.9 g, 3.9g, 4.16g and 3.2g using SB, SBAC, Alginate-bentonite/SBAC and Nanocellulose/PVA respectively. Adsorbent mass in 8 cm height of adsorbent column is 6.7g, 6.2g, 5.67g and 4.15g using SB, SBAC, Alginate-bentonite/SBAC and Nanocellulose/PVA respectively. Feed containing flouride of 10 mg/L concentration and pH 4.0 was passed through the fixed bed column at flow rate of 5 mL/min at different bed height. The C_t/C_0 versus time plot show that when bed height increased from 4.0 cm to 8.0 cm, breakthrough time of the fixed-bed column containing SBAC particles increased from 60 to 250 min leading to steeper breakthrough curve at small bed height (Fig. 6.34(b)). Fig. 6.35 (b) show that on increasing bed height from 4.0 to 8.0 cm using alginate-bentonite/SBAC beads the breakthrough time increased from 240 to 445 min. Using Nanocellulose/PVA composite as adsorbent, Fig. 6.36(b) breakthrough time changed from 210 min to 405min for the same change in bed height.

Influence of feed flow rate

In order to evaluate the defluoridation capability of raw SB, SBAC, Alginate-bentonite/SBAC and Nanocellulose/PVA in fixed bed reactor at varying inlet flow rate (ranging from 5 to 13

ml/min) experiment was done at pH 4.0, initial fluoride concentration (10 mg/L) and bed height (4 cm) constant. From C_t/C_0 versus time plot (Fig. 6.33(c), Fig. 6.34(c), Fig. 6.35(c), and Fig. 6.36(c)), it was observed that breakthrough achieved was faster at a higher influent flow rate. On increasing flow rate from 5 to 13 ml/min, the breakthrough time of the fixed-bed column containing raw SB particles (Fig. 6.33(c)) SBAC particles (Fig. 6.34(c)), Alginate-bentonite/SBAC beads (Fig. 6.35(c)) and nanocellulose/PVA (Fig. 6.36(c)) decreased from 65 min to about 30 min, from 115min to 60 min, from 240 min to about 110 min and from 210min to 95 min respectively.

Influence of initial fluoride concentration

The effect of initial fluoride concentration on breakthrough curve was studied by varying the inlet feed concentration in fixed-bed reactor using biosorbents for individual study. The influence of feed concentration on breakthrough characteristic have been shown C_t/C_0 versus time graph. It is observed that with increase in feed concentration, breakthrough time decreased resulting in sharpness of breakthrough curves. Using Alginate-bentonite/SBAC beads as adsorbent, breakthrough time reduced from 240 to 165 min with increasing feed concentration of fluoride solution (from 10 to 14 mg/L) in fixed-bed reactor (Fig. 6.35(d)). Similarly, with Nanocellulose/PVA composite as adsorbent breakthrough curves (Fig. 6.36(d) revealed that with an increase in the concentration of fluoride solution (as of 10 to 14 mg/L), the time required for breakthrough reduced from 210 min to 140 min.

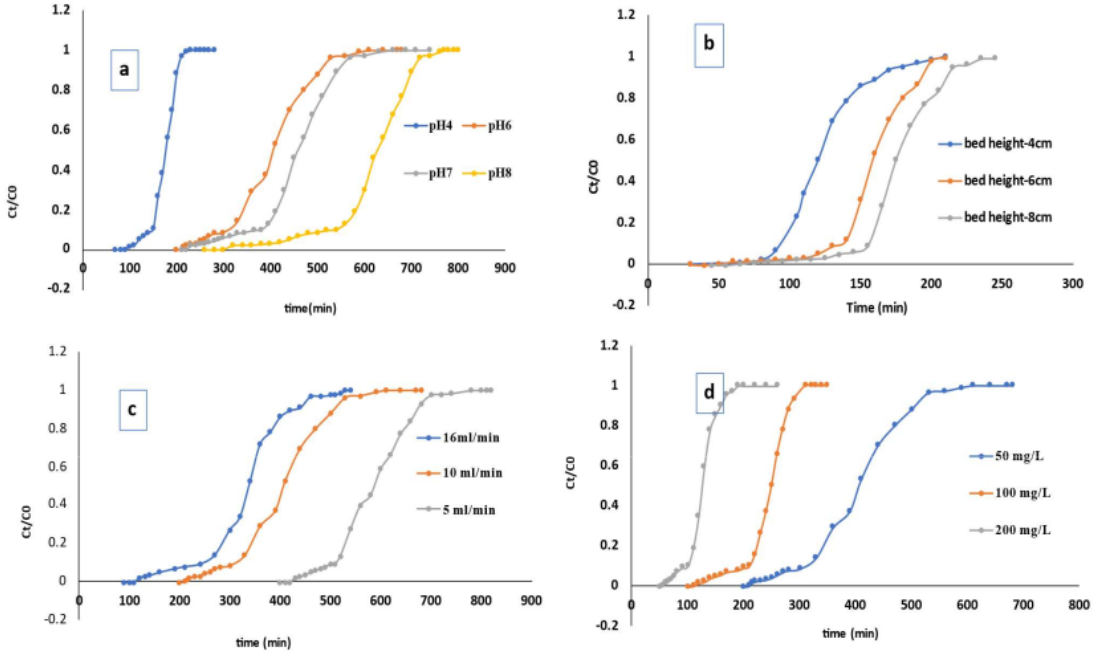

Fig. 6.33: Effect of of various operational conditions on breakthrough curve for fluoride adsorption in fixed-bed containing raw SB

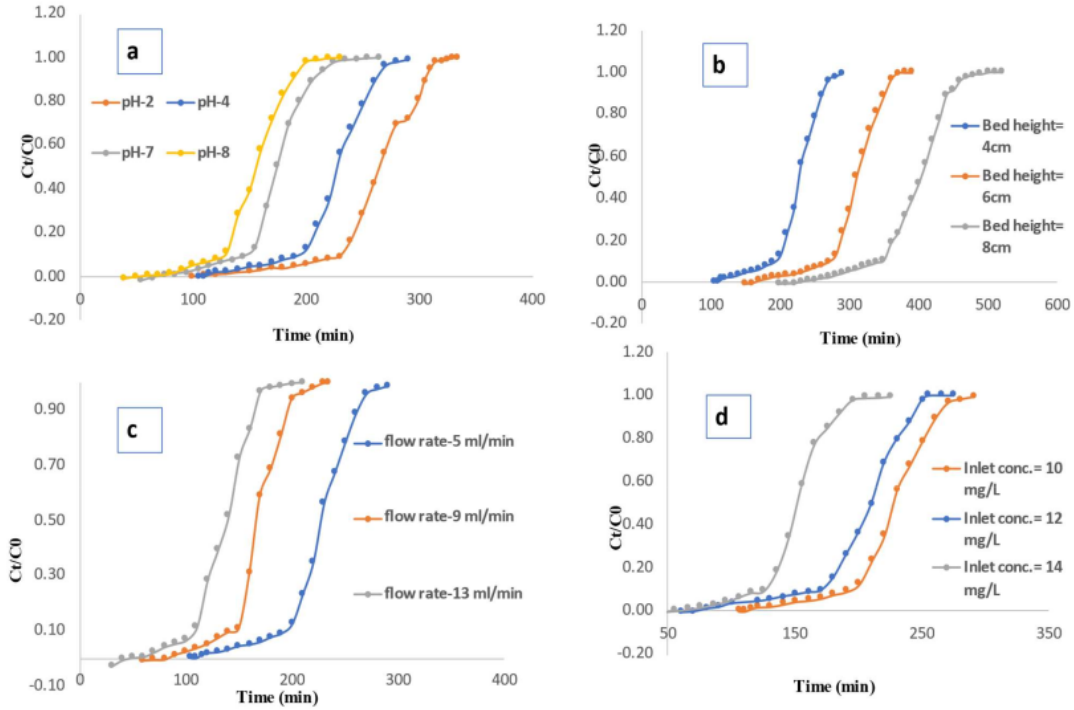

Fig. 6.34: Effect of various operational conditions on breakthrough curve for fluoride adsorption in fixed-bed containing SBAC

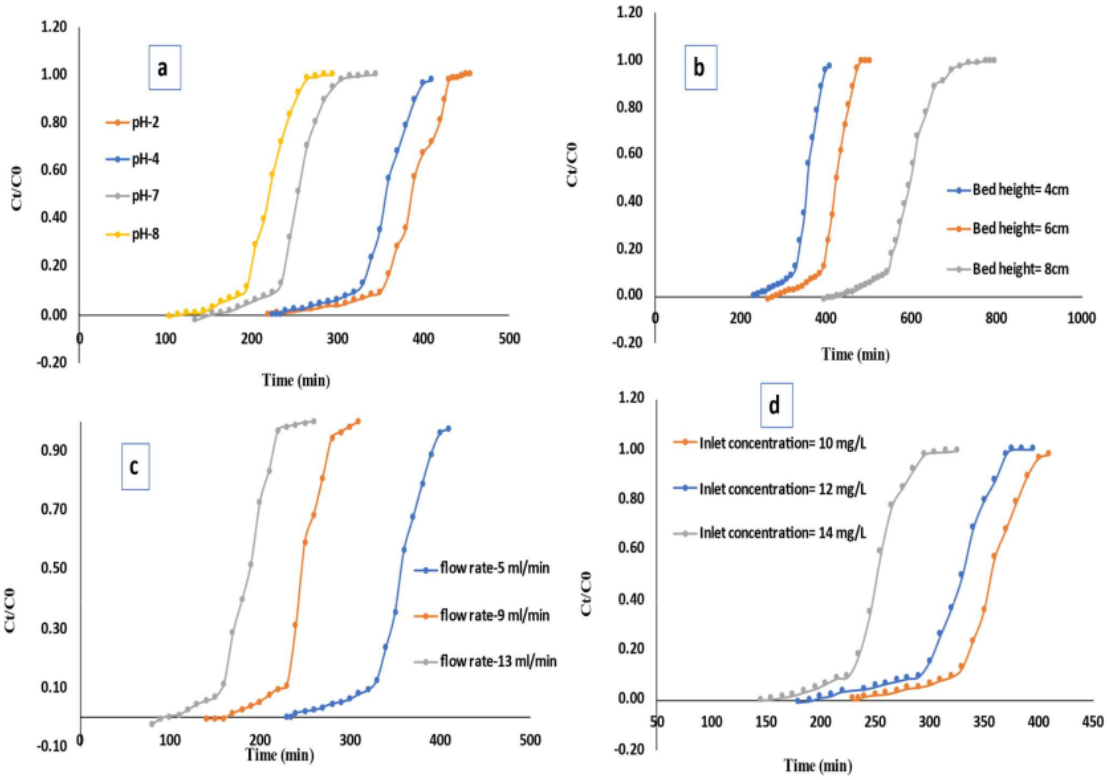

Fig. 6.35: Effect of various operational conditions on breakthrough curve for Fluoride adsorption in fixed-bed column containing Alginate-bentonite/SBAC beads

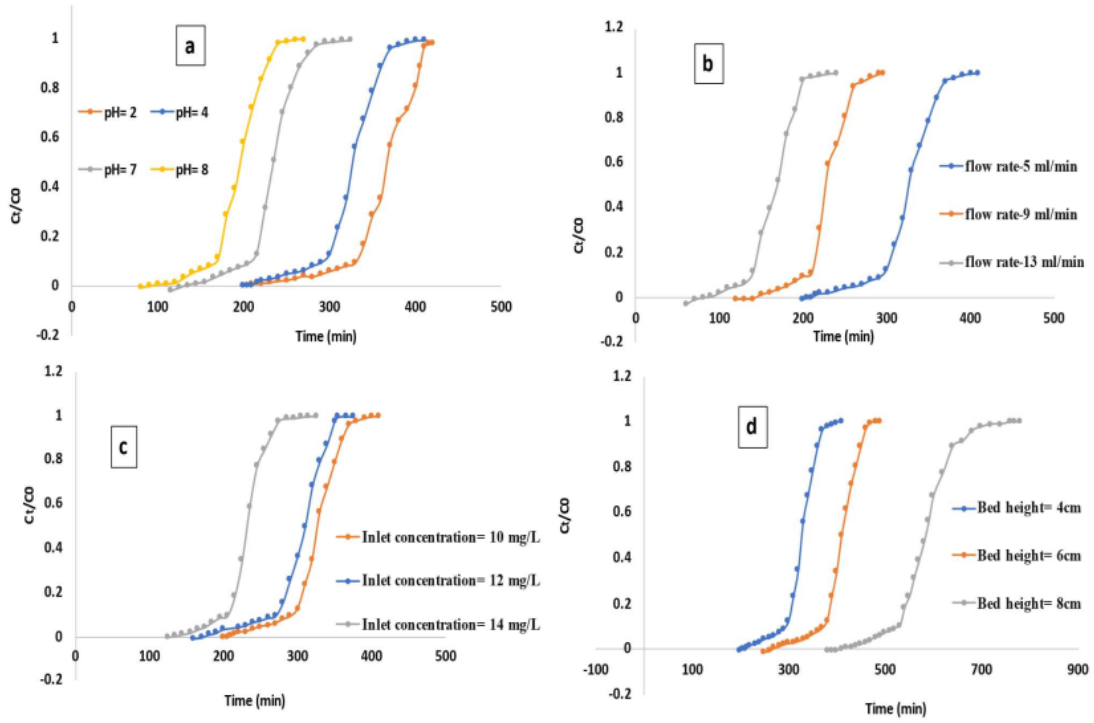

Fig. 6.36: Effect of various operational conditions on breakthrough curve for fluoride adsorption onto nanocellulose/PVA (under various pH level (a), at different inlet flow rate (b), at various inlet concentrations (c), and at several column bed height (d))

Table 6.10: Parameters of the breakthrough curves for fluoride adoption onto raw SB

Q(ml/min)	C_0 (mg/L)	pH	L_b(cm)	t_b	t_t (min)	M_{tot} (mg)	S_{tot}	S_b/S_{tot}	R (%)	S_{eq}(mg/mg)
5	8	4	4	65	136.96	8.6	5.478	0.593206	63.70	1.480
5	10	4	4	80	133.28	10.5	6.664	0.720285	63.46	1.801
5	12	4	4	20	76.014	7.5	4.560	0.438511	60.81	1.232
10	10	4	4	45	104.21	18	10.421	0.561343	57.89	2.816
13	10	4	4	30	87.77	19.5	11.411	0.131449	58.51	3.084
5	10	4	6	70	155.74	10.5	7.787	0.44946	74.163	1.052
5	10	4	8	85	174.90	12.25	8.745	0.48599	71.38	0.945
5	10	6	4	35	88.48	7.25	4.424	0.39555	61.023	1.195
5	10	8	4	25	81.38	6.75	4.069	0	60.282	1.099

Table 6.11: Parameters of the breakthrough curves for fluoride adsorption onto SBAC

Q(ml/min)	C_0 (mg/L)	pH	L_b(cm)	t_b	t_t (min)	M_{tot} (mg)	S_{tot}	S_b/S_{tot}	R (%)	S_{eq}(mg/mg)
5	8	4	4	115	219.1699	11.6	8.766795	0.524707	75.57	3.130998
5	10	4	4	65	146.9578	11.25	7.347889	0.442304	65.31	2.624246
5	12	4	4	80	187.3636	16.5	11.24182	0.426977	68.13	4.014935
9	10	4	4	90	160.1515	21.15	14.41364	0.561968	68.149	5.147727
13	10	4	4	60	127.4295	27.3	16.56584	0.470849	60.68	5.91637
5	10	4	6	180	290.081	19.5	14.50405	0.620516	74.379	3.718987
5	10	4	8	250	381.9213	26	19.09606	0.654585	73.44	3.929231
5	10	2	4	130	246.0385	16.75	12.30193	0.528372	73.444	4.393545
5	10	7	4	85	168.5308	16.25	8.42654	0.504359	51.855	3.009479
5	10	8	4	80	146.3932	11.5	7.319661	0.546473	63.6492	2.614164

Table 6.12: Parameters of the breakthrough curves for Fluoride adsorption onto Alginate-bentonite/SBAC beads

Q(ml/min)	C_0 (mg/L)	pH	L_b(cm)	t_b	t_t (min)	M_{tot} (mg)	S_{tot}	S_b/S_{tot}	R (%)	S_{eq}(mg/mg)
5	10	4	4	240	369.4632	21.5	18.47316	0.649591	85.921	5.597928
5	12	4	4	200	336.1814	23.4	20.17089	0.594917	86.200	6.11239
5	14	4	4	165	261.8996	22.4	18.33297	0.630013	81.843	5.55544
9	10	4	4	160	249.1088	27.9	22.41979	0.64229	80.357	6.793875
13	10	4	4	110	189.1455	33.8	24.58892	0.581563	72.748	7.451187
5	10	4	6	295	445.7772	24.25	22.28886	0.661766	91.912	3.980154
5	10	4	8	445	622.1307	39.25	31.10653	0.715284	79.252	4.147538
5	10	2	4	250	405.0258	22.25	20.25129	0.617245	91.017	6.136755
5	10	7	4	165	273.75	17.25	13.6875	0.60274	79.347	4.14772
5	10	8	4	145	216.5169	14.75	10.82584	0.669694	73.395	3.28055

Table 6.13: Parameters of the breakthrough curves for fluoride adsorption onto nanocellulose/PVA

Q(ml/min)	C_0 (mg/L)	pH	L_b(cm)	t_b	t_t (min)	M_{tot} (mg)	S_{tot}	S_b/S_{tot}	R (%)	S_{eq}(mg/mg)
5	10	4	4	225	341.607	20.5	17.080	0.6147	83.318	8.1335
9	10	4	4	150	239.11	26.55	21.519	0.6273	81.054	10.247
13	10	4	4	95	170.53	31.2	22.168	0.5277	71.054	10.556
5	10	2	4	230	373.98	21.75	18.699	0.6150	85.972	8.904
5	10	7	4	145	253.75	16.25	12.687	0.5714	78.076	6.041
5	10	8	4	110	212.042	13.5	10.602	0.5187	78.534	5.048
5	10	4	6	275	401.87	24.5	20.093	0.6843	82.014	6.279
5	10	4	8	405	593.44	39	29.672	0.6824	76.082	7.14988
5	12	4	4	180	294.107	22.5	17.646	0.6120	78.428	8.403
5	14	4	4	140	231.364	22.75	16.195	0.6267	71.188	7.712

Kinetic Modelling data of fixed-bed column adsorption of Fluoride

Estimated values of model parameters, k_{YN} (L/min), under various operational conditions are listed in the Table 6.14, Table 6.15, Table 6.16 and Table 6.17. The table revealed that the magnitude of k_{YN} increased with both pH value of feed solution and concentration of feed, whereas k_{YN} decreased under such conditions. k_{YN} increased with the rate of inlet flow but decreased with increasing depth of the column bed containing biosorbent. Derived values of k_{TH}, q_0, and the value of R^2 (correlation coefficient) were listed in Table 6.14, Table 6.15, Table 6.16 and Table 6.17. Results indicated that q_0 increased with both the depth of the column and the flow-rate of feed solution. Whereas, k_{TH} decreased with increasing pH of the inlet solution. On the other hand, k_{Th} decreased with increasing depth of the adsorbent column but increased with both pH value of the inlet fluoride solution and the feed flow rate (Dhanasekaran et al. 2017). Results revealed that the Yoon-Nelson and Thomas model seemed to be well fit the investigational data of the fixed-bed adsorption experiment for the fluoride removal using raw SB, SBAC Alginate-bentonite/SBAC, Nanocellulose/PVA as biosorbent.

Table 6.14: Derived Parameters of column kinetic models for fluoride adsorption on raw SB at different experimental conditions

Operational conditions				Thomas model			Yoon-Nelson		
F(ml/min)	C_0(mg/L)	Z(cm)	pH	k_{TH} (L/mg min)	q_0(×10 mg/g)	R^2	k_{YN} (L/min)	τ (min)	R^2
5	8	4	4	0.00577	148.073	0.976	0.0462	136.96	0.976
5	10	4	4	0.00759	165.0455	0.953	0.0759	133.28	0.953
5	12	4	4	0.00732	123.2111	0.988	0.0878	76.014	0.988
10	10	4	4	0.00714	281.6602	0.962	0.0714	104.21	0.962
13	10	4	4	0.00793	308.405	0.985	0.0793	87.779	0.985
5	10	6	4	0.00617	199.676	0.948	0.0617	155.74	0.948
5	10	8	4	0.00604	911.0272	0.964	0.0604	174.90	0.964
5	10	4	6	0.00929	119.5735	0.984	0.0929	88.484	0.984
5	10	4	8	0.00917	109.9782	0.985	0.0917	81.381	0.985

Table 6.15: Derived Parameters of column kinetic models for fluoride adsorption on SBAC at different experimental conditions

Operational conditions				Thomas model			Yoon-Nelson		
F(ml/min)	C_0(mg/L)	Z(cm)	pH	k_{TH} (L/mg min)	q_0(×10 mg/g)	R^2	k_{YN} (L/min)	τ (min)	R^2
5	8	4	4	0.00647	313.09	0.946	0.0518	219.1699	0.946
5	10	4	4	0.00687	262.424	0.964	0.0687	146.9578	0.964
5	12	4	4	0.00421	401.493	0.948	0.0506	187.3636	0.948
9	10	4	4	0.0066	514.773	0.944	0.066	160.1515	0.944
13	10	4	4	0.00759	591.64	0.977	0.0759	127.4295	0.977
5	10	6	4	0.00494	371.898	0.906	0.0494	290.081	0.906
5	10	8	4	0.00432	392.9.23	0.954	0.0432	381.9213	0.954
5	10	4	2	0.00467	439.35	0.901	0.0467	246.0385	0.901
5	10	4	7	0.00633	300.95	0.974	0.0633	168.5308	0.974
5	10	4	8	0.00707	261.4.16	0.970	0.0707	146.3932	0.970

Table 6.16: Derived Parameters of column kinetic models for Fluoride adsorption onto Alginate-bentonite/SBAC at different experimental conditions

Operational conditions				Thomas model			Yoon-Nelson		
F(ml/min)	C_0(mg/L)	Z(cm)	pH	k_{TH} (L/mg min)	q_0(×10 mg/g)	R^2	k_{YN} (L/min)	τ (min)	R^2
5	10	4	4	0.00503	5294.897	0.95	0.0503	349.463	0.95
5	12	4	4	0.00395	5657.844	0.969	0.0474	311.181	0.969
5	14	4	4	0.00490	5237.263	0.964	0.0687	246.899	0.964
9	10	4	4	0.00662	6248.421	0.95	0.0662	229.108	0.95
13	10	4	4	0.00749	7057.248	0.977	0.0749	179.145	0.977
5	10	6	4	0.00386	3756.939	0.946	0.0386	420.777	0.946
5	10	8	4	0.00352	3980.871	0.961	0.0352	597.130	0.961
5	10	4	2	0.00387	5757.967	0.94	0.0387	380.025	0.94
5	10	4	7	0.0064	3768.939	0.981	0.064	248.75	0.981
5	10	4	8	0.00712	3204.801	0.966	0.0712	211.516	0.966

Table 6.17: Derived Parameters of column kinetic models for fluoride adsorption on polymeric composite at different experimental conditions

Operational condition				Yoon-Nelson			Thomas		
F(ml min^{-1})	C_0 (mg L^{-1})	Z (cm)	pH	k_{YN} (L min^{-1})	τ (min)	R^2	k_{TH} (L mg^{-1} min^{-1})	q_0 ×10^2 (mg g^{-1})	R^2
5	10	4	4	0.056	316.607	0.946	0.0056	75.383	0.946
9	10	4	4	0.073	224.11	0.952	0.0073	96.047	0.952
13	10	4	4	0.076	160.53	0.983	0.0076	99.373	0.983
5	10	4	2	0.049	348.98	0.899	0.0047	82.32	0.899
5	10	4	7	0.064	228.75	0.981	0.0064	54.464	0.981
5	10	4	8	0.071	187.042	0.966	0.0071	44.534	0.966
5	10	6	4	0.049	391.87	0.882	0.0049	61.225	0.882
5	10	8	4	0.032	588.44	0.988	0.0032	70.896	0.988
5	12	4	4	0.056	289.107	0.847	0.00467	82.543	0.847
5	14	4	4	0.066	226.364	0.983	0.00471	75.523	0.983

4.4. Summary

- In batch study, the fluoride adsorption potential of the prepared composite was observed to be significantly dependent on the various operational factors including pH, experimental time, composite mass.
- Under all investigational condition, nanocellulose/PVA composite showed excellent results towards fluoride adsorption compared to other biosorbents
- Fluoride adsorption isotherm showed that the estimated value of monolayer adsorption capacity were 19.88, 20.53, 22.22, 23.809, 14.75, 28.41, and 23.809 mg/g for SB powder, SBC, SBAC, Alginate-Bentonite/SBAC beads, Cellulose, NanoCellulose/PVA, Alginate-Nanocellulose beads respectively
- The nature of rate limiting steps involved in adsorption process might be well predicted by the Pseudo-second-order kinetics ($R^2 = 0.999$).
- Values of parameters obtained from the thermodynamic analysis show that the decolorization and defluoridation method was spontaneous, exothermic and feasible.
- Yoon-Nelson model and Thomas model showed excellent conformity of the experimental data of fixed-bed study with the breakthrough curves and effectively explained the fluoride uptake process
- At higher initial fluoride concentration and at basic condition (pH>7), breakthrough was reached faster on increasing depth of the adsorbent column.
- The fluoride adsorption efficiency of the composite column increased with both the bed depth of the composite column and the inlet flow rate, while it decreased with increasing pH of the inlet fluoride solution.

Chapter.7

Dye and Fluoride remediation using polymeric materials-based composite: Fluidized-bed study

7.1. Introduction

The solid-liquid fluidized-bed adsorption system have been used for many applications in various sector of the chemical and biochemical industries. In a fluidized bed system, complete mixing between solid particles and fluid can be established, thus creating more suitable environments for effective heat and mass-transfer (Davoodi et al., 2021). In recent years, this system has been applied in the wastewater purification process (Sureshkumar et al., 2020). The benefits of this system besides preventing clogging in associated with fixed bed are better adsorbate-adsorbents interaction leading to higher removal/uptake efficiency and less adsorbent quantity requirement (Lan et al., 2002).

In this chapter, the results obtained on application of Alginate-nanocellulose composite beads for MG dye decolorization and defluoridation process in fluidized-bed system have been presented. Experimental data were evaluated by designing mathematical modeling.

7.2. Results and Discussion

7.2.1. *Fluidized-bed study for Dye removal using Alginate-nanocellulose beads*

Characteristics of fluidized-bed

Minimum fluidization velocity' was calculated using adsorbent-bed height (H) vs. superficial velocity (U) plot (Fig. 7.1) and corresponds to the point where the changes from stationary solid adsorbent bed to solid-liquid fluidized-bed happens through increase in fluidization velocity. Experimentally obtained U_{mf} value and the fluidization velocity for different height of adsorbent-bed was represented in Fig. 7.1 using adsorbent mass of 4g. It is seen that the velocity must be maintained above 0.06217 cm min^{-1} for attainment of fluidized condition. High superficial velocity leads to increase in loss of fine adsorbent material (B. Lv et al., 2021).

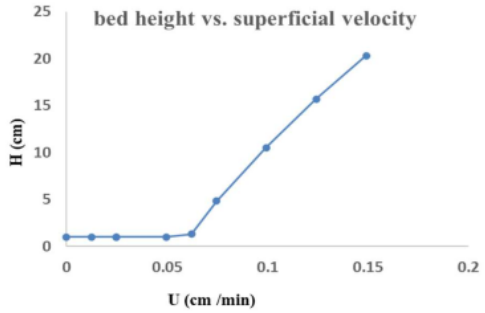

Fig. 7.1**:** Fluidization curve for determination of the minimum fluidization velocity (adsorbent mass=4g, fixed bed height=8cm, adsorbent beads diameter= 0.25mm)

Effect of feed concentration

Influence of initial feed concentration on MG dye adsorption in fluidized-bed column (continuous adsorption experiments) with fixed biosorbent-bed weight of 4g Alginate-nanocellulose beads was investigated by varying feed concentration (50, 75, 100 mg/L) at constant inlet flow rate of 50 ml/min using 0.25 mm beads size. The curves presented (Fig. 7.2(a)) show that the rate of defluoridation in fluidized-bed is better at lower feed solutions. So feed concentration of 50 mg/L was used for further experiments. The reduced adsorption efficiency on increasing feed concentrations of dye solution could be associated with the competition between large amount of adsorbate molecules for active sites on composite beads surface (B. Lv et al., 2021).

Effect of adsorbent bed weight

Weight of biosorbent bed is another significant factor in the fluidized-bed adsorption process. Effects of bed depth on the performance of column adsorption process were investigated in fluidized-bed reactor at different bed weight (4, 6, and 8 g) with the feed flow rate, concentration of feed and beads size kept constant at 50 mL/min, 50 mg/L and 0.25 mm respectively. The results at various bed weight has been presented in Fig. 7.2(b). It is noted that an increase in adsorbent-bed weight from 4g to 8g fluoride removal efficiency decreased. With increasing weight of biosorbent mass, movement/suspension of particles in fluidized media of the column reduced which leads to the decreased in adsorbent-adsorbate interaction (or contact in between adsorbate and adsorbent) and reduce the removal proficiency. Hence, weight of column bed for further study was kept by around 4g.

Effect of feed flowrate

Influence of the initial feed flow rates on fluoride adsorption performance of continuous fluidized-bed system containing Alginate-nanocellulose as biosorbent was examined under varying feed flow rate (30-50 mL/min) for a constant mass of biosorbent-bed (4g), initial feed concentration of 8 mg/L and bead diameter 0.25 mm. The sorption behaviours attained at various feed flowrates are presented in Fig. 7.2(c). Results indicated that as rate of feed flow was increased better dye adsorption was obtained with lengthier saturation period. Feed flow

rate of 50 mL/min correspond to minimum fluidization velocity at which the fixed bed become fluidized. Fluidization increases the adsorbate molecule-adsorbent particle interaction and improves efficiency.

Effect of composite beads size

The influence of average adsorbate breads size (in diameter) on MG dye adsorption performance in continuous fluidized-bed reactor was investigated at varying adsorbent bead diameter (0.25mm, 0.53mm, 0.97mm) while the feed flowrate, adsorbent mass and feed concentration were kept constant as 50 mL/min, 4g and 50 mg/L respectively. Mass of adsorbent in column taken in each run was kept constant (4g). Beads of different diameter was prepared by allowing the suspension to flow into the calcium chloride solution from openings of different diameter. Fig. 7.2(d) represented the effects of composite beads size upon biosorption proficiency. A decrease in biosorbent beads diameter from 0.97 to 0.25 mm show higher defluoridation performance and lengthier biosorption process. Removal proficiency is improved by using smaller size of solid particle because of higher adsorbent surface area for better interaction with adsorbate molecule at the same adsorbent mass.

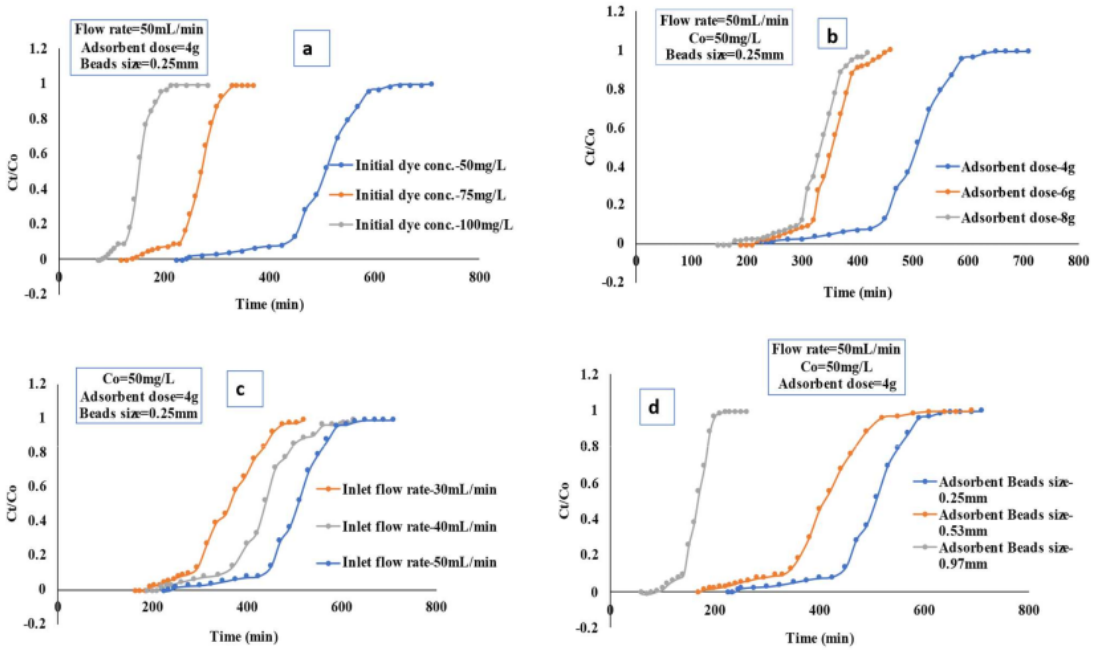

Fig. 7.2: Influence of different experimental variables on adsorbent performance of the continuous fluidized-bed for MG dye removal

7.2.2. Fluidized bed column kinetic models for MG dye removal study

Parameters obtained from Yoon-Nelson model are presented in Table 7.1. On the basis of resulted data, it is observed that the value of k_{YN} and τ decreased on increasing both feed flow rate and pH of feed solution. The value of τ was maximum at 8 cm bed height.

Calculated values of k_{Th}, q_0, and regression coefficients obtained from Thomas model are presented in Table 7.1. Results suggested that with an increase in the feed flow rate, the value of Thomas rate constant (k_{Th}) reduced but the bed capacity (q_0) increased. Contrarily, q_0 increased and the value of k_{Th} reduced with an increase in column bed height. The reasonably high value of regression coefficients (R^2 >0.95) at all the investigational situations signify that the data obtained from the column study could be suitably explained by Thomas model and Yoon Nelson model.

Table 7.1: Derived Parameters of continuous fluidized bed column kinetic models for dye adsorption on composite at different experimental conditions

Operational condition				Yoon-Nelson model			Thomas model		
F (L/min)	C_0 (mg/L)	W (g)	Adsorbent beads dia. (mm)	k_{YN} (L/min)	τ (min)	R^2	$k_{TH} \times 10^2$ (L/mg.min)	q_0 (mg/g)	R^2
0.05	50	4	0.25	0.0225	483.955	0.966	0.045	336.080	0.966
0.05	50	6	0.25	0.0192	711.406	0.984	0.0384	296.419	0.984
0.05	50	8	0.25	0.0175	828.971	0.993	0.035	262.333	0.993
0.04	50	4	0.25	0.0209	373.827	0.987	0.041	207.682	0.987
0.03	50	4	0.25	0.0257	35.875	0.993	0.0514	14.948	0.993
0.05	75	4	0.25	0.0452	257.079	0.954	0.060	267.791	0.954
0.05	100	4	0.25	0.0543	157.311	0.963	0.054	218.487	0.963
0.05	50	4	0.97	0.065	165.384	0.962	0.13	114.850	0.962
0.05	50	4	0.53	0.0195	683.589	0..985	0.039	474.715	0..985
0.05	50	4	0.25	0.0225	483.955	0.966	0.045	336.0802	0.966

7.2.3. Fluidized-bed study for Fluoride removal using Alginate-nanocellulose beads

Fluoride adsorption behaviour in fluidized bed was investigated using Alginate-nanocellulose beads as adsorbent by varying parameters including feed concentration (8, 10, 12 mg/L), feed

flowrate (30, 40, 50 mL/min), adsorbent beads size (0.25, 0.53, 0.97mm), adsorbent bed weight (4, 6, and 8g). The trends of the results are similar to that obtained in the dye removal study in fluidized bed column under all experimental conditions.

Effect of feed concentration

Influence of initial feed concentration on fluoride adsorption in fluidized-bed column of Alginate-nanocellulose beads was investigated by varying feed concentration (8-12 mg/L) at constant biosorbent-bed weight (4 g), constant feed flowrate of 50 ml/min using 0.25 mm beads size. The curves presented (fig. 7.3(a)) show that the performance of fluidized-bed was better at feed concentration of 8 mg/L.

Effect of adsorbent bed weight

Effects of bed depth on the performance of column adsorption process were investigated in fluidized-bed reactor at different bed weight (4, 6, and 8 g) where the feed flowrate and concentration of feed were kept constant at 50 mL/min and 8 mg/L respectively. The results are presented in Fig. 7.3(b). It was noticed with increase in adsorbent-bed weight defluoridation rate decreased.

Effect of feed flowrate

The effect of feed flowrates on fluoride adsorption performance of continuous fluidized-bed system was examined under varying feed flowrate (30-50 mL/min) for fixed weight of biosorbent-bed (4g), beads size of 0.25 mm and feed concentration of 8 mg/L. The sorption behaviours attained at various feed flowrates were presented in Fig. 7.3(c). Results indicated that as rate of feed flow was enhanced to 50 mL/min better fluoride adsorption was obtained.

Effect of composite beads size

The influence of average adsorbate breads size (in diameter) on fluoride adsorption performance in continuous fluidized-bed reactor was investigated at varying adsorbent bead diameter (0.25mm, 0.53mm, 0.97mm) while the initial feed flow rate and feed concentration were kept constant as 50 mL/min and 8 mg/L, respectively. It was noticed that a decrease in biosorbent beads diameter from 0.97 to 0.25 mm showed higher defluoridation performance and lengthy biosoption process.

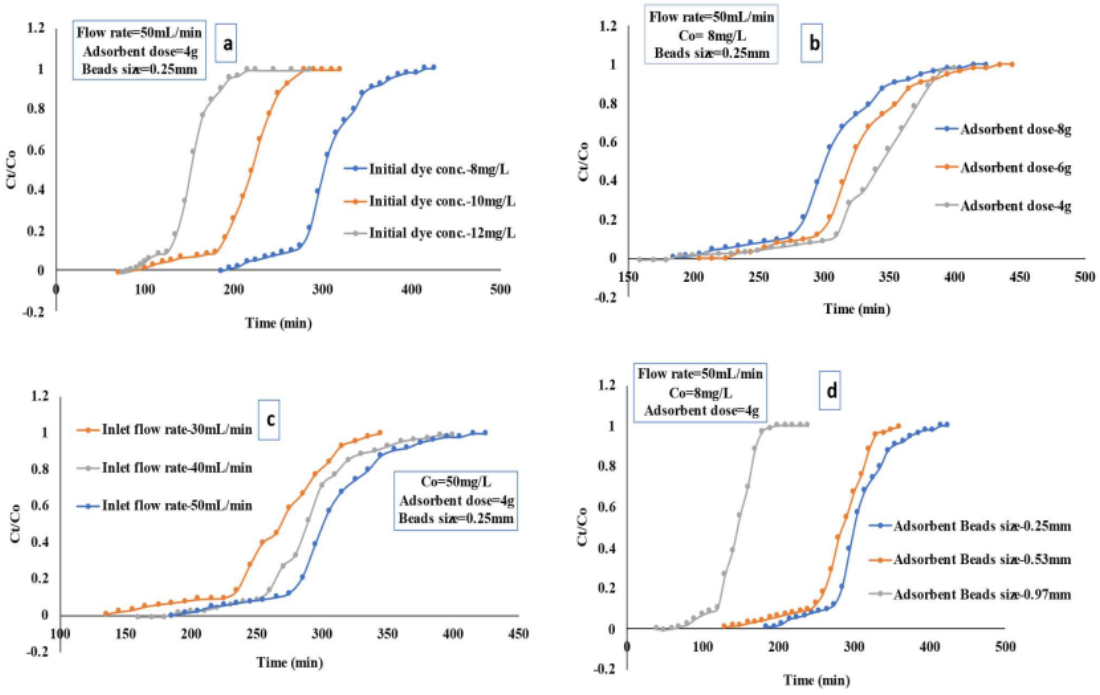

Fig. 7.3: Influence of different experimental variables on adsorbent performance of the continuous fluidized-bed for fluoride removal

7.2.4. Fluidized bed column kinetic models for fluoride removal study

The calculated values of parameters obtained from Yoon-Nelson model, k_{YN} and τ are shown in table 7.2. Results showed that the model parameter k_{YN} increased with an initial concentration of feed solution and the value of τ decreased under such conditions. The magnitude of these parameters decreased with increase in flow rate of feed solution and adsorbent beads size. The value of τ increased with the weight of the adsorbent bed but that of k_{YN} decreased. Calculated values of Thomas model parameters k_{Th} and q_0 with coefficients of regression analysis (R^2) for each set of experimental conditions are presented in Table 7.2. Resulted data indicated that both the Thomas model and Yoon-Nelson models were suitable to predict the biosorption performance for fluoride adsorption onto Alginate-nanocellulose composite beads in a fluidized-bed system. As seen in Table 7.2, it is observed that k_{Th} decreased with increasing both the adsorbent bed weight and the flow rate of the feed solution, whereas q_0 increased for these trend. The value of q_0 increased with increasing both the inlet concentration and beads size whereas k_{Th} decreased.

Table 7.2: Derived Parameters of kinetic models for continuous fluidized bed column for Fluoride adsorption using Alginate-nanocellulose at different experimental conditions

Operational condition				Yoon-Nelson model			Thomas model		
F (L/min)	C_0 (mg/L)	W (g)	Adsorbent beads dia. (mm)	k_{YN} (L/min)	τ (min)	R^2	$k_{TH} \times 10^2$ (L mg/min)	$q_0 \times 10^3$ (mg/g)	R^2
0.05	50	4	0.25	0.039	296.035	0.983	0.0079	205.580106	0.983
0.05	50	6	0.25	0.045	324.201	0.978	0.0091	135.083880	0.978
0.05	50	8	0.25	0.036	335.467	0.992	0.0072	106.160453	0.992
0.04	50	4	0.25	0.044	291.715	0.990	0.0088	162.064208	0.990
0.03	50	4	0.25	0.044	256.892	0.957	0.0088	107.038288	0.957
0.05	75	4	0.25	0.045	207.124	0.954	0.0602	215.754056	0.954
0.05	100	4	0.25	0.054	157.311	0.930	0.0054	218.487824	0.930
0.05	50	4	0.97	0.072	138.152	0.965	0.0145	95.9386973	0.965
0.05	50	4	0.53	0.033	327.848	0.950	0.0066	227.672558	0.950

7.3. Summary

Decolourization and defluoridation characteristics of fluidized bed was examined using Alginate-nanocellulose beads are presented in this chapter. Concluded summery of this research work are as follows:

- With increasing bed weight, the adsorption rate increased
- The adsorption efficiency reduced by rising initial feed concentrations
- Results indicated that as rate of feed flow was enhanced better fluoride adsorption was ascended along with lengthier saturation period due to increase in the adsorbent-adsorbate contact frequency.
- It was noticed that a decrease in biosorbent beads diameter showed higher defluoridation performance and lengthy biosoption process.

These results suggested that fluidized bed in conjunction with Alginate-nanocellulose composite can be used as a suitable efficient biosorbent in decolourization and defluoridation process in treatment of polluted water.

Chapter.8

Evaluation on Regeneration and Biodegradation study of pollutant-loaded composites

8.1. Introduction

Recyclability and reuse of adsorbent are important factors in evaluation of economy of adsorption process. Pollutant elimination by biosorption process is reasonable and beneficial if the pollutant loaded biosorbent can be regenerated. Regeneration helps to prolong serviceability of adsorbent, recuperate the uptake capability and saves expenses for adsorbent preparation. Disposing the used adsorbent has many undesirous effect on the environment. This could be reduced by biodegradation of the adsorbent. After several cycle of reuse, as the removal efficiency of adsorbent is reduced, the pollutant loaded adsorbents were biodegraded by isolated microorganism before dispose them to the environment.

Biodegradation is the microbial process of decaying or reduction of different organic materials and toxic metals to their nontoxic form with the help of microorganisms. The biodegradation process is a simple, eco-friendly and cost-effective process that requires low capital and operating cost and generates no hazardous end products. In this method nutrients and physical conditions plays important role. Temperature and pH are the important physical variables and shows a significant impact on degradation behavior. Biodegradation of dye (Banerjee et al., 2017) and fluoride (Singh & Gothalwal (2018); Mukherjee et al., (2015) occurs as a result of the activity of a large number of microorganisms including bacteria, fungi and actinomycetes. Bacterial species including *Bacillus sp*, *Pseudomonas sp*, *Streptomyces sp* etc have proved to be efficient in biodegradation of dye (Kalyani et al., 2008; Katiyar et al., 2020) whereas microorganism such as Aspergillus sp., Rhizopus sp., Acinetobacter sp. RH5 are also proved to be efficient in biodegradation of sodium fluoride (Tamilvani et al., 2015; Mukherjee et al., 2015). Though there is huge volume of work on the biodegradation of pollutants from wastewater such as *Bacillus sp.* used to biodegrade 2, 4, 6-TNT (Lin et al., 2013), *Pseudomonas sp* used for bioremediation of Reactive Red 2 (Kalyani et al., 2008; Banerjee et al., 2017), etc. But research on use of micro-organism for degradation of pollutant loaded adsorbent is still a not much researched area.

This present chapter describes the experimental results on the regeneration and biodegradation of the pollutant loaded biosorbents after use in wastewater treatment process. In regeneration study, loaded biosorbent post-adsorption of dye/fluoride was regenerated and then again used in adsorption study. After a few cycles, the loaded biosorbent were biodegraded using isolated microorganism. The biodegradation of dye-loaded adsorbents and fluoride-loaded adsorbents was carried out using isolated microorganism (*Lysinibacillus sp*.

(GenBank accession no: SUB9070461 seq1PDMW596888). The biodegradation behavior was observed in terms of % weight loss with time.

8.2. Material and method

8.2.1. Regeneration experiment

Experiment on the recyclability of the adsorbent was done at 30°C. 1 g/L of adsorbent was kept in contact with 50 mL of dye solution (20 mg/L) for 60 min under agitation. MG dye loaded adsorbent was added into 0.1 M NaOH or 0.1 M HCl solution and stirred for 120 min. The adsorbent mass was then separated and washed with deionized water two times to remove the residual NaOH or HCl solution and then vacuum dried at 80 °C and reused for adsorption. This process was repeated for several cycles in the following manner.

Regeneration study of fluoride-loaded adsorbents was conducted at 30 °C. 2 g/L of adsorbent was added to 50 ml of fluoride solution of strength 6 mg/L. The suspension was stirred for 90 min. Fluoride loaded adsorbent was the separated and added into NaOH (0.05 M) solution and was stirred for 90 min at 30 °C. Thereafter the adsorbent was again separated from the solution and washed away two or three times with DI water. Then, it was vacuum dried at 80 °C. This cycle was again repeated a few times.

8.2.2. Isolation and culture of micro-organism

Bacteria were isolated from soil samples taken from Bantala industrial complex, Kolkata, West Bengal. Bacterial colonies were cultured by serial dilution of the solution of soil sample and plating them on the nutrient agar plate. After several subcultures purest culture was stored at 4°C for further use. There are different types of culture mechanism for the organism growth. Slant culture and liquid solution culture have been used in this study.

- 100 ml nutrient broth solution was prepared taking 1.3gm of broth and distilled water. The solution was sterilized at 15 psig pressure for 15 minutes in an autoclave and cooled. The bacteria were inoculated into this solution aseptically. The inoculated media was incubated in a BOD shaker for one day for uniform growth of the organism.
- 50 ml nutrient agar solution was prepared. The solution was sterilized for 15 minutes in an autoclave at 15 psig pressure and then the solution was equally divided into ten test tube. Mouth of the test tubes were sealed with the help of nonabsorbent cotton. The test tubes were kept slightly slanted manner. When solution in the test tube become solidified then small

amount of micro-organism was inoculated with the help of nip wire. Then the test tubes mouths were plugged with nonabsorbent cotton and kept in incubator for 24 hours at 35°C.

8.2.3. Characteristics of the isolated micro-organism

Gram stain characterization was implemented to detect the cellular morphology and gram nature of the isolated strain.

Morphological characteristics of the isolated strain

Gram staining is a common technique used to differentiate two large groups of bacteria based on their different cell wall constituents. The Gram stain procedure distinguishes between Gram positive and Gram-negative groups by coloring these cells red or violet. Gram positive bacteria stain violet due to the presence of a thick layer of peptidoglycan in their cell walls, which retains the crystal violet these cells are stained with. Alternatively, Gram negative bacteria stain red, which is attributed to a thinner peptidoglycan wall, which does not retain the crystal violet during the decoloring process

Procedure of Gram staining

- A smear was prepared from the 24 hr old plate culture of the isolated strain
- The smear was air dried.
- Air-dried smear was then heat-fixed.
- The smear was covered with crystal violet stain and allowed to stand for 1 min.
- The primary stain was washed with Gram's iodine solution and it was allowed to stand for 60 min.
- The smear was washed with 95% ethyl alcohol and washed with water.
- The secondary stain safranine was applied and the smear was exposed for1 min
- The slide was washed with water and dried
- Slide was examined under microscope.

8.2.4. Determination of bacterial growth

Total viable count: Standard method of viable count was performed to quantify number of cells to be used as inoculums of the reaction mixture. Total Viable Count (TVC) gives a quantitative idea about the presence of microorganisms in a sample. The count actually represents the number of colony forming units (CFU) per ml of the sample. The standard plate count method consists of diluting a sample with sterile saline diluents until the bacteria are dilute enough to count accurately.

- A TVC is achieved by plating dilutions of the culture until 30-300 colonies exist on a single plate.

***Turbidometric analysis*:** Biomass was separated by centrifugation at 8000 RPM for 10 min. The pellet was washed and re-suspended in equal volume sterile saline solution and measured for OD at 600nm (optical density measuring at this wavelength reduces the absorbance of the culture media and corresponds to the discrete light interactions of the microorganism).

Standard plate count method

- In order to check OD of growth media 5ml was taken (at 550nm wavelength).1ml from rest of this add to 9ml double distillate water (autoclaved) in a test tube (1). Taking 0.1ml from test tube (1) spreading was done in a Petri plate (1). then from test tube (1) 1ml was taken and added with another test tube (2). Then 0.1ml from this test tube was used for spreading in a Petri plate (2). from test tube (2) 1 ml was taken and similarly this process was go on up to Petri plate (7).
- OD of those test tube samples was checked before spreading culture and counting CFU from plate culture.

Standard curve (OD_{600} corresponds to CFU/mL)

The procedure adopted for standard curve from bacterial growth is stated below

- 1. Bacteria were grew at different time period in broth (4 time period i,e.: 18 hours 24 hours, 36 hours and 48 hours), The OD600 was measured for each growth condition
- 2. The broth was taken from the conditions mentioned above; the serial dilution and streak were done onto agar plate
- 3. The plates were incubated and counted the CFU/mL for each growth conditions (18 hours, 24 hours, 36 hours and 48 hours)
- 4. Standard curve (OD600 vs CFU/mL) was plotted

CFU measurement in Petridis = (colony number × dilution factor)/volume plated

8.2.5. Biodegradation study of pollutant-loaded composite and weight loss analysis

After the adsorption process, dye-loaded composites and fluoride-loaded composites were biodegraded using isolated selected stain Lysinibacillus Sp. (GenBank accession no: SUB9070461 seq1PDMW596888). Biodegradation studies were performed at different experimental conditions such as varying pH, inoculums volume, system temperature, dye-loaded composite mass, salinity and agitation speed. The biodegradation potential of isolated bacteria was evaluated by the weight loss method. Collected dye-loaded composite beads

from the post-adsorption process were disinfected in an autoclave. Sterilized dye-loaded composite was then weighed and inoculated with isolated microorganisms and kept in a BOD shaker at 35°C for 5, 10, 15, 20, 25, 30, 35, 40, and 45 days under various operational conditions. After a certain time period of incubation samples were washed with sterile DI water and ethanol to wash excess inoculated bacteria, and then vacuum dried and weighed. Percentage Weight loss was determined in each case of the experimental condition by following equation (Eqn.8.1) (Sarkhel et al., 2020).

$$\% \text{ Weight loss } = \frac{T_0 - T_f}{T_0} \times 100 \ldots\ldots\ldots\ldots (8.1)$$

Where, T_0 (g) and T_f (g) denoted the initial weight of the dye-loaded composite before the treatment of biodegradation and the final weight of the biodegraded dye-loaded composite at certain time intervals.

8.3. Results and discussions

8.3.1. Regeneration Study of dye-loaded and fluoride-loaded adsorbents

Desorption experiment

The adsorbents used were sugarcane bagasse activated biochar (SBAC), cellulose, Alginate-bentonite/SBAC, nanocellulose/PVA, Alginate-nanocellulose beads. The % desorption of the MG dye-adsorbed adsorbents and fluoride-adsorbed adsorbents using a 5% (*v*/*v*) NaOH solution after 2 h is shown in Fig. 8.1(a) and Fig. 8.1(b).

Regeneration study

Fig. 8.2 show the effect of recovery cycles on the adsorption capacities of dye and fluoride onto prepared adsorbents. The result of % removal of dye and fluoride for six adsorption-desorption cycles are illustrated in Fig. 8.2a and Fig. 8.2b. Table 8.1 and Table 8.2 show that the amount of dye and fluoride adsorbed in each cycle. The results show that the decrease in uptake of cellulose alginate beads were not large for malachite green (MG). However, for fluoride the uptake decreased significantly after two cycles. These promising results demonstrated that adsorbent could be regenerated and repeatedly used in dye and fluoride removal.

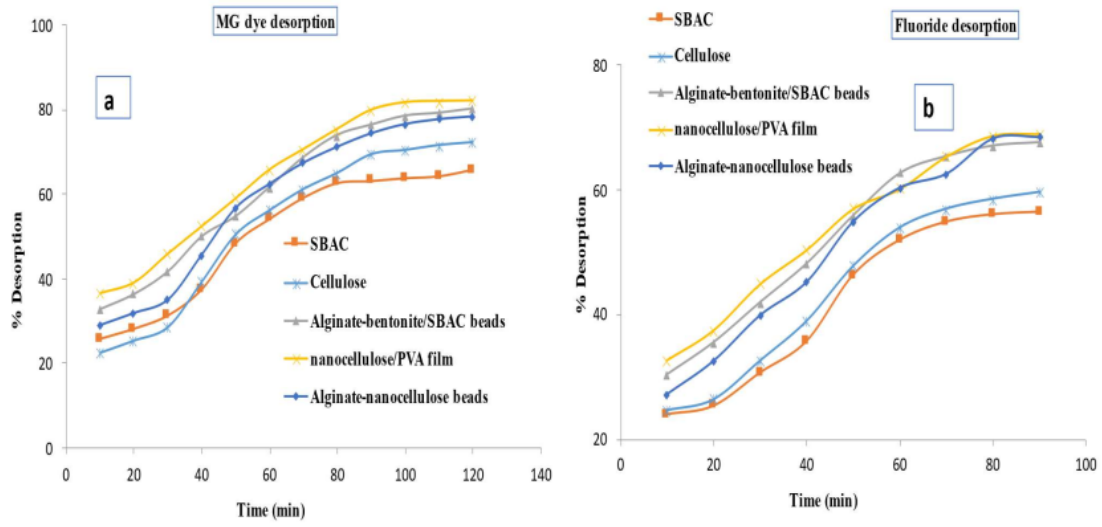

Fig. 8.1: The % desorption of dye and fluoride over time with the use of 5% (*v/v*) ethanol.

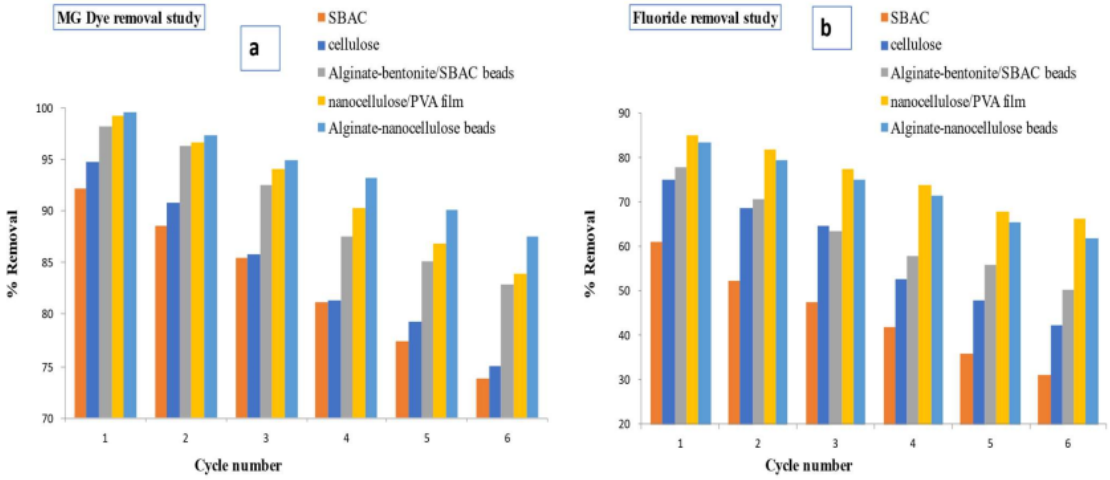

Fig. 8.2: Effect of recovery cycles on the dye and fluoride adsorption efficiency of prepared adsorbents

Table. 8.1: Results of regeneration study for MG dye-loaded adsorbents

Adsorbent		Cycle I	Cycle II	Cycle III	Cycle IV	Cycle V	Cycle VI
SBAC	%R	92.15	88.51	85.5	81.155	77.507	73.85
	q	18.43	17.702	17.1	16.231	15.5014	14.77
Cellulose	%R	94.72	90.85	85.85	81.41	79.25	75.085

	q	18.944	18.17	17.17	16.282	15.85	15.017
SBAC-alginate beads	%R	98.21	96.241	92.52	87.533	85.15	82.9
	q	19.642	19.2482	18.504	17.5066	17.03	16.58
Cellulose-PVA film	%R	99.23	96.6	94.02	90.3	86.92	84.012
	q	19.846	19.32	18.804	18.06	17.384	16.8024
Cellulose-alginate beads	%R	99.57	97.345	94.94	93.15	90.185	87.585
	q	19.914	19.469	18.988	18.63	18.037	17.517

Table 8.2: Results of regeneration study fluoride-loaded adsorbents

Adsorbent		Cycle I	Cycle II	Cycle III	Cycle IV	Cycle V	Cycle VI
SBAC	%R	60.94	52.167	47.38	41.88	35.716	31.16
	q	1.828	1.565	1.421	1.256	1.071	0.93
Cellulose	%R	75.11	68.76	64.83	52.8	48	42.5
	q	2.2533	2.063	1.945	1.584	1.44	1.275
SBAC-alginate beads	%R	77.82	70.80	63.4	57.76	56.05	50.3
	q	2.334	2.12	1.902	1.733	1.6815	1.509
Cellulose-PVA film	%R	85.14	82	77.57	74	67.93	66.4
	q	2.5542	2.46	2.327	2.22	2.038	1.992
Cellulose-alginate beads	%R	83.53	79.48	75.13	71.4	65.43	61.75
	q	9.88	9.38	8.16	7.68	6.92	5.906

8.3.2. Characteristics of isolated bacteria stain

The isolated strain was identified and showed the closest homology with *Lysinibacillus sp.* (Closer to macrolides). *Lysinibacillus macrolides* (GenBank accession no: SUB9070461 seq1PDMW596888) strain L1 NC110221A. The isolated bacteria stain showed gram-positive characteristics.

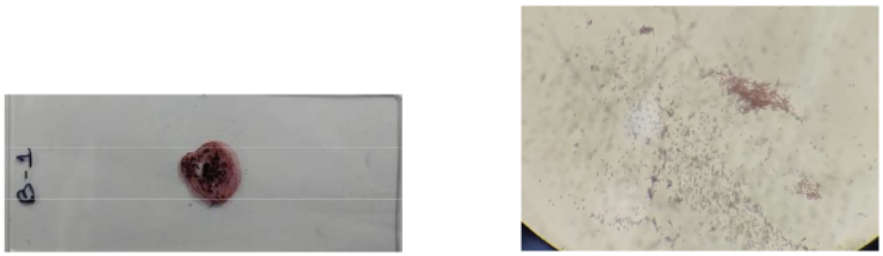

Fig. 8.3: Microscopic view of isolated bacteria, Gram staining results: **Gram positive bacteria**

8.3.3. Microbial Growth study at different experimental conditions

Effect of temperature on bacterial growth:

Temperature has significant effects on the biodegradation rate as it plays an importance role in the growth of microorganisms. Temperature affects microbes in two contradictory ways: with increasing temperature (Fig. 8.4a), chemical and enzymatic reactions occur at more rapid rates, and the growth rate increases. But above a definite temperature, proteins are permanently damaged. In this experiment, 50 ml medium was distributed in a series of 100 ml flask, plugged with non-adsorbent cotton and wrapped with brown paper. Then the entire contents were sterilized in an autoclaved at 15 psi pressure for 15 min. Then each medium was inoculated with 1 ml of bacterial cells. The media were then maintained in a BOD incubator at different temperature ranges (25-55°C) and 150 RPM. The growth curve is depicted in Fig. 8.4. The organism showed maximum growth at 35°C and showed a good consistent growth at temperature ranging from 25 to 55°C. Microbial membrane are damaged at high temperature. At very low temperature, cell membrane solidify and enzyme's activities reduces.

Effect of pH on growth of the organism

The pH level of an environment can either enhance or harm the microbial growth. The effect of different pH on the bacterial growth was investigated at various pH ranges (2-11) in BOD incubator at 150 RPM under 35 °C temperature and the growth curve is shown in Fig. 8.4(b). The gram-positive bacteria were grown in mineral salt medium for 360 min at different pH. Maximum amount of cell mass was produced at pH 8. Intracellular pH can reduce significantly when the microbial cell is exposed to the acidic or basic environment. As maximum enzymes are very sensitive to pH, the growth inhibitions that are observed under acidic condition occur through direct influence of H^+ on cellular components.

Effect of salinity on bacterial growth

Salt concentration inhibits bacterial growth in various ways. Salt dehydrates microbial cell as the salt around the external part of the cell membrane draws water molecules out and substitutes them with salt molecules. Very high density of salt harms or destroys microorganism by drawing water out of them. To investigate the effect of salt concentration on growth of the isolated bacteria a series of liquid culture have been observed at different concentration of sodium chloride salt (1%, 2%, 4% w/v) in mineral salt medium culture and

growth curve was presented in fig. 8.4. It was observed that bacterial growth rate was higher and stable at 2% (w/v) salt concentration in liquid culture.

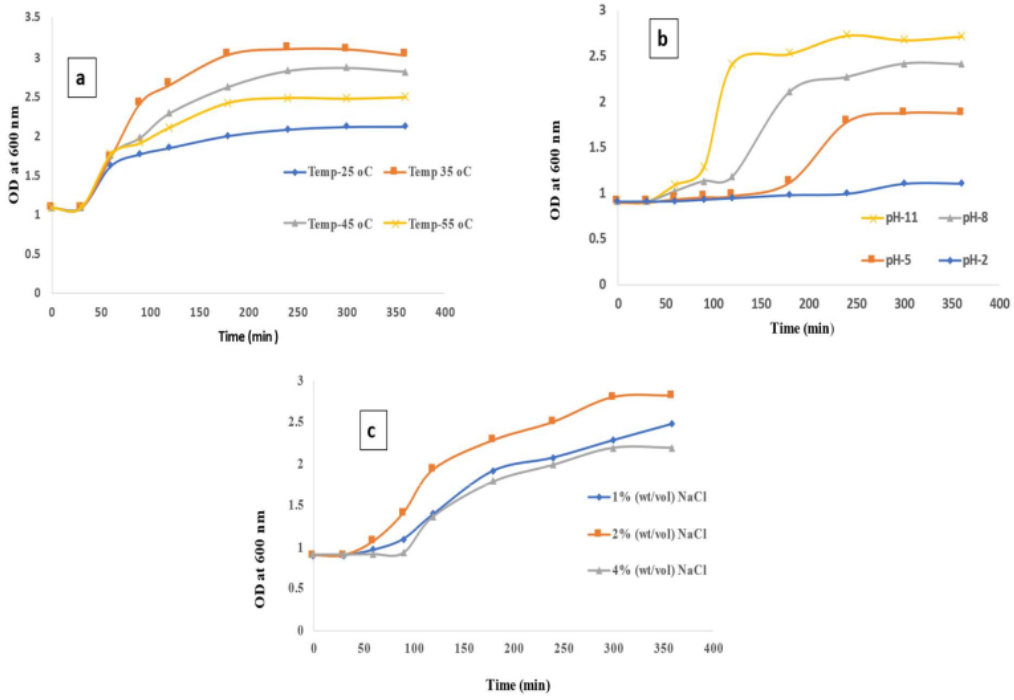

Fig. 8.4: Bacterial growth at various temperatures (a), at various pH levels (b), at different concentration of NaCl salt (c)

Effect of incubation time on bacterial growth at presence of dye and fluoride

In order to examine the effect of incubation time on bacterial growth in presence of dye and fluoride, isolated bacteria were grown in mineral salt medium containing either malachite green (100 mg/L) or fluoride (6 mg/L) for the individual study. The time dependent growth curve of isolated bacteria in presence of dye and fluoride is shown in fig. 8.5. In both the cases the organism entered its log phase after 1 hours of its growth from inoculation into fresh media. The two graphs suggest that the organism reaches its stationary stage after 8 hours. Increase of MG concentration increased from 100 mg/L to 200 mg/L reduced the bacterial growth rate. CFU numbers decreased at higher concentration of MG dye (500 mg/L) and fluoride (15mg/L) due to toxic effect of MG and fluoride on the bacteria.

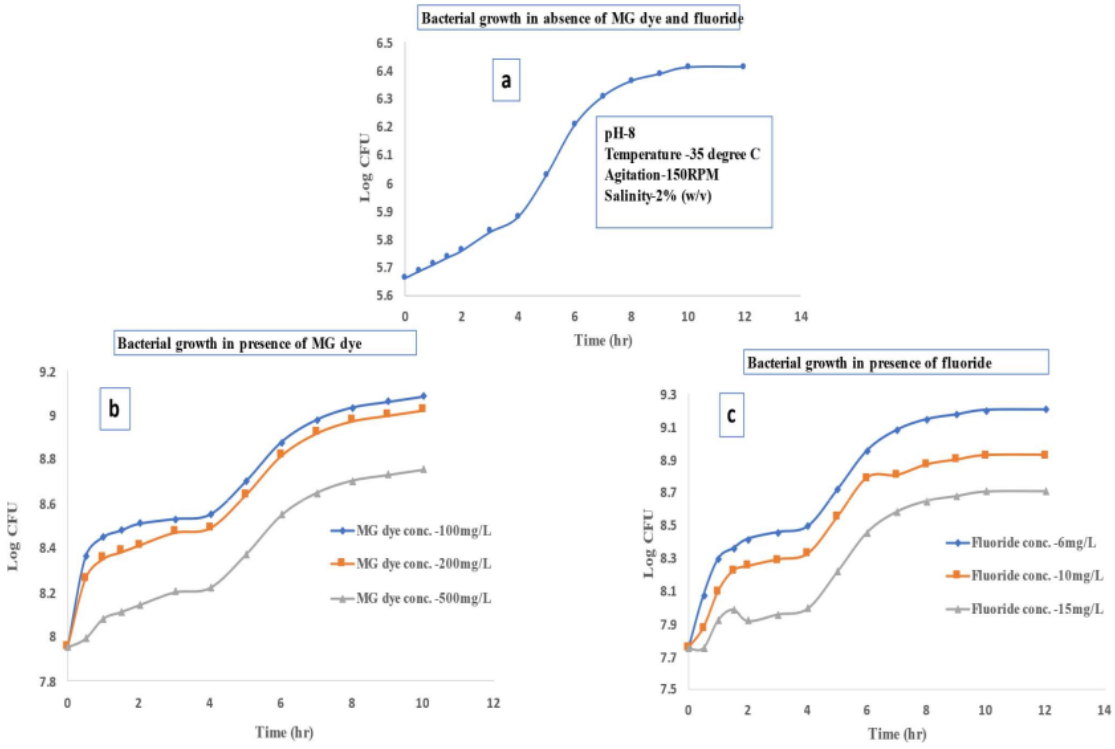

Fig. 8.5: Bacterial growth curve with time in presence of MG dye and Fluoride at different initial concentrations

The growth characteristics of the organism were optimized in order to increase the yield. The organism was found to be a neutrophile, which grows best at neutral pH (5-8), prefers a temperature of 35°C and a rotation speed of 150 rpm. The growth curve of the organism showed that it reached its doubling phase after 1 hours of its growth.

8.3.4. Biodegradation study of MG dye-loaded and fluoride-loaded composite

Effect of pH on biodegradation rate

Influence of system pH on dye-loaded and fluoride-loaded composites degradation using *Lysinibacillus sp* (GenBank accession no: SUB9070461) bacteria has been examined at different pH: 2-11 for period of 45 days under specified operational conditions (Initial Inoculums volume-0.3 $\times 10^9$ CFU/mL (0.4g/L), rotation speed-150 rpm, Temperature 35 °C). The data is presented in %weight loss vs. time graph in Fig. 8.6. It is observed that with changing pH level from 2.0 to 8.0, % weight loss of on dye-loaded and fluoride-loaded

composites increased after biodegradation. The growth or degradation inhibitions that are observed at acidic conditions (pH-2) might be affected through the direct influence of H^+ ion on cellular elements (James B. Russell et al. 2001). The isolated bacteria favor growth at basic environments (pH 5-8). However, it sustains a neutral cytoplasmic pH to avoid acidic or alkali variable macro-molecules in the microbe cell. This leads to very less biodegradation rate at pH=2 and moderate above pH=8 (such as pH=11 shown in fig. 8.6(c)).

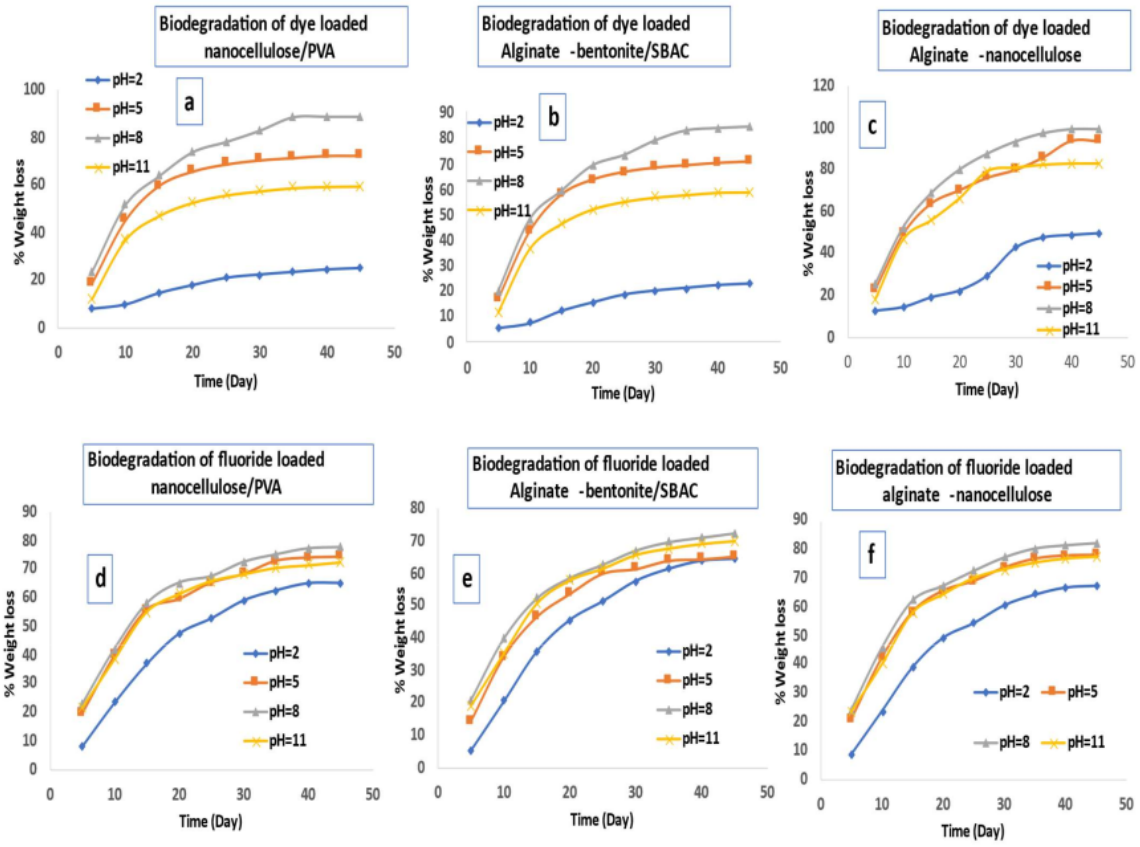

Fig. 8.6: Time dependent %weight loss data at different pH condition for biodegradation of dye and Fluoride-loaded composites (Inoculum dose-0.3×10^9 CFU/mL, Composite dose-1g/L, Temperature-35℃, Agitation speed-150 RPM)

Effect of temperature on biodegradation rate

In these studies, the temperature was varied from 30°C to 45°C. The results are presented graphically in fig. 8.7. All other operational parameters including initial inoculums volume-.3 $\times10^9$ CFU/mL (0.4g/L), agitation speed-150 rpm, pH-8, dye-loaded composite dose-1g/L were

kept constant. Results indicated that the biodegradation rate of on dye-loaded and fluoride-loaded composites showed an increasing trend as temperature was increased from 30 to 35°C. The rate then decreased with further increase of temperature to 40°C. At higher temperature, bacterial growth was less which leads to the lower biodegradation rate of pollutant-loaded polymeric composites material.

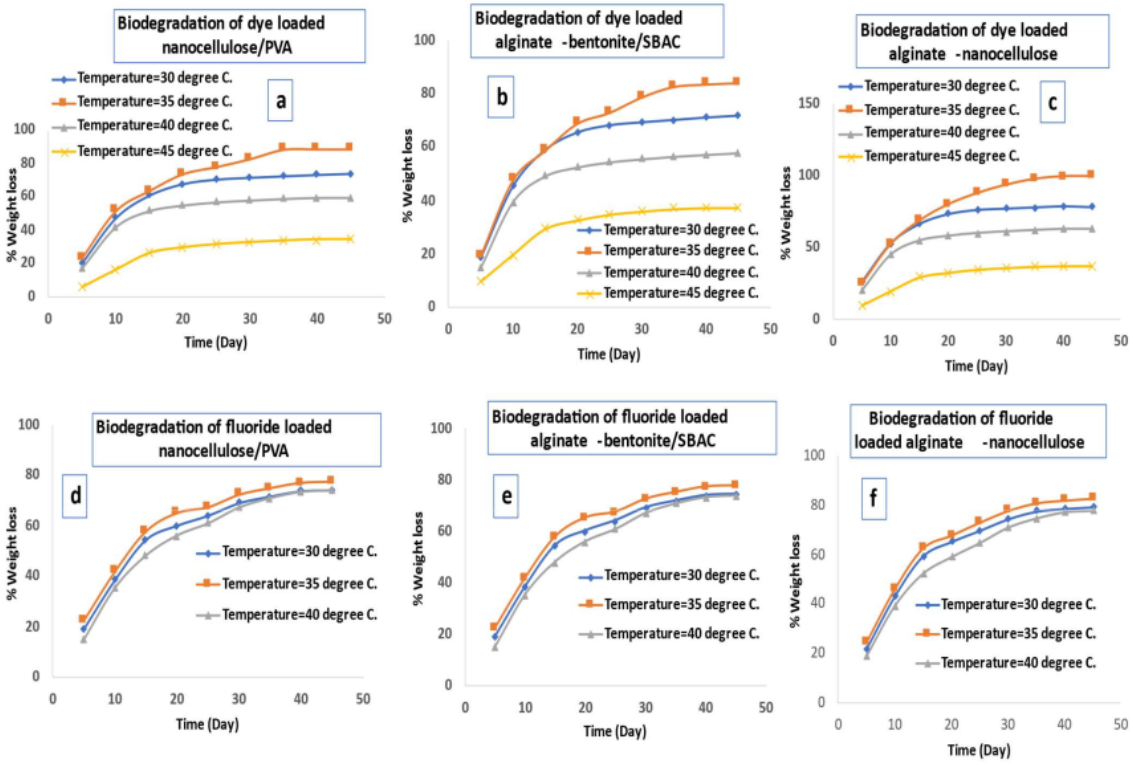

Fig. 8.7: Time dependent %weight loss data at different Temperature for biodegradation of dye and Fluoride-loaded composites (Inoculum dose-0.3×10^9 CFU/mL, Composite dose-1g/L, Agitation speed-150 RPM, pH-8)

Effect of pollutant-loaded composite dose on biodegradation rate

Effect of dye-loaded adsorbent mass on biodegradation of on dye-loaded and fluoride-loaded composites composite by *Lysinibacillus sp* (GenBank accession no: SUB9070461) has been observed at different doses 1-2g/L for 45 days at constant operational conditions (Initial Inoculums volume-0.3 $\times10^9$ CFU/mL (0.4g/L), rotation speed-150 rpm, pH-8, temperature 35°C). The results presented in Fig. 8.8 shows that degradation rate is higher at lower dosage of pollutant loaded adsorbent. At a higher dosage of dye-loaded and fluoride-loaded composites, bacterial growth was less which leads to the less biodegradation rate of composites

material. This is happened due to the toxic effect of excess composite on the bacteria (Sarkhel et al., 2020; Polman et al., 2021).

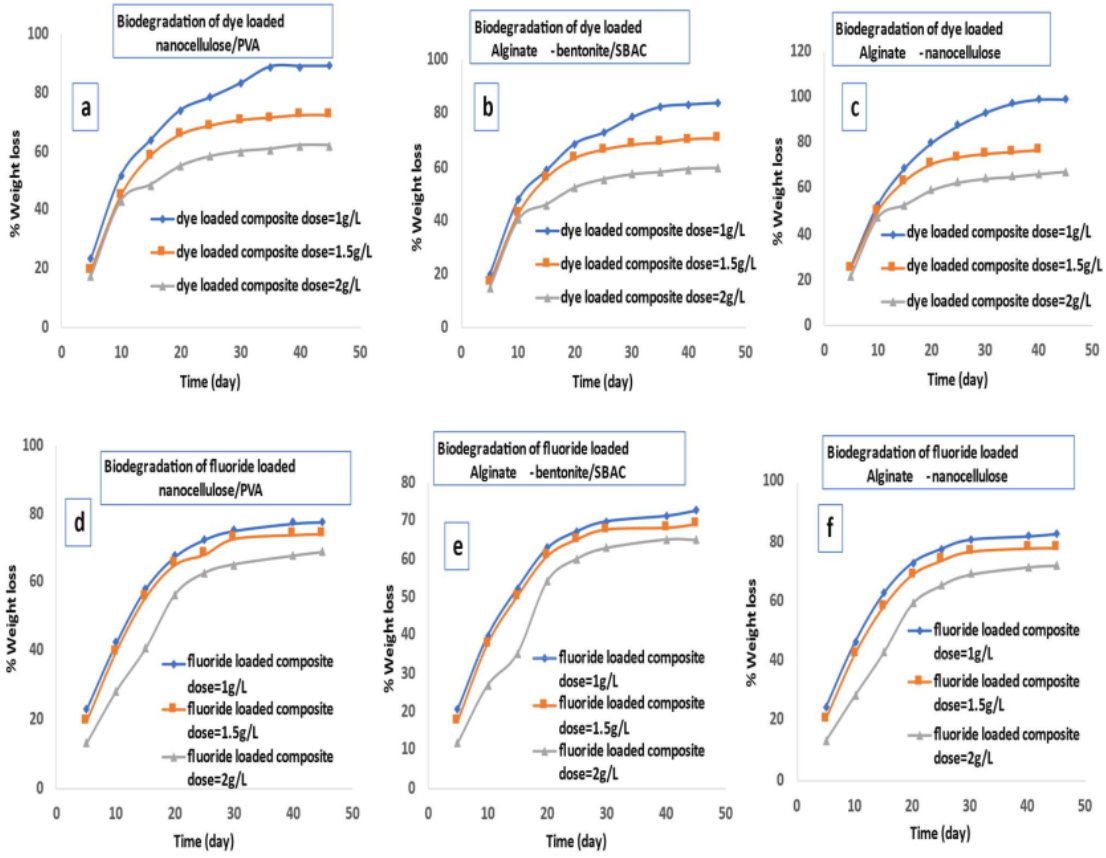

Fig. 8.8: Time dependent %weight loss data at different dosage for biodegradation of dye and Fluoride-loaded composites (Inoculum dose-0.3×10^9 CFU/mL, Temperatur-35 ℃, Agitation speed-150 RPM, pH-8)

Effect of inoculums volume on biodegradation rate

The inoculums volume is an essential parameter that significantly affects the growth rate of microbes as well as biodegradation rate. Generally, a lesser amount of inoculums volume is inadequate to biodegrade the dye-loaded polymeric composite, whereas a very high dosage of inoculums volume induces less biodegradation rate (Verma & Kuila, 2019; Polman et al., 2021). Hence, the suitable dosage of inoculums volume is essential for the biodegradation study. Biodegradation study of dye-loaded Ca-Alginate/biochar composite by *Lysinibacillus sp* (GenBank accession no: SUB9070461) was carried out for 45 days at different inoculums

concentrations (0.1- 0.3×10^9 CFU/mL) keeping all other operational factors constant (agitation speed 150 rpm, pH-8, and temperature 35°C, dye-loaded composite dose-1g/L). The time-dependent biodegradation response is depicted in terms of % weight loss vs. time graph in fig. 8.9. It is seen in the graph that with raise in inoculums dosage from 0.1 ×10^9 CFU/mL (0.1g/L) to 0.3 ×10^9 CFU/mL (0.4g/L), % weight loss of pollutant-loaded composite after biodegradation treatment increased.

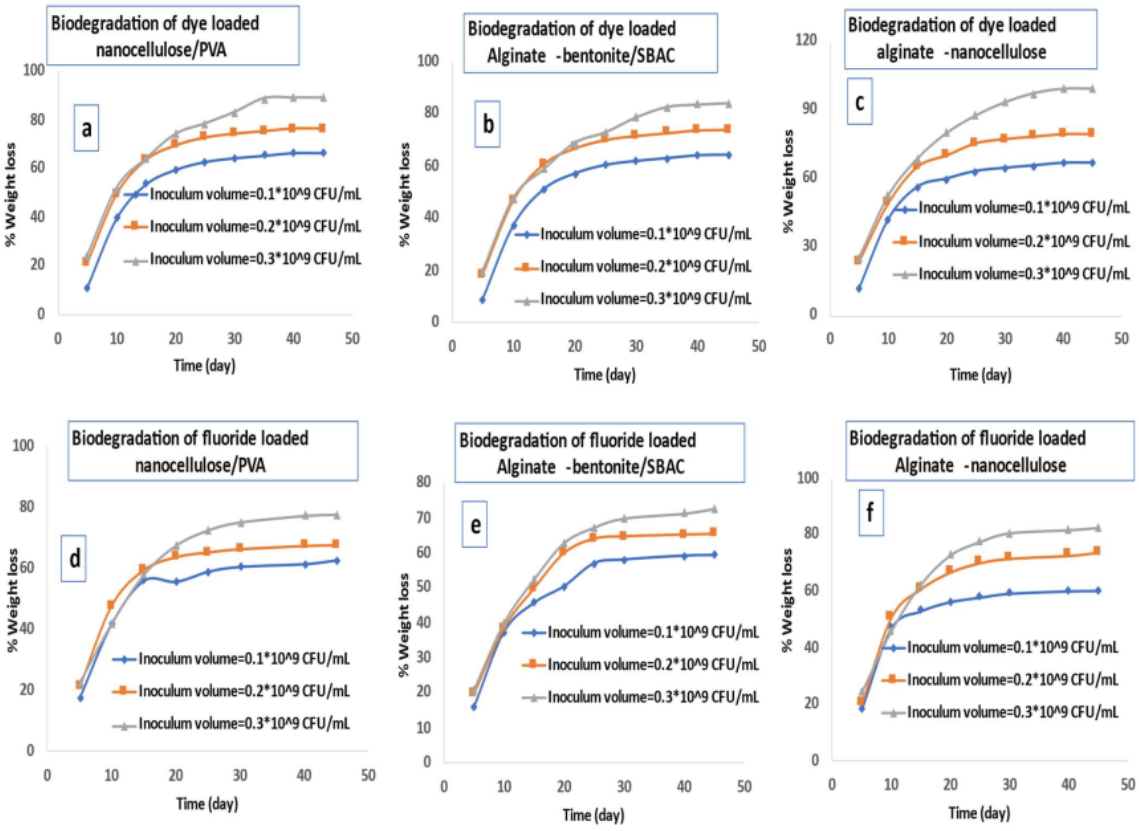

Fig. 8.9: Time dependent %weight loss data at various Inoculum volume for biodegradation of dye and Fluoride-loaded composites (Composite dose- 1g/L, Temperatur-35 ℃, Agitation speed-150 RPM, pH-8)

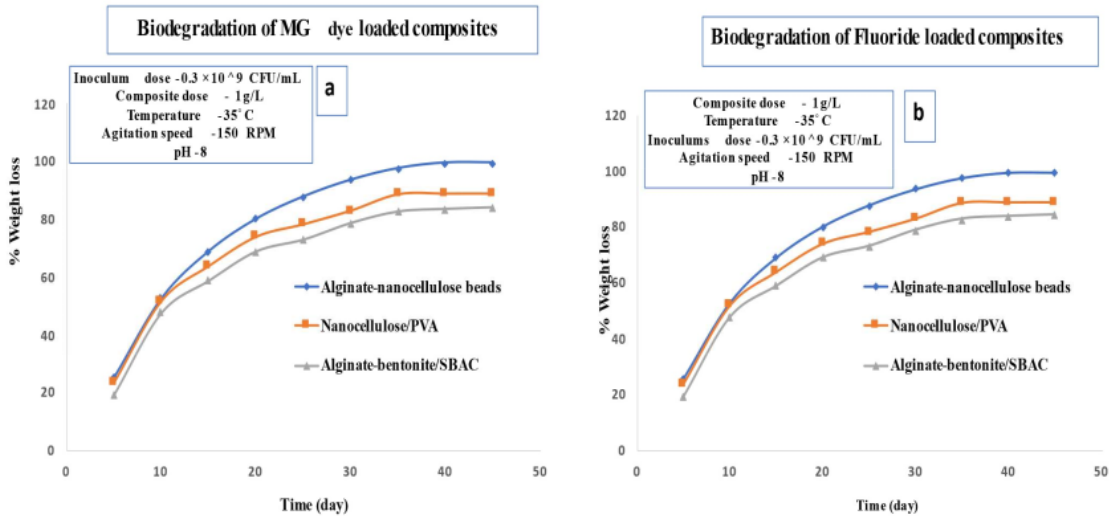

Fig. 8.10: Graphical presentation for Biodegradation of MG dye-loaded and Fluoride-loaded composites at optimum condition (Composite dose- 1g/L, salinity-2% (w/v), Temperature-35℃, Inoculums dose-0.3 $\times 10^9$ CFU/mL, Agitation speed-150 RPM, pH-8)

8.4. SEM image of biodegraded composites

SEM images of biodegraded composites (Alginate-bentonite/SBAC beads, Alginate-nanocellulose beads, nanocellulose/PVA hydrogel composite) are presented in fig. 8.11. The figure suggests that the surface of the composite after the biodegradation process showed a disrupted surface compared to the untreated composite (mentioned in previous chapters). After the treatment of the biodegradation process, the surface of the pollutant-loaded composite showed more unevenness, cavities and cracks with large interconnected holes around the surface.

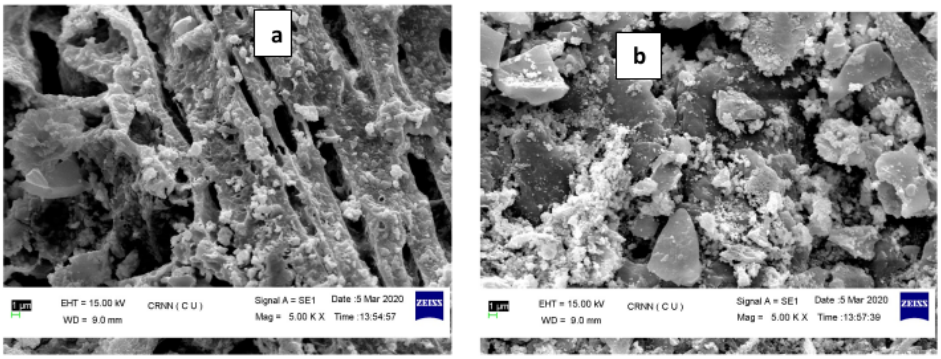

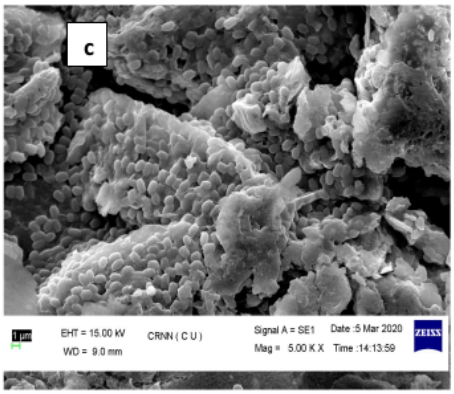

Fig. 8.11: SEM image of biodegraded dye-loaded composites: Alginate-bentonite/SBAC beads (a), Alginate-nanocellulose beads (b), nanocellulose/PVA hydrogel composite (c)

8.5. Summary

- After five adsorption-desorption cycles, the average adsorption efficiency for MG dye removal dropped to ~70 %, whereas the average adsorption efficiency for fluoride removal study dropped to ~40%.
- After six cycles, MG dye adsorption efficiency was 87.58% and fluoride adsorption efficiency obtained was 61.75% with Alginate-nanocellulose composite beads, whereas MG dye adsorption efficiency obtained as 84% and fluoride adsorption efficiency obtained as 66.4% for Nanocellulose/PVA composite film after six cycles.
- **Biodegradation** study of dye-loaded and fluoride-loaded composite by isolated bacteria, Lysinibacillus Sp. (GenBank accession no: SUB9070461 seq1PDMW596888) were observed for 45 days under aerobic conditions by varying different operational parameters (pH, inoculum dosage, salinity, temperature, etc.) and high biodegradation efficiency was found (after 45 days % weight loss >80%).
- Biodegradation rate of dye-loaded composites and fluoride-loaded composites showed an increasing trend with pH. The maximum biodegradation rate was obtained at pH 8.0.
- Maximum biodegradation capability was observed at 35°C temperature
- At the higher dosage of pollutant-loaded composites, bacterial growth was found to be less which leads to a less biodegradation rate.

Chapter.9

Overall Conclusion and Future scope

9.1. Overall Conclusions

Fluoride enters into ground-water because of natural leaching of fluoride rich rock sand Volcanic ash (such as Fluorspar, cryolite, fluorapatite and sellaite etc.). Discharging effluents of numerous industrial activities for instance, coal-burning stations, steel production, aluminum, phosphorus, production of bricks, glass, plastic, cement, and HF acid (hydrofluoric acid) contains fluoride which affects the ecosystem and living beings by contaminating water, air, soil, crops and vegetables. The effluent of many industries such as textile, leather tanning, paper, food contain considerable amount of dyes. Dye is of environmental concern due to its hazardous and toxic effects on human being and aquatic life.

The effluent needs to be treated before discharge into open waterbodies. The technique that have been focused on in this study was adsorption. The objective was to evaluate the removal efficiency of carbonaceous materials and polymer grafted composites derived from agro-waste for adsorption of MG dye and fluoride from wastewater and make these processes economically attractive. Agro-waste, Sugarcane bagasse was selected to derive carbonaceous material and to extract biopolymer from it. Kinetic and equilibrium studies were conducted in batch reactor. Batch process is not much suitable when large volume of wastewater needs to be treated. Therefore, dye and fluoride adsorption studies were also carried out in continuous mode in fixed bed and fluidized bed contactor. The removal efficiency of prepared composites with its base materials or components were compared for identifying the suitability of prepared composites for MG dye and fluoride remediation processes.

Overall conclusion of these study includes:

- Dye and Fluoride Removal efficiency depends on the parameters; such as: adsorbate concentration, adsorbent dosage, contact time, pH, temperature and rotational speed.
- Dye adsorption Isotherm showed that the estimated value of monolayer adsorption capacity were 169.49, 172.414, 185.185, 196.078, 188.68, 212.76, and 263.158 mg/g for SB powder, SBC, SBAC, Alginate-Bentonite/SBAC beads, Cellulose, NanoCellulose/PVA, Alginate-Nanocellulose beads respectively.
- Fluoride adsorption Isotherm showed that the estimated value of monolayer adsorption capacity ware19.88, 20.53, 22.22, 23.809, 14.75, 28.41, and 23.809 mg/g for SB powder, SBC, SBAC, Alginate-Bentonite/SBAC beads, Cellulose, NanoCellulose/PVA, Alginate-Nanocellulose beads respectively.

- Adsorption kinetic study indicated that the pollutant removal using beads would better describe by Pseudo-second-order kinetic model
- Negative value of Gibbs free energy and negative Enthalpy value indicated the spontaneous nature of the reaction and pollutant elimination process was exothermic
- RSM modeling showed that optimization was effectively correlated with batch experimental data.
- The breakthrough in fixed bed study was achieved faster at a higher influent flow rate. With increasing inlet dye concentration breakthrough time decreased. On the other hand, with rising bed height and pH the breakthrough time increased
- With increasing feed flow rate, adsorption rate in fluidized bed increased but with increasing bed weight the adsorption rate decreased.
- After five cycles, the average adsorption efficiency for MG dye removal dropped to 70 %. The adsorption efficiency for Fluoride removal study was just over 40%.
- The regenerability or recyclability of adsorbents were better with dye s compared with fluoride.
- Isolated Bacteria was Gram positive bacteria and showed better growth rate at pH 5-8 and at 35 °C temperature
- Bio-degradation of dye loaded exhausted adsorbents using isolated bacteria showed appreciated results

Table 9.1: Dye adsorption capacity results for different type of prepared adsorbents

Prepared adsorbents	%Removal	Initial dye concentration (mg/L)	Adsorbent mass used in Dye adsorption	Adsorption capacity (mg/g)	Chemical used in composites
Sugar cane bagasse (SB) powder	83.04 %	20 mg/L	1 g/L	169.49 mg/g	-
SB Biochar (SBC)	90.64%	20 mg/L	1g/L	172.414 mg/g	-
NaOH Activated Biochar (SBAC)	93.42%	20 mg/L	1g/L	185.185 mg/g	SBC:NaOH (15%)=1:10
Sodium alginate-Bentonite/SBAC beads	98.21%	20 mg/L	1g/L	196.078 mg/g	1g SBC, 2%(w/v) of sodium alginate ,2% (w/v) bentonite clay

Cellulose	94,78%	20 mg/L	1g/L	188.68 mg/g	0.75% $NaClO_2$, 2% $NaHSO_3$, 17% NaOH
NanoCellulose/PVA	99.23%	20 mg/L	1g/L	212.76 mg/g	0.5g cellulose ,4% (w/v) PVA
Alginate-Nanocellulose beads	99.63%	20 mg/L	1g/L	**263.158** mg/g	0.5g cellulose, 2% (w/v) of sodium alginate

Table 9.2: Fluoride adsorption capacity results for different type of prepared adsorbents

Prepared adsorbents	**%Removal**	**Initial fluoride concentration (mg/L)**	**Adsorbent mass used in Dye adsorption**	**Fluoride Adsorption capacity (mg/g)**	**Chemical used in composites**
Sugar cane bagasse (SB) powder	54.63 %	6 mg/L	2g/L	19.88 mg/g	-
SB Biochar (SBC)	57.68%	6 mg/L	2g/L	20.53 mg/g	-
NaOH Activated Biochar (SBAC)	60.72%	6 mg/L	2g/L	22.22 mg/g	SBC:NaOH (15%)=1:10
Sodium alginate-Bentonite/SBAC beads	76.65%	6 mg/L	2g/L	23.06 mg/g	1g SBC, 2%(w/v) of sodium alginate ,2% (w/v) bentonite clay
Cellulose	75.96%	6 mg/L	2g/L	14.75 mg/g	0.75% $NaClO_2$, 2% $NaHSO_3$, 17% NaOH
NanoCellulose/PVA	83.44%	6 mg/L	2g/L	**28.41** mg/g	0.5g cellulose ,4% (w/v) PVA
Alginate-Nanocellulose beads	83.23%	6 mg/L	2g/L	23.809 mg/g	0.5g cellulose, 2% (w/v) of sodium alginate

The present study demonstrated that proposed composites (Alginate-Bentonite/SBAC beads, NanoCellulose/PVA, Alginate-Nanocellulose composite polymeric beads) are efficient, high-potential biodegradable biosorbent and could be used as potential alternatives for decolorization and defluoridation of wastewater.

9.2. Future Scope

Further studies need to be undertaken for the practical application of this system. These include:

- Actual industrial effluents contain various type of pollutants rather than just a single pollutant (dye or fluoride; selected as pollutant in this study). This may affect the adsorptive capacity of the biomass for the specific pollutant. Hence, it is very important to investigate the remediation performance of the target pollutant in presence of the other species.
- Performance evaluation of prepared composites needs to be investigated with the real industrial effluents.
    - The influence of common ions usually present in wastewater such as phosphate, calcium chloride on the fluoride adsorption process.
    - Investigation of different types of contractors to improve adsorption efficiency in continuous mode.
    - Development of more efficient degradation method of loaded biosorbent that will be discarded post adsorption.

Chapter.10

References

Abdelrahman, E.A., Hegazey, R.M., 2019. Utilization of waste aluminum cans in the fabrication of hydroxysodalite nanoparticles and their chitosan biopolymer composites for the removal of Ni(II) and Pb(II) ions from aqueous solutions: Kinetic, equilibrium, and reusability studies. Microchem. J. https://doi.org/10.1016/j.microc.2018.10.016

Aksu, Z., Gönen, F., 2004. Biosorption of phenol by immobilized activated sludge in a continuous packed bed: Prediction of breakthrough curves. Process Biochem. https://doi.org/10.1016/S0032-9592(03)00132-8

Aljeboree, A.M., Alshirifi, A.N., Alkaim, A.F., 2017. Kinetics and equilibrium study for the adsorption of textile dyes on coconut shell activated carbon. Arab. J. Chem. 10, S3381–S3393. https://doi.org/10.1016/j.arabjc.2014.01.020

Amalraj, A., Pius, A., 2013. Health risk from fluoride exposure of a population in selected areas of Tamil Nadu South India. Food Sci. Hum. Wellness 2, 75–86. https://doi.org/10.1016/j.fshw.2013.03.005

Amir, M.N.I., Muhd Julkapli, N., Hamid, S.B.A., (2017). Effective adsorption and photodegradation of methyl orange by TiO2-chitosan supported glass plate photocatalysis. Mater. Technol. https://doi.org/10.1080/10667857.2016.1201635

Ammavasi N, Mariappan R, Enhanced removal of hazardous fluoride from drinking water by using a smart material: magnetic iron oxide fabricated layered double hydroxide/cellulose composite, Journal of Environmental Chemical Engineering (2018), https://doi.org/10.1016/j.jece.2018.08.071

Anirudhan, T.S., Suchithra, P.S., (2009). Adsorption characteristics of humic acid-immobilized amine modified polyacrylamide/bentonite composite for cationic dyesin aqueous solutions. J. Environ. Sci. https://doi.org/10.1016/S1001-0742(08)62358-X

Asadi, S., Eris, S., Azizian, S., (2018). Alginate-Based Hydrogel Beads as a Biocompatible and Efficient Adsorbent for Dye Removal from Aqueous Solutions. ACS Omega. https://doi.org/10.1021/acsomega.8b02498

Ayoob, S., Gupta, A.K., 2006. Fluoride in drinking water: A review on the status and stress effects. Crit. Rev. Environ. Sci. Technol. https://doi.org/10.1080/10643380600678112

Aziz, Faissal; El Achaby, Mounir; Lissaneddine, Amina; Aziz, Khalid; Ouazzani, Naaila; Mamouni, Rachid; Mandi, Laila (2019). Composites with alginate beads: A novel design of nano-adsorbents impregnation for large-scale continuous flow wastewater treatment pilots. Saudi Journal of Biological Sciences, , S1319562X19302530–. doi:10.1016/j.sjbs.2019.11.019

Azizi Samir, M.A.S., Alloin, F., Dufresne, A., (2005). Review of Recent Research into Cellulosic Whiskers, Their Properties and Their Application in Nanocomposite Field. Biomacromolecules 6, 612–626. https://doi.org/10.1021/bm0493685

Azman, I., Mutalib, S.A., Yusoff, S.F.M., Fazry, S., Noordin, A., Kumaran, M., Mat Lazim, A., (2016). Novel Dioscorea hispida starch-based hydrogels and their beneficial use as disinfectants. J. Bioact. Compat. Polym. 31, 42–59. https://doi.org/10.1177/0883911515597704

Banerjee, P., Barman, S.R., Sikdar, D., Roy, U., Mukhopadhayay, A., Das, P., 2017. Enhanced degradation of ternary dye effluent by developed bacterial consortium with RSM optimization, ANN modeling and toxicity evaluation. Desalin. WATER TREATMEN 72, 249–265. https://doi.org/10.5004/dwt.2017.20422

Belhouchat, N., Zaghouane-Boudiaf, H., Viseras, C., 2017. Removal of anionic and cationic dyes from aqueous solution with activated organo-bentonite/sodium alginate encapsulated beads. Appl. Clay Sci. 135, 9–15. https://doi.org/10.1016/j.clay.2016.08.031

Bhatnagar, A., Kumar, E., Sillanpää, M., 2011. Fluoride removal from water by adsorption-A review. Chem. Eng. J. https://doi.org/10.1016/j.cej.2011.05.028

Bhattacharyya, A., Banerjee, B., Ghorai, S., Rana, D., Roy, I., Sarkar, G., Saha, N.R., De, S., Ghosh, T.K., Sadhukhan, S., Chattopadhyay, D., (2018). Development of an auto-phase separable and reusable graphene oxide-potato starch based cross-linked bio-composite adsorbent for removal of methylene blue dye. Int. J. Biol. Macromol. https://doi.org/10.1016/j.ijbiomac.2018.05.069

Bhupinderkaur & chanchal, (2016). Environmental and health concerns of the textile industry. Int. J. Civil, Struct. Environ. Infrastruct. Eng. Res. Dev.

Brown, R.M., (2004). Cellulose Structure and Biosynthesis: What is in Store for the 21st Century?, in: Journal of Polymer Science, Part A: Polymer Chemistry. https://doi.org/10.1002/pola.10877

Bulgariu, D., Bulgariu, L., 2013. Sorption of Pb(II) onto a mixture of algae waste biomass and anion exchanger resin in a packed-bed column. Bioresour. Technol. https://doi.org/10.1016/j.biortech.2012.10.142

Chatterjee, Sandipan, Chatterjee, Sudipta, Chatterjee, B.P., Guha, A.K., (2007). Adsorptive removal of congo red, a carcinogenic textile dye by chitosan hydrobeads: Binding mechanism, equilibrium and kinetics. Colloids Surfaces A Physicochem. Eng. Asp. https://doi.org/10.1016/j.colsurfa.2006.11.036

Chen, N.; Zhang, Z.; Feng, C.; Li, M.; Zhu, D.; Sugiura, N. Studies on fluoride adsorption of iron-impregnated granular ceramics from aqueous solution. Mater. Chem. Phys. 2011, 125, 293–298.

Chen, S., Yue, Q., Gao, B., Li, Q., Xu, X., Fu, K., 2012. Adsorption of hexavalent chromium from aqueous solution by modified corn stalk: A fixed-bed column study. Bioresour. Technol. https://doi.org/10.1016/j.biortech.2011.11.110

Chen, Y. H.; Shen, C. S.; Rashid, S.; Li, S.; Ali, B. A.; Liu, J. S., Biopolymer-induced morphology control of brushite for enhanced defluorination of drinking water. Journal of Colloid and Interface Science 2017, 491, 207-215

Cheng, C.S., Deng, J., Lei, B., He, A., Zhang, X., Ma, L., Li, S., Zhao, C., (2013). Toward 3D graphene oxide gels based adsorbents for high-efficient water treatment via the promotion of biopolymers. J. Hazard. Mater. https://doi.org/10.1016/j.jhazmat.2013.09.065

Choubisa SL (2012a) Status of fluorosis in animals. Proc Nat Acad Sci India Sect B: Biol Sci 82(3):331–339

Choubisa, Shanti Lal; Choubisa, Darshana (2016). Status of industrial fluoride pollution and its diverse adverse health effects in man and domestic animals in India. Environmental Science and Pollution Research, 23(8), 7244–7254. doi:10.1007/s11356-016-6319-8

Chowdhury S., Mishra R., Saha P., Kushwaha P., Adsorption thermodynamics, kinetics and isosteric heat of adsorption of malachite green onto chemically modified rice husk, Desalination 265 (2011)159-168. https://doi.org/10.1016/j.desal.2010.07.047

Chowdhury, S., Chakraborty, S., Saha, P. Das, 2013. Response surface optimization of a dynamic dye adsorption process: A case study of crystal violet adsorption onto NaOH-modified rice husk. Environ. Sci. Pollut. Res. https://doi.org/10.1007/s11356-012-0989-7

Chowdhury, S., Mishra, R., Saha, P., Kushwaha, P., 2011. Adsorption thermodynamics, kinetics and isosteric heat of adsorption of malachite green onto chemically modified rice husk. Desalination. https://doi.org/10.1016/j.desal.2010.07.047

Chowdhury, S., Saha, P., 2010. Sea shell powder as a new adsorbent to remove Basic Green 4 (Malachite Green) from aqueous solutions: Equilibrium, kinetic and thermodynamic studies. Chem. Eng. J. https://doi.org/10.1016/j.cej.2010.08.050

Crini,G., Lichtfouse. E.,2019. Advantages and disadvantages of techniques used for wastewater treatment. Environmental Chemistry Letters. Springer Verlag, 17, 145-155. ff10.1007/s10311-018-0785-9ff. ffhal-02082890f

Dai, H., Huang, Y., Huang, H., (2018). Eco-friendly polyvinyl alcohol/carboxymethyl cellulose hydrogels reinforced with graphene oxide and bentonite for enhanced adsorption of methylene blue. Carbohydr. Polym. https://doi.org/10.1016/j.carbpol.2017.12.073

Davila Jimenez M.M., Elizalde Gonzalez M.P., Pelaez-Cid A.A.. Adsorption interaction between natural adsorbents and textile dyes in aqueous solution, Colloids and Surfaces A: Physicochem. Eng. Aspects (2005). 254, 107–114

Datta P. S., Deb D. L., and Tyagi S. K., "Stable isotope (18O) investigations on the processes controlling fluoride contamination of groundwater," Journal of Nanocellulose-Reinforced Organo-Inorganic Nanocomposite for Synergistic and Affordable Defluoridation of Water and an Evaluation of Its Sustainability Metrics Contaminant Hydrology, vol. 24, no. 1, pp. 85–96, 1996.

Davoodi, S.M., Brar, S.K., Galvez-Cloutier, R., Martel, R., 2021. Performance of packed and fluidized bed columns for the removal of unconventional oil using modified dolomite. Fuel 285, 119191. https://doi.org/10.1016/j.fuel.2020.119191

De Castro Silva, F., Da Silva, M.M.F., Lima, L.C.B., Osajima, J.A., Da Silva Filho, E.C., (2016). Integrating chloroethyl phosphate with biopolymer cellulose and assessing their potential for absorbing brilliant green dye. J. Environ. Chem. Eng. https://doi.org/10.1016/j.jece.2016.07.010

Deniz, F., Karaman, S., 2011. Removal of an azo-metal complex textile dye from colored aqueous solutions using an agro-residue. Microchem. J. https://doi.org/10.1016/j.microc.2011.05.021

Dhanasekaran, P., Satya Sai, P.M., Gnanasekar, K.I., 2017. Fixed bed adsorption of fluoride by Artocarpus hirsutus based adsorbent. J. Fluor. Chem. 195, 37–46. https://doi.org/10.1016/j.jfluchem.2017.01.003

Dhillon, A.; Nair, M.; Bhargava, S. K.; Kumar, D., Excellent fluoride decontamination and antibacterial efficacy of Fe-Ca-Zr hybrid metal oxide nanomaterial. Journal of Colloid and Interface Science 2015, 457, 289-297

Dhillon, A.; Sapna; Choudhary, B. L.; Kumar, D.; Prasad, S., Excellent disinfection and fluoride removal using bifunctional nanocomposite. Chemical Engineering Journal 2018, 337, 193-200

Dongre RS. Biosorption of fluoride from water by fabricated chitosan doped graphite novel composite. Research & Development in Material Science. 2018;7(1):1-9

Du, Q., Wang, Y., Li, A., Yang, H., (2018). Scale-inhibition and flocculation dual-functionality of poly(acrylic acid) grafted starch. J. Environ. Manage. https://doi.org/10.1016/j.jenvman.2018.01.016

Fan, L., Luo, C., Sun, M., Li, X., Lu, F., Qiu, H., (2012). Preparation of novel magnetic chitosan/graphene oxide composite as effective adsorbents toward methylene blue. Bioresour. Technol. https://doi.org/10.1016/j.biortech.2012.02.067

Fernandez, M.E., Nunell, G.V., Bonelli, P.R., Cukierman, A.L., 2014. Activated carbon developed from orange peels: Batch and dynamic competitive adsorption of basic dyes. Ind. Crops Prod. https://doi.org/10.1016/j.indcrop.2014.09.015

Freundlich, H., Heller, W., 1939. The Adsorption of cis - and trans -Azobenzene. J. Am. Chem. Soc. 61, 2228–2230. https://doi.org/10.1021/ja01877a071
Fritz, W., Schluender, E.-U., 1974. Simultaneous adsorption equilibria of organic solutes in dilute aqueous solutions on activated carbon. Chem. Eng. Sci. 29, 1279–1282. https://doi.org/10.1016/0009-2509(74)80128-4
Galiano, F., Briceño, K., Marino, T., Molino, A., Christensen, K.V., Figoli, A., (2018). Advances in biopolymer-based membrane preparation and applications. J. Memb. Sci. https://doi.org/10.1016/j.memsci.2018.07.059
Ganguly, P., Sengupta, S., Das, P., Bhowal, A., 2020. Valorization of food waste: Extraction of cellulose, lignin and their application in energy use and water treatment. Fuel 280. https://doi.org/10.1016/j.fuel.2020.118581
Getachew T., Hussen A. and Rao V.M., ―Defluoridation of water by activated carbon prepared from banana (Musa paradisiaca) peel and coffee (Coffea arabica) husk‖, Int. J. Environ. Sci. Technol., vol. 12, pp.1857–1866, 2015.
Ghorai,S., Pant,K.K, 2005. Equilibrium, kinetics and breakthrough studies for adsorption of fluoride on activated alumina. Separation and Purification Technology 42, 3, 265–271, 2005. https://doi.org/10.1016/j.seppur.2004.09.001
Gong, G., Zhang, F., Cheng, Z., Zhou, L., (2015). Facile fabrication of magnetic carboxymethyl starch/poly(vinyl alcohol) composite gel for methylene blue removal. Int. J. Biol. Macromol. https://doi.org/10.1016/j.ijbiomac.2015.07.061
Hafshejani, L. D.; Tangsir, S.; Daneshvar, E.; Maljanen, M.; Lahde, A.; Jokiniemi, J.; Naushad, M.; Bhatnagar, A., Optimization of fluoride removal from aqueous solution by Al2O3 nanoparticles. Journal of Molecular Liquids 2017, 238, 254-262.
Tahir Hajira, Muhammad Sultan, Nasir Akhtar, Uzma Hameed, Tahreem Abid. Application of natural and modified sugar cane bagasse for the removal of dye from aqueous solution. Journal of Saudi Chemical Society (2016) 20, S115–S121. http://dx.doi.org/10.1016/j.jscs.2012.09.007
Hasan, M.M., Shenashen, M.A., Hasan, M.N., Znad, H., Salman, M.S., Awual, M.R., (2021). Natural biodegradable polymeric bioadsorbents for efficient cationic dye encapsulation from wastewater. J. Mol. Liq. https://doi.org/10.1016/j.molliq.2020.114587
Hussaini Jagaba, A., (2018). Wastewater Treatment Using Alum, the Combinations of Alum-Ferric Chloride, Alum-Chitosan, Alum-Zeolite and Alum- <i>Moringa Oleifera</i> as Adsorbent and Coagulant. Int. J. Eng. Manag. https://doi.org/10.11648/j.ijem.20180203.13
Jaman, H., Chakraborty, D., Saha, P., 2009. A study of the thermodynamics and kinetics of copper adsorption using chemically modified rice husk. Clean - Soil, Air, Water. https://doi.org/10.1002/clen.200900138
Jeon, Y.S., Lei, J., Kim, J.H., (2008). Dye adsorption characteristics of alginate/polyaspartate hydrogels. J. Ind. Eng. Chem. https://doi.org/10.1016/j.jiec.2008.07.007
Jin, H. Y.; Ji, Z. J.; Yuan, J.; Li, J.; Liu, M.; Xu, C. H.; Dong, J.; Hou, P.; Hou, S., Research on removal of fluoride in aqueous solution by alumina-modified expanded graphite composite. Journal of Alloys and Compounds 2015, 620, 361-367
Kadam, A.A., Lee, D.S., (2015). Glutaraldehyde cross-linked magnetic chitosan nanocomposites: Reduction precipitation synthesis, characterization, and application for removal of hazardous textile dyes. Bioresour. Technol. https://doi.org/10.1016/j.biortech.2015.06.148
Kagne, S., Jagtap, S., Thakare, D., Devotta, S., Rayalu, S.S., 2009. Bleaching powder: a versatile adsorbent for the removal of fluoride from aqueous solution. Desalination 243, 22-31. 10.1016/j.desal.2008.04.012
Kalyani, D.C., Telke, A.A., Dhanve, R.S., Jadhav, J.P., 2009. Ecofriendly biodegradation and detoxification of Reactive Red 2 textile dye by newly isolated Pseudomonas sp. SUK1. J. Hazard. Mater. https://doi.org/10.1016/j.jhazmat.2008.07.020
Kamga E.T., Ngameni E. and Darchen A., ―Evaluation of removal efficiency of fluoride from aqueous solution using new charcoals that contain calcium compounds‖, J. Colloid Interf. Sci., vol. 346, pp. 494–499, 2010.
Kardam, A., Raj, K.R., Srivastava, S., Srivastava, M.M., (2014). Nanocellulose fibers for biosorption of cadmium, nickel, and lead ions from aqueous solution. Clean Technol. Environ. Policy 16, 385–393. https://doi.org/10.1007/s10098-013-0634-2
Karim, Z., Mathew, A.P., Grahn, M., Mouzon, J., Oksman, K., (2014). Nanoporous membranes with cellulose nanocrystals as functional entity in chitosan: Removal of dyes from water. Carbohydr. Polym. https://doi.org/10.1016/j.carbpol.2014.06.048
Kerrou, Meryem & Bouslamti, Najia & Raada, Abdelaziz & Elanssari, Abdellah & Mrani, Driss & Slimani, My. (2021). The Use of Sugarcane Bagasse to Remove the Organic Dyes from Wastewater. International journal of analytical chemistry. 2021. 5570806. 10.1155/2021/5570806.
Karthikeyan M., and K.P. Elango, ―Removal of fluoride from aqueous solution using graphite: A kinetic and thermodynamic study‖, Indian J. Chem. Technol., vol. 15, pp. 525–532, 2008
Katiyar, P., Pandey, N., & Sahu, K. K. (2020). Biological approaches of fluoride remediation: potential for environmental clean-up. In Environmental Science and Pollution Research (Vol. 27, Issue 12). https://doi.org/10.1007/s11356-020-08224-2

Kooh, M.R.R., Dahri, M.K., Lim, L.B.L., Lim, L.H., Malik, O.A., 2016. Batch adsorption studies of the removal of methyl violet 2B by soya bean waste: isotherm, kinetics and artificial neural network modelling. Environ. Earth Sci. 75, 783. https://doi.org/10.1007/s12665-016-5582-9

Kuang, Y., Du, J., Zhou, R., Chen, Z., Megharaj, M., Naidu, R., (2015). Calcium alginate encapsulated Ni/Fe nanoparticles beads for simultaneous removal of Cu (II) and monochlorobenzene. J. Colloid Interface Sci. https://doi.org/10.1016/j.jcis.2015.01.080

Kumar, Vicky & Othman, Norzila & Mohd Asharuddin, Syazwani. (2017). Applications of Natural Coagulants to Treat Wastewater − A Review. MATEC Web of Conferences. 103. 10.1051/matecconf/201710306016.

Lan, Q., Bassi, A.S., Zhu, J.-X. (Jesse), Margaritis, A., 2002. Continuous protein recovery with a liquid–solid circulating fluidized-bed ion exchanger. AIChE J. 48, 252–261. https://doi.org/10.1002/aic.690480209

Le Corre, D., Bras, J., Dufresne, A., (2010). Starch nanoparticles: A review. Biomacromolecules. https://doi.org/10.1021/bm901428y

Li, P., Gao, B., Li, A., Yang, H., (2020). Evaluation of the selective adsorption of silica-sand/anionized-starch composite for removal of dyes and Cupper(II) from their aqueous mixtures. Int. J. Biol. Macromol. https://doi.org/10.1016/j.ijbiomac.2020.02.047

Li, W., Wei, H., Liu, Y., Li, S., Wang, G., Han, H., (2021). Fabrication of novel starch-based composite hydrogel microspheres combining Diels-Alder reaction with spray drying for MB adsorption. J. Environ. Chem. Eng. 9, 105929. https://doi.org/10.1016/j.jece.2021.105929

Li, X., Qi, Y., Li, Y., Zhang, Y., He, X., Wang, Y., (2013). Novel magnetic beads based on sodium alginate gel crosslinked by zirconium(IV) and their effective removal for Pb2+ in aqueous solutions by using a batch and continuous systems. Bioresour. Technol. https://doi.org/10.1016/j.biortech.2013.05.081

Li, Y., Du, Q., Liu, T., Sun, J., Wang, Y., Wu, S., Wang, Z., Xia, Y., Xia, L., (2013). Methylene blue adsorption on graphene oxide/calcium alginate composites. Carbohydr. Polym. https://doi.org/10.1016/j.carbpol.2013.01.094

Li, Y., Zhang, P., Du, Q., Peng, X., Liu, T., Wang, Z., Xia, Y., Zhang, W., Wang, K., Zhu, H., Wu, D., 2011. Adsorption of fluoride from aqueous solution by graphene. J. Colloid Interface Sci. 363, 348–354. https://doi.org/10.1016/j.jcis.2011.07.032

Lin, D., Shi, M., Zhang, Y., Wang, D., Cao, J., Yang, J., Peng, C., (2019). 3D crateriform and honeycomb polymer capsule with nano re-entrant and screen mesh structures for the removal of Multi-component cationic dyes from water. Chem. Eng. J. https://doi.org/10.1016/j.cej.2019.121911

Lin, H., Yu, C.-P., Chen, Z., 2013. Aerobic and anaerobic biodegradation of TNT by newly isolated Bacillus mycoides. Ecol. Eng. 52, 270–277. https://doi.org/10.1016/j.ecoleng.2012.11.004

Linares-Solano, A., Lillo-Ródenas, M. A., Marco-Lozar, J. P., Kunowsky, M., & Romero-Anaya, A. J. (2012). NaOH and KOH for preparing activated carbons used in energy and environmental applications. International Journal of Energy, Environment and Economics, 20(4).

Luo, X., Zhang, L., (2009). High effective adsorption of organic dyes on magnetic cellulose beads entrapping activated carbon. J. Hazard. Mater. https://doi.org/10.1016/j.jhazmat.2009.06.009

Lv, B., Zhao, Z., Deng, X., Fang, C., Xing, B., Dong, B., 2021. Hydrodynamics and adsorption performance of liquid–solid fluidized bed with granular activated carbon for removal of copper ions from wastewater. J. Clean. Prod. https://doi.org/10.1016/j.jclepro.2021.129627

Ma W, Ya FQ, Han M, et al. Characteristics of equilibrium, kinetics studies for adsorption of fluoride on magnetic–chitosan particle. Journal of Hazardous Materials. 2007;143 (1–2):296–302.

Ma, W., Song, X. Y., Pan, Y. Q., Cheng, Z. H., Xin, G., Wang, B. D., et al. (2012). Adsorption behavior of crystal violet onto opal and reuse feasibility of opal-dye sludge for binding heavy metals from aqueous solutions. Chemical Engineering Journal, 193–194, 381–390.

Ma, Y., Qi, P., Ju, J., Wang, Q., Hao, L., Wang, R., Sui, K., Tan, Y., (2019). Gelatin/alginate composite nanofiber membranes for effective and even adsorption of cationic dyes. Compos. Part B Eng. https://doi.org/10.1016/j.compositesb.2019.01.048

Madhusudana Rao, K., Krishna Rao, K.S.V., Sudhakar, P., Chowdoji Rao, K., Subha, M.C.S., (2013). Synthesis and characterization of biodegradable poly (vinyl caprolactam) grafted on to sodium alginate and its microgels for controlled release studies of an anticancer drug. J. Appl. Pharm. Sci. https://doi.org/10.7324/JAPS.2013.3609

Mahmoodi, N.M., Hayati, B., Arami, M., Bahrami, H., (2011). Preparation, characterization and dye adsorption properties of biocompatible composite (alginate/titania nanoparticle). Desalination. https://doi.org/10.1016/j.desal.2011.02.034

Mandal, A., & Chakrabarty, D. (2011). Isolation of nanocellulose from waste sugarcane bagasse (SCB) and its characterization. Carbohydrate Polymers, 86, 1291–1299.

Manna, S., Saha, P., Roy, D., Adhikari, B., & Das, P. (2018). Fixed bed column study for water defluoridation using neem oil-phenolic resin treated plant bio-sorbent. Journal of Environmental Management, 212, 424 432. doi:10.1016/j.jenvman.2018.02.037 10.1016/j.jenvman.2018.02.037

Markeb AA, Alonso A, Sánchez A, et al. Adsorption process of fluoride from drinking water with magnetic core–shell Ce–Ti@ Fe 3 O 4 and Ce–Ti oxide nanoparticles. Sci Total Environ. 2017;598:949–958

Marrakchi, F., Khanday, W.A., Asif, M., Hameed, B.H., (2016). Cross-linked chitosan/sepiolite composite for the adsorption of methylene blue and reactive orange 16. Int. J. Biol. Macromol. https://doi.org/10.1016/j.ijbiomac.2016.09.069

Martel, B., Devassine, M., Crini, G., Weltrowski, M., Bourdonneau, M., Morcellet, M., (2001). Preparation and sorption properties of a β-cyclodextrin-linked chitosan derivative. J. Polym. Sci. Part A Polym. Chem. https://doi.org/10.1002/1099-0518(20010101)39:1<169::AID-POLA190>3.0.CO;2-G

Matei, E., Rapa, M., Covaliu, C.I., Predescu, A.M., Turcanu, A., Predescu, C., Ignat, D., Vlad, G., 2020. Sodium alginate-cellulose-nano-clay composite adsorbent applied for lead removal from wastewater. Rev. Chim. https://doi.org/10.37358/RC.20.3.8015

Md. Munjur, H., Hasan, M.N., Awual, M.R., Islam, M.M., Shenashen, M.A., Iqbal, J., (2020). Biodegradable natural carbohydrate polymeric sustainable adsorbents for efficient toxic dye removal from wastewater. J. Mol. Liq. https://doi.org/10.1016/j.molliq.2020.114356

Meimoun, J., Wiatz, V., Saint-Loup, R., Parcq, J., Favrelle, A., Bonnet, F., Zinck, P., (2018). Modification of starch by graft copolymerization. Starch/Staerke. https://doi.org/10.1002/star.201600351

Mohammadi, A., Daemi, H., Barikani, M., 2014. Fast removal of malachite green dye using novel superparamagnetic sodium alginate-coated Fe3O4 nanoparticles. Int. J. Biol. Macromol. https://doi.org/10.1016/j.ijbiomac.2014.05.042

Mohammed, N., Grishkewich, N., Waeijen, H. A., Berry, R. M., & Tam, K. C. (2016). Continuous flow adsorption of methylene blue by cellulose nanocrystal-alginate hydrogel beads in fixed bed columns. Carbohydrate Polymers, 136, 1194–1202. doi:10.1016/j.carbpol.2015.09.099

Mohan, Dinesh; Sharma, Rupa; Singh, Vinod K.; Steele, Philip; Pittman, Charles U. (2012). Fluoride Removal from Water using Bio-Char, a Green Waste, Low-Cost Adsorbent: Equilibrium Uptake and Sorption Dynamics Modeling. Industrial & Engineering Chemistry Research, 51(2), 900–914. doi:10.1021/ie202189v

Mohapatra M., S. Anand, B. K. Mishra, D. E. Giles, and P. Singh, "Review of fluoride removal from drinking water," Journal of Environmental Management, vol. 91, no. 1, pp. 67–77, 2009.

Moharrami, P., Motamedi, E., (2020). Application of cellulose nanocrystals prepared from agricultural wastes for synthesis of starch-based hydrogel nanocomposites: Efficient and selective nanoadsorbent for removal of cationic dyes from water. Bioresour. Technol. https://doi.org/10.1016/j.biortech.2020.123661

Mohseni–Bandpi A, Kakavandi B, Kalantary RR, et al. Development of a novel magnetite chitosan composite for the removal of fluoride from drinking water: adsorption modeling and optimization. RSC Advances. 2015;5(89):73279–73289.

Mukherjee, S., Yadav, V., Mondal, M., Banerjee, S. and Halder, G.(2015) Characterization of a Fluoride Resistant BacteriumAcinetobacter sp. RH5 Towards Assessment of its WaterDefluoridation Capability. Appl. Water Sci.,7, 1923–1930.

Mukherjee, S.; Ramireddy, H.; Baidya, A.; Amala, A. K.; Sudhakar, C.; Mondal, B.; Philip, L.; Pradeep, T.,. Acs Sustainable Chemistry & Engineering 2020, 8 (1), 139-147.

Nasrollahzadeh, M., Sajjadi, M., Iravani, S., Varma, R.S., (2021). Starch, cellulose, pectin, gum, alginate, chitin and chitosan derived (nano)materials for sustainable water treatment: A review. Carbohydr. Polym. https://doi.org/10.1016/j.carbpol.2020.116986

Ndazi, B.S., Karlsson, S., Tesha, J. V., Nyahumwa, C.W., 2007. Chemical and physical modifications of rice husks for use as composite panels. Compos. Part A Appl. Sci. Manuf. https://doi.org/10.1016/j.compositesa.2006.07.004

Nekouei F., Nekouei S., Tayagi I., Gupta V.K., Kinetic, thermodynamic and isotherm studies for acid blue 129 removal from liquids using copper oxide nanoparticle-modified activated carbon as a novel adsorbent, J. Molecular Liq. 201 (2015) 124-133. https://doi.org/10.1016/j.molliq.2014.09.027

Ng, T. S., Ching, Y.C., Awanis, N., Ishenny, N., Rahman, M. R. (2014). Effect of bleaching condition on thermal properties and UV-transmittance of PVA/cellulose biocomposites. Mater. Res. Innov. 18, 400-404. https://doi.org/10.1179/1432891714Z.000000000986

Nikfar, S., Jaberidoost, M., (2014). Dyes and Colorants, in: Encyclopedia of Toxicology: Third Edition. https://doi.org/10.1016/B978-0-12-386454-3.00602-3

Njoku V.O., Foo K.Y., Asif M., Hameed B.H., Preparation of activated carbons from rambutan (Nephelium lappaceum) peel by microwave-induced KOH activation for acid yellow 17 dye adsorption, Chem. Eng. J. 250 (2014) 198–204. https://doi.org/10.1016/j.cej.2014.03.115

Noor, N.M., Othman, R., Mubarak, N.M., Abdullah, E.C., 2017. Agricultural biomass-derived magnetic adsorbents: Preparation and application for heavy metals removal. J. Taiwan Inst. Chem. Eng. 78, 168–177. https://doi.org/10.1016/j.jtice.2017.05.023

Onyango, M.S.; Kojima, Y.; Aoyi, O.; Bernardo, E.C.; Matsuda, H. Adsorption equilibrium modeling and solution chemistry dependence of fluoride removal from water by trivalent-cation-exchanged zeolite F-9. J. Colloid Interface Sci. 2004, 279, 341–350.

Parlayici, Ş., (2019). Alginate-coated perlite beads for the efficient removal of methylene blue, malachite green, and methyl violet from aqueous solutions: kinetic, thermodynamic, and equilibrium studies. J. Anal. Sci. Technol. https://doi.org/10.1186/s40543-019-0165-5

Polman, E.M.N., Gruter, G.-J.M., Parsons, J.R., Tietema, A., 2021. Comparison of the aerobic biodegradation of biopolymers and the corresponding bioplastics: A review. Sci. Total Environ. 753, 141953. https://doi.org/10.1016/j.scitotenv.2020.141953

Pourjavadi, A., Ghasemzadeh, H., Soleyman, R., (2007). Synthesis, characterization, and swelling behavior of alginate-g-poly(sodium acrylate)/kaolin superabsorbent hydrogel composites. J. Appl. Polym. Sci. 105, 2631–2639. https://doi.org/10.1002/app.26345

Sekhar, P. C., Kalidhasan, S., Rajesh, V., Rajesh, N., (2009). Bio-polymer adsorbent for the removal of malachite green from aqueous solution. Chemosphere. https://doi.org/10.1016/j.chemosphere.2009.07.068

Premraj R, M., 2005. Bidegradation of polymers. Indian J.Biotechnology 4, 186–193.

Puvaneswari, N., Muthukrishnan, J., Gunasekaran, P., (2006). Toxicity assessment and microbial degradation of azo dyes. Indian J. Exp. Biol.

Raghav, S.; Kumar, D., Comparative kinetics and thermodynamic studies of fluoride adsorption by two novel synthesized biopolymer composites. Carbohydrate Polymers 2019, 203, 430-440.

Ramesh S. T., Gandhimathi R., Nidheesh P. V. and Taywade M. Batch and Column Operations for the Removal of Fluoride from Aqueous Solution Using Bottom Ash. Environmental Research, Engineering and Management, 2012. No. 2(60), P. 12-20. http://dx.doi.org/10.5755/j01.erem.60.2.1396

Ranjana kumara et al., 2022, Aluminium fumarate-based polymer matrix composite for selective removal of fluoride from groundwater.https://doi.org/10.1016/j.enmm.2022.100642

Rao DN, Pal D (1978) Cattle fluorosis problem around an aluminium factory. Environ Physio Eco Plant 2:399–406

Raval, N.P., Shah, P.U., Shah, N.K., (2016). Nanoparticles Loaded Biopolymer as Effective Adsorbent for Adsorptive Removal of Malachite Green from Aqueous Solution. Water Conserv. Sci. Eng. https://doi.org/10.1007/s41101-016-0004-0

Reddy, M.M., Vivekanandhan, S., Misra, M., Bhatia, S.K., Mohanty, A.K., (2013). Biobased plastics and bionanocomposites: Current status and future opportunities. Prog. Polym. Sci. https://doi.org/10.1016/j.progpolymsci.2013.05.006

Rosa, S., Laranjeira, M.C.M., Riela, H.G., Fávere, V.T., (2008). Cross-linked quaternary chitosan as an adsorbent for the removal of the reactive dye from aqueous solutions. J. Hazard. Mater. https://doi.org/10.1016/j.jhazmat.2007.11.059

Roy, S., Sengupta, S., Manna, S., Das, P., 2018. Chemically reduced tea waste biochar and its application in treatment of fluoride containing wastewater: Batch and optimization using response surface methodology. Process Saf. Environ. Prot. 116, 553–563. https://doi.org/10.1016/j.psep.2018.03.009

Sadeghi-Kiakhani, M., Arami, M., Gharanjig, K., (2013). Preparation of chitosan-ethyl acrylate as a biopolymer adsorbent for basic dyes removal from colored solutions. J. Environ. Chem. Eng. https://doi.org/10.1016/j.jece.2013.06.001

Saha, N., Das, L., Das, P., Bhowal, A., Bhattacharjee, C., 2021. Comparative experimental and mathematical analysis on removal of dye using raw rice husk, rice husk charcoal and activated rice husk charcoal: batch, fixed-bed column, and mathematical modeling. Biomass Convers. Biorefinery. https://doi.org/10.1007/s13399-021-01996-8

Saha, P. Das, Chakraborty, S., Chowdhury, S., 2012. Batch and continuous (fixed-bed column) biosorption of crystal violet by Artocarpus heterophyllus (jackfruit) leaf powder. Colloids Surfaces B Biointerfaces. https://doi.org/10.1016/j.colsurfb.2011.11.057

Sairam Sundaram, C.; Viswanathan, N.; Meenakshi, S. Uptake of fluoride by nano-hydroxyapatite/chitosan, a bioinorganic composite. Bioresour. Technol. 2008, 99, 8226–8230.

Salisu, A., Sanagi, M.M., Naim, A.A., Karim, K.J., (2015). Removal of methylene blue dye from aqueous solution using alginate grafted polyacrylonitrile beads. Der Pharma Chem.

Salleh, M.A.M., Mahmoud, D.K., Karim, W.A.W.A., Idris, A., (2011). Cationic and anionic dye adsorption by agricultural solid wastes: A comprehensive review. Desalination. https://doi.org/10.1016/j.desal.2011.07.019

Sami, A.J., Khalid, M., Iqbal, S., Afzal, M., Shakoori, A.R., (2016). Synthesis and Application of Chitosan-Starch Based Nanocomposite in Wastewater Treatment for the Removal of Anionic Commercial Dyes. Pak. J. Zool. https://doi.org/10.17582/journal.pjz/2017.49.1.21.26

Sankararamakrishnan, N.; Srivastava, I.; Mishra, S., Studies on novel nano-bimetal doped cellulose nanofibers derived from agrowaste towards deflouridation. International Journal of Biological Macromolecules 2019, 128, 556-565

Sarkhel, R., Sengupta, S., Das, P., Bhowal, A., 2020. Comparative biodegradation study of polymer from plastic bottle waste using novel isolated bacteria and fungi from marine source. J. Polym. Res. 27, 16. https://doi.org/10.1007/s10965-019-1973-4
Scott, C.D., Woodward, C.A., Thompson, J.E., 1989. Solute diffusion in biocatalyst gel beads containing biocatalysis and other additives. Enzyme Microb. Technol. https://doi.org/10.1016/0141-0229(89)90040-9
Sen, G., Ghosh, S., Jha, U., Pal, S., (2011). Hydrolyzed polyacrylamide grafted carboxymethylstarch (Hyd. CMS-g-PAM): An efficient flocculant for the treatment of textile industry wastewater. Chem. Eng. J. 171, 495–501. https://doi.org/10.1016/j.cej.2011.04.016
Shrestha R., Ban S., Devkota S., Sharma S., Joshi R., Tiwari A.P., Kim H., Joshi M.K., Technological trends in heavy metals removal from industrial wastewater: A review. J. Environ. Chem. Eng. 9 (2021) 105688.
Silva Filho, E. C., Lima, L. C., Silva, F. C., Sousa, K. S., Fonseca, M. G., & Santana, S. A. (2013). Immobilization of ethylene sulfide in aminated cellulose for removal of the divalent cations. Carbohydrate Polymers, 92, 1203–1210.
Silva, L.S., Lima, L.C.B., Silva, F.C., Matos, J.M.E., Santos, M.R.M.C., Santos Júnior, L.S., Sousa, K.S., da Silva Filho, E.C., (2013). Dye anionic sorption in aqueous solution onto a cellulose surface chemically modified with aminoethanethiol. Chem. Eng. J. https://doi.org/10.1016/j.cej.2012.11.118
Singh, A., & Gothalwal, R. (2018). A reappraisal on biodegradation of fluoride compounds: role of microbes. Water and Environment Journal, 32(3). https://doi.org/10.1111/wej.12322
Singh, B., Sharma, V., Kumar, S., (2011). Synthesis of smart hydrogels by radiation polymerisation for use as slow drug delivery devices. Can. J. Chem. Eng. https://doi.org/10.1002/cjce.20456
Singh, Kalpana; Lataye, Dilip H.; Wasewar, Kailas L. (2015). Removal of Fluoride from Aqueous Solution by Using Low-Cost Sugarcane Bagasse: Kinetic Study and Equilibrium Isotherm Analyses. Journal of Hazardous, Toxic, and Radioactive Waste, 04015024. doi:10.1061/(ASCE)HZ.2153-5515.0000309
Sivasankar V., "A world ubiquitous compound, its chemistry, and ways of contamination," in Surface Modified Carbons as Scavengers for Fluoride from Water—2016, p. 5,Springer International Publishing, Cham, Switzerland, 2016.
Soleimani M., Kaghazchi T., Agricultural waste conversion to activated carbon by chemical activation with phosphoric acid, Chem. Eng. Technol. 30 (2007) 649–654. https://doi.org/10.1002/ceat.200600325.
Somasekhara Reddy, M.C.; Nirmala, V. (2014). Bengal gram seed husk as an adsorbent for the removal of dyes from aqueous solutions – Column studies. Arabian Journal of Chemistry, (), S1878535214001889–. doi:10.1016/j.arabjc.2014.08.026
Sonawane, S.H., Chaudhari, P.L., Ghodke, S.A., Parande, M.G., Bhandari, V.M., Mishra, S., Kulkarni, R.D., (2009). Ultrasound assisted synthesis of polyacrylic acid-nanoclay nanocomposite and its application in sonosorption studies of malachite green dye. Ultrason. Sonochem. https://doi.org/10.1016/j.ultsonch.2008.10.008
Song, Wen, Gao, B., Xu, X., Xing, L., Han, S., Duan, P., Song, Wuchang, Jia, R., (2016). Adsorption-desorption behavior of magnetic amine/Fe3O4 functionalized biopolymer resin towards anionic dyes from wastewater. Bioresour. Technol. https://doi.org/10.1016/j.biortech.2016.01.078
Srivastava, S., Sinha, R., & Roy, D. (2004). Toxicological effects of malachite green. In Aquatic Toxicology (Vol. 66, Issue 3). https://doi.org/10.1016/j.aquatox.2003.09.008
Stan, M., Lung, I., Soran, M.L., Opris, O., Leostean, C., Popa, A., Copaciu, F., Lazar, M.D., Kacso, I., Silipas, T.D., Porav, A.S., (2019). Starch-coated green synthesized magnetite nanoparticles for removal of textile dye Optilan Blue from aqueous media. J. Taiwan Inst. Chem. Eng. https://doi.org/10.1016/j.jtice.2019.04.006
Sudha, M., Saranya, (2014). Microbial degradation of Azo Dyes: A review. Int. J. Curr. Microbiol. 3, 670-690. ISSN: 2319-7706
Sundaram, C. S., Viswanathan, N., & Meenakshi, S. (2009). Defluoridation of water using magnesia/chitosan composite. Journal of Hazardous Materials, 163(2–3), 618–624.
Sureshkumar, N., Bhat, S., Srinivasan, S., Gnanasundaram, N., Thanapalan, M., Krishnamoorthy, R., Abuhimd, H., Ahmed, F., Show, P.L., 2020. Continuous phenol removal using a liquid–solid circulating fluidized bed. Energies. https://doi.org/10.3390/en13153839
Swain, S.K., Patnaik, T., Dey, R.K., (2013). Efficient removal of fluoride using new composite material of biopolymer alginate entrapped mixed metal oxide nanomaterials. Desalin. Water Treat. https://doi.org/10.1080/19443994.2012.749426
Tamilvani, T., King Solomon, E. and Rajesh Kannan, V. (2015) Biodegradation on Fluoride Contaminated Soil and Water in Dharmapuri District of Tamilnadu India. CIBTech J. Microbiol.,4, 78–84
Tang Q , Duan T, Li P, Zhang P, Wu D. Enhanced defluoridation capacity from aqueous media via hydroxyapatite decorated with carbon nanotube. Frontiers in Chemistry. 2018;6. Article 104
Tavakolian, Mandana; Wiebe, Hannah; Sadeghi, Mohammad Amin; van de Ven, Theo G.M. (2019). Dye removal using hairy nanocellulose: experimental and theoretical investigations. ACS Applied Materials & Interfaces, (), acsami.9b18679–. doi:10.1021/acsami.9b18679

Valdez-Alegria, C. J.; Fuentes-Rivas, R. M.; Garcia-Rivas, J. L.; Arce, R. E. Z.; Nunez, M. D. J.; Garcia-Gaitan, B., Synthesis of Chitosan-Polyvinyl Alcohol Biopolymers to Eliminate Fluorides from Water. Biomolecules 2020, 10 (1), 1-15.
Varghese, A.G., Paul, S.A., Latha, M.S., (2019). Remediation of heavy metals and dyes from wastewater using cellulose-based adsorbents. Environ. Chem. Lett. https://doi.org/10.1007/s10311-018-00843-z
Varil T., Bergna D., Lahti R., Romar H., Hu T., Lassi U., Activated carbon production from peat using ZnCl2: Characterization and applications, BioResources. 12 (2017) 8078–8092. https://doi.org/10.15376/biores.12.4.8078-8092.
Verma, A., Thakur, S., Mamba, G., Prateek, Gupta, R.K., Thakur, P., Thakur, V.K., 2020. Graphite modified sodium alginate hydrogel composite for efficient removal of malachite green dye. Int. J. Biol. Macromol. https://doi.org/10.1016/j.ijbiomac.2020.01.142
Verma, S., Kuila, A., 2019. Bioremediation of heavy metals by microbial process. Environ. Technol. Innov. 14, 100369. https://doi.org/10.1016/j.eti.2019.100369
Viswanathan, N.; Prabhu, S.M.; Meenakshi, S. Development of amine functionalized co-polymeric resins for selective fluoride sorption. J. Fluor. Chem. 2013, 153, 143–150.
Wagner, P.A., Little, B.J., Hart, K.R., Ray, R.I., 1996. Biodegradation of composite materials. Int. Biodeterior. Biodegrad. https://doi.org/10.1016/S0964-8305(96)00036-4
Wahyuningsih, K. & Iriani, Evi & Fahma, Farah. (2016). Utilization of cellulose from pineapple leaf fibers as nanofiller in polyvinyl alcohol-based film. 16. 181-189. 10.14499/ijc-v16i2p181-189.
Wambu, E.W., Ambusso, W.O., Onindo, C., Muthakia, G.K., 2016. Review of fluoride removal from water by adsorption using soil adsorbents – An evaluation of the status. J. Water Reuse Desalin. https://doi.org/10.2166/wrd.2015.073
Wang, X., Cheng, F., Liu, J., Smått, J.H., Gepperth, D., Lastusaari, M., Xu, C., Hupa, L., 2016. Biocomposites of copper-containing mesoporous bioactive glass and nanofibrillated cellulose: Biocompatibility and angiogenic promotion in chronic wound healing application. Acta Biomater. 46, 286–298. https://doi.org/10.1016/j.actbio.2016.09.021
Wang, Y., Zhang, Xiaofang, He, X., Zhang, W., Zhang, Xinxing, Lu, C., (2014). In situ synthesis of MnO2 coated cellulose nanofibers hybrid for effective removal of methylene blue. Carbohydr. Polym. https://doi.org/10.1016/j.carbpol.2014.04.008
Wu, N., Wei, H., Zhang, L., (2012). Efficient Removal of Heavy Metal Ions with Biopolymer Template Synthesized Mesoporous Titania Beads of Hundreds of Micrometers Size. Environ. Sci. Technol. 46, 419–425. https://doi.org/10.1021/es202043u
Wu, Z., Joo, H., Lee, K., 2005. Kinetics and thermodynamics of the organic dye adsorption on the mesoporous hybrid xerogel. Chem. Eng. J. https://doi.org/10.1016/j.cej.2005.07.011
Wulandari, W. T., Rochliadi, A., & Arcana, I. M. (2016). Nanocellulose prepared by acid hydrolysis of isolated cellulose from sugarcane bagasse. Materials Science and Engineering, 107, 12–45.
Xia, K., Liu, X., Wang, W., Yang, X., Zhang, X., (2020). Synthesis of modified starch/polyvinyl alcohol composite for treating textile wastewater. Polymers (Basel). https://doi.org/10.3390/polym12020289
Xu Xuezhu, Fei Liuu, Long Jiang, J. Y. Zhu, 2013. Darrin Haagenson, Dennis P. Wiesenborn. (Cellulose Nanocrystals vs. Cellulose Nanofibrils: A Comparative Study on Their Microstructures and Effects as Polymer Reinforcing Agents.CS Appl. Mater. Interfaces 5, 8, 2999–3009. https://doi.org/10.1021/am302624t
Yadav, S., Asthana, A., Chakraborty, R., Jain, B., Singh, A.K., Carabineiro, S.A.C., Susan, M.A.B.H., 2020. Cationic dye removal using novel magnetic/activated charcoal/β-cyclodextrin/alginate polymer nanocomposite. Nanomaterials. https://doi.org/10.3390/nano10010170
Yadav, Asheesh Kumar; Abbassi, Rouzbeh; Gupta, Asha; Dadashzadeh, Mohammad (2013). Removal of fluoride from aqueous solution and groundwater by wheat straw, sawdust and activated bagasse carbon of sugarcane. Ecological Engineering, 52(), 211–218. doi:10.1016/j.ecoleng.2012.12.069
Yang, X., Chen, K., Zhang, Y., Liu, H., Chen, W., Yao, J., (2017). Polyacrylamide grafted cellulose as an eco-friendly flocculant: Efficient removal of organic dye from aqueous solution. Fibers Polym. https://doi.org/10.1007/s12221-017-1216-4
Yang, X., Zhang, Q., Wang, Y., Chen, H., Zhang, H., Gao, F., Liu, L., (2008). Self-aggregated nanoparticles from methoxy poly(ethylene glycol)-modified chitosan: Synthesis; characterization; aggregation and methotrexate release in vitro. Colloids Surfaces B Biointerfaces 61, 125–131. https://doi.org/10.1016/j.colsurfb.2007.07.012
Yin, J., Deng, B., (2015). Polymer-matrix nanocomposite membranes for water treatment. J. Memb. Sci. https://doi.org/10.1016/j.memsci.2014.11.019
Yu, Xiaolin; Tong, Shengrui; Ge, Maofa; Zuo, Junchao (2013). Removal of fluoride from drinking water by cellulose@hydroxyapatite nanocomposites. Carbohydrate Polymers, 92(1), 269–275. doi:10.1016/j.carbpol.2012.09.045

Zare et al., 2022, Fluoride removal from aqueous solutions using alginate beads modified with functionalized silica particles.https://doi.org/10.1016/j.molstruc.2021.132217
Zeng, L., Xie, M., Zhang, Q., Kang, Y., Guo, X., Xiao, H., Peng, Y., Luo, J., (2015). Chitosan/organic rectorite composite for the magnetic uptake of methylene blue and methyl orange. Carbohydr. Polym. https://doi.org/10.1016/j.carbpol.2015.01.021
Zhang C, Li Y, Wang TJ, et al. Adsorption of drinking water fluoride on a micron–sized magnetic Fe3O4@ Fe–Ti composite adsorbent. Applied Surface Science. 2016;363:507–515
Zhang, J.; Chen, N.; Su, P. Y.; Li, M.; Feng, C. P., Fluoride removal from aqueous solution by Zirconium-Chitosan/Graphene Oxide Membrane. Reactive & Functional Polymers 2017, 114, 127-135.
Zhang, X., Yu, H., Yang, H., Wan, Y., Hu, H., Zhai, Z., Qin, J., (2015). Graphene oxide caged in cellulose microbeads for removal of malachite green dye from aqueous solution. J. Colloid Interface Sci. https://doi.org/10.1016/j.jcis.2014.09.048
Zhao X, Wang J, Wu F, et al. Removal of fluoride from aqueous media by Fe3O4@Al (OH)3 magnetic nanoparticles. J Hazard Mater. 2010;173(1):102–109.
Zhao, Y., Wang, L., (2012). Adsorption characteristics of Congo red from aqueous solution on the carboxymethylcellulose/montmorillonite nanocomposite, in: Advanced Materials Research. https://doi.org/10.4028/www.scientific.net/AMR.450-451.769
Zhao, Y.; Li, X.; Liu, L.; Chen, F. Fluoride removal by Fe(III)-loaded ligand exchange cotton cellulose adsorbent from drinking water. Carbohydr. Polym. 2008, 72, 144–150
Zhou, L., Jin, J., Liu, Z., Liang, X., Shang, C., (2011). Adsorption of acid dyes from aqueous solutions by the ethylenediamine-modified magnetic chitosan nanoparticles. J. Hazard. Mater. https://doi.org/10.1016/j.jhazmat.2010.10.012
Zhou, L., Zhou, H., Yang, X., (2019). Preparation and performance of a novel starch-based inorganic/organic composite coagulant for textile wastewater treatment. Sep. Purif. Technol. https://doi.org/10.1016/j.seppur.2018.07.089
Zhu H, Wang H, Wang G, Zhang K. Removal of fluorine from water by the aluminum-modified bone char. In: 2010 International Conference on Biology, Environment and Chemistry, IPCBEE; Singapore. Vol. 1. 2011. pp. 455-457
Zou, J., Zhu, H., Wang, F., Sui, H., Fan, J., (2011). Preparation of a new inorganic-organic composite flocculant used in solid-liquid separation for waste drilling fluid. Chem. Eng. J. https://doi.org/10.1016/j.cej.2011.03.100

Final thesisLOPA.pdf

ORIGINALITY REPORT

9%
SIMILARITY INDEX

PRIMARY SOURCES

1	www.researchgate.net Internet	344 words — 1%
2	link.springer.com Internet	310 words — 1%
3	Aofei Li, Jie Liu, Ziwei Qin, Lu Wang, Lu Li, Keyong Tang, Ying Pei. "Black wattle tannin - immobilized mesostructured collagen as a promising adsorbent for cationic organic dyes (methylene blue) removal in batch and continuous fixed - bed systems", Journal of Applied Polymer Science, 2022 Crossref	126 words — < 1%
4	serc.carleton.edu Internet	96 words — < 1%
5	www.tandfonline.com Internet	90 words — < 1%
6	Prangya Ranjan Rout, Rajesh Roshan Dash, Puspendu Bhunia. "Nutrient removal from binary aqueous phase by dolochar: Highlighting optimization, single and binary adsorption isotherms and nutrient release", Process Safety and Environmental Protection, 2016 Crossref	85 words — < 1%

7	Shamik Chowdhury, Papita Das Saha. "Adsorption of malachite green from aqueous solution by naoh-modified rice husk: Fixed-bed column studies", Environmental Progress & Sustainable Energy, 2013 Crossref	71 words —	< 1%
8	manualzz.com Internet	63 words —	< 1%
9	acikbilim.yok.gov.tr Internet	60 words —	< 1%
10	Mustafa T. Yagub, Tushar Kanti Sen, Sharmeen Afroze, H.M. Ang. "Fixed-bed dynamic column adsorption study of methylene blue (MB) onto pine cone", Desalination and Water Treatment, 2014 Crossref	58 words —	< 1%
11	Swapnila Roy, Shubhalakshmi Sengupta, Papita Das. "Integral approach of adsorption and chemical treatment of fluoride containing wastewater: Batch and optimization using RSM", Journal of Environmental Chemical Engineering, 2017 Crossref	55 words —	< 1%
12	typeset.io Internet	52 words —	< 1%
13	ebin.pub Internet	51 words —	< 1%
14	Wang, Shu Dong, Song Cheng, Jian Zhang, Hai Ying Zhao, Xun Jing Ma, and Xiao Min Zhu. "Adsorptive Removal of Cr(VI) from Aqueous Solution over Material: Optimisation through Response Surface Methodology", Applied Mechanics and Materials, 2014. Crossref	50 words —	< 1%

15	scholar.najah.edu Internet	46 words — < 1%
16	doczz.net Internet	44 words — < 1%
17	Uttariya Roy, Shubhalakshmi Sengupta, Priya Banerjee, Papita Das, Avijit Bhowal, Siddhartha Datta. "Assessment on the decolourization of textile dye (Reactive Yellow) using Pseudomonas sp. immobilized on fly ash: Response surface methodology optimization and toxicity evaluation", Journal of Environmental Management, 2018 Crossref	39 words — < 1%
18	www.science.gov Internet	38 words — < 1%
19	Asheesh Kumar Yadav, Rouzbeh Abbassi, Asha Gupta, Mohammad Dadashzadeh. "Removal of fluoride from aqueous solution and groundwater by wheat straw, sawdust and activated bagasse carbon of sugarcane", Ecological Engineering, 2013 Crossref	34 words — < 1%
20	Arpita Ghosh, Papita Das. "Optimization of Copper Adsorption by Soil of Polluted Wasteland using Response Surface Methodology", Indian Chemical Engineer, 2014 Crossref	33 words — < 1%
21	Noureddine El Messaoudi, Mohammed El Khomri, Abdellah Dbik, Safae Bentahar, Abdellah Lacherai, Bahcine Bakiz. "Biosorption of Congo red in a fixed-bed column from aqueous solution using jujube shell: Experimental and mathematical modeling", Journal of Environmental Chemical Engineering, 2016 Crossref	33 words — < 1%

22	etd.aau.edu.et Internet	33 words — < 1%
23	krishikosh.egranth.ac.in Internet	33 words — < 1%
24	"Emerging Nanostructured Materials for Energy and Environmental Science", Springer Nature, 2019 Crossref	32 words — < 1%
25	www.ijert.org Internet	32 words — < 1%
26	mdpi-res.com Internet	31 words — < 1%
27	Beekam Kebede, Abebe Beyene, Fekadu Fufa, Moa Megersa, Michael Behm. "Experimental evaluation of sorptive removal of fluoride from drinking water using iron ore", Applied Water Science, 2014 Crossref	30 words — < 1%
28	M. A. Khapre, R. M. Jugade. "Hierarchical approach towards adsorptive removal of Alizarin Red S dye using native chitosan and its successively modified versions", Water Science and Technology, 2020 Crossref	30 words — < 1%
29	pubs.rsc.org Internet	30 words — < 1%
30	A. Dhanapal, S. Rajendra Boopathy, V. Balasubramanian. "Comparative Evaluation of Corrosion Behavior of Friction Stir Welded AZ61A Magnesium Alloy Weldments in Immersion Corrosion Tests and Salt Spray	29 words — < 1%

Corrosion Tests Using Response Surface Methodology", Transactions of the Indian Institute of Metals, 2012
Crossref

31	dokumen.pub Internet	29 words — < 1%
32	phd-dissertations.unizik.edu.ng Internet	29 words — < 1%
33	edoc.pub Internet	26 words — < 1%
34	Faten B. Hussein, Brooke K. Mayer. "Fixed-bed column study of phosphate adsorption using immobilized phosphate-binding protein", Chemosphere, 2022 Crossref	25 words — < 1%
35	Sivaraju Sugashini, Khadhar Mohamed Meera Sheriffa Begum. "Performance of ozone treated rice husk carbon (OTRHC) for continuous adsorption of Cr (VI) ions from synthetic effluent", Journal of Environmental Chemical Engineering, 2013 Crossref	25 words — < 1%
36	baadalsg.inflibnet.ac.in Internet	25 words — < 1%
37	uir.unisa.ac.za Internet	25 words — < 1%
38	Sharmeen Afroze, Tushar Kanti Sen, H. M. Ang. "Adsorption performance of continuous fixed bed column for the removal of methylene blue (MB) dye using Eucalyptus sheathiana bark biomass", Research on Chemical Intermediates, 2015 Crossref	24 words — < 1%

39	ajehe.umsha.ac.ir Internet	24 words — < 1%
40	fdocuments.in Internet	24 words — < 1%
41	www.politesi.polimi.it Internet	24 words — < 1%
42	Krishnamoorthy Shanmugaraj, Ramalinga Viswanathan Mangalaraja, Cristian H. Campos, Dinesh Pratap Singh et al. "Gold nanoparticles decorated two-dimensional TiO2 nanosheets as effective catalyst for nitroarenes and rhodamine B dye reduction in batch and continuous flow methods", Inorganic Chemistry Communications, 2023 Crossref	23 words — < 1%
43	Desagani Dayananda, Venkateswara R. Sarva, Sivankutty V. Prasad, Jayaraman Arunachalam et al. "Synthesis of MgO nanoparticle loaded mesoporous Al2O3 and its defluoridation study", Applied Surface Science, 2015 Crossref	22 words — < 1%
44	Nishil Mohammed, Nathan Grishkewich, Herman Ambrose Waeijen, Richard M. Berry, Kam Chiu Tam. "Continuous flow adsorption of methylene blue by cellulose nanocrystal-alginate hydrogel beads in fixed bed columns", Carbohydrate Polymers, 2016 Crossref	22 words — < 1%
45	He, Yinhai, Hai Lin, Yingbo Dong, Quanli Liu, and Liang Wang. "Simultaneous removal of phosphate and ammonium using salt–thermal-activated and lanthanum-doped zeolite: fixed-bed column and mechanism study", Desalination and Water Treatment, 2016. Crossref	21 words — < 1%

46	Kyung-Won Jung, Tae-Un Jeong, Brian Hyun Choi, Ho- Jeong Kang, Kyu-Hong Ahn. " Phosphate adsorption from aqueous solution by -derived biochar-calcium alginate beads in a fixed-bed column: Experiments and prediction of breakthrough curves ", Environmental Progress & Sustainable Energy, 2017 Crossref	21 words — < 1%
47	cyberleninka.org Internet	21 words — < 1%
48	gyan.iitg.ernet.in Internet	21 words — < 1%
49	"Advanced Magnetic Adsorbents for Water Treatment", Springer Science and Business Media LLC, 2021 Crossref	20 words — < 1%
50	Ahmed Thabet, Ahmed Elfaky, Wael Mohamed, Ahmed El-Zaref, Zein Elbahy. "Synthesis and Characterization of Chitosan/ZrO2 Nanocomposite and Its Application in the Removal of Rose Bengal Dye", Egyptian Journal of Chemistry, 2022 Crossref	20 words — < 1%
51	Halil Hasar, Yakup Cuci, Erdal Obek, M. Fatih Dilekoglu. "Removal of Zinc(II) by Activated Carbon Prepared from Almond Husks under Different Conditions", Adsorption Science & Technology, 2016 Crossref	20 words — < 1%
52	Jalal Parsa, Mahmood Abbasi. "Modeling and optimizing of sonochemical degradation of Basic Blue 41 via response surface methodology", Open Chemistry, 2010 Crossref	20 words — < 1%

53	P. Kanmani, J. Aravind, M. Kamaraj, P. Sureshbabu, S. Karthikeyan. "Environmental applications of chitosan and cellulosic biopolymers: A comprehensive outlook", Bioresource Technology, 2017 Crossref	20 words — < 1%
54	Song, Shiow-Tien, Norasikin Saman, Khairiraihanna Johari, and Hanapi Mat. "Removal of Hg(II) from Aqueous Solution by Adsorption Using Raw and Chemically Modified Rice Straw As Novel Adsorbents", Industrial & Engineering Chemistry Research, 2013. Crossref	20 words — < 1%
55	Zongping Wang, Miaomiao Xue, Kai Huang, Zizheng Liu. "Chapter 5 Textile Dyeing Wastewater Treatment", IntechOpen, 2011 Crossref	20 words — < 1%
56	dspace.lboro.ac.uk Internet	20 words — < 1%
57	troindia.in Internet	20 words — < 1%
58	library.cvasu.ac.bd:8080 Internet	19 words — < 1%
59	www.ijcce.ac.ir Internet	19 words — < 1%
60	Rajan Mariappan, Raj Vairamuthu, Alagumuthu Ganapathy. "Use of chemically activated cotton nut shell carbon for the removal of fluoride contaminated drinking water: Kinetics evaluation", Chinese Journal of Chemical Engineering, 2015 Crossref	18 words — < 1%

61	investigacionfitopatologiaumar.files.wordpress.com Internet	17 words — < 1%
62	irepos.unijos.edu.ng Internet	16 words — < 1%
63	repository.futminna.edu.ng:8080 Internet	16 words — < 1%
64	A. Öztürk, E. Malkoc. "Cationic Basic Yellow 2 (BY2) adsorption onto manure ash: surface properties and adsorption mechanism", Desalination and Water Treatment, 2014 Crossref	15 words — < 1%
65	assets.researchsquare.com Internet	15 words — < 1%
66	iicbe.org Internet	15 words — < 1%
67	pt.scribd.com Internet	15 words — < 1%
68	scholar.sun.ac.za Internet	15 words — < 1%
69	www-air.larc.nasa.gov Internet	15 words — < 1%
70	A. Teutli-Sequeira, Marcos Solache-Ríos, P. Balderas-Hernández. "Modification Effects of Hematite with Aluminum Hydroxide on the Removal of Fluoride Ions from Water", Water, Air, & Soil Pollution, 2011 Crossref	14 words — < 1%

71	C. Prathibha, Anjana Biswas, L.A. Avinash Chunduri, Shiva Konda Reddy et al. "Zr(IV) functionalized Graphene oxide anchored sand as potential and economic adsorbent for fluoride removal from water", Diamond and Related Materials, 2020 Crossref	14 words — < 1%
72	Chakraborty, S.. "Adsorption of Crystal Violet from aqueous solution onto NaOH-modified rice husk", Carbohydrate Polymers, 20111015 Crossref	14 words — < 1%
73	Rudrapatnam N. Tharanathan, Farooqahmed S. Kittur. "Chitin — The Undisputed Biomolecule of Great Potential", Critical Reviews in Food Science and Nutrition, 2003 Crossref	14 words — < 1%
74	Sharififard, Hakimeh, Farzin Zokaee Ashtiani, and Mansooreh Soleimani. "Adsorption of palladium and platinum from aqueous solutions by chitosan and activated carbon coated with chitosan : ADSORPTION OF PALLADIUM AND PLATINUM IONS FROM AQUEOUS SOLUTIONS", Asia-Pacific Journal of Chemical Engineering, 2012. Crossref	14 words — < 1%
75	repositorium.uminho.pt Internet	14 words — < 1%
76	www.thieme-connect.de Internet	14 words — < 1%
77	www2.mdpi.com Internet	14 words — < 1%
78	Abhishek Walia, Preeti Mehta, Anjali Chauhan, C. K. Shirkot. "Production of Alkalophilic Xylanases	13 words — < 1%

by Paenibacillus polymyxa CKWX1 Isolated from Decomposing Wood", Proceedings of the National Academy of Sciences, India Section B: Biological Sciences, 2012
Crossref

79 Debiparna De, Sukka Santosha, Vineet Aniya, Aravindu Sreeramoju, Satyavathi B.. "Assessing the applicability of an agro-industrial waste to Engineered Bio-char as a dynamic adsorbent for Fluoride Sorption", Journal of Environmental Chemical Engineering, 2018 — 13 words — < 1%
Crossref

80 Imran Ali, Zeid A. Al-Othman, Abdulrahman Alwarthan, Mohd Asim, Tabrez A. Khan. "Removal of arsenic species from water by batch and column operations on bagasse fly ash", Environmental Science and Pollution Research, 2013 — 13 words — < 1%
Crossref

81 Jian Liu, Ying Yan, Huiping Zhang. "Preparation of Microfibrous Entrapped Activated Carbon Composites and its Application for Benzene Adsorption", Separation Science and Technology, 2014 — 13 words — < 1%
Crossref

82 Parveen Kumar, Shruti Vashishth, Isha Sharma, Vivek Verma. "Porous SnO2 ceramic-based hydroelectric cells for green power generation", Journal of Materials Science: Materials in Electronics, 2020 — 13 words — < 1%
Crossref

83 Prathibha Chinnakoti, Avinash L.A. Chunduri, Ranganayakulu K. Vankayala, Sandeep Patnaik, Venkataramaniah Kamisetti. "Enhanced fluoride adsorption by nano crystalline y-alumina: adsorption kinetics, isotherm modeling and thermodynamic studies", Applied Water Science, 2016 — 13 words — < 1%
Crossref

84	Qi Zuo, Hong Zheng, Pengyi Zhang, Yu Zhang. "Functionalized Activated Carbon Fibers by Hydrogen Peroxide and Polydopamine for Efficient Trace Lead Removal from Drinking Water", Langmuir, 2021 Crossref	13 words — < 1%
85	Tiyasha Kanjilal, Chiranjib Bhattacharjee, Siddhartha Datta. "Bio-degradation of acetamiprid from wetland wastewater using indigenous Micrococcus luteus strain SC 1204: Optimization, evaluation of kinetic parameter and toxicity", Journal of Water Process Engineering, 2015 Crossref	13 words — < 1%
86	Yuzhe Zhang, Meiwen Zhao, Qian Cheng, Chao Wang, Hongjian Li, Xiaogang Han, Zhenhao Fan, Gaoyuan Su, Deng Pan, Zhongyu Li. "Research progress of adsorption and removal of heavy metals by chitosan and its derivatives: A review", Chemosphere, 2021 Crossref	13 words — < 1%
87	en.wikipedia.org Internet	13 words — < 1%
88	www.mdpi.com Internet	13 words — < 1%
89	www.textiletoday.com.bd Internet	13 words — < 1%
90	zzybot.net Internet	13 words — < 1%
91	Chen, Gui-jie, Chuan-yi Peng, Jiang-yu Fang, Yang-yang Dong, Xiao-hui Zhu, and Hui-mei Cai. "Biosorption of fluoride from drinking water using spent	12 words — < 1%

mushroom compost biochar coated with aluminum hydroxide", Desalination and Water Treatment, 2015.
Crossref

92 Dibya Ranjan Rout, Hara Mohan Jena. "Removal of malachite green dye from aqueous solution using reduced graphene oxide as an adsorbent", Materials Today: Proceedings, 2021 — 12 words — < 1%
Crossref

93 Kerstin I. Andersson, Marie Eriksson, Magnus Norgren. "Removal of Lignin from Wastewater Generated by Mechanical Pulping Using Activated Charcoal and Fly Ash: Adsorption Kinetics", Industrial & Engineering Chemistry Research, 2011 — 12 words — < 1%
Crossref

94 Nan Li, Jing Ren, Lin Zhao, Zhong-liang Wang. "Removal of Cr(VI) ions from wastewater using nanosized ferric oxyhydroxide loaded anion exchanger on a fixedbed column", Desalination and Water Treatment, 2013 — 12 words — < 1%
Crossref

95 Qingxi Zhang, Qipeng Yuan. "Modeling of Nanofiltration Process for Solvent Recovery from Aqueous Ethanol Solution of Soybean Isoflavones", Separation Science and Technology, 2009 — 12 words — < 1%
Crossref

96 S. S. Baral, S. N. Das, P. Rath, G. Roy Chaudhury, Y. V. Swamy. " Removal of Cr(VI) from aqueous solution using waste weed, ", Chemistry and Ecology, 2007 — 12 words — < 1%
Crossref

97 U.T. Uthappa, Shrinath Bhat, Sung Soo Han, Heon-Ho Jeong, Tariq Altalhi, Ho-Young Jung, Mahaveer D. Kurkuri. "Tailoring of 2D MoS2 microspheres on 3D low-cost DE for the efficient removal of hazardous cationic — 12 words — < 1%

dyes", Advanced Powder Technology, 2022
Crossref

98	ijeab.com Internet	12 words — < 1%
99	iwaponline.com Internet	12 words — < 1%
100	theses.hal.science Internet	12 words — < 1%
101	utpedia.utp.edu.my Internet	12 words — < 1%
102	Ali Akbar Babaei, Alireza Khataee, Elham Ahmadpour, Mohsen Sheydaei, Babak Kakavandi, Zahra Alaee. "Optimization of cationic dye adsorption on activated spent tea: Equilibrium, kinetics, thermodynamic and artificial neural network modeling", Korean Journal of Chemical Engineering, 2015 Crossref	11 words — < 1%
103	C. NAMASIVAYAM, S. SENTHILKUMAR. "Adsorption of Copper(II) by “Waste” Fe(III)/Cr(III) Hydroxide from Aqueous Solution and Radiator Manufacturing Industry Wastewater", Separation Science and Technology, 1999 Crossref	11 words — < 1%
104	Disha Khandare, Somnath Mukherjee. "A Review of Metal oxide Nanomaterials for Fluoride decontamination from Water Environment", Materials Today: Proceedings, 2019 Crossref	11 words — < 1%

105 Fu, Zhijie. "Hydrodynamics Studies of Air Dense Medium Fluidized Bed with Binary Mixtures for Dry Coal Beneficiation", The University of Western Ontario (Canada), 2022
ProQuest
11 words — < 1%

106 Gong, Ji-Lai, Yong-Liang Zhang, Yan Jiang, Guang-Ming Zeng, Zhi-Hui Cui, Ke Liu, Can-Hui Deng, Qiu-Ya Niu, Jiu-Hua Deng, and Shuang-Yan Huan. "Continuous adsorption of Pb(II) and methylene blue by engineered graphite oxide coated sand in fixed-bed column", Applied Surface Science, 2015.
Crossref
11 words — < 1%

107 Khitous, Mohamed, Samir Moussous, Ammar Selatnia, and Mohamed Kherat. "Biosorption of Cd(II) by Pleurotus mutilus biomass in fixed-bed column: experimental and breakthrough curves analysis", Desalination and Water Treatment, 2015.
Crossref
11 words — < 1%

108 M. Ihsan Danish, Ishtiaq A. Qazi, Akif Zeb, Amir Habib, M. Ali Awan, Zahiruddin Khan. "Arsenic Removal from Aqueous Solution Using Pure and Metal-Doped Titania Nanoparticles Coated on Glass Beads: Adsorption and Column Studies", Journal of Nanomaterials, 2013
Crossref
11 words — < 1%

109 Manohara H M, Supratim Chakraborty, Kanakaraj Aruchamy, Debasis Ghosh et al. "Engineering Fe-doped highly oxygenated solvothermal carbon from glucose-based eutectic system as active microcleaner and efficient carbocatalyst", Journal of Materials Chemistry A, 2019
Crossref
11 words — < 1%

110 Sapna Raghav, Dinesh Kumar. "Fabrication of aluminium and iron impregnated pectin
11 words — < 1%

biopolymeric material for effective utilization of fluoride adsorption studies", Groundwater for Sustainable Development, 2019
Crossref

111 Srividya, K.. "Biosorption of hexavalent chromium from aqueous solutions by Catla catla scales: Equilibrium and kinetics studies", Chemical Engineering Journal, 20091215
Crossref
11 words — < 1%

112 Teck Nam Ang, Brent R. Young, Matthew Taylor, Rob Burrell, Mohamed Kheireddine Aroua, Saeid Baroutian. "Breakthrough analysis of continuous fixed-bed adsorption of sevoflurane using activated carbons", Chemosphere, 2020
Crossref
11 words — < 1%

113 Ulises Emiliano Rodriguez-Castrejón, Alma Hortensia Serafin-Muñoz, Aurelio Alvarez-Vargas, Gustavo Cruz Jimenez et al. "Isolation and Molecular identification of native As-resistant bacteria: As(III) and As(V) removal capacity and possible mechanism of detoxification", Research Square Platform LLC, 2021
Crossref Posted Content
11 words — < 1%

114 daneshyari.com
Internet
11 words — < 1%

115 hdl.handle.net
Internet
11 words — < 1%

116 ir.library.osaka-u.ac.jp
Internet
11 words — < 1%

117 rasayanjournal.co.in
Internet
11 words — < 1%

118	www.ijrte.org Internet	11 words — < 1%
119	"Green Photocatalysts", Springer Science and Business Media LLC, 2020 Crossref	10 words — < 1%
120	"Recent Trends in Waste Water Treatment and Water Resource Management", Springer Science and Business Media LLC, 2020 Crossref	10 words — < 1%
121	"Recent Trends in Wastewater Treatment", Springer Science and Business Media LLC, 2022 Crossref	10 words — < 1%
122	Berhane Desta Gebrewold, Pimluck Kijjanapanich, Eldon R. Rene, Piet N. L. Lens, Ajit P. Annachhatre. "Fluoride removal from groundwater using chemically modified rice husk and corn cob activated carbon", Environmental Technology, 2018 Crossref	10 words — < 1%
123	Chubaakum Pongener, Parimal Chandra Bhomick, Aola Supong, Mridushmita Baruah, Upasana Bora Sinha, Dipak Sinha. "Adsorption of Fluoride onto activated carbon synthesized from Manihot esculenta biomass —Equilibrium, kinetic and thermodynamic studies", Journal of Environmental Chemical Engineering, 2018 Crossref	10 words — < 1%
124	Deli Liu, Dezhi Sun. "Simulation of indigo carmine dye adsorption on polymer doped sawdust in fixed-bed systems", Desalination and Water Treatment, 2011 Crossref	10 words — < 1%
125	Duanhao Wang, Jiahua Tian, Jian Guan, Yiwen Ding, Ming Li Wang, Brandon Tonnis, Jiayang Liu,	10 words — < 1%

Qingguo Huang. "Valorization of sugarcane bagasse for sugar extraction and residue as an adsorbent for pollutant removal", Frontiers in Bioengineering and Biotechnology, 2022
Crossref

126 Ganesh Jethave, Umesh Fegade, Sanjay Attarde, Sopan Ingle. "Facile synthesis of Lead Doped Zinc-Aluminum Oxide Nanoparticles (LD-ZAO-NPs) for efficient adsorption of anionic dye: Kinetic, isotherm and thermodynamic behaviors", Journal of Industrial and Engineering Chemistry, 2017 — 10 words — < 1%
Crossref

127 Gietu Yirga Abate, Adugna Nigatu Alene, Adere Tarekegne Habte, Desiew Mekuanint Getahun. "Adsorptive removal of malachite green dye from aqueous solution onto activated carbon of Catha edulis stem as a low cost bio-adsorbent", Environmental Systems Research, 2020 — 10 words — < 1%
Crossref

128 Hasan, S. H., and Preeti Srivastava. "Biosorptive Abatement of Cd²⁺ by Water Using Immobilized Biomass of Arthrobacter sp.: Response Surface Methodological Approach", Industrial & Engineering Chemistry Research, 2011. — 10 words — < 1%
Crossref

129 Irene M. C. Lo, Jing Hu, Guohua Chen. "Iron-Based Magnetic Nanoparticles for Removal of Heavy Metals from Electroplating and Metal-Finishing Wastewater", American Society of Civil Engineers (ASCE), 2009 — 10 words — < 1%
Crossref

130 Issam Mechnou, Sarra Meskini, Imane Mourtah, Laurent Lebrun, Miloudi Hlaibi. "Use of phosphorus-doped microporous carbon from olive mill — 10 words — < 1%

wastewater for effective removal of Crystal violet and Methylene blue", Journal of Cleaner Production, 2023
Crossref

131 Krishna Kumar Yadav, Neha Gupta, Vinit Kumar, Shakeel Ahmad Khan, Amit Kumar. "A review of emerging adsorbents and current demand for defluoridation of water: Bright future in water sustainability", Environment International, 2018 — 10 words — < 1%
Crossref

132 Ling Wei Low, Tjoon Tow Teng, Norhashimah Morad, Baharin Azahari. "Optimization of the column studies into the adsorption of basic dye using tartaric acid-treated bagasse", Desalination and Water Treatment, 2013 — 10 words — < 1%
Crossref

133 Mai Thi Vu, Huan-Ping Chao, Tuyen Van Trinh, Trinh Thi Le, Chu-Ching Lin, Hai Nguyen Tran. "Removal of ammonium from groundwater using NaOH-treated activated carbon derived from corncob wastes: Batch and column experiments", Journal of Cleaner Production, 2018 — 10 words — < 1%
Crossref

134 Md. M. R. Khan, M. Z. B. Mukhlish, M. S. I. Mazumder, K. Ferdous, D. M. R. Prasad, Z. Hassan. "Uptake of Indosol Dark-blue GL dye from aqueous solution by water hyacinth roots powder: adsorption and desorption study", International Journal of Environmental Science and Technology, 2013 — 10 words — < 1%
Crossref

135 Mohammed K. Al Mesfer, Mohd Danish, Mumtaj Shah. "Optimization of fluoride adsorption from aqueous solution over mesoporous titania - alumina composites using Taguchi method", Water Environment Research, 2021 — 10 words — < 1%

Crossref

136 Moni U. Khobragade, Ashish Kumar Nayak, Anjali Pal. "Application of response surface methodology to evaluate the removal efficiency of Mn(II), Ni(II), and Cu(II) by surfactant-modified alumina", Clean Technologies and Environmental Policy, 2016 — 10 words — < 1%
Crossref

137 N. Saranya, Abhishek Ajmani, V. Sivasubramanian, N. Selvaraju. "Hexavalent chromium removal from simulated and real effluents using Artocarpus heterophyllus peel biosorbent - Batch and continuous studies", Journal of Molecular Liquids, 2018 — 10 words — < 1%
Crossref

138 Payam Arabkhani, Arash Asfaram. "Development of a novel three-dimensional magnetic polymer aerogel as an efficient adsorbent for malachite green removal", Journal of Hazardous Materials, 2020 — 10 words — < 1%
Crossref

139 S. L. Pala, W. K. Biftu, M. Suneetha, K. Ravindhranath. "De-fluoridation studies: using Lanthanum-alginate-beads impregnated with green synthesized nSiO2 and active carbon of Terminalia Ivorensis plant as an effective adsorbent", International Journal of Environmental Science and Technology, 2021 — 10 words — < 1%
Crossref

140 Sanjay P. Kamble, Gunavant Deshpande, Prashant P. Barve, Sadhana Rayalu et al. "Adsorption of fluoride from aqueous solution by alumina of alkoxide nature: Batch and continuous operation", Desalination, 2010 — 10 words — < 1%
Crossref

141 Saurabhkumar Singh, Sachin Gondhalekar, Sanjeev R. Shukla. "Continuous column study of Cu(II) and Pb(II) ions on alkali-treated coir", Desalination and Water Treatment, 2015 — 10 words — < 1%
Crossref

142 Shu Hui Tang, Muhammad Abbas Ahmad Zaini. "Microporous activated carbon prepared from yarn processing sludge via composite chemical activation for excellent adsorptive removal of malachite green", Surfaces and Interfaces, 2021 — 10 words — < 1%
Crossref

143 Soumia Bakhta, Zahra Sadaoui, Ulla Lassi, Henrik Romar, Riikka Kupila, Julien Vieillard. "Performances of metals modified activated carbons for fluoride removal from aqueous solutions", Chemical Physics Letters, 2020 — 10 words — < 1%
Crossref

144 Tomar, Geetanjali, Arushi Thareja, and Sudipta Sarkar. "Fluoride removal by a hybrid fluoride-selective adsorbent", Water Science & Technology Water Supply, 2014. — 10 words — < 1%
Crossref

145 Usha Kumari, Asmita Mishra, Hammad Siddiqi, B.C. Meikap. "Effective defluoridation of industrial wastewater by using acid modified alumina in fixed-bed adsorption column: Experimental and breakthrough curves analysis", Journal of Cleaner Production, 2020 — 10 words — < 1%
Crossref

146 Wang, S.. "Environmental-benign utilisation of fly ash as low-cost adsorbents", Journal of Hazardous Materials, 20060825 — 10 words — < 1%
Crossref

147	Xiuli Han. "Adsorption characteristics of methylene blue onto agricultural wastes lotus leaf in bath and column modes", Water Science & Technology, 08/2011 Crossref	10 words — < 1%
148	cwww.intechopen.com Internet	10 words — < 1%
149	dergipark.org.tr Internet	10 words — < 1%
150	etheses.whiterose.ac.uk Internet	10 words — < 1%
151	lib.buet.ac.bd:8080 Internet	10 words — < 1%
152	lutpub.lut.fi Internet	10 words — < 1%
153	patents.google.com Internet	10 words — < 1%
154	prr.hec.gov.pk Internet	10 words — < 1%
155	worldwidescience.org Internet	10 words — < 1%
156	www.icontrolpollution.com Internet	10 words — < 1%
157	ynu.repo.nii.ac.jp Internet	10 words — < 1%

158 Şerife Parlayici. "Alginate-coated perlite beads for the efficient removal of methylene blue, malachite green, and methyl violet from aqueous solutions: kinetic, thermodynamic, and equilibrium studies", Journal of Analytical Science and Technology, 2019
Crossref

10 words — < 1%

EXCLUDE QUOTES	OFF	EXCLUDE SOURCES	< 10 WORDS
EXCLUDE BIBLIOGRAPHY	ON	EXCLUDE MATCHES	< 10 WORDS